PETROLOGY, GEOCHEMISTRY AND FLUID INCLUSION STUDIES OF AMPHIBOLITE - GRANULITE FACIES TRANSITION ZONE AROUND SOMVARPET, DHARWAR CRATON - IMPLICATION ON CRUSTAL EVOLUTION

Thesis submitted to Kuvempu University for the award of the degree of

DOCTOR OF PHILOSOPHY

in

APPLIED GEOLOGY

By

Mr. JAYARAM GANAPATI NAIK

Under the Guidance of

Guide:

Dr. K.S. ANANTHA MURTHY
Professor
Dept. of P.G. Studies and
Research in Applied Geology,
Kuvempu University
Shankaraghatta – 577 451

Co-Guide:

Dr. GOVINDRAJU
Assistant Professor
Dept. of P.G. Studies and
Research in Applied Geology
Kuvempu University
Shankaraghatta – 577 451

KUVEMPU UNIVERSITY

Department of P.G. Studies and Research in Applied Geology
Jnana Sahyadri, Shankaraghatta – 577 451
Shivamogga District, Karnataka, INDIA

2016

Declaration

I, **Jayaram Ganapati Naik,** hereby declare that the thesis entitled **"Petrology, Geochemistry and Fluid Inclusion Studies of Amphibolite - Granulite Facies Transition Zone Around Somvarpet, Dharwar Craton - Implication on Crustal Evolution"** submitted to Kuvempu University for the award of **Doctor of Philosophy in Applied Geology,** is the original work carried out by me under the guidance of **Dr. K.S. Anantha Murthy**, Professor and **Dr. Govindraju**, Assistant Professor, Department of P.G. Studies and Research in Applied Geology, Kuvempu University, Shankaraghatta. This thesis or any part of it has not been previously submitted elsewhere, for any other degree or diploma of any other University/Institute.

JAYARAM GANAPATI NAIK

Date: 23/05/16

Place: Shankaraghatta

Certificate

This is to certify that the thesis entitled *"***Petrology, Geochemistry and Fluid Inclusion Studies of Amphibolite - Granulite Facies Transition Zone Around Somvarpet, Dharwar Craton - Implication on Crustal Evolution"** submitted to Kuvempu University by **Mr. Jayaram Ganapati Naik,** for the award of the degree of **Doctor of Philosophy in Applied Geology** is based on the results of experiments carried out by him under our supervision. The content of thesis or any part of it has not been previously submitted for the award of any other degree or diploma of any other University/Institute.

Dr. K.S. ANANTHA MURTHY
Professor
Dept. of P.G. Studies and
Research in Applied Geology
Kuvempu University
Shankaraghatta – 577 451

Date: 23rd May 2014
Place: Tirumakudalu

Dr. GOVINDRAJU
Assistant Professor
Dept. of P.G. Studies and
Research in Applied Geology
Kuvempu University
Shankaraghatta – 577 451

Date:
Place:

ACKNOWLEDGEMENTS

It gives me immense pleasure to express sincere gratitude to my research guides **Dr. K. S. Anantha Murthy**, Professor and **Dr. Govindraju**, Assistant Professor, Applied Geology, Kuvempu University under whose guidance this work has been carried out. I am greatly benefited by their valuable guidance, suggestions and encouragement throughout the course of this research work.

I express my sincere thanks to all the Chair Persons and The Co-ordinators, UGC Innovative Program, UGC-SAP(DRS) Phase I & II and DST- FIST of the Department of Applied Geology, Kuvempu University for extending the all the available facilities.

I am highly indebted to all my Teachers; **Prof. G. Chandrakantha, Prof. K. N. Chandrashekarappa** and **Prof. Syed Ashfaq Ahmed,** Dept. of Applied Geology, Kuvempu University, **Dr. M. Lingadevaru**, Department of Geology, Central University of Karnataka, Kalaburgi for their continuous encouragement and support in various ways at different stages of this work.

I would like place on record my sincere thanks to **Dr. T. C. Devaraju**, Formerly Professor of Geology, Karnatak University, Dharwad. He has spent his valuable time with us during time of field work and also gave his valuable inputs.

I express my sincere thanks to **Dr. J. N. Pattan**, Scientist 'F', NIO, Goa, for extending ICP-AAS facility and **Dr. G. R. Ravindra Kumar.** Scientist 'G', NCESS, Kerala for extending XRF facility and D**r. Ananthanarayan** DDG (Rtd), **Dr. Girish** and **Dr. Mahesh**, Mineralogists, PPOD lab, GSI, Bangalore for helping me in obtaining EPMA and Fluid inclusions data.

I am highly thankful to my friends **Mr. Umapathi, B. N., Mr. Jaykumar, P. D**., **Dr. Gobi, Mr. Manohar, Mr. Shivaprasad, Mr. Somesh, Mr. Lalu, Mr. Kumar, Mr. Ganesh Prasanna, Mr. Bathish, Mr. Lingadevaru, Ms. Shashikala** and other research colleagues helped in various ways and also for the finalization of draft.

I extend my sincere regards to all the **non-teaching staff** of the Dept. of Applied Geology, helped at different stages of the work.

I am highly thankful to University Grants Commission, New Delhi for the financial assistance through major research project **F.No: 37-257/2009(SR): Dated: 12-01-2010.**

This work has seen the light of the day because of the affection, constant encouragement, support and the blessings of my **parents** and **family members**.

Finally, I would like to express my thanks to all those who are close to me and who have offered support directly or indirectly during the course of my work.

JAYARAM GANAPATI NAIK

LIST OF TABLES

LIST OF FIGURES

CONTENTS

ABSTRACT

Nature and composition of the middle to lower crust is inferred from the study of amphibolite - granulite facies rocks. Somvarpet area forms a part of the amphibolite – granulite facies transition zone of the Western Dharwar Craton and covers the western most part of Fermer's Orthopyroxene Isograde line. Amphibolite facies gneisses, incipient charnockite, foliated charnockite, pyroxene granulite, hornblende schist and younger mafic intrusives represented by dolerite forms important lithologies of the area. The present study provides petrological data base for the Somvarpet amphibolite – granulite facies transition zone.

Migmatized amphibolite facies gneisses, represented by grey-biotite/hornblende gneiss and pink garnetiferous gneiss which are predominant in the northern part of the area are often over printed by greasy brown patches of incipient charnockite. Quite often, the gneissic foliation is bent or swerved at the borders of the charnockite patches. Greasy looking, granulitic textured foliated charnockite which is dominant in the middle of the study area contain both the feldspars with quartz, hypersthene, biotite and hornblende. Whereas, medium to fine grained and greenish black to black pyroxene granulite is ubiquitous in the southern part of the area, exhibits granulitic texture and contains both ortho and clinopyroxenes and plagioclase with subordinate amounts of garnet. Excluding the dolerites all the lithologies of the area have undergone two events of deformation resulted in the N-S to NNW regional in the study area.

The chemistry of amphibolite facies gneisses, incipient charnockite and foliated charnockite indicate they are high Al_2O_3 TTG. The depletion of LIL elements in charnockites is correlated to the granulite facies rocks, elsewhere. The relative higher contents of LIL elements in incipient charnockites compared to foliated charnockite attributed to their enrichment during fluid induced metamorphism.

Relatively, low density carbonic inclusion and their entrapment at relatively low P-T compared of CO_2 inclusions of incipient charnockite compare to foliated charnockite may be attributed to re-entrapment of earlier CO_2 during the formation of incipient charnockite.

Geothermobarometry, mineral stability, mineral isograde and fluid inclusion data demonstrate the P-T conditions along N-S traverse of the study area, increases gradually from 738^{o}C/4.5-5kb in amphibolite facies gneisses to 764^{o}C/5.8-6.3kb in incipient charnockite and 898 – 945^{o}C/6.3-6.7kb in foliated charnockite in the further south. This is not only reflects increasing temperature and pressure of metamorphism but also a change in the fluid regime from amphibolite to granulite facies.

Chapter - I

INTRODUCTION

1.1. Introduction

Knowledge about the nature and composition of the deep continental crust and its interaction with the underlying mantle and overlying upper crust is essential to understand the formation and stabilization of the continents. Most of the exposed continental crust in Precambrian terrains are of the granulite grade and are considered as windows to deep continental crust. The amphibolite – granulite facies transition zones are recognized as a fundamental boundary within the crust, and are commonly considered to designate the transition from middle to lower crustal levels. Hence, the study of these can provide us constraints on the probable nature and composition of the lower crust (Bholen, 1987; Harley, 1989; Brown and White, 2008). Understanding the spatial and temporal relationships within the amphibolite–granulite facies boundary is a key in discerning the crustal architecture, thus, inferring the crustal behavior. Particularly, the exposed crustal cross sections offer an unparalleled perspective on the nature and history, and significance of the metamorphic boundaries. In general, the petrological studies and thermo barometric calculations indicate 5-10kb paleo-pressures and 600-850^{o}C temperatures for granulite facies metamorphism. The diverse P-T-t paths like, clock-wise, anticlockwise or both, suggests different tectonic process like continental collision, extensional, subduction and magmatic under platting. Fluids (CO_2, CH_4, N, H_2O-NaCl, etc.,) play a significant role in controlling the mineral stability, heat flow, melting and deformation of the deep crust (Newton, 1989). CO_2 fluids appear to play an important role in the lower crustal process, particularly, syn and post metamorphic CO_2 fluid processes have been suggested by Touret and Hortel (1990), Lamb (1990) and Srikantappa *et al.*, (1992 and 1994). Further, based on studies of granulite terrains across

the world, several models have been proposed by geoscientist to explain the processes of formation of granulites. They include;

1. ***Partial anatexis*** - by Fyfe (1973), Pride and Muecke (1980) and Powell (1983). According to this model granulites are formed by dehydration melting of amphibolite facies rocks and removal of water enriched silicate melts leaving behind, essentially dry granulite residue and CO_2 enriched fluid phase.

2. ***Influx of CO_2 rich fluids and concomitant reduction of water activity*** - by Touret (1971); Janardhan *et al.,* (1979) and Newton *et al.,* (1980, 2014). The model emphasizes the transformation of amphibolite facies rocks to granulite facies due to strong reduction of water activity as a result of massive influx of CO_2 fluids of deep seated origin.

3. ***Sudden decrease in fluid pressure*** - by Srikantappa *et al.,* in 1985. The model assumes that the amphibolite grade protoliths contain intergranular fluids and these fluids escaped along a system of fractures which are developed when the deformational behavior has changed from ductile to brittle. The sudden decrease in fluid pressure relative to lithostatic pressure led to break down of the hydrous mineral assemblages.

4. ***Granulite formation by dehydration of amphibolite facies rocks under fluid absent conditions*** (e.g. Adirondock granulites, Namaqualand granulites) - by Valley *et al.*, 1984, Thompson, 1984, Waters and Whales, 1984. The model emphasize, reduction of H_2O activity resulted from the production of silicate melt by a vapor absent Fe-Mg reaction (Bt+Sill+Qtz=Gt+K-feldspar+liquid, Hbd+Qtz=Opx+Cpx+Pl+L), which affects Fe-rich compositions before vapor absent melting occurs in Mg-rich rocks, and segregations represent the solid and liquid reaction products. Such processes imply local control of activity of H_2O, and indicate the granulite transition did not result from a regional influx of metasomasing fluids.

In all the above models, heat, pressure and fluids are the most important parameters in granulite formation. The sources of heat and fluids are the subjects of current day debate. Harris *et al.,* (1982), Rajesh *et al.,* (2004), Santhosh *et al.,* (1992, 2003, 2006 and 2011) and Drury *et al.,* (1984) have suggested mantle outgassing was the source of heat and fluids. On the contrary, Wickham (1987) and Touret (1971) have proposed basaltic under plating at the base of continental crust. However, geochemical studies suggest both magmatic and sedimentary protoliths with varying pre-crustal histories (Janardhan *et al.,* 1982; Mahabaleshwar *et al.,* 1995). The distinct mineralogical and geochemical changes attend the regional metamorphism, depletion in large ion lithophile elements (LILE) being one of the characteristic features (Tarney, 1976; Rollinson and Windley, 1980). Geochemical characterization of prograde metamorphism has been largely inferred from the variations in elemental abundance between amphibolite and granulite facies litho-units. Hence, geochemical investigations of unbroken gneiss - granulite successions, in an independently exposed and regionally metamorphosed terrain are of fundamental relevance in quantifying the elemental mobility. When such an association occurs together in an exposure, within the scale of a few decimeters, apparently represent isochemical transformation of gneiss to granulite, hence, it provides a unique opportunity to evaluate elemental mobility.

Southern Peninsular India exposes one of the largest granulite terrains of the world. The most characteristic features of the terrain are; the continuous gradation from green schist facies – amphibolite facies - granulite facies with increasing P-T conditions (Raase *et al.,* 1986), and the presence of syn-metamorphic high density CO_2 fluids. The Dharwar Craton which forms a part of the Southern Indian shield expose a large section of continental crust, principally composed of TTG with in the folded supracrustal rocks and bounded by the late Archean juvenile terrains in the south. Calc-alkaline to K-rich

granites forms the latest magmatic events in the Craton. One of the most significant features of the Dharwar Craton is the continuous unbroken amphibolite - granulite transition. This transition zone has received the much attention in recent years, particularly, Eastern and Central part of the 'Former's orthopyroxene isograde line in the southern Dharwar Craton namely; Kabbaldurga, B.R.Hills, Coorg and Kushalnagara in Karnataka and Krishnagiri - Salem in Tamilnadu. A large volume of petrological, mineralogical, geochemical and geochronological data have been generated on these areas by geoscientists viz., Pichamuthu (1960); Janardhan *et al.,* (1979, 1982, 1994 and 1995); Friend (1981); Condie et.al, (1982); Hansen *et al.,* (1984 and1995); Battacharya and Sen, (1986); Gopalkrishna *et al.,* (1986); Lingadevaru *et al.,* (2007); Stahle *et al.,* (1987); Peucat et al, (1989 and 1993); Sen and Battacharya, (1990); Srikantappa, (1992); Basavarajappa, (1992); Srikantappa *et al.,* (1992 and1994); and Mahabaleshwar *et al.,* (1995).

1.2. Previous work on the study area

The study area is located in south western part of the Western Ghats in Karnataka and forms western most part of the amphibolite – granulite facies transition zone known as ''Former's orthopyroxene isograde line" of the Dharwar craton. except, Geological Survey of India mapping (1973, 1994) no other information on geology of the Somvarpet area and few works on adjacent area by Srikantappa *et al.,* 1994; Gopalkrishna *et al.,* 1986; Peucat *et al.* 2013; Santhosh *et al.,* 2013.

Gopalkrishna *et al.* (1984) have mapped the Kushalnagar area with emphasis on charnockite development in relation to several episodes of structure formation. They have

obtained temperatures of 700-800^{o}C across the transition based on thermometric calculations.

Srikantappa *et al.* (1994) have obtained 7 to 8.5 kb pressure and 720 to 760^{o}C peak granulite facies P-T conditions of metamorphism for the Coorg granulites. Their fluid inclusion studies have indicated that Coorg charnockites contain high density (1.07 to 1.09 g/cc) carbonic inclusions.

Peucat *et al.* (2013) have obtained Sm–Nd whole-rock isochron ages of 3700 - 2910 Ma for the charnockites, mafic granulites and migmatitic gneisses from the Coorg Block.

Santosh *et al.,* (2013) have carried out detailed geological, geochemical and geochronological studies of the Coorg granulites. Based on major, trace and REE data, they opined arc-related signatures for the Coorg rocks. Their Zircon U-Pb Isotopic data indicate the age of 3153.4±9 to 3275±5.1 Ma for the Coorg granulites and their mineral P-T data indicate 820-870^{o}C temperature and 6 kb pressure for the granulite facies lithologies of this area.

Review of literature of the area around Somvarpet which forms western most part of the Amphibolite-Granulite transition zone (Former's orthopyroxene isograde line) reveal the area has not been studied in detail, probably due to its rugged topography with thick natural and manmade vegetation, limited outcrops and inaccessibility. Hence, the geological database of this area is very scanty though, the area provides an excellent opportunity to understand the nature, composition and evolution of deep continental crust. Therefore, the present study has been carried out with the following aim and objectives.

1.3. Aim

The main aim of the present study is to understand the nature, composition and evolution of deep continental crust with the following objectives;

1.4. Objectives

- To understand gneiss-charnockite relationship – based on a detailed geological investigation and mapping
- To understand the P-T history and P-T-t paths – based on mineral chemistry.
- To know the nature and composition of metamorphic fluids – based on fluid inclusion studies
- To understand the nature of protoliths – by geochemical analysis for major, trace and REE of lithounits of amphibolite – granulite facies transition.

1.5. Methodology

In order to achieve the enumerated objectives the following methodology has been adopted.

1.5.1. Literature Review

To update the knowledge on crustal evolution in general and granulites facies rocks of southern India and Somavarpet area in particular by referring to journals/books, and web and internet sources.

1.5.2. Field investigations

The geological map of the study area has been prepared by carrying out detailed Geological field investigations. While, compiling the geological map of the study area, the data obtained during the field visit and resource map of Hassan and Kodagu district has been integrated on GIS platform (Arc GIS, 9.2).

1.5.3. Laboratory Investigations

Representative rock samples collected during field investigation has been subjected laboratory studies;

- ***Petrography***: Petrographic work has been carried out for all the collected samples by using Olympus OLYMPUL-CX31 and Swift Prior in the Department of Applied Geology, Kuvempu University, Shankaraghatta.
- ***Mineral chemistry***: Elemental analyses of co-existing mineral pairs were analyzed using a wave dispersive CAMECA-SX100, electron microprobe analyzer for 10 probe sections at PPOD lab, Geological Survey of India, Bangalore. Mineral phase equilibria and P-T conditions of metamorphism were used to formulate P-T-t paths.
- ***Fluid inclusions:*** 12 doubly polished thin sections were prepared at the Dept. of Earth Science studies, University of Mysore, Mysore for fluid inclusion studies. The micro-thermometric studies were carried out on a Linkam THMSG 600 heating/freezing stage fitted on an Olympus BX 50 transmitted light microscope at PPOD laboratory, Geological Survey of India Bangalore.
- ***Geochemistry:*** Based on the petrographic study, 45 rock samples representing different litho units were selected geochemical analysis. Powdering of all these rock samples has been carried out using Jaw crusher for coarse grinding. Disc mill for fine powdering at PPOD laboratory, Geological Survey of India. 10 rock samples whole rock geochemical analysis has been carried out in ICP-MS laboratory, at Act lab, Canada. 35 rock samples Trace and REE geochemical analysis has been carried out in ICP-MS laboratory, at CSIR lab, National institute of Oceanography, Goa. 35 rock samples Major oxide analysis has been carried out using XRF at Centre for Earth Science studies, CSIR lab, Trivandrum, Kerala.

1.5.4. Data compilation and analysis

The data obtained from all the above studies has been computed and analysed to formulate metamorphic evolutionary history of deep continental crust.

1.6. Study area

1.6.1. Location and Accessibility

The study area forms a part of Hassan and Kodagu district covering an area of 450 Km^2, and located in the southwestern part of Karnataka state, lying between the longitude 75° 45'-75° 55' E and latitude 12° 35'-12° 56' N and falls in the Survey of India Toposheet No 48P/13 and 48P/14. Somvarpet, which is the taluk head quarter of Kodagu District is the main town of the study area and is well connected with all season road network. The National Highway NH-48 which connects port city of Mangalore with capital city Bangalore and State highway SH-88 are passing through the area. The study area is lies about 262 km south west of Bangalore (State Capital), 128 km west of Mysore and 130 km east of Mangalore.

1.6.2. Climate

The area enjoys typical tropical climate characterized by slight to medium humidity due to proximity to coast (about 32 Km). It is known to be quite pleasant and healthy, characterized by high humidity, heavy rainfall and cool summer. A major part of the year consists of rainy season as the monsoon period starting in June lasts till the ends of September. Even during the post monsoon months of October and November certain parts of the area receive a significant amount of rainfall. Because of the cloudy weather, the day would be quite sultry during October and it is only during the second half of the November that the weather becomes brighter. The period from December to February is

the cold season marked by a bright weather, foggy mornings and chilled nights. The day temperature begins to rise sharply during March and marks the commencement of the summer season, which lasts till the end of May. The analysis of the meteorological data for the last 10 years, reveals that the highest rainfall (Average 3302.46 mm) has occurred in the Western part of the area which is thickly forested and the lowest (Average 2105.22 mm) in the northern part of the area having comparatively less forest cover. The area lies in the Malnad region on the magnificent hills of the biodiversity hotspot, the Western Ghats. It has a temperate climate surrounded with lofty green hills full of Coffee, Cardamom, Orange, Pepper and Areca plantations. Large timber yielding trees such as Silver oak, Rose wood and Jack fruit trees provide shade for these coffee bushes and add to the economy of the region. .

1.6.3. Topography

The physical features of study area are varied. Topographically the area is characterized by long and elongated ridges, run from east to west. These chains of hill range have an elevation ranging from 1000 to 1700 meters above the msl. The high hilltops are generally grassy with valley of dense mixed vegetation, and the mounds hill range are generally under cultivation with plantation crops.

1.6.4. Soil

The soils of the area are of a heterogeneous profile and consist of sandy, sandy loam and lateritic debris found in different stages of weathering and lateritization. The valleys and slopes have fertile red loamy soils that are suitable for cultivation. In the eastern part of the area, the dark clay soil is predominant, and it is often get water logged during monsoon, and deep cracks appear during the summer months. While, the central part is predominantly covered by loamy soil whereas, in the western part, the soil is lateritic in nature and tend to be quite shallow. The northern part appears to be more of sandy soil.

1.6.5. Outcrops

Due to rugged topography, thick vegetation and soil cover has made most part the area inaccessible. The only accessible parts for geological observation and sampling are; active/abundant quarries around Kodlipet, Shanthahalli, Jakkanahalli, Banavara and Alur Siddapura; road cuttings between; Sakalashpura - Kodlipete, Kodlipete - Sanivarasanthe, Somvarpet - Banavara, Shanthahalli - Kutti, Somvarpet - Doddakunda, Surlabi - Garvale; and river (Hemavathi river) and stream banks, besides few exposers around Sanivarsanthe, Doddakunda, Rudragiri betta, Malambi betta and Vanguru.

Chapter - II

GEOLOGY

2.1. Geology of Southern India

Precambrian shield of the Indian subcontinent has been divided into cratonic nuclei of Dharwar, Singbhum and Bastar cratons, surrounded by mobile belts of successively younger ages (Radhakrishna and Naqvi, 1986). The Dharwar craton in the southern shield records geological events that occurred essentially during 3.4 to 0.5 Ga. The craton can be divided into two principal terrains based on the grade of metamorphism i.e., (1) southern high-grade granulite terrain and (2) northern low grade granite-greenstone terrain. The boundary between these two terrains appears to be a kind of transition which is superimposed across the structural grain. The southern high-grade terrain encompasses large areas in Tamil Nadu, Kerela and southern part of Karnataka, and essentially composed of gneisses punctuated with rafts of supracrustal rocks. The rocks of the terrain exhibit a polymetamorphic history, with the youngest event recorded at 500 Ma, which may be correlated with the Pan-African orogeny (Chacko *et al.*, 1987). The northern low- grade terrain is spread over major parts of Karnataka and Goa, and parts of Andhra Pradesh. It is composed of several greenstone belts surrounded by gneisses and granitoids. The central part consists of granite-greenstone terrain characterized by green schist to lower amphibolite facies metamorphism and surrounded by a mobile belt consisting of charnockite and migmatitic gneisses, and are well exposed in the eastern portion of the south Indian shield.

In general, the south Indian Peninsular region includes representatives of all the three principal rock associations, which is a characteristic of Archean terrains, viz., (i) granulites - the high-grade associations of Tamilnadu and Kerala (ii) older

supracrustals - the granite-greenstone association and, (iii) Dharwars - the Craton-basin association. Perhaps, in no other part of the world, all the three associations brought together in such a well-knit composite unit as in South India, affording excellent opportunities for a close study and understanding of the stages in the evolution of the early crust.

2.2. Dharwar Craton

The Dharwar Craton (Fig. 2.1) is bordered by the Arabian Sea in the west and high-grade terrain of Tamil Nadu – Kerala in the south. The crescent shaped Cuddapah Basin (1600 Ma) covers a good part of the gneissic terrain in the east and the northern extensions of the cratonic block is hidden beneath the cover of Deccan Traps of Mesozoic - Tertiary age. Dharwar craton comprising of a number of sub parallel schist belts, set in a matrix of polyphase gneisses bordered by granulites in the south, and granites to the east (Radhakrishna and Naqvi, 1986; Radhakrishna and Ramakrishnan, 1988; Ramkrishanan and Vidyanadhan, 2008). The available geochronological ages spanning between 3.4 and 2.0 b.y, highlights the major early Precambrian events in the Craton. The Dharwar craton has been subdivided into eastern and western blocks (Swamin Nath et al. 1976). These Eastern and Western blocks have major differences in lithology and age. The dividing line is being a steeply dipping mylonite zone (Chitradurga Shear) and that is being interpreted as ristric structure by Chadwic *et al.,* (1992), and as a low angle thrust which becomes shallow at depth as proposed by Kalia *et al.,* (1979). The Closepet Granite is a good approximation of the western boundary (Ramakrishnan and Vaidyanadhan, 2008), and Chitradurga shear zone marks the boundary between Western Dharwar and Eastern Dharwar Craton. The western block has much broader expression of the Dharwar's and Sargur's, whereas, the eastern block has fewer supracrustals, but many have discrete granite bodies, especially the elongate N-S Closepet granite, and a collection of number

of individual plutons of late Archean or early Proterozoic age, which traverse the eastern block near its western extremity. The strong N-S trending fabric of the Dharwar craton is partly a result of late Archean transcurrent shearing episode (Drury and Holt, 1980; Chadwick *et al.,* 1989) and is contemporaneous with the emplacement of the Closepet granite (Jayananda and Mahabaleshwar, 1991).

The most characteristic feature of the Dharwar craton is the transition from low to medium grade metamorphism in the north to high grade metamorphism in the south through a transition zone (Swami Nath and Ramakrishnan, 1981; Janardhan *et al.,* 1982; Radhakrishna, 1983; Jayananda *et al.,* 2013). The existence of a gradual progression in metamorphic grade from north to south across the Dharwar craton was recognized by Pichamuthu (1965). The actinolite-chlorite metamorphism exhibited by both greenstones and enclosing gneisses in the north of the craton gives way steadily southward to amphibolite facies, and eventually the granulite facies in the southern margins, where orthopyroxene appears almost simultaneously in gneisses and metabasic lenses. A diffuse regional orthopyroxene isograde has been traced across the southern end of India (Subramaniam, 1967). The paleo-pressures increase from 3kb (in mafic rocks) in central Karnataka to 8-9kb (in both felsic and mafic rocks) in the south (Raith *et al.,* 1983; Hansen *et al.,* 1984; Raase *et al.,* 1986; Eckert and Newton, 1993). The increase of P-T towards south is not linked to any particular tectonic features or breaks (Raith *et al.,* 1983; Pichamuthu and Srinivasan, 1984; Raase *et al.,* 1986).

2.3. Western Dharwar Craton

The Western Dharwar Craton (WDC) is bound by Eastern Dharwar Craton (EDC) in the east, to the west by the Arabian Sea, and to the south by "Southern Granulite Terrain". The remaining boundary to the north is buried under younger sediments and the Cretaceous Deccan Traps. WDC comprises of Holenarsipur, Bababudan, Shimoga-North Kanara, and Chitradurga - Gadag schist belts. The available radiometric dates of

supracrustal rocks and gneisses appear to be in consistent with the broad two-fold division, wherein, the Sargur group of rocks have formed during 3.8-3.2 b.y (Nutman *et al.,* 1992; Peucat *et al.,* 1995; Jayananda *et al.,* 2008) and supracrustal rocks of Dharwar super group accumulated during 2.91-2.72 b.y. (Taylor *et al.,* 1984; Nutman *et al.,* 1996; Trendall *et al.,* 1997; Jyananad *et al.,* 2013). The polyphase migmatitic gneisses yielded radiometric ages of 3.4 - 2.2 Ga (Pecat *et al.,* 1995; Jayananda *et al.,* 2008), but larger area recorded 3.0 Ga. The supracrustal rocks and Peninsular gneisses are further intruded by K-rich granites which are 2.5 Ga. old (Taylor *et al.,* 1984 and Bhaskar Rao *et al.,* 1992). The status of Super group as a separate unit has however been disputed by Naha *et al.,* (1993), who questioned the validity of attaching stratigraphic significance to the Peninsular gneisses which constitutes a polyphase gneiss evolved over a long span of time ranging from 3.3 -2.9 Ga. High grade supracrustal rocks underlying the basal unconformity have been referred to as "Sargurs" by Swami Nath and Ramakrishnan (1981). The younger Dharwar super group has been subdivided into (a) the lower Bababudan group and (b) the upper Chitradurga group and (c) Shigegudda schist belt based on the presence of a thin persistent oligomict quartz pebble conglomerate horizon marking the unconformity between these two groups. The supracrustal rocks of Sargur occur as thin slivers within the Peninsular gneiss and are mainly confined to the southern fringes of the Craton. In the southern parts of Craton, the supracrustal rocks of the Sargur group have been subjected to granulite facies metamorphism. Radimetric ages of detrital zircon present in quartzites led to propose a sialic basement for the Sargur by Chadwick *et al.,* (1986) and Nutman *et al.,* (1992). The Sargur group encompasses a diversified group of volcanic and sedimentary lithologies, represented by ultramafic-mafic volcanic rocks, pelites, quartzites, impure carbonates, iron formation and intrusive ultramafic-mafic and gabbro-anorthosite complexes (Swaminath and Ramakrishnan, 1981). Further, they reported concordant contact of the

Sargur enclaves with the surrounding gneisses and migmaties implying their involvement in ductile deformation along with the gneisses. The greenstone belts of the Western Block are characterized by mature, sediment-dominated supracrustals with subordinate volcanics and are recrystallized in intermediate pressure metamorphism. However, development of greenstone belts in the western block of the Dharwar Craton proceeded through three major depositional cycles such as volcanism and sedimentation terminating with the intrusion of syn- to post-kinematic granites on minor scale.

2.4. Geology of the study area

The study area falls on the Amphibolite – granulite facies transition zone and represent western most part of the "Former orthopyroxene isograd". The major lithologies of the area are amphibolites facies gneisses, incipient charnockite, foliated charnockite, pyroxene granulite, enclaves of hornblende schist and intruded by pegmatites and younger mafic dykes.

Amphibolite facies gneisses are the major lithounits and at places they are intensely migmatised to varying degrees and overprinted by greasy brown patches of incipient charnockite. These patches generally vary in size from centimetre to ½ a meter. The development of orthopyroxene is confined to shear planes across/along foliation, limbs/hinges of small scale folds with the variable degree of obliteration of earlier foliation of the gneisses. The banded charnockite and pyroxene granulites are the next dominant litho units. The mafic (Dolerite) dykes are the later intrusives trendig in E-W, NW-SE and NNW-SSE directions and cutting across all the litho units.

The lithologies of the area have under gone two events of deformation. The first event of deformation is represented by tight isoclinal folds. Second event of deformation is represented by tight folds with steep axial planes. Two deformational eposodes gives rise to the dominan N-S regional grain.

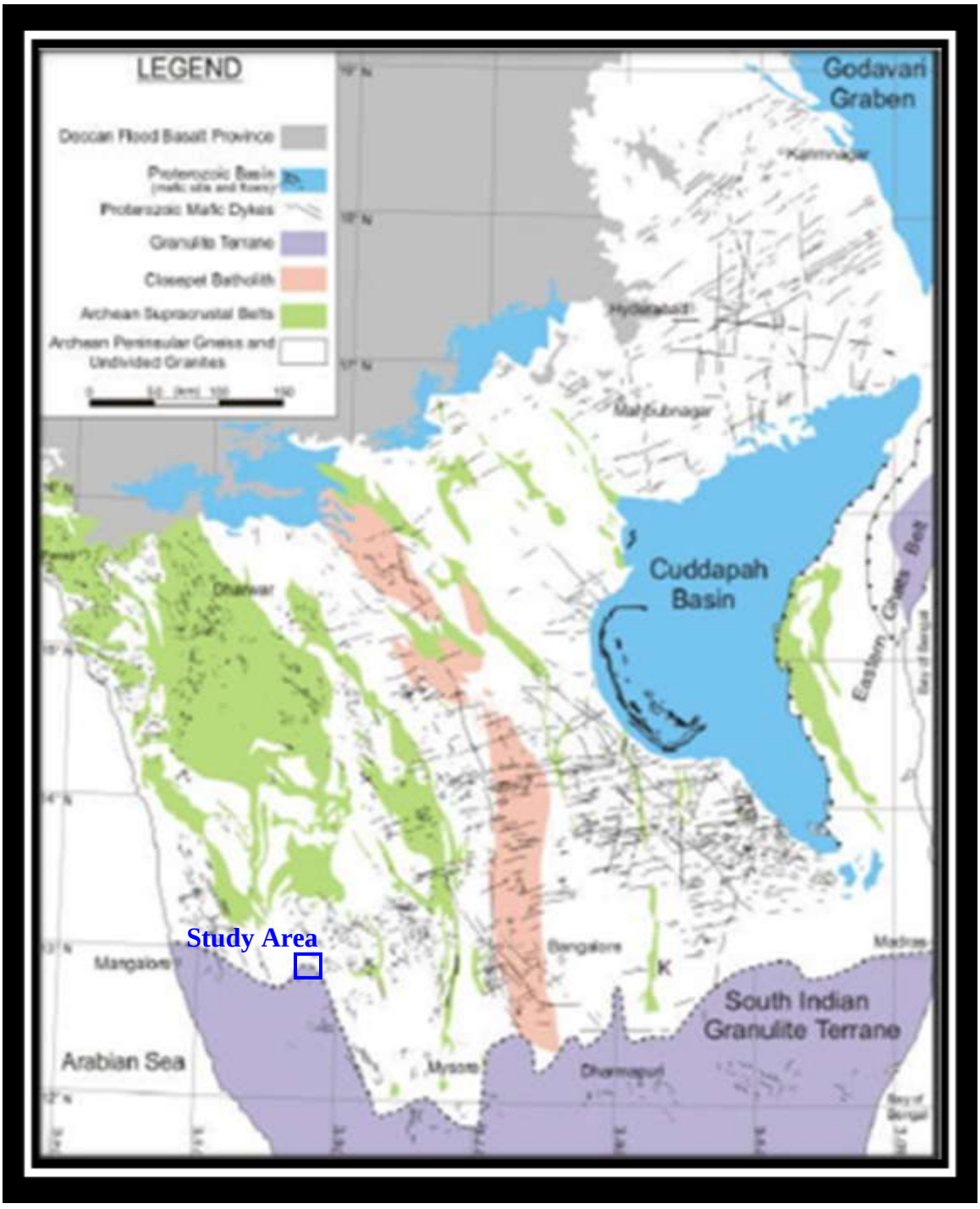

Fig. 2.1. Geological map of Dharwar Craton

Chapter - III

FIELD RELATIONS AND STRUCTURES

3.1. Introduction

The amphibolite – granulite transition zone of Somvarpet area forms a part of the Western Ghats, which is highly undulated and rouged terrain, comprising of steep hill ranges and deep valleys, covered with thick natural forest and coffee plantation that has made most part of the area as inaccessible. However, the availability of few old and active quarries, road cuttings and stream channels, and very few out crops close to roads have made it possible for geological field observation and sampling. The Geological map (Fig.3.1) and the field data presented in this chapter is based on the observation of few exposures i.e., quarries, road cuttings and stream channels, and accessible exposures across the study area.

3.2. Gneisses

Gneisses are the most dominant rock types covering 70% of the study area. They occupy the elongated hill ranges, often subdued, round and flat mounds. Based on the field observation two type gneisses are distinguished and are;

1. Garnetiferous - Leucocratic gneiss
2. Non garnetiferous - Grey gneiss

The occurrence of ***garnetiferous - Leucocratic gneiss*** is confined to northern part of study area (Kenchammana Hoskote, Balupet and Banavar). The garnetiferous gneiss is medium to coarse grained and exhibit typical gneissose texture and banding (Fig. 3.2, 3.3). Mineralogically, the rock is essentially composed of quartz, orthoclase and plagioclase feldspars representing felsic layers and mafic layer is essentially composed of biotite/hornblende, whereas, porphyroblasts of garnet are mostly confined to felsic layers and giving its pink color to the layer.

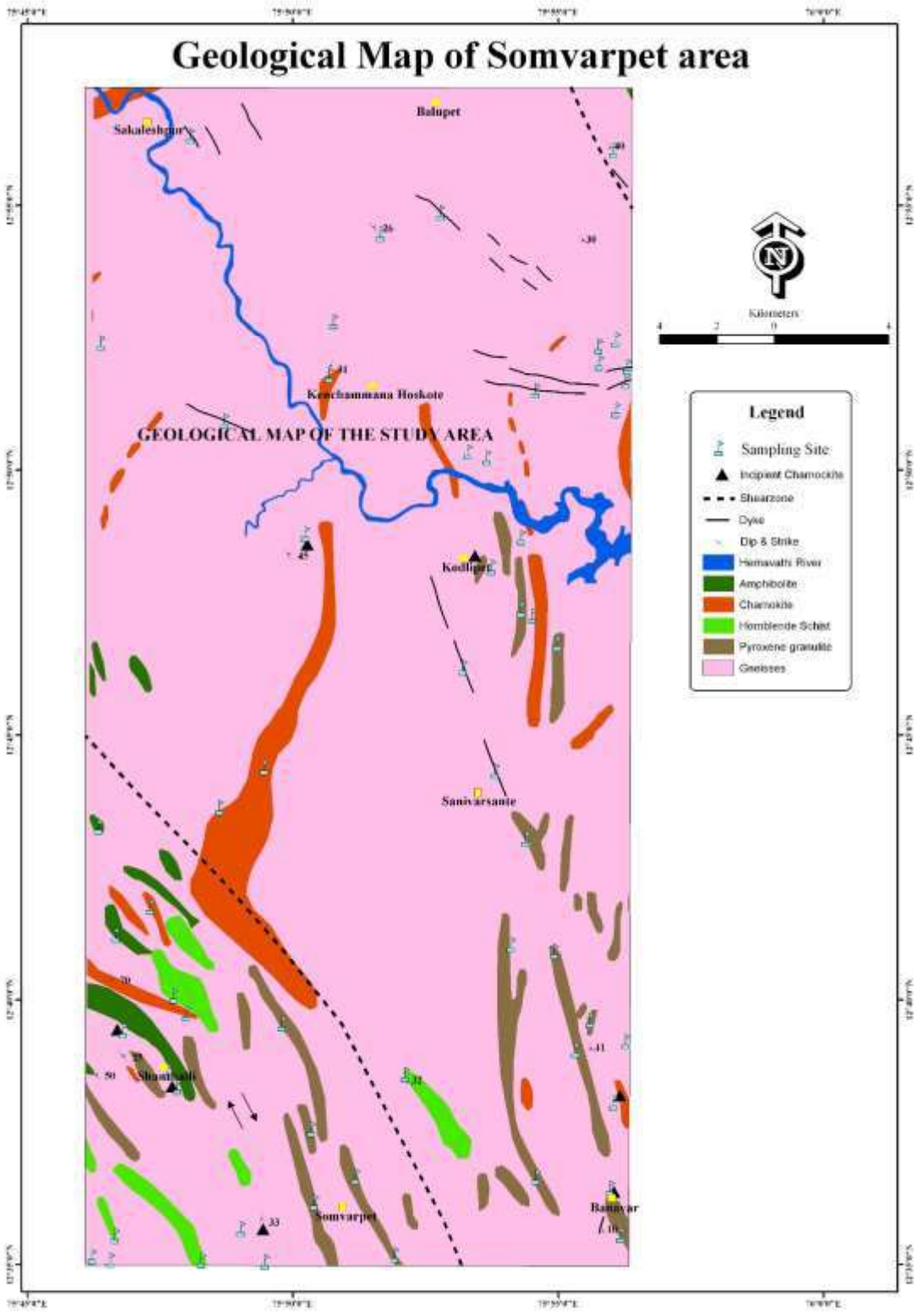

Fig. 3.1. Geological Map of Somvarpet area

The medium to coarse grained ***non-garnetiferous - gray gneiss*** occur in the southern part of the area particularly around Kodlipet (Fig. 3.4), Shanthalli, Jakkanahalli and exhibit typical gneissic texture. Mineralogically, the Gray gneiss is essentially consists of quartz, orthoclase and plagioclase feldspars, biotite/hornblende resembling typical amphibolite facies gneiss. The gneiss often shows migmatization to varying degrees with segregation granitic melt at places. In the central part of the study area (Kodlipet and Banavar quarries), it is observed that the dark biotite flakes with or without hornblende occur as patches/lenses/enclaves. The migmatized gray gneiss is often overprinted by patches of greasy brown incipient charnockite.

3.3. Incipient Charnockite

The greasy looking incipient charnockite occur as patches, discrete veins within the gneisses. These incipient charnockite patches generally vary in size from 2-5cm, and it reaches to a maximum width of ½ mtr (Fig. 3.5 and 3.6) and in some instances plates of orthopyroxene develops as tiny veins. The development of brownish greasy orthopyroxene is seen along the border of Biotite/Hornblende and concentrated in sheared limbs, foliations and hinges of small scale folds. The development of irregular greasy charnockite patches often seen which obliterating earlier foliation of the gneisses at variable degree (Fig. 3.7). Quite often, the gneissic foliation is bent or swerved at the borders of the charnockite patches. Close observation (Banavar quarry) reveals the developments of orthopyroxene along conjugate shears trending N 30° W and N 15° E.

3.4. Foliated Charnockite

Foliated Charnockite is one of the prominent litho unit of the study area. It is a greasy looking, medium to coarse grained occur as a massive out crops. The out crops of foliated charnockite also occur as discrete bands, boudins (Fig. 3.8 & 3.9), and often

contain small enclaves of pyroxene granulite. The major mineralogical assemblages are orthopyroxene, plagioclase, alkali feldspar, quartz, occasionally biotite, garnet and clinopyroxene. The garnet bearing charnockite band is observed only in Vanaguru road cuttings. On fresh surface, charnockites are massive in appearance, but, the weathered surface show well developed foliation trending in NE-SW with moderate to steep dips due East.

3.5. Pyroxene Granulite

The pyroxene granulite which is also referred as basic granulites or mafic granulites is one of the major litho units in the southernmost part of the study area. It is dark grey to black in colour, medium to fine grained in nature and occur as large bands trending N-S to NW–SE and traceable over a distance of more than a kilometre. The maximum width of the pyroxene granulite band is seen in south of Somvarpet along the Surlabi and Garvale road cuttings (Fig. 3.10), which is more than 100mts in width. Pyroxene granulite often occurs as disrupted boulders, boudins and enclaves within foliated charnockite and amphibolite facies gneisses. The major mineralogical constituents are orthopyroxene, clinopyroxene, plagioclase, hornblende and quartz, rarely garnet. Garnet bearing pyroxene granulite bands are noticed near BTCS College, Somvarpet and in the road cuttings between Doddakund and Nirgod (Fig. 3.11).

3.6. Hornblende Schist

Hornblende schist is the minor litho unit in the study area, generally occurs in association with mafic granulites as enclaves. The enclaves of hornblende schist are observed in the south western part of the study area near Garvale and south of Somvarpet. The rock is medium to course grained exhibits schistose fabric consisting mainly hornblende and plagioclase.

3.7. Pegmatite

The pegmatite veins forms a minor litho unit and essentially composed of quartz and pink feldspar. The veins ranging from less than a centimetre to a meter thick are found permeating the gneisses along and across the gneissic foliation (Fig. 3.12). Occurrence of these pegmatite veins is more prominent in the northern part of the study area particularly in Banavar and Kenchammana Hoskote quarries.

3.8. Mafic dyke

Mafic dykes of the study area are represented by dolerites have intrusive contacts with all the other litho units, and trending E-W, NW-SE and NNW-SSE direction. Their occurrence is more ubiquitous in northern part of the study area (Fig. 3.13) and occurs as bouldary outcrops with typical spheroidal weathering. Mafic dykes are fine to medium grained, dark in colour and exhibit ophitic to sub-ophitic texture. Mineralogically, they essentially consist of plagioclase and pyroxene with minor amounts of quartz.

Fig. 3.2. Garnetiferous leucocratic gneiss collected at Alur Siddapura quarry

Fig. 3.3. Leucocratic gneiss with typical foliation can see and the sample was collected at Jakkanhalli quarry

Fig. 3.4. Typical gneissose texture gray gneiss collected at Kodlipet quarry

Fig. 3.5. Typical Incipient charnockite patches observed within a gray gneiss at Shanthalli quarry

Fig. 3.6. Typical Incipient charnockite patches observed within leucocratic gneiss at Kodlipet quarry

Fig. 3.7. Development of orthopyroxene along the foliation of the gneiss at Jakkanahalli quarry

Fig. 3.8. Foliated charnockite sample collected at Kutti road cuttings

Fig. 3.9. Typical foliated charnockite with an intrusion of pyroxene granulites at Shanthalli quarry

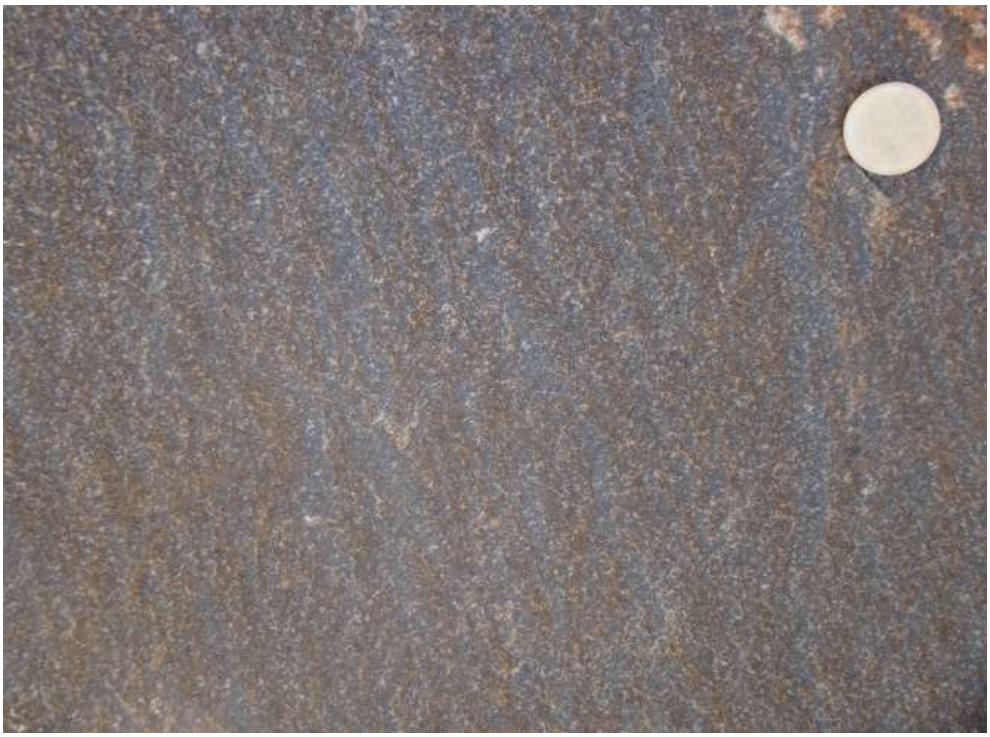

Fig. 3.10. Typical Pyroxene granulite sample collected at Rudragiri betta near Doddakunda

Fig. 3.11. Garnetiferous pyroxene granulite sample collected at BTCS College near Somvarpet

Fig. 3.12. The pegmatitic veins ranging from less than a centimetre to a meter thick are permeating along and across the foliation of gneiss at Banavara quarry

Fig. 3.13. The sharp contact between typical NW-SE trending dolerite dyke and migmatitic gneiss at Banavar quarry

3.9. Structures

3.9.1. Foliation

Foliation is the common planar structures noticed in gneisses, charnockite and hornblende schists. The most common type of foliation noticed in gneisses is compositional layering wherein, platy, flaky and lenticular minerals show preferred orientation with alternate layers of felsic mafic minerals(Fig. 3.14 and 3.15).

3.9.2. Shear zones

Shear zones are the zones of faulting in which the displacement is accommodated across and along a zone rather than on a single plane. These are typically produced when volumes of rock metamorphosed or intruded at high temperature are reworked under lower temperature conditions. Set of NW-SE trending sinistral shear zones within the peninsular gneisses are common but, the most prominently shear zones of the study area are observed at Jakkanahalli and Shanthalli quarry (Fig. 3.16). Chetty *et al.,* (2012), while mapping shear zones of southern Dharwar craton have described the enclaves of granulitic crust in Sakaleshpur and Somvarpet as highly elongated shears oriented parallel to the foliation trajectories.

3.9.3. Deformational episodes

During a detailed mapping and field study based on fold interference patterns, three phases of deformations have been identified. The structures related to three phases of deformation are seen as individual folds and combination of more than one.

3.9.3.1. Structures of D1 deformation

D1 is the earliest deformational event that affected the litho units. The first phase of deformation (D1) has produced folds (F1) which are invariably overturned, tight to isoclinals and occur as intrafolial and rootless folds. These folds resulted in the formation of axial planar foliation (S1) which is most pervasively developed structural element, defining the regional gneissosity. Structures related D1 deformation is observed in the grey gneiss at Kodlipet quarry (Fig. 3.17).

3.9.3.2. Structures of D2 Deformation

Structures of D2 deformation are represented by tight to rarely open upright isoclinal folds. The D2 deformation resulted in the development of F2 folds, related lineation and axial planar foliation (S2) were aligned in a general NE-SW (Fig. 3.18). Granitic material in the migmatites was plastic during F2 and minerals often aligned themselves parallel to S2.

3.9.3.3. Structures of D3 Deformation

The D3 deformation has resulted in the development of numerous E-W trending F3 warps throughout the area. This is the major deformational episodes, which is intensive as well as penetrative in the medium to high grade terrain, resulted in refolding of D2 deformation. The interference of F3 folds on earlier F1 and F2 folds has resulted in the formation of culmination, depression and compressional structures. These minor folds, with amplitudes of one meter or more, normally developed cylindrical, concentric forms with sub-vertical axial planes and E-W trending axes. The D3 structures are quite common in Banavar quarry

3.9.4. Joints

Joints are divisional planes found in all kinds of igneous and metamorphic rocks. In the study area, amphibolite facies gneisses exhibit three sets of joints, one set of joint is more or less horizontal, and the other two are vertical and perpendicular to each other. These three sets of partings are more or less equally spaced, which often give rise to a cuboidal block structures (Fig. 3.19). The horizontal joints are often closely spaced and produce a sheet structure. The thickness of the sheets reduces and become thinner and thinner near to the surface, and usually show some degree of parallelism to the surface.

Fig. 3.14. Common type of foliation noticed in gneisses at Jakkanahalli

Fig. 3.15. Common type of foliation noticed in foliated charnockite at Shanthalli quarry

Fig. 3.16. NW-SE trending sinistral shear zones within the peninsular gneiss noticed at Shanthalli quarry

Fig. 3.17. D1 deformation is observed in the gray gneisses at Kodlipet quarry

Fig. 3.18. Open upright isoclinals folds observed at Kodlipet quarry

Fig. 3.19. Three sets of joints (mural) in leucocratic gneiss observed at Banavara quarry

Chapter - IV

PETROGRAPHY

4.1. Introduction

The lithologies of the sudy area includes; amphibolite facies gneisses, incipient charnockite, foliated charnockite, pyroxene granulite, hornblende schist and dolerite dyke. In this chapter an attempt has been made to present a detailed petrographic description of all the lithologies.

4.2. Amphibolite facies gneisses

Amphibolite facies gneisses are medium to coarse grained, grey to pink coloured and exhibit the typical gneissosity and banding. Based on the colour and mineralogy, the gneisses have been classified ino two types. Namely;

1. Non garnetiferous - Grey gneiss

2. Garnetiferous - Leucocratic gneiss

Grey gneiss - Biotite/hornblende gneiss is the most prominent litho unit in the southern part covering more than 70% the area, and essentially contains quartz, both potash and plagioclase feldspars in the felsic layers and, biotite/hornblende minerals in the mafic layers, apatite, zircon and monazite occur as accessary minerals. Flakes of biotite, occur as a major mineral in mafic layer, is of two generation. The early formed biotite show reddish brown to dark brown colour, and the second generation biotite show greenish colour (Fig. 4.1). This kind of variation in colour of biotite is attributed to the enrichment of Fe and Ti during its formation (Chetty *et.al*., 2012)). The hornblende occur as prismatic grains in mafic layer and exhibit reddish brown to green pleochroic

colour. Laths plagioclase exhibit perthite and often antiperthitic texture. K-feldspar is represented by microcline and oocur as euhdral grains exhibit typical cross hatch twinning. Anhedral grains of quartz show marginal granulation which indicates that the rock has suffered defomation.

Garnetiferous-Leucocratic gneiss is medium to coarse grained and exhibit weak foliation,. Mineralogically, it is mainly composed of quartz, plagioclase, microcline, biotite, and garnet as an essential minerals and rutile, zircon and opaques forms the important accessory phase. The brownish coloured biotite in the mafic layer occur as elongated flakes. the weak foliation exhibited by the garnetiferous – leucocratic gneiss is to the alignment of biotite flakes in sub-parallel fashion. Garnet, which occur as Anhedral to subhedral grains along with the laths plagioclase often show, idioblastic to subidioblastic texture and contain inclusions of quartz (Fig. 4.2). Microcline, which exhibits subidioblastic to xenoblastic texture show fine perthitic lamellae of albite and cross-hatched twinning

4.3. Incipient charnockite

The incipient charnockite occur as small geasy stringers, patches and lenses confined to the shear planes with in the gneisses and exhibit xenoblastic texture. Mineralogical assemblage of the incipient charnockite is as follows:

Quartz + plagioclase + K-feldspar + hypersthene $\pm$ Biotite $\pm$ Hornblende

Large plates of greenish brown to dark brown hypersthene occurs as xenoblasts along micro fracture/shear planes of the gneisses. Plagioclase occur as subhedral laths are highly stretched and deformed and exhibiting xenomorphic texture with polygonal

aggregates, and occasionally show antiperthitic texture. K-feldspar occurs as subhedral to anhedral grains and show cross hatched twinning. The occurrence of hyperthene along micro fracture/shear planes of the gneisses indicate the mineral might be have formed at the expense of either biotite/hornblede (Fig. 4.3). The formation of hypersthene by breakdown of biotite and/or hornblende in the presence of quartz has been explained by Janardhan et al, 1979; Friend, 1981; Hansen et al, 1984, with the following the reaction:

$$\text{Biotite} + \text{Quartz} \pm \text{Hornblende} \longrightarrow \text{Hypersthene} + \text{K-feldspar}$$

4.4. Foliated Charnockite

The foliated charnockite are greasy looking, medium to coarse grained in nature and in thin section it exhibits a granular texture. Both Plagioclase and K-feldspar are the most abundant minerals with minor amounts of quartz, biotite, hornblende and pyroxene. Zircon, apatite, ilmenite and magnetite are the accessory minerals. The mineral assemblage of charnockite is as follows.

Orthopyroxene ± Clinopyroxene + Quartz + Plagioclase + K-feldspar ± Garnet +Biotite+opaques

The subhedral plates of orthopyroxene show brownish to pink in color and it is moderately pleochroic (Light pink to brown). The unstable orthopyroxene often show alteration to biotite/ hornblende along the grain boundaries and fracture planes at varying degrees (Fig. 4.4). Plates of bluish green Clinopyroxene are found in few sections, and show alteration to biotite and amphibole with the release of iron oxides along grain boundaries. Idioblastic to subidioblastic garnets occur as minor mineral often surrounded by orthopyroxene and plagioclase symplectites (Fig. 4.5). Biotite which is a minor constituent ocurr as typically bent flaks, show yellowish brown to greenish brown pleochroic color.

4.5. Pyroxene granulite

The pyroxene granulite is one of the prominent lithounits of the study area, is fine to medium grained and greenish black to balck in colour and exhibits granulitic texture (Fig. 4.6). Light green subhedral plates of clinopyroxene show various stages of alteration to honblende. Garnet occurs as subhidiblatic grains and occassionaly contain inclusions of pyroxene and plagioclase. Intergrowth of garnet and quartz often found in contact with plagioclase and pyroxenes. Ilmenite and magnetite ocurr as opaques are important accessory minerals found in almost all the pyroxene granulite samples studied. Plagioclase is the dominant feldspar in pyroxene granulites occurs as large subhedral laths with polysynthetic twinning. Anhedral grains of quartz form the minor phase and generally occurs as vermicular intergrowth with garnet around pyroxenes. Petrographic study revels the occurrence of the following mineral assemblages;

M1. Clinopyroxene + Orthopyroxene + Garnet ± Hornblende + Plagioclase ± Quartz ± Opaques

M2. Clinopyroxene + Orthopyroxene + Plagioclase ± Quartz ± Hornblende ± Opaque

M1 type pyroxene granulite, show coronitic texture (Fig. 4.7) where, the occurrence of garnet both as porphyroblast and symplectitic intergrowth with quartz between pyroxene and plagioclase grains, indicating on set of retrograde process. The coronitic texture seems to indicate the incomplete reaction due to upliftment/exumation of the terrain, sudden change of P&T (Ellis and Green, 1985; S.L.Harley, 1989). Further, reaction rims of garnet, quartz aroud pyroxenes and Fe oxides (Fig. 4.8) indicates resorption of pyroxenes by the following reactions (Ellis and Green, 1985; Harley, S. L., 1989).

1. Opx+Pl=Grt+qtz
2. Opx+Pl=Grt+Cpx+Qtz
3. Cpx+Pl=Grt+Qtz

4.6. Hornblende schist

Hornblende schist is highly foliated and essentially contains hornblende and plagioclase with minor amounts of quartz, biotite and opaques and exhibit typical schistose texture. Hornblende occurs as elongate prismatic grains with reddish brown to green color (Fig. 4.9). Laths of Plagiclase exhibits polysynthetic twinning, and anheradal grains of quartz occur as intersticial grains. Biotite is also present as small flakes and show brownish green to brown colour.

4.7. Dolerite

Fine to medium grained dolerite exhibits ophitic to sub-ophitic texture. The major mineral composition of this lithounit include plagioclase and clinopyroxene with hornblende and quartz as minor phase. Ilmenite and magnetite forms the usual accessory minral phases. Lath shaped plagioclase grains showing multiple twinning. Clinopyroxene is pale green in color and is feebly pleochroic and show some marginal alteration to bluish green hornblende with opaques (Fig. 4.11).

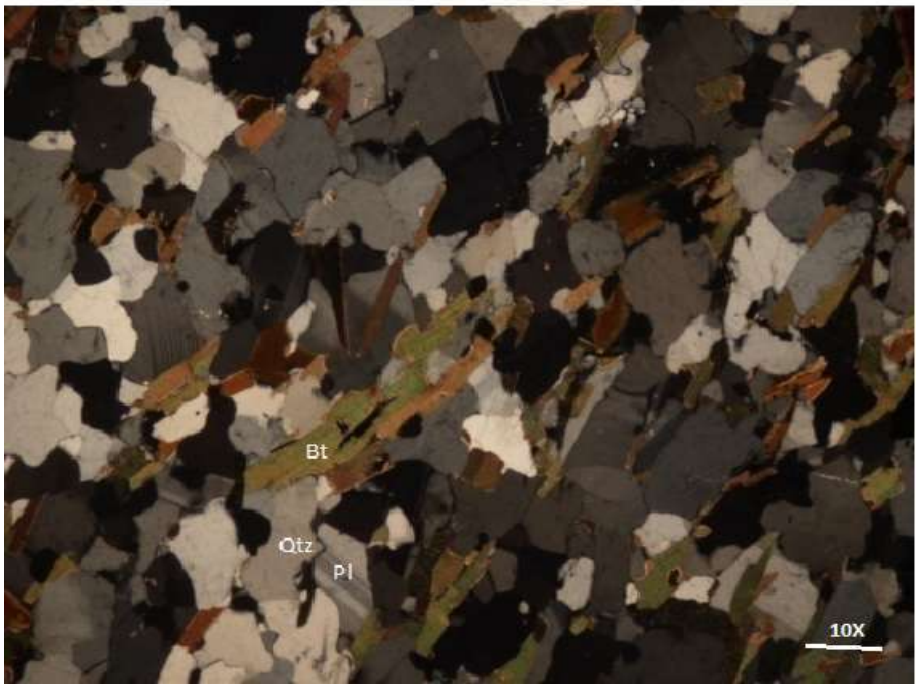

Fig. 4.1. Microphotograph of gray gneiss (XPL)

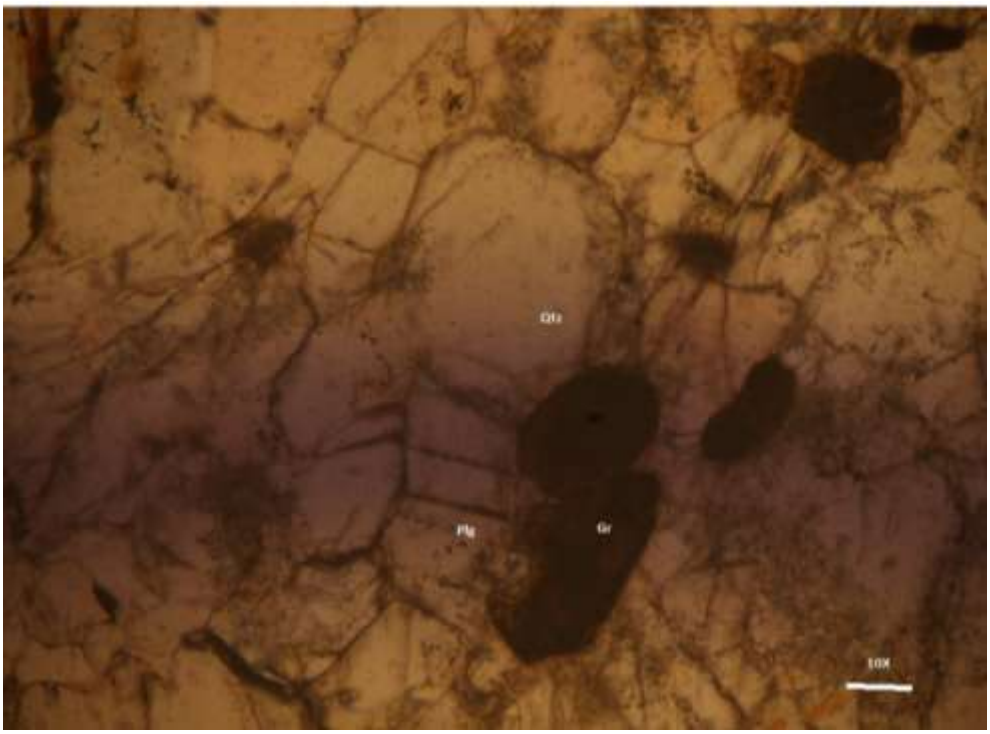

Fig. 4.2. Microphotograph of garnetiferous gneiss (PPL)

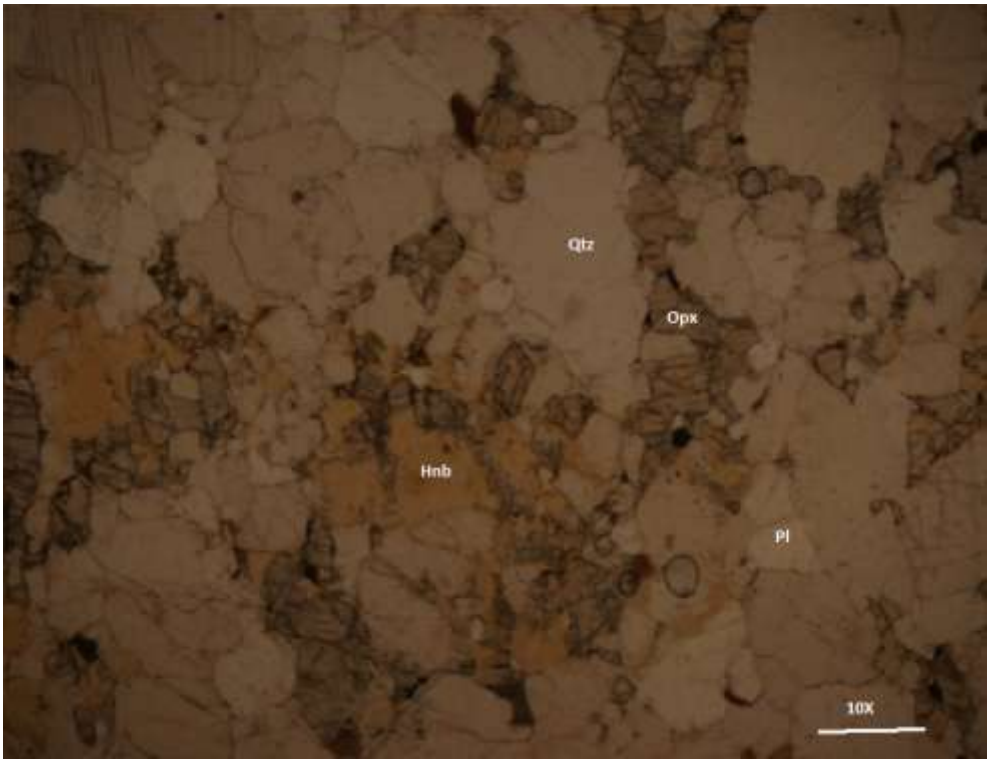

Fig. 4.3. Microphotograph of incipient charnockite. Note the Xenomorphic texture the replacement of bitite by orthopyroxene (PPL)

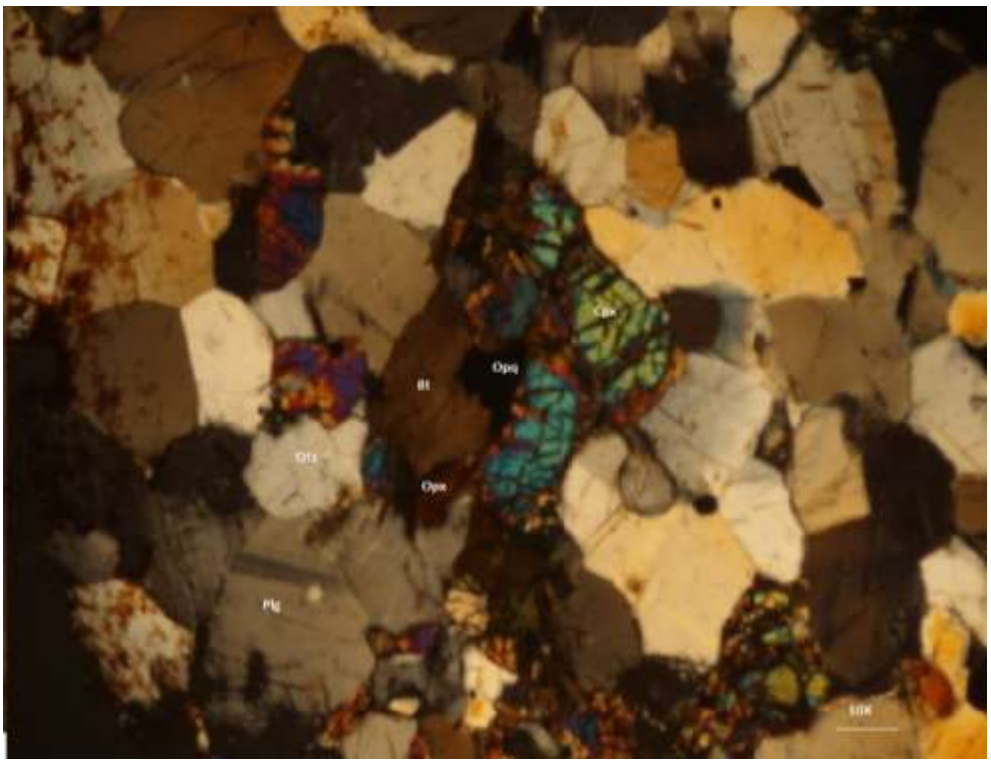

Fig. 4.4. Microphotograph of foliated charnockite, note the replacement of orthopyroxene by biotite (XPL)

Fig. 4.5. Microphotograph of garnetifeours foliated charnockite (XPL)

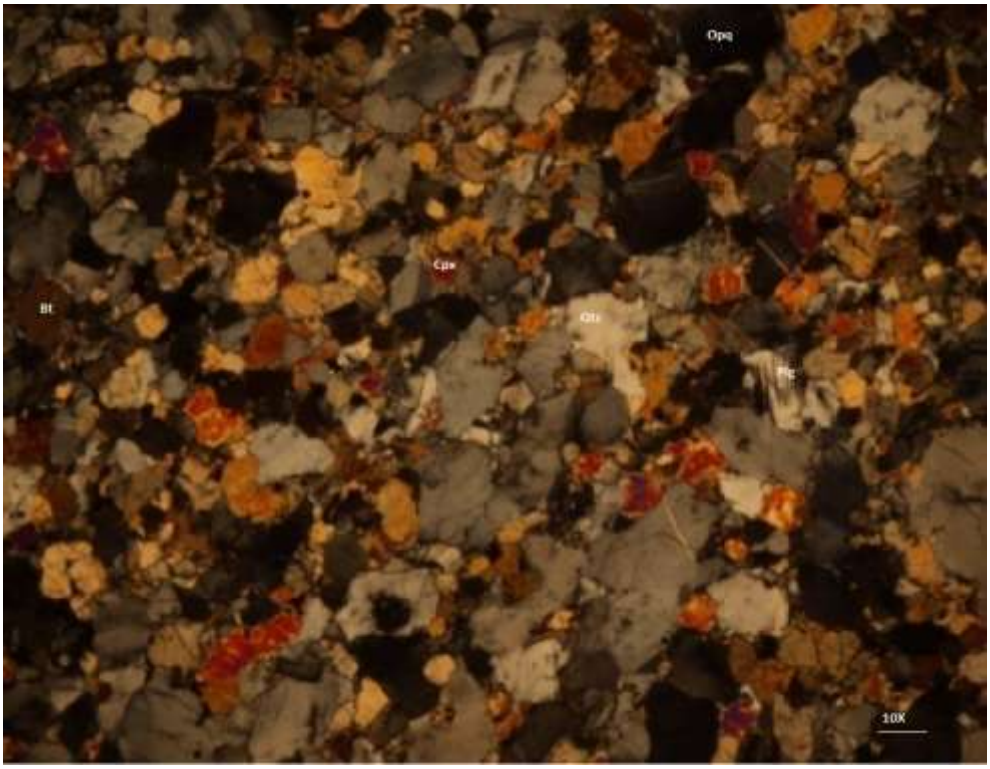

Fig. 4.6. Microphotograph of pyroxene granulite (XPL)

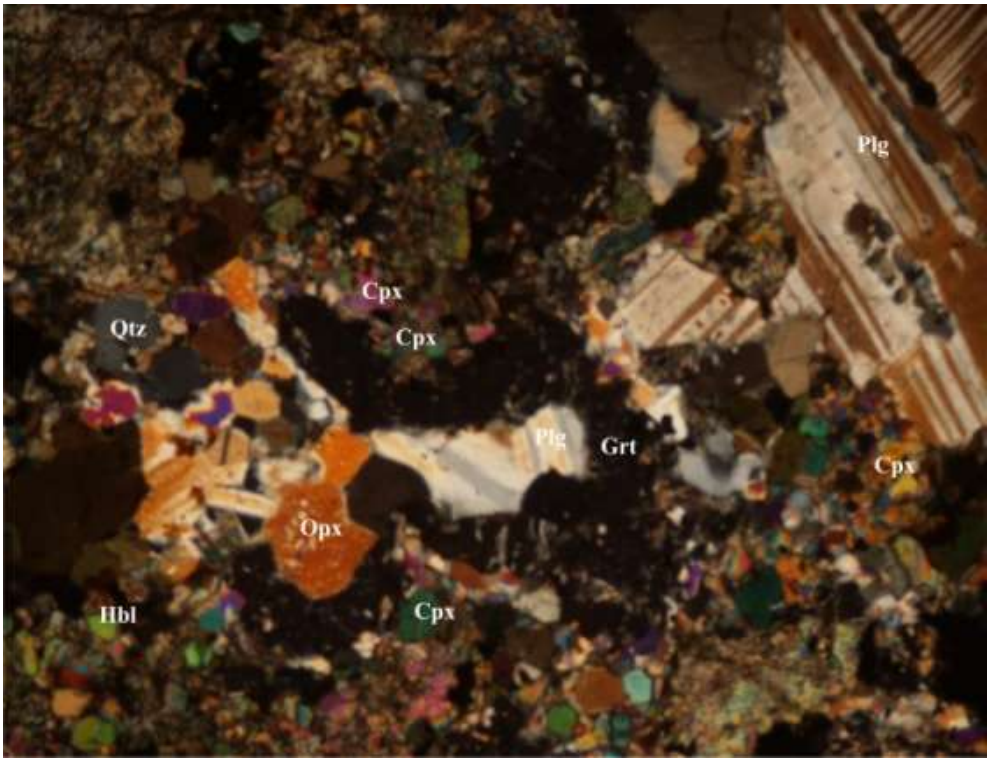

Fig. 4.7. Micro photograph of pyroxene granulite. Note the garnet-quartz simplectite between plagioclase and pyrxenes (XPL)

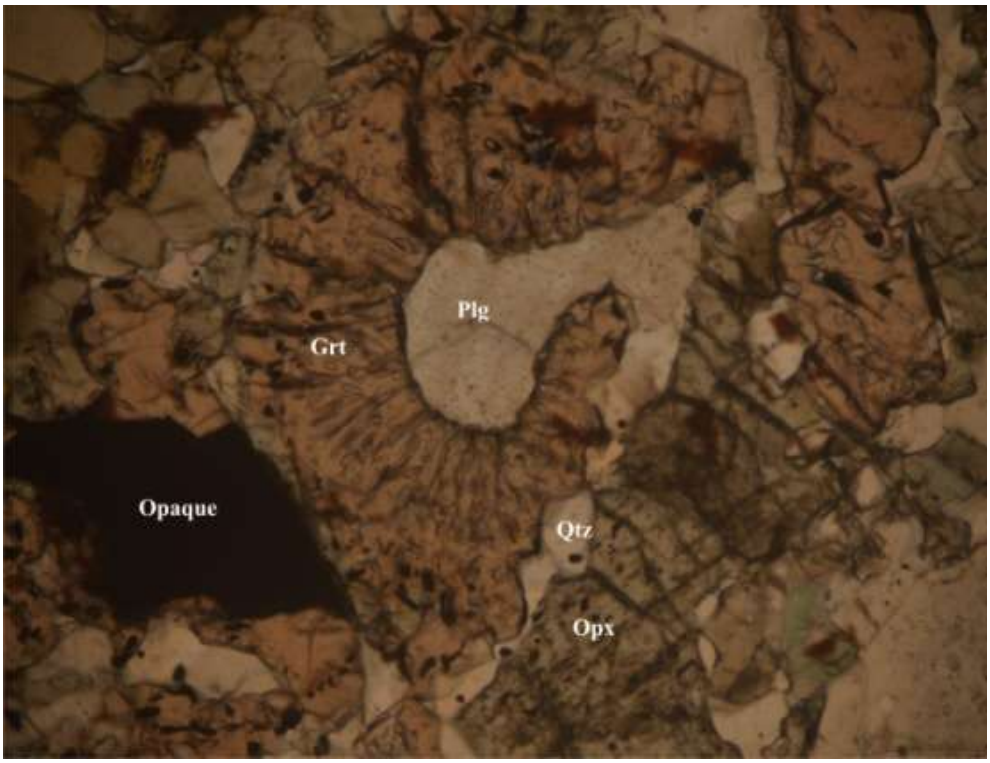

Fig. 4.8. Microphotograph of pyroxene granulite. Note the garnet-qartz simplectite aroud pyroxenes and opaques (PPL)

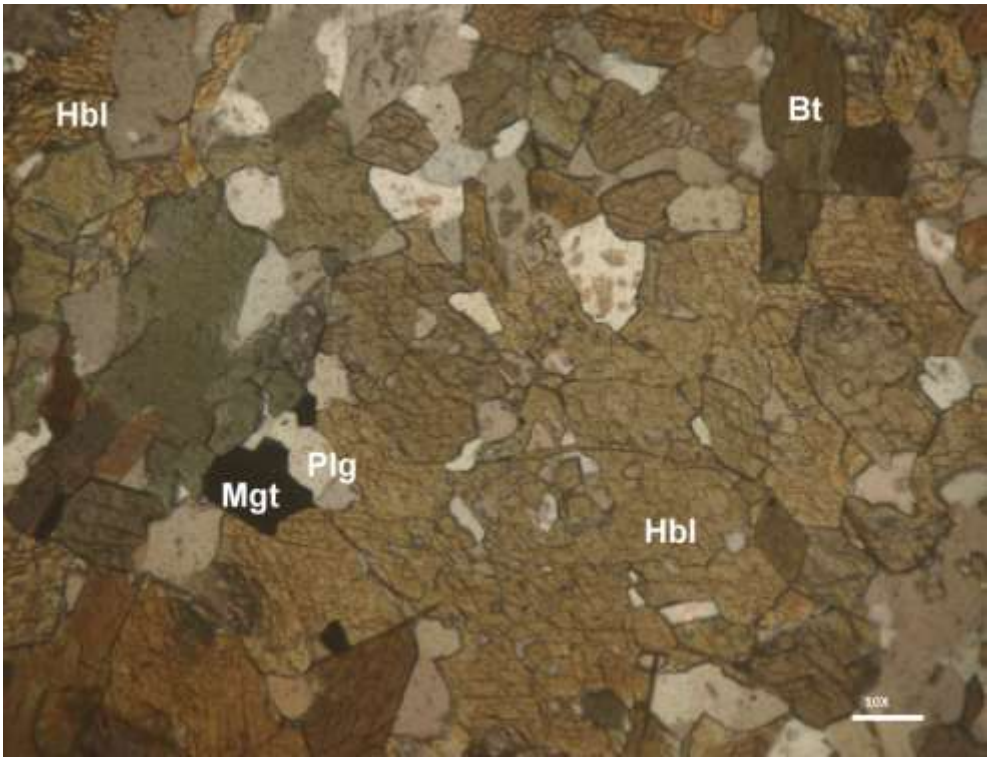

Fig. 4.9. Microphotograph of hornblede schist (XPL)

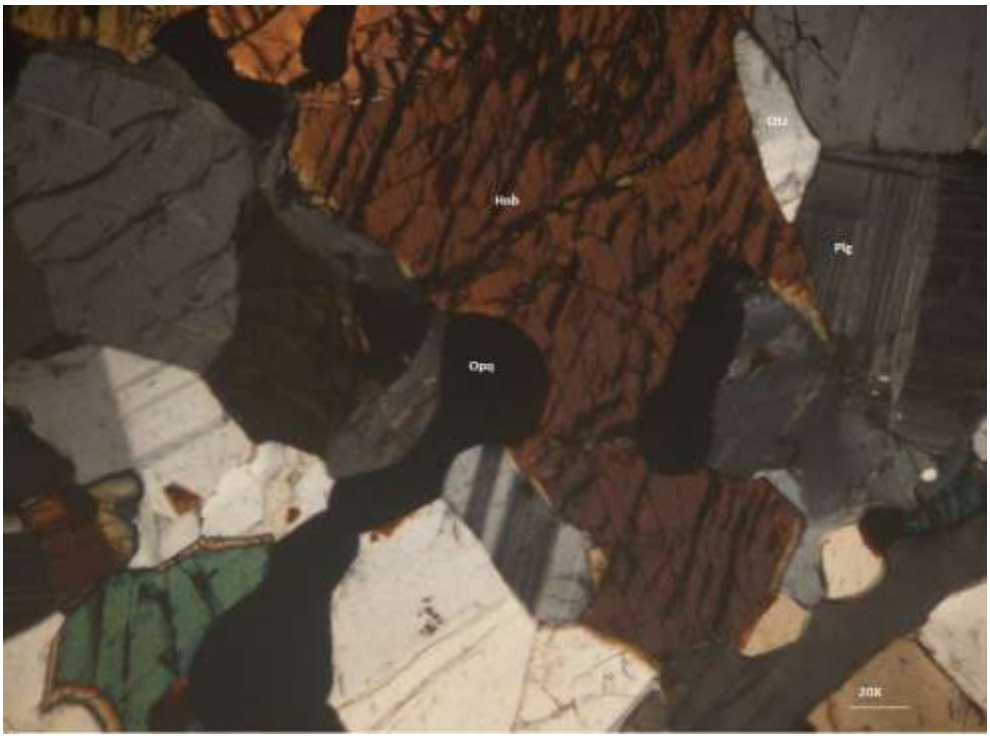

Fig. 4.10. Microphotograph of Hornblende schist. Note the alteration of hornblede to biotite along the cleavage plane with release of Fe-Ti oxides (XPL)

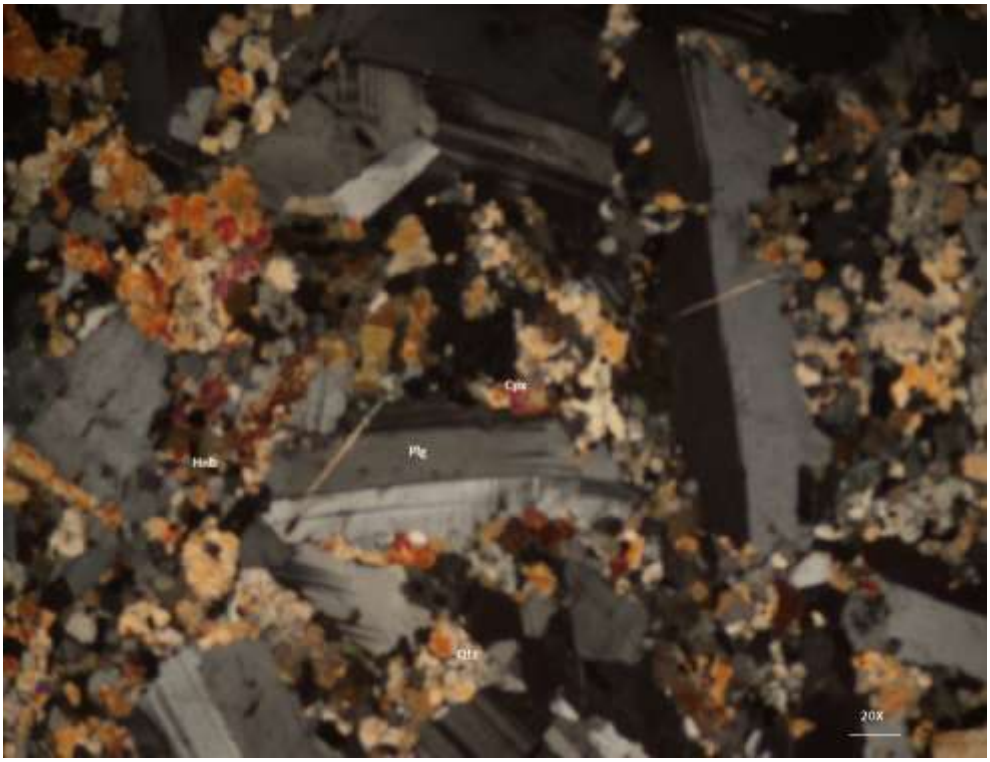

Fig. 4.11. Microphotograph of dolerite showing ophitic texture (XPL)

Chapter - V

MINERAL CHEMISTRY AND P-T ESTIMATES

5.1. Introduction

Metamorphism is a non-static process, characterized by changing P-T conditions hence, understanding of these changes with respect to time is more important. Pressure – Temperature -time (P-T-t) history of a rock is the function of tectonic processes. So, the retrieval of quantitative P-T-t information from the mineral assemblages of the rocks under the study considered as the primary goal in understanding the thermo-tectonic history of the area, which presents a better picture of the tectonic processes that operated in the deep continental crust. Therefore, in this chapter the P-T estimates carried out using mineral chemistry of silicate phase, viz., orthopyroxene, clinopyroxene, garnet, hornblende, plagioclase, K-feldspar that occur in different lithologies of the study area and the results of the same is presented in the proceeding sections.

5.2. Details of the samples

The samples selected for EPMA and thermo-barometric study based on the field relationships and petrography of the rock types. The following table presents the details of the samples used for EPMA and thermo-barometric studies.

5.3. Analytical methods

Mineral chemistry of the constituents were determined using a wave dispersive CAMECA-SX100, Electron Microprobe Analyzer at PPOD lab, Geological Survey of India (GSI), Bangalore. Measurement conditions were 5-50 kV and sample current was 10^{-7} amp with a one-micrometer beam spot. Natural and synthetic mineral were used as standards.

Table 5.1. Details of the EPMA samples of the study area

Sl. No	Sample No.	Sample location (Lat. & Long.)	Rock type	Mineralogy
01	J-11-2	Kenchammana Hoskote (12º48'09.8" &75º50'03.4")	Grey gneiss	Quartz, plagioclase, K-feldspar, Amphibole, Monazite, Apatite and zircon (Fig. 5.1).
02	J-11-27	Banavar quarry (12º35'48.0"&75º56'01.5")	Incipient Charnockite	Quartz, plagioclase, K-feldspar, Orthopyroxene, biotite and perthite (Fig. 5.2).
03	J-11-19A	Shanthalli quarry (12º38'37.1" & 75º 47'20.8")	Foliated Charnockite	Orthopyroxene, clinopyroxenes, amphibole, plagioclase, K-feldspar, quartz with minor amounts of Ilmenite and magnetite. ((Fig. 5.3).
04	J-11-20	Vanaguru road cutting (12º43'39.5" & 75º44'40.4")	Garnetiferous foliated charnockite	Garnet, orthopyroxene, clinopyroxene, amphibole, plagioclase, K-feldspar and quartz with Fe-Ti oxides (ilmenite and magnetite) with zircon and pyrite grains as accessory phases ((Fig. 5.4).
05	J-11-32	Somvarpet-Surlabi road cuttings (12º35'31.6" & 75º49'46.8")	Foliated charnockite	Orthopyroxene, clino10pyroxene, amphibole, plagioclase, quartz and oxides (ilmenite and magnetite) ((Fig. 5.5).
06	J-11-37	Gurvale-Surlabi road cutting (12º34'11.8" & 75º45'40.4")	Foliated charnockite	Orthopyroxene, amphibole, plagioclase, quartz, K-feldspar and exsolution of magnetite within ilmenite ((Fig. 5.6).
07	J-11-22	BTCS college, Somvarpet (12º36'26.3"& 75º51'10.5")	Garnetiferous pyroxene granulite	Orthopyroxene, clinopyroxene, garnet, amphibole, and plagioclase, exsolution of magnetite within ilmenite and coronitic growth of garnet + quartz between plagioclase and pyroxene ((Fig. 5.7 & 5.8).
08	J-11-34	Near Gurvale village (12º34'54.3" & 75º46'33.7")	pyroxene granulite	Orthopyroxene, clinopyroxene, amphibole and plagioclase (Fig. 5.9).
09	SM-18	Banavar - Bannur road cutting (12º36'41.1" & 75º57'26.7")	Garnetiferous pyroxene granulite	Porphyroblastic texture and comprises of garnet, orthopyroxene, clinopyroxene, plagioclase and minor amount of Ilmenite, phyrotite, magnetite and chalcopyrite (Fig. 5.10).
10	SM-8-1	Near Malambi betta (12º41' & 75º54'06")	pyroxene granulite	Orthopyroxene, clinopyroxene, plagioclase associated with amphibole and minor amount of Ilmenite, magnetite and pyrite specs (Fig. 5.11).

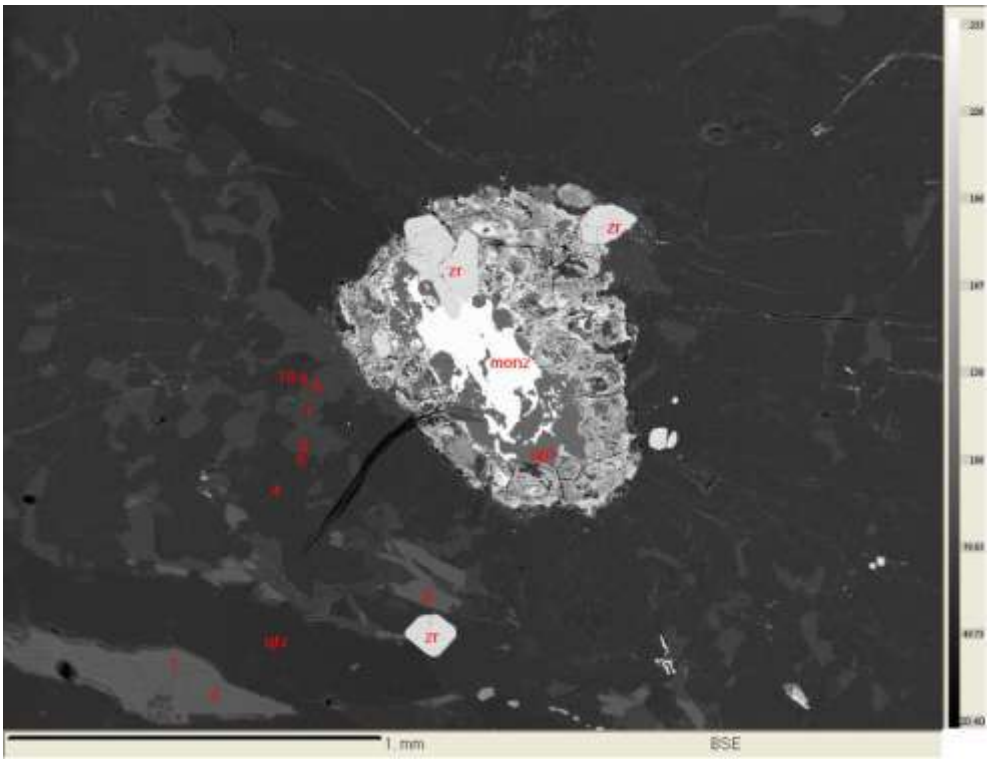

Fig. 5.1. Base point image of gneiss (J-11-2)

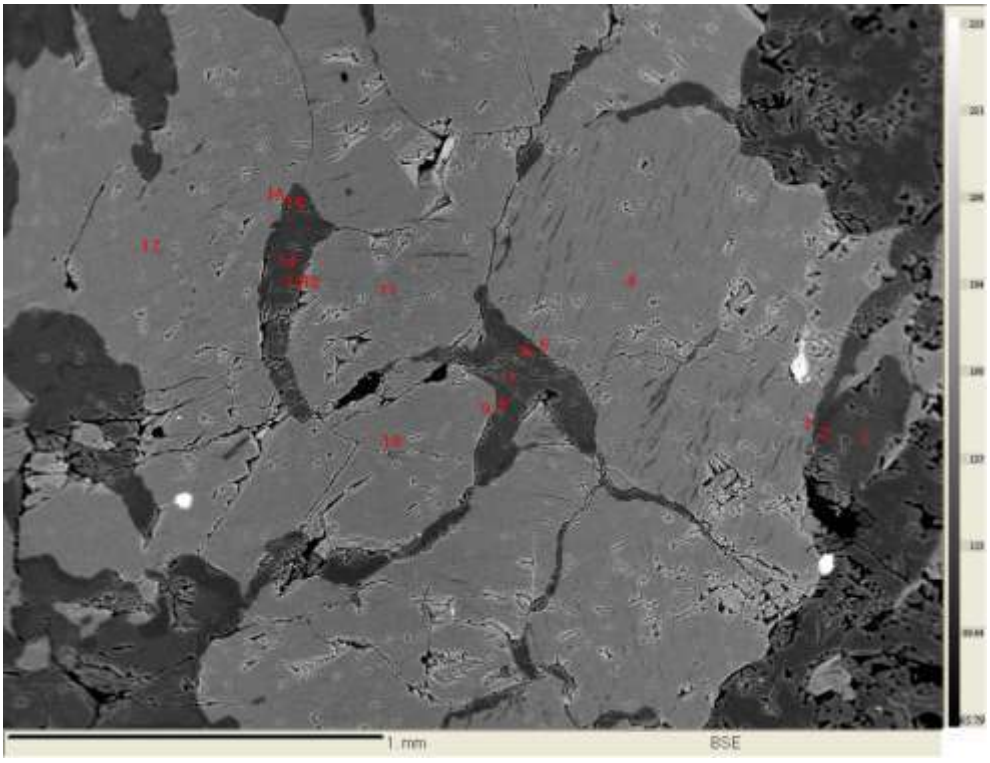

Fig. 5.2. Base point image of incipient charnockite (J-11-27)

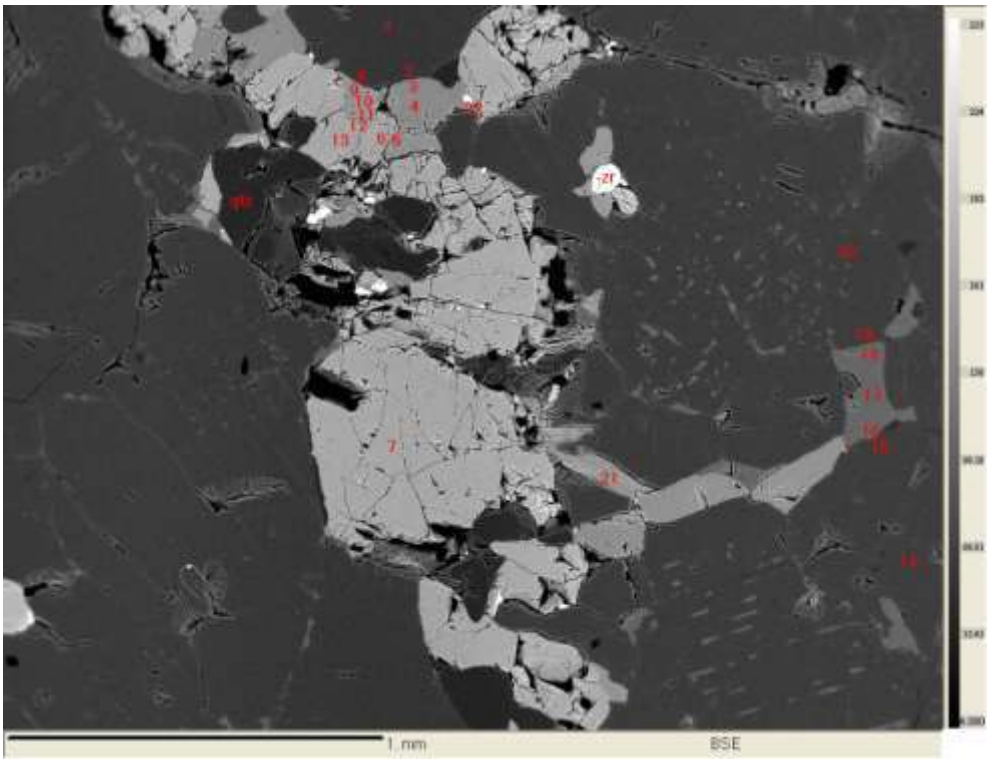

Fig. 5.3. Base point image of foliated charnockite (J-11-19A)

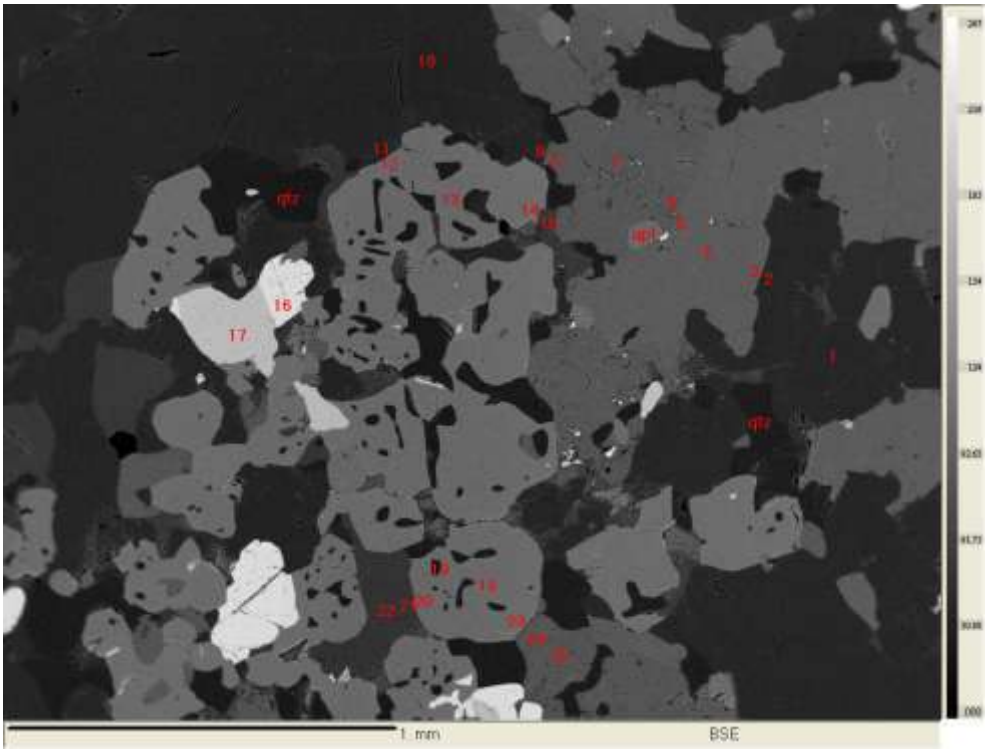

Fig. 5.4. Base point image of garnetiferous foliated charnockite (J-11-20)

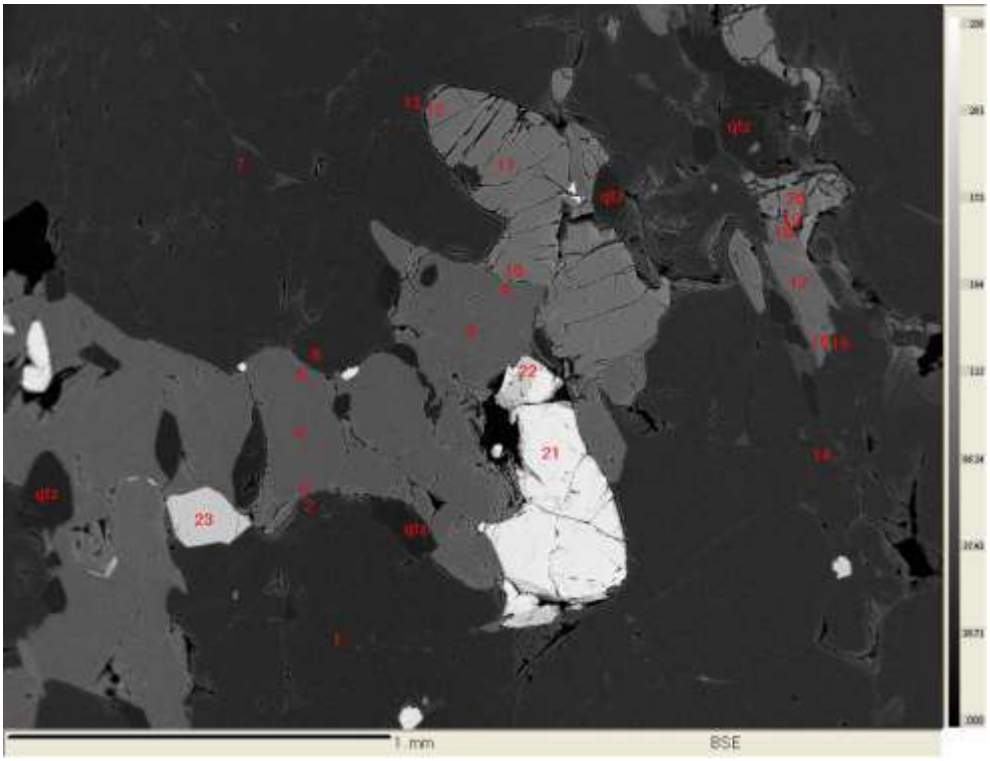

Fig. 5.5. Base point image of foliated Charnockite (J-11-32)

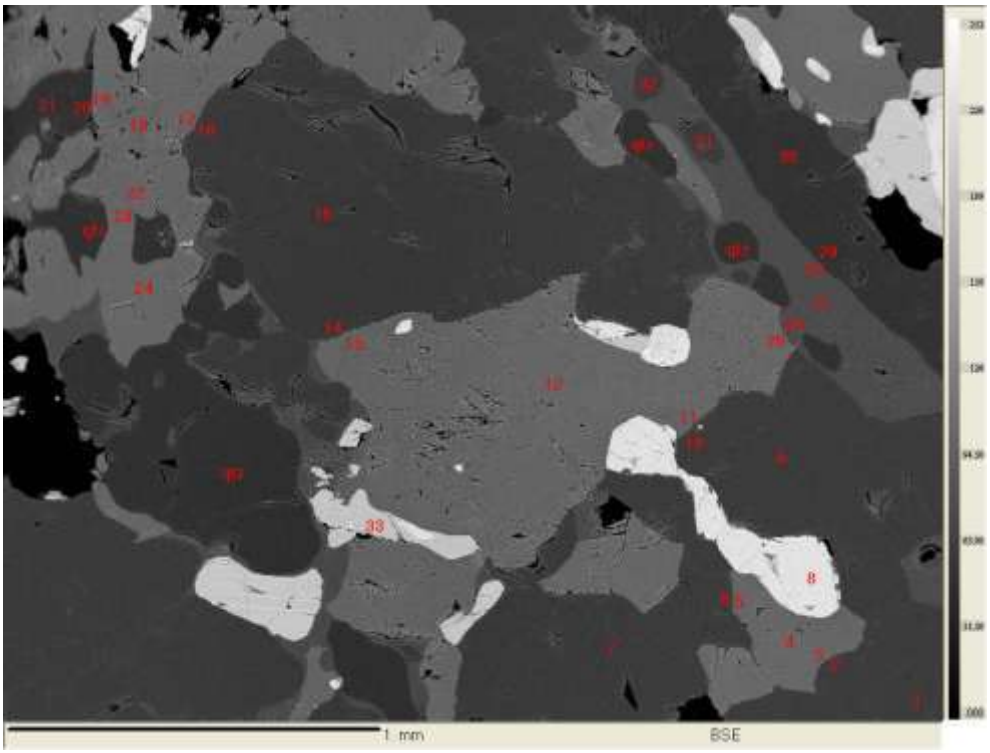

Fig. 5.6. Base point image of foliated charnockite (J-11-37)

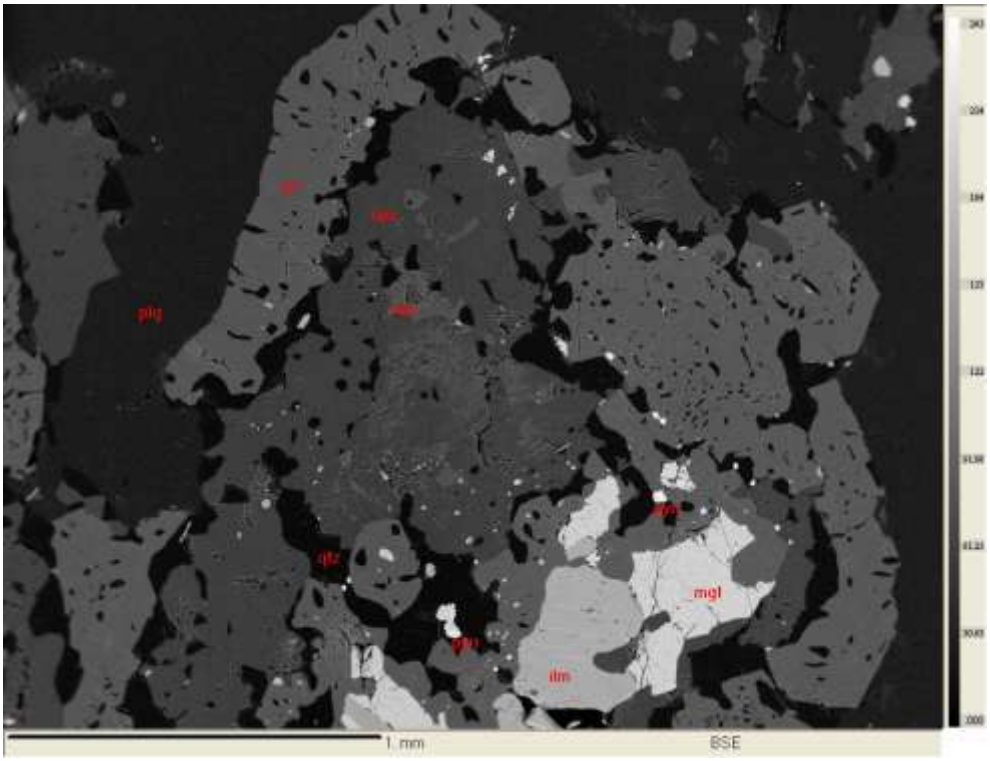

Fig. 5.7. Base point image of pyroxene granulite (J-11-22)

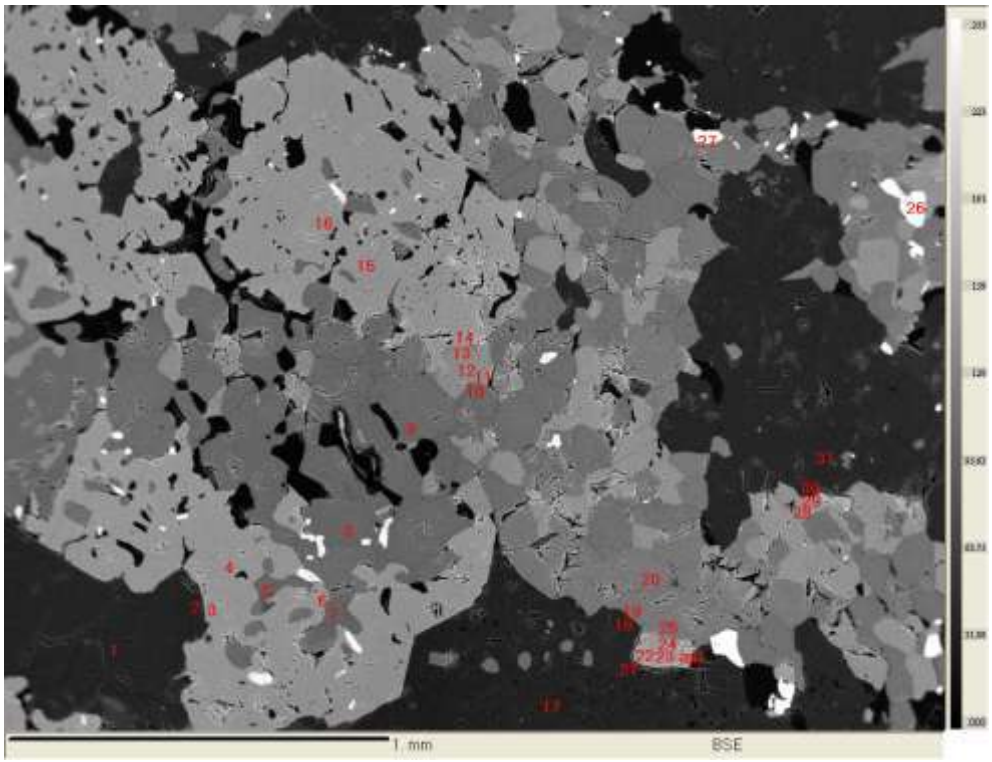

Fig. 5.8. Base point image of pyroxene granulite (J-11-22)

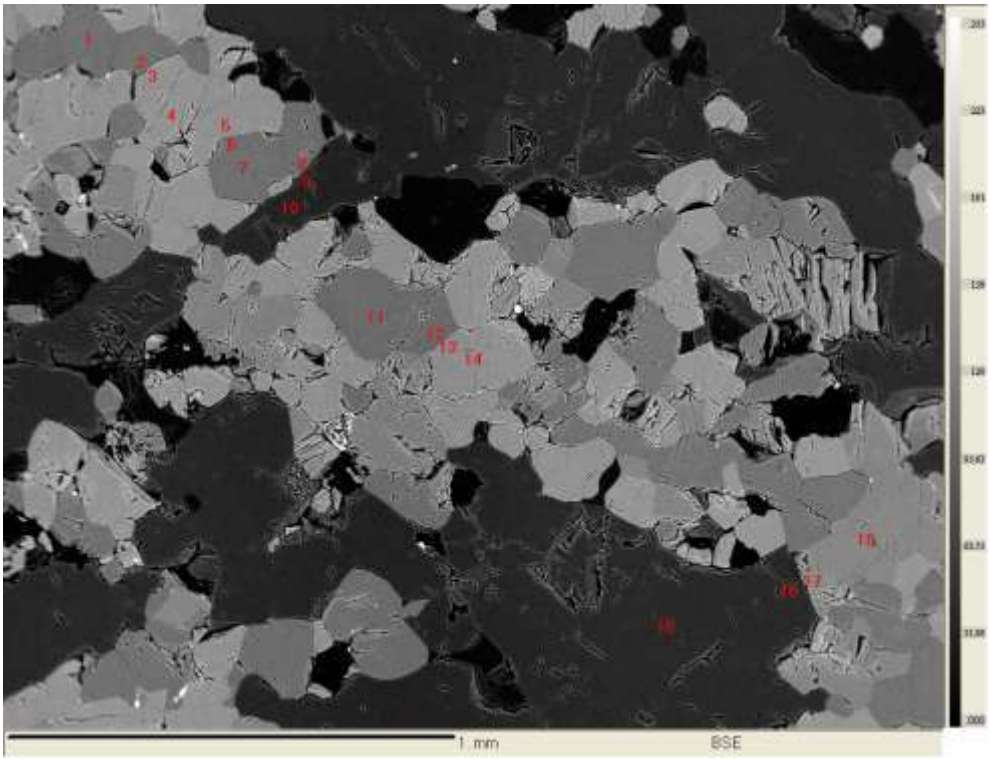

Fig. 5.9. Base point image of Pyroxene granulite (J-11-34)

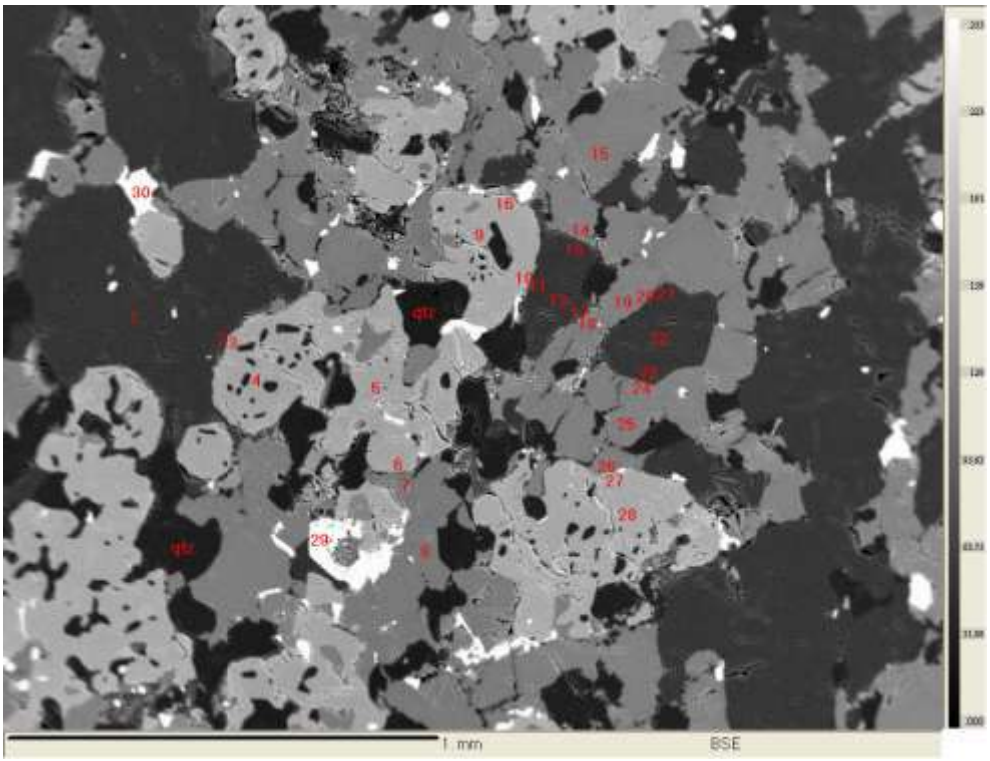

Fig. 5.10. Base point image of pyroxene granulite (SM-18)

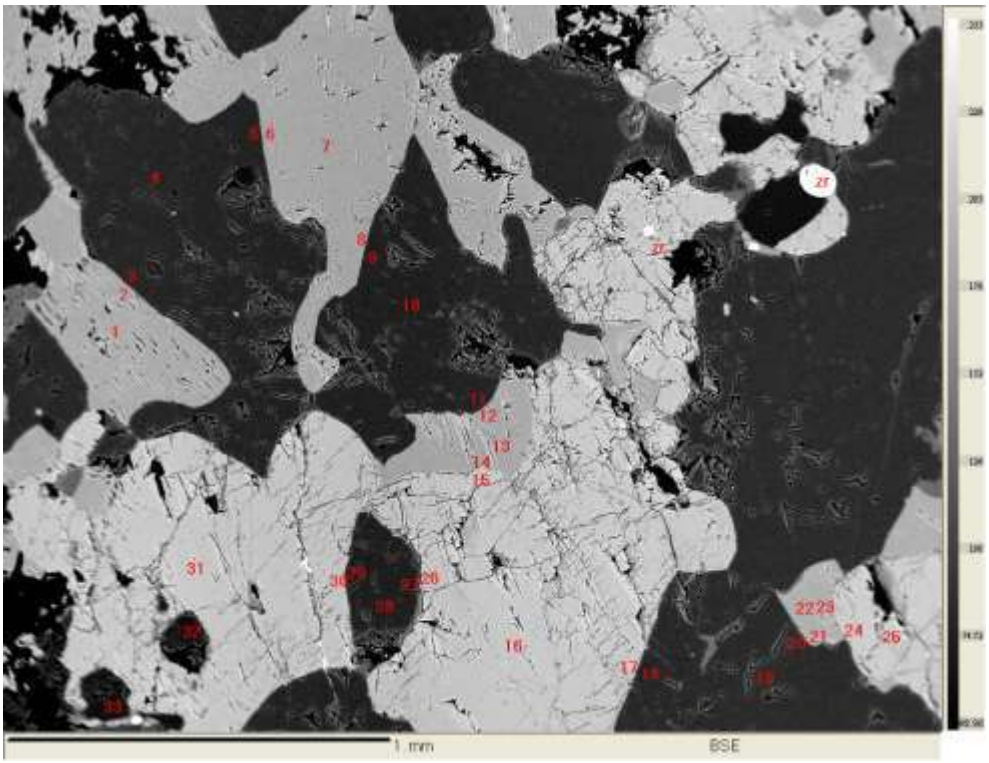

Fig. 5.11. Base point image of pyroxene granulite (SM-8-1)

5.4. Mineral Chemistry

5.4.1. Orthopyroxene

Microprobe data of Orthopyroxenes (Opx) from pyroxene granulite and foliated charnockite is presented in table 5.2. Compositionally, Opx from the foliated charnockite and pyroxene granulite represent hypersthene to ferro-hypersthene. Al_2O_3 content of Opx of foliated charnockite and pyroxene granulite ranges from 0.63 to 0.89 (av. 0.82%), and 0.68 to 1.73%, (av. 1.07%), respectively, and distinctly lower than the coexisting Clinopyroxene (Cpx). The moderate content of Al_2O_3 of Opx of pyroxene granulite compared to the values reported for Opx from low land (1.31%) and high land (2.2%) foliated charnockites by Janardhan et al., (1982), may indicate the formation of orthopyroxene at medium P-T conditions. The FeO content of Opx of foliated

charnockites and pyroxene granulite varies from 28.47-28.92 wt.% (av. 28.71%) and 29.41 – 32.07wt % (av. 30.77%), respectively. The content of MgO varies from 17.49 to 18.11 wt.% (av. 17.72%) in the Opx of foliated charnockites, and 14.76 – 17.43 wt % (av. 16%) in pyroxene granulite. The MgO content of Opx of foliated charnockite is slightly higher than pyroxene granulite (Table 5.2). The average MnO content of Opx of pyroxene granulites ranges from 0.41-1.18 (av. 0.82%) and, Opx of foliated charnockites ranges from 0.79-1.18 wt. % (av. 1.05%). The MnO values obtained for Opx of both foliated charnockite and pyroxene granulites is high, compared to the reported value of 0.21% for high land charnockites (Janardhan et al., 1982). The X_{mg} for foliated charnockites and pyroxene granulites for Opx ranges from 0.99-1.03 and 0.86 – 0.99, respectively. Whereas, Mn and Ca in Opx of both foliated charnockites and pyroxene granulites are low, and Ti is almost absent in foliated charnockite. The content Ca varies from 0.02-0.03 in the Opx of foliated charnockite and pyroxene granulites. However, the Opx, which co-exists with Cpx generally, show similar Ca content. The Opx of foliated charnockites characterized by relatively low Fe and Al contents when compared to the Opx of pyroxene granulites. The Mg content is similar in Opx of pyroxene granulites, whereas, charnockite Opx have slightly higher Mg in the core, and the content decreases towards the rim.

Chemistry of the Opx plotted on Al_2O_3 Vs (MgO+FeO) of Rietmeizer (1983) diagram which show, the Opx of foliated charnockites falls in the field of transition zone, and Opx of pyroxene granulites falls in the metamorphic field (Fig 5.12). Further, to know the metamorphic pressure and temperature, the data of Opx plotted on (Fe^{+2}/Fe^{+2}+Mg) Vs (100 Ca/ Fe+Mg+Mn) diagram of Reitmeizer (1983). The plot falls in the field of medium pressure and temperature of metamorphism (Fig. 5.13).

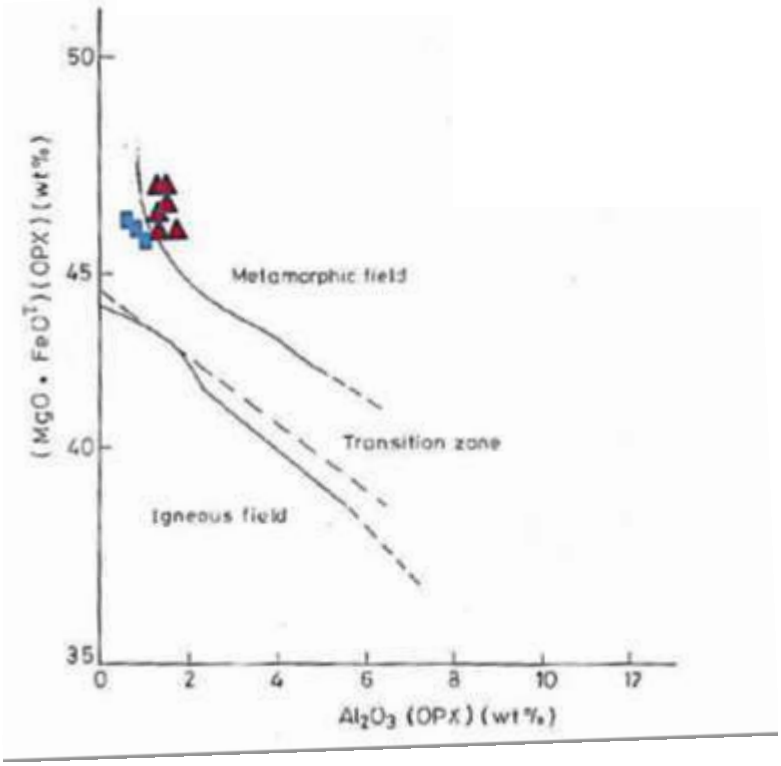

Fig. 5.12. Al_2O_3 Vs ($MgO+FeO^T$) diagram after Reitmeizer (1983)

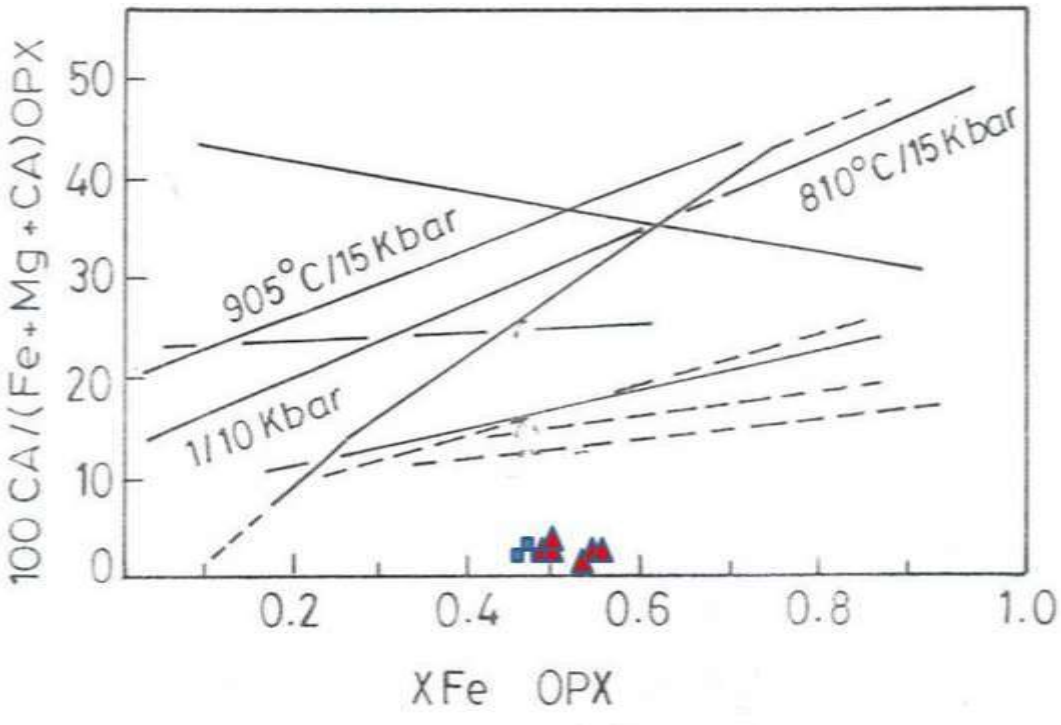

Fig. 5.13. (Fe^{+2}/Fe^{+2}+Mg) Vs (100 Ca/ Fe+Mg+Mn) diagram after Reitmeizer (1983)

5.4.2. Clinopyroxene

The microprobe data of clinopyroxenes (Cpx) from pyroxene granulites and foliated charnockites is listed in table 5.3. Chemically, the Cpx from the pyroxene granulite and foliated charnockites have wollastanite or diopside in composition. The Cpx of the present study have high Al_2O_3 content (0.44-2.06% in foliated charnockite, 1.38-3.39% in pyroxene granulites), which is characteristics of high-grade granulites. The range of Al content (0.02-0.09) of Cpx in foliated charnockites and 0.07-0.14 in pyroxene granulites of study area is almost similar to the values reported from Sargur - Mysore area (0.07-0.16) by Raith *et al.,* (1983). The alkali content in Cpx is very low, and mainly represented by Na, which ranges from 0.002-0.06 in foliated charnockites and 0.028-0.048 in pyroxene granulite. The content of Ti, Cr and Mn are very low. Ca and Mg of Cpx increases towards the margin with decreasing Fe, Al and Ti, and to a lesser extent Na, which reflects slight compositional zoning in Cpx.

5.4.3. Garnet

Microprobe data of garnets from foliated charnockite and pyroxene granulites is presented in table 5.4, along with structural formula calculated based on 12 oxygen atoms. The garnets of the present study have the composition of almandine - pyrope – grossular solid solution with a minor amount of spessartine. In the foliated charnockites, almandine-grossular content is comparatively more than the pyrope - spessartine fraction. Garnets of the present study are mainly almandine in composition (61.77-63.66%, table 5.4). However, pyrope content increase with decrease in spessartine towards the core (Fig. 5.14). This represents typical retrograde diffusion zoning of garnet (Toriumi and Nomizo, 2000).

All the garnets of pyroxene granulites show an Mg enriched core and Fe enriched rim. However, the garnets of foliated charnockites show slight decrease in Mg and Fe^{+2} with increasing Ca towards rim, indicating re-equilibration during the metamorphism. The variation in chemistry of the garnet in different lithologies and may be attributed to the bulk rock chemistry of the precursor and grade of metamorphism. Garnets of pyroxene granulites are characterized by high grossular content (19.78-20.06%) in contrast to the garnets in foliated charnockites, where, the grossular content is relatively low (18.45-19.64%). On (FeO+MgO) Vs (CaO+MnO) variation diagram (Fig. 5.15), after Sturt (1982), the garnets of both pyroxene granulites and foliated charnockite fall in the garnet zone, without any significant variation.

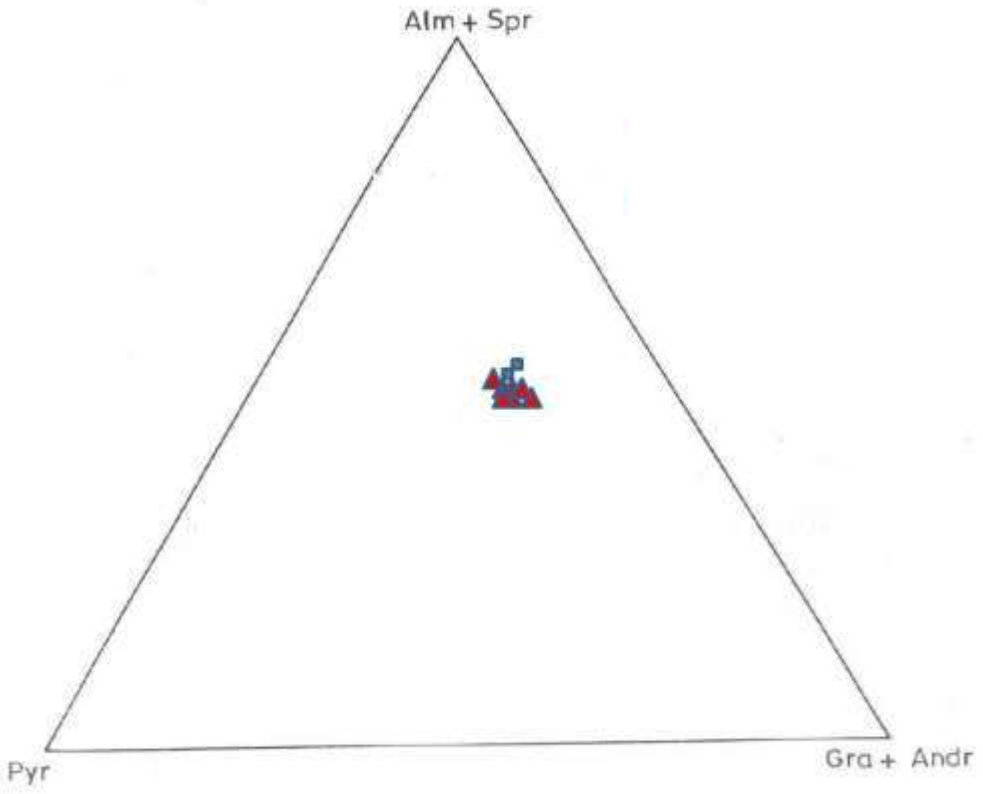

Fig. 5.14. Variation of end members of garnet on ternary diagram

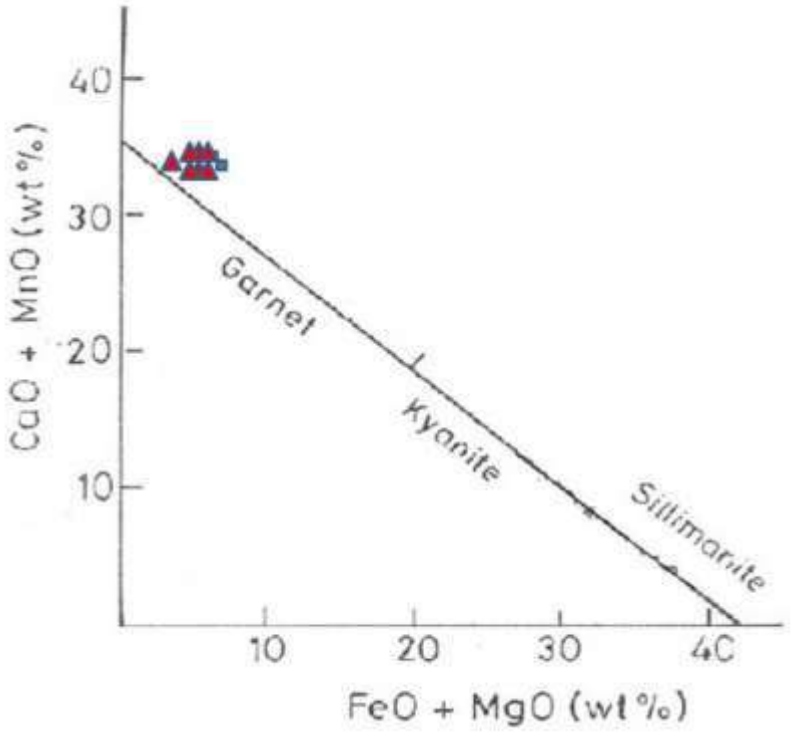

Fig. 5.15. (FeO+MgO) Vs (CaO+MnO) diagram after Sturt (1982)

5.4.4. Amphibole

The microprobe data of amphibole is presented in table 5.5. The structural formula is calculated on the basis of 23 oxygen atoms. The amphiboles analyzed are from grey gneiss, foliated charnockites and pyroxene granulites. The amphiboles of the study area are found to be calcic sub group (hornblende), where Ca>Na. The CaO content ranges from 0.0 - 0.02 wt%, 8.04-11.72wt% and 11.09-11.88 wt % in the amphiboles of gneiss, foliated charnockites and in pyroxene granulite, respectively. Na_2O ranges between 0.03 – 0.09 wt%, 0.04 – 1.65 wt% and 1.32 – 1.67 wt% in amphiboles of gneiss, foliated charnockite and pyroxene granulite, respectively. On Si Vs (Na+K) and ($Mg/Mg+Fe^{+2}$) Vs Si diagrams (Fig. 5.16 & 5.17) of Leake (1978) the amphiboles of the present study falls in the field of Pargasite and Ferroan pargasite.

Ti content of the amphiboles varies from 0.3 - 0.41 in gneiss, 0.2 – 0.57 in foliated charnockite and 0.24 – 0.28 in pyroxene granulite. The Ti content of amphiboles depends on metamorphic grade. Raase, (1974 & 1986) 1and Spear (1981) have suggested that the Ti content in calcic amphiboles is strongly temperature dependent and nearly independent of pressure. Hence, the variation in Ti content of amphiboles of different lithounits of the same area may be related to chemistry of parent rock.

The K content in the amphiboles which ranges from 1.8 – 1.85 in gneisses, 0.28 – 1.78 in foliated charnockite and 0.31 – 0.43 in pyroxene granulite, is relatively high when compared to the amphiboles from low-grade terrains elsewhere. The K content of amphiboles increases with metamorphic grade and attributed to increase in temperature, which favors the introduction of potassium into the amphibole structure during metamorphism (Raase *et al.,* 1986).

Mg content of the amphiboles varies from 2.11 – 2.14 in gneiss, 1.81 – 2.52 in foliated charnockite and 1.84 – 2.05 in pyroxene granulite. Whereas Fe content varies from 2.39 – 2.43 in gneiss, 0.32 – 2.3 in foliated charnockite and 2.12 – 2.47 in pyroxene granulite. The Mg/Fe ratios of amphiboles are 0.86 – 0.88 in gneiss, 1.09 – 5.65 in foliated charnockite and 0.86 – 0.91 in pyroxene granulite. The Mg/Fe ratio of amphiboles is mainly due to the change in the partitioning related to co-existing minerals (Leake, 1978). Kamineni (1986) has attributed to low Fe/Mg ratio to the amounts of Fe and Mg available in the host rock.

On (Na+K) Vs Ti diagram (Fig. 5.18), amphiboles of the present study falls in the granulite facies field (IV), and this may indicate the development of hornblende by replacement of orthopyroxene. The mineral chemistry of amphibole, particularly, Al and Na can be used as a pressure indicator (Raase, 1974; Raase *et al.*, 1986). In Si Vs Na+K+Ca discriminative diagram (Leake, 1978) the amphiboles of presented study of

gneiss fall in the magmatic field (Fig.5.19). On 100 Al/ (Si+Al) Vs 100 Na/ (Ca+Na) diagram of Laird and Albee (1981), the amphiboles of foliated charnockite and pyroxene granulites fall in the medium to low pressure metamorphic field (Fig. 5.20).

Note : Blue square indicates foliated charnockite, red triangle indicates pyroxene granulite and green circle indicates gneisses.

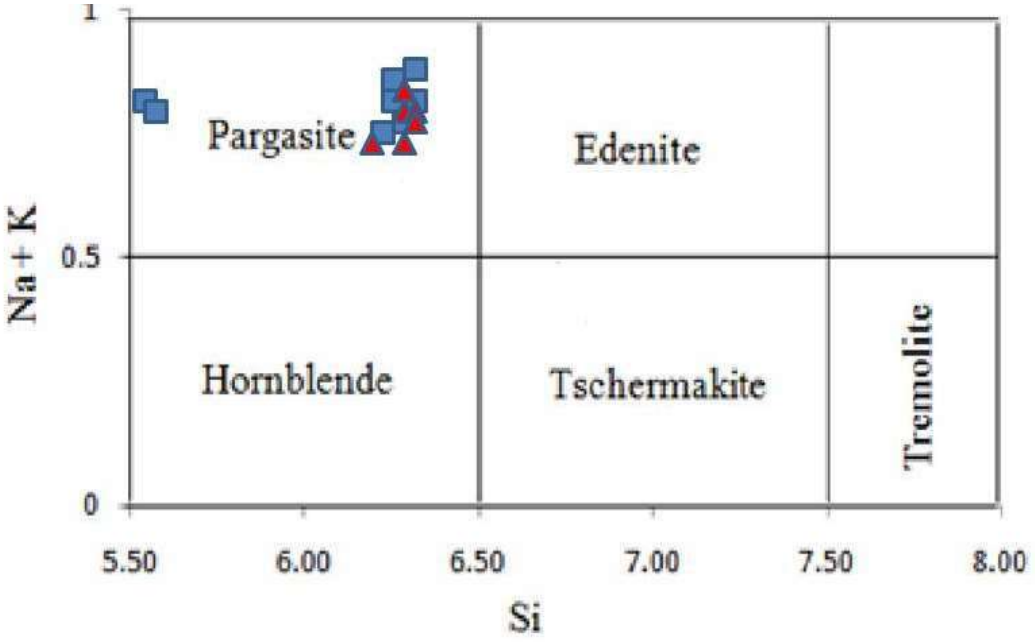

Fig. 5.16. Classification of amphiboles on the basis of Si Vs (Na+K) after Leake (1978).

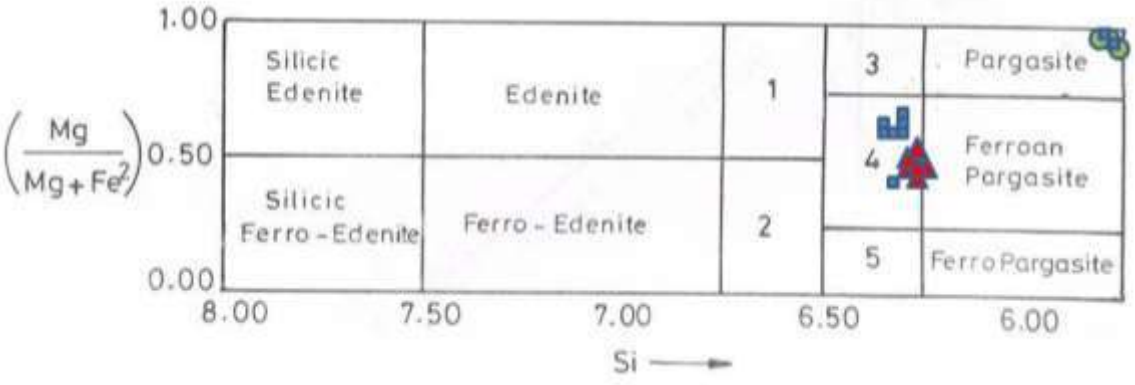

Fig. 5.17. Amphiboles classified on the basis of (Mg/Mg+Fe^{+2}) Vs Si, after Leake (1978).

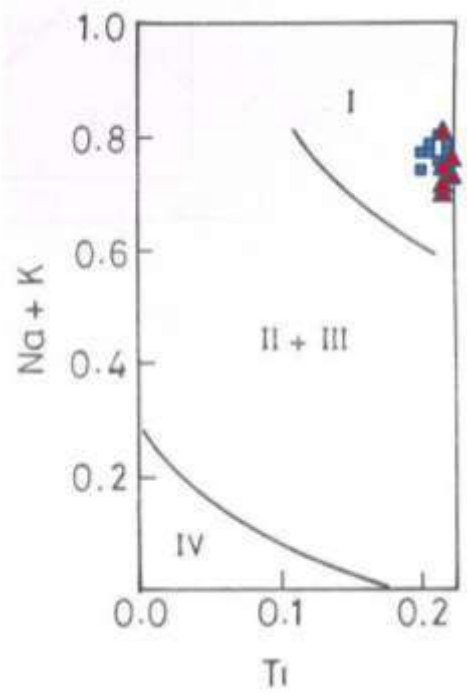

Fig. 5.18. Ti Vs (Na+K) diagram are after Yurkova *et al.*, (1985). I- Granulite facies, II & III- amphibolite and Epidote-amphibolite facies and IV- Green schist facies

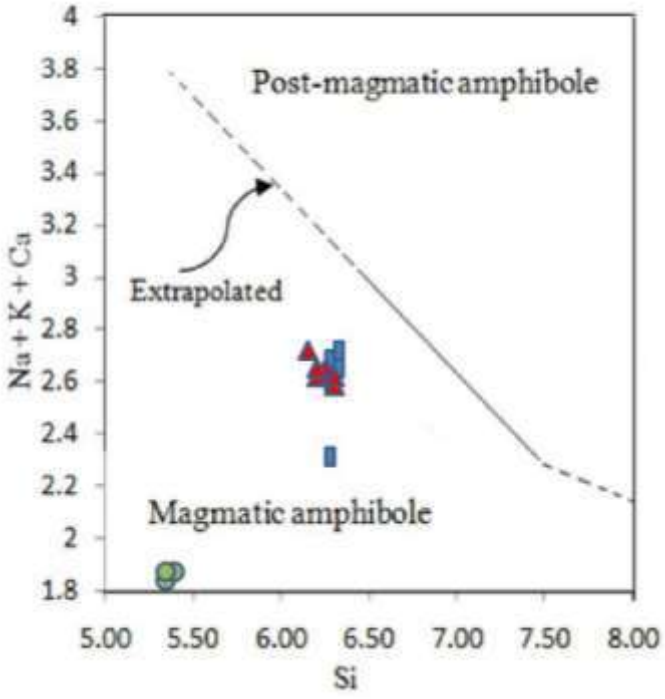

Fig. 5.19. Si Vs (Na+K+Ca) diagram after Leake (1978)

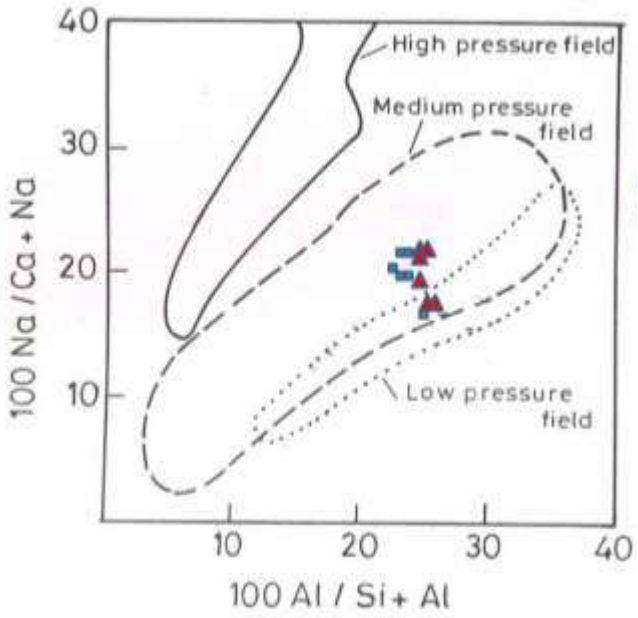

Fig. 5.20. (100 Al/Si+Al) Vs (100 Na/ Ca+Na) diagram of Laird and Albee (1981)

5.4.5. Plagioclase feldspar

The analyzed data of plagioclase feldspar from gneiss, incipient charnockite and foliated Charnockite is presented in table 5.6. The plagioclase feldspars of the present study are characterized by low K-content and most of them are albite rich, only few plagioclase of pyroxene granulite are anorthite in composition (50.16- 57.90%). High anorthite content of plagioclase in pyroxene granulite is probably due to grade of metamorphism and bulk composition of host rock. Plagioclases often contain exsolution laths of antiperthite with the composition almost alkali feldspar with only minor amounts of albite.

5.4.6. K-feldspar

The analyzed data of K-feldspar from gneiss, incipient charnockite and foliated Charnockite and data is presented in table 5.7. The Na content of K-feldspars varies between 4.6 – 7.70% in gneiss, 5.3 – 7.8% in incipient Charnockite and 2.39 – 5.98% in foliated Charnockite. K-feldspar often shows myrmekitic intergrowth with plagioclase.

5.5. P-T estimates

The peak metamorphic condition of granulites ranges from 700 to1000^{o}C temperature and 4-12kb (Newton and Perkins, 1982; Bohlen et al, 1983; Bohlen, 1987; Harley, 1989; Bohlen 1991; Indares and Martignole, 2003). Despite this general range, there exist diversity in the P-T conditions deduced from mineral textures and thermobarometry. Determination of peak metamorphic P-T regime in high temperature granulites is often hampered by retrograde reactions and diffusion cation exchange resulted in compositional changes of mineral phases (Harley, 1989, 1998; Fitzsimons and Harley, 1994). Knowledge of P-T time history of granulites is critical in understanding the thermal and tectonic processes that have operated in the deep continental crust. Granulite facies rocks are particularly amenable to quantitative geothermobarometric studies because many rock types of this facies include pyroxenes, garnet, amphiboles, plagioclase and K-feldspars, which have been studied experimentally at P-T conditions overlapping the granulites or not too far from granulites. Various geothermobarometers are applicable to the mineral assemblages in granulite facies rocks. In the present study an attempt has been made to find out the peak metamorphic conditions by selecting suitable samples that are affected by less retrogressive reactions.

5.6. Thermometry

5.6.1. Two Pyroxene Thermometry

While, calculating the metamorphic temperature for foliated charnockites and pyroxene granulites two pyroxene geothermometer of Brey and Kohler (1990) and Putrika (2008) are used in the present study. The results of temperature estimates are presented in table 5.10. The temperatures calculated for the foliated charnockites using Brey and Kohler (1990) method ranges from 699 – 901^{o}C with a mean temperature of 811^{o}C and Putrika (2008) method the temperature range from 687 – 861^{o}C with a mean 773^{o}C for core to rim respectively.

Temperature estimates for garnetiferous pyroxene granulites by using Brey and Kohler (1990) and Putrika (2008) thermometers ranges from 770 –1013^{o}C (an average of 893^{o}C), and 703 – 925^{o}C (an average of 822^{o}C) for core and rim respectively. The non-garnetiferous pyroxene granulites yield the temperatures of 754 – 940^{o}C (an average of 847^{o}C), and 704 –911^{o}C (an average of 808^{o}C) for core and rim respectively.

5.6.2. Orthopyroxene-Garnet thermometry

The Co-existing pair of garnet-orthopyroxene (Gt-Opx) is considered as potential indicators of the P-T conditions for formation of mineral assemblages, particularly those formed at granulite facies metamorphism. In the present study, Gt-Opx thermometers, calibrated by Lee and Ganguly (1988), Carswell and Harley (1990), Bhattachary et al., (1991), Lal (1993), Arnovich and Newton (1997) and Sen and Bhattachary (1998) are used. There is a large variation in the temperatures obtained for the garnetiferous pyroxene granulite (Table 5.11). Off these estimates, Opx- Gt thermometer of Harley (1984) yields very low temperatures (651 – 664^{o}C) and Arnovich and Newton (1997) yields very high temperature (984 – 994^{o}C) for core and rim respectively. The overall estimated temperatures obtained for garnetiferous pyroxene granulites of the study area ranges between 657 – 994^{o}C (an average of 749^{o}C) and 643 – 984^{o}C (an average of 735^{o}C) for core to rim composition respectively. The temperature estimates using Gt-Qtz symplectites around Opx-Pl show significant differences in core and rim compositions (55-150^{o}C). According to Harley (1989), the garnet+quartz symplectite texture between clinopyroxene and plagioclase of pyroxene granulites indicate isobaric cooling P-T paths.

5.6.3. Garnet-Clinopyroxene - Plagioclase thermometry

Many workers (Raheim and Green, 1979; Ellis and Green, 1979, Newton and Pattison, 1989) have studied Fe-Mg distribution between garnet and clinopyroxene to

estimate the metamorphic temperatures. Johnsen et al., (1983) have opined that Gt-Cpx calibrations, give more consistent results for regional geothermometry. In the present study, Krogh (1988, 2001), Raheim and Green (1979), Ellis, Green (1979), and Ai (1994) Gt-Cpx-Plg thermometers are used and the result are presented in table 5.13. Cpx bearing foliated charnockites have yielded the lowest temperatures of 640 – 618^{o}C by Krogh (1988) method for core and rim, and the highest temperature of 697 – 676^{o}C by Ellis and Green (1979) method for core to rim. The minimum and maximum temperate obtained by all the methods range from 640 – 697^{o}C for core with an average of 659^{o}C, and 570 – 676^{o}C with an average of 613^{o}C for rim. Whereas, temperature range of Pyroxene granulite for core is 612 – 702^{o}C with an average of 652^{o}C and 544–635^{o}C with an average of 581^{o}C for rim.

5.6.4. Plagioclase – K-feldspar thermometry

Plagioclase-K-feldspar thermometer of Putrika (2008) is used to estimate the temperature for gray gneiss, incipient charnockite and foliated charnockite of the present study and the data is presented in table 5.12. The estimated temperature for gneiss are 727 - 749^{o}C (avg. 738^{o}C) and 723 – 742^{o}C (avg. 732^{o}C) for core and rim respectively. Whereas, obtained for incipient charnockite yield temperature range for core and rim between 729 - 765^{o}C (avg.747^{o}C) and 726 – 764^{o}C (avg. 745^{o}C) respectively. The estimated temperature range for foliated charnockite is between 905 – 929^{o}C (avg.917^{o}C) and 900 – 911^{o}C (avg. 905^{o}C) for core to rim respectively.

5.7. Barometers

5.7.1. Garnet-Orthopyroxene barometer

Garnet-Orthopyroxene-plagioclase-quartz (Gt-Opx-Plg-Qtz) assemblage is extensively used for geobarometry, because of large volume changes on reaction. The

Opx-Gt geobarometers include two metastable mineral equilibria, namely pyrope-grossular-enstatite-anorthite-quartz and almadine-grossular-ferrosilite-anorthite-quartz called as Mg end member and Fe end member equilibrium, respectively. Various methods have been used to calibrate these end member equilibria, namely; Newton and Perkins (1982), Perkins and Chipera (1985), Powel and Hollanad (1988), Bhattacharya et al (1991), Eckert et al (1991)and Lal (1993). The pressures estimates obtained by above mentioned methods are presented in table 5.11, ranges from 7-13.7kb (avg. 9.62kb) and 6.8 – 13.7kb (avg. 9.48kb) for core and rim, respectively.

5.7.2. Garnet-Clinopyroxene barometer

Co-existing minerals of garnet and clinopyroxenes mineral pairs are used to estimate the pressure by using Powell and Holland (1988), Newton and Perkins (1982) and Eckert et al (1991) barometers, and the data obtained is presented in table 5.13. The estimated pressure for core and rim for co-existing minerals of garnet and clinopyroxenes mineral pairs of foliated charnockites yielded of 7 – 8.4kb (avg.7.6kb) and 6 – 8.3kb (avg. 7.2kb) for core and rim respectively. Whereas, the pressure obtained for pyroxene granulite ranges between 7 – 8.9kb with an average of 7.9kb, and 6.8 – 8.5kb, average of 7.6kb for core to rim, respectively.

5.8. P-T-t path

Any thermobarometric calibration based on an internally consistent data set should always utilize the same thermodynamic data and activity models for all the phases, which provides a better constrains to estimate the P-T conditions. Calculated P-T conditions of different rock types combined with textural studies are used to constrain P-T-t path of the study area. In the present study, the highest estimated temperatures from pre-exsolution composition of co-existing plagioclase and K-feldspar of gneiss yielded 738 – 732^{o}C and the incipient charnockite of the same exsolution of co-existing minerals

have given 747 – 744^{o}C for core to rim, respectively. Whereas, foliated charnockites exhibits varied temperature and pressure. Feldspar thermometry of Putrika (2008), has yielded temperature range of 917 – 911^{o}C and 811– 773^{o}C for core to rim, respectively. Garnet-Cpx-Plagioclase thermometry of Raheim and Green, (1979) and Krogh (2001) have yielded peak metamorphic temperature range of 699–901^{o}C. Whereas, Powell & Holland (1988) and Eckert et al., (1991) have yielded 6.9 – 8.4 kb peak metamorphic pressure. This assemblage was equilibrated at or near isothermal decompression, as indicated by P-T data obtained.

The pyroxene granulites of Somvarpet show two metamorphic events. The estimated temperatures for non garnetiferous pyroxene granulites by using two pyroxene thermometer of Putrika (2008) yield 1017 – 939^{o}C (avg.978^{o}C) for core and rim, respectively. This temperature seems to be higher, probably; this temperature is of metamorphic or magmatic cooling temperature of pyroxene granulite intrusion. P-T data of Gt- pyroxene thermometry indicate two pyroxene assemblages was equilibrated at or near isobaric cooling. Further, Gt-Opx thermobarometry of Sen and Bhattacharya (1998), indicate 747 - 734^{o}C temperature and 10.6 – 11 kb peak pressure for core and rim respectively. The Gt-Cpx-plg thermobarometry of Krogh (2001) indicates 583^{o}C temperature and pressure of 8.7 kb. Newton and Perkins (1982) barometer for the assemblage Opx-Gt-Pl-Qtz of pyroxene granulites yields 8.2kb and 8kb pressure for core and rim, respectively.

The mineral chemistry and thermobarometric studies of pyroxene granulites exhibits two metamorphic events. The non garnetiferous pyroxene granulites exhibit isothermal decompression path. The presence of gt+qtz symplectites between plagioclase and pyroxene in garnetiferous pyroxene granulites suggest isobaric cooling path. All the above evidences suggest isobaric cooling and isothermal decompression (ITD) path for the Somvarpet granulites.

Table 5.2. Microprobe data of orthopyroxene

	Foliated charnockite							Pyroxene granulite		
	J-11-19A		J-11-32					J-11-22		
	Core	Rim	Rim	Core	Rim	Rim	Core	Rim	Core	Rim
SiO_2	52.04	51.51	51.47	51.43	51.47	52.29	51.61	50.87	50.89	51.2
TiO_2	0.04	0.13	0.08	0.07	0.08	0.07	0.03	0.04	0	0.07
Al_2O_3	0.63	0.89	0.73	0.81	0.84	0.71	0.83	1.19	1.1	0.94
Cr_2O_3	0.03	0	0	0	0.01	0	0.01	0.01	0	0.01
FeO	28.47	28.72	27.78	28.88	28.8	29.35	28.92	29.73	30.61	29.36
MnO	0.95	0.79	1.2	1.18	1.08	1.14	1.04	0.55	0.58	0.41
MgO	18.11	17.74	17.63	17.49	17.44	18.28	17.36	16.93	16.99	17.35
CaO	0.39	0.59	0.47	0.64	0.55	0.54	0.55	0.45	0.39	0.41
Na_2O	0	0	0	0.01	0	0.02	0.03	0.03	0	0.02
K_2O	0	0	0	0.01	0	0.03	0.02	0	0	0
Total	100.66	100.38	99.37	100.51	100.27	102.42	100.41	99.79	100.55	99.77
	Cations calculated based on 6(O)									
Si	1.99	1.97	1.99	1.97	1.98	1.96	1.98	1.97	1.96	1.97
Al	0.03	0.04	0.03	0.04	0.04	0.03	0.04	0.05	0.05	0.04
Fe+3	0	0.01	0	0.02	0	0.04	0	0.01	0.04	0
Fe+2	0.91	0.91	0.90	0.91	0.92	0.88	0.93	0.95	0.95	0.94
Mn	0.03	0.03	0.04	0.04	0.04	0.04	0.03	0.02	0.02	0.01
Mg	1.03	1.01	1.02	1.00	1.00	1.02	0.99	0.98	0.97	0.99
Ca	0.02	0.02	0.02	0.03	0.02	0.02	0.02	0.02	0.02	0.01

Contd. . . . .

Pyroxene granulite													
	SM-8-1								J-11-34				
	Rim	**Core**	**Rim**	**Rim**	**Core**	**Rim**	**Rim**	**Core**	**Rim**	**Core**	**Rim**	**Rim**	**Core**
SiO_2	50.87	50.71	51.17	50.67	49.9	50.64	50.87	50.55	50.79	51.32	50.78	50.07	50.49
TiO_2	0.07	0.11	0.09	0.11	0.09	0	0.13	0.09	0.04	0.12	0.01	0.08	0.09
Al_2O_3	0.75	1.06	0.68	0.76	1.16	0.8	0.72	0.98	1.55	1.38	1.6	1.62	1.73
Cr_2O_3	0	0.05	0.01	0	0.01	0.01	0	0	0.04	0.03	0.01	0.06	0.03
FeO	31.54	32.07	32.35	31.37	32.2	31.61	31.35	31.66	29.88	29.73	29.97	29.52	29.41
MnO	0.92	0.98	0.87	0.97	1.06	0.97	0.85	0.92	0.66	0.6	0.61	0.63	0.65
MgO	15.01	14.76	14.85	14.99	14.89	15.14	15.1	15.04	17.05	17.43	17.19	16.93	17.26
CaO	0.46	0.71	0.49	0.47	0.81	0.51	0.5	0.55	0.48	0.4	0.47	0.5	0.52
Na_2O	0.03	0	-0.01	0.02	0	0	0.01	0.02	0.02	0.01	0.01	0.01	0
K_2O	0.01	0.01	0	0.02	0	0	0	0	0	0.01	0	0	0
Total	99.66	100.45	100.51	99.37	100.12	99.68	99.54	99.81	100.51	101.01	100.65	99.42	100.18
Cations calculated based on 6(O)													
Si	2.00	1.98	2.00	1.99	1.95	1.99	2.00	1.98	1.95	1.96	1.95	1.94	1.94
Al	0.03	0.05	0.03	0.04	0.05	0.04	0.03	0.05	0.07	0.06	0.07	0.07	0.08
Fe^{+3}	0	0	0	0	0.04	0	0	0	0.03	0.02	0.04	0.04	0.03
Fe^{+2}	1.04	1.05	1.06	1.03	1.02	1.04	1.03	1.04	0.93	0.93	0.92	0.92	0.91
Mn	0.03	0.03	0.03	0.03	0.04	0.03	0.03	0.03	0.02	0.02	0.02	0.02	0.02
Mg	0.88	0.86	0.86	0.88	0.87	0.89	0.88	0.88	0.98	0.99	0.98	0.98	0.99
Ca	0.02	0.03	0.02	0.02	0.03	0.02	0.02	0.02	0.02	0.02	0.02	0.02	0.02

Table 5.3. Microprobe data of Clinopyroxenes

	Pyroxene Granulite							Foliated Charnockite							
	J-11-34							J-11-19A			J-11-32				
	Core	**Rim**	**Rim**	**Core**	**Rim**	**Core**	**Rim**	**Rim**	**Core**	**Core**	**Rim**	**Core**	**Rim**	**Core**	**Rim**
SiO_2	50.35	51.45	51.2	50.69	51.19	50.43	50.92	52.4	52.05	51.85	52.27	51.81	51.79	52.44	52.22
TiO_2	0.31	0.18	0.2	0.39	0.23	0.4	0.26	0.13	0.15	0.02	0.17	0.18	0.15	0.15	0.19
Al_2O_3	3.14	2.48	2.57	3.39	2.33	3.33	2.6	1.76	1.95	0.62	1.69	2.06	1.82	2.06	1.74
Fe_2O_3	0.05	0.03	0.05	0.06	0.07	0.05	0.05	0.01	0.02	0.01	0	0.01	0.02	0.02	0.02
FeO	11.81	11.13	11.19	11.34	11.36	12.3	11.1	11.15	11.24	28.93	10.2	11.6	10.9	11.97	10.43
MnO	0.28	0.12	0.32	0.24	0.23	0.2	0.25	0.2	0.33	0.85	0.35	0.36	0.43	0.46	0.41
MgO	11.2	12.04	11.91	11.22	11.74	11.36	11.92	11.88	11.76	17.48	12.28	11.75	11.89	11.79	12.45
CaO	21.89	22.6	22.49	22.67	22.39	22.04	22.54	22.15	22.1	0.77	22.68	21.52	22.04	21.46	22.43
Na_2O	0.54	0.48	0.46	0.63	0.49	0.55	0.39	0.7	0.79	0.03	0.63	0.81	0.72	0.9	0.65
K_2O	0	0	0	0	0	0.01	0.02	0	0	0.02	0	0.01	0.01	0	0
Total	99.57	100.51	100.38	100.63	100.02	100.67	100.05	100.4	100.38	100.59	100.27	100.14	99.76	101.27	100.55
Cations calculated based on 6(O)															
Si	1.907	1.923	1.918	1.896	1.926	1.889	1.914	1.961	1.948	1.985	1.953	1.945	1.949	1.947	1.946
Ti	0.009	0.005	0.006	0.11	0.007	0.011	0.007	0.004	0.004	0.001	0.005	0.005	0.004	0.004	0.005
Al	0.14	0.109	0.113	0.149	0.103	0.147	0.115	0.078	0.086	0.028	0.074	0.091	0.081	0.09	0.076
Fe3+	0.067	0.069	0.072	0.081	0.065	0.091	0.07	0.043	0.067	0.004	0.055	0.068	0.065	0.071	0.068
Fe2+	0.307	0.279	0.279	0.274	0.293	0.294	0.279	0.306	0.285	0.922	0.263	0.297	0.278	0.301	0.257
Mn	0.009	0.004	0.01	0.008	0.007	0.006	0.008	0.006	0.01	0.028	0.011	0.011	0.014	0.014	0.013
MgO	0.632	0.671	0.665	0.626	0.659	0.634	0.668	0.663	0.656	0.998	0.684	0.658	0.667	0.653	0.692
Ca	0.888	0.905	0.903	0.908	0.903	0.885	0.908	0.888	0.886	0.032	0.908	0.866	0.889	0.854	0.895
Na	0.04	0.035	0.033	0.046	0.036	0.04	0.028	0.051	0.057	0.002	0.046	0.059	0.053	0.065	0.047
End member calculations															
Otho and calcic Cpx															
Wollastonite	48.61	48.8	48.88	50.25	48.69	48.79	48.95	47.83	48.5	1.62	48.94	47.57	48.47	47.24	48.56
Enstatite	34.6	36.17	36.02	34.6	35.52	34.99	36.01	35.7	35.91	51.12	36.87	36.14	36.38	36.11	37.5
Ferrosilite	16.79	15.03	15.1	15.15	15.78	16.22	15.04	16.47	15.59	47.26	14.2	16.3	15.15	16.65	13.95
Sodic and calcic Cpx															
Aegerine	7.247	7.355	7.662	8.478	6.912	9.859	7.48	4.599	7.103	11.374	5.796	7.315	6.936	7.709	7.197
Jaderite	-2.974	-3.654	-4.093	-3.69	-3.103	-5.539	-4.444	0.81	-1.028	-4.789	-1.01	-0.938	-1.355	-0.655	-2.215
Diopside	95.727	96.299	96.431	95.212	96.191	95.679	96.964	94.591	93.924	93.414	95.214	93.623	94.419	92.946	95.017

Contd…..

	Garnetiferous foliated charnockite					Garnetiferous pyroxene granulite											
	J-11-20					J-11-22					SM-18						
	Cpx	**Rim**	**Core**	**Core**	**Rim**	**Rim**	**Core**	**Rim**	**Rim**	**Core**	**Rim**	**Core**	**Rim**	**Core**	**Rim**	**Core**	**Rim**
SiO_2	51.78	52.15	51.55	51.55	51.89	51.62	51.68	51.32	51.16	51.49	52.77	51.55	52.13	51.69	52.24	51.47	52.81
TiO_2	0.14	0.12	0.22	0.29	0.18	0.12	0.14	0.06	0.15	0.2	0.08	0.14	0.07	0.31	0.09	0.22	0.14
Al_2O_3	2.11	1.38	1.9	2.32	1.88	1.57	1.61	1.55	1.79	1.85	1.78	2.02	1.53	2.37	1.72	2.4	1.38
Fe_2O_3	0	0	0.04	0	0	0	0.01	0	0.01	0	0.02	0.03	0.03	0.02	0.04	0.02	0.01
FeO	11.3	10.53	10.62	11.8	11.42	13.48	14.25	13.01	12.86	13.98	10.35	11.52	9.84	11.11	9.99	11.78	9.36
MnO	0.22	0.19	0.14	0.15	0.21	0.35	0.29	0.34	0.37	0.3	0.11	0.1	0.1	0.05	0.13	0.16	0.1
MgO	11.98	12.7	11.86	11.42	11.8	11	10.84	11.06	10.94	11.11	12.75	11.98	12.36	11.61	12.57	11.84	12.99
CaO	22.23	23.21	22.06	22.02	22.05	21.83	21.2	21.4	21.43	21.12	22.93	21.99	23.25	22.19	22.81	21.83	23.14
Na_2O	0.46	0.43	0.47	0.52	0.51	0.53	0.65	0.65	0.63	0.59	0.51	0.6	0.33	0.64	0.39	0.66	0.46
K_2O	0	0	0	0	0	0.01	0	0.01	0.02	0.02	0	0	0	0	0	0	0.01
Total	100.22	100.71	98.85	100.07	99.93	100.52	100.67	99.39	99.37	100.66	101.3	99.94	99.65	99.99	99.98	100.38	100.41
Cations calculated based on 6(O)																	
Si	1.943	1.941	1.96	1.943	1.955	1.949	1.95	1.954	1.949	1.941	1.95	1.939	1.962	1.943	1.957	1.928	1.965
Ti	0.004	0.003	0.006	0.008	0.005	0.003	0.004	0.002	0.004	0.006	0.002	0.004	0.002	0.009	0.003	0.006	0.004
Al	0.093	0.061	0.085	0.103	0.083	0.07	0.072	0.07	0.08	0.082	0.078	0.09	0.068	0.105	0.076	0.106	0.061
Fe3+	0.046	0.082	0.016	0.032	0.034	0.065	0.067	0.067	0.059	0.069	0.054	0.068	0.028	0.037	0.032	0.073	0.036
Fe2+	0.309	0.246	0.322	0.339	0.326	0.36	0.383	0.347	0.35	0.371	0.265	0.294	0.282	0.313	0.281	0.296	0.255
Mn	0.007	0.006	0.005	0.005	0.007	0.011	0.009	0.011	0.012	0.01	0.003	0.003	0.003	0.002	0.004	0.005	0.003
MgO	0.67	0.705	0.672	0.642	0.663	0.619	0.61	0.628	0.621	0.624	0.702	0.672	0.693	0.651	0.702	0.661	0.720
Ca	0.894	0.926	0.899	0.889	0.89	0.883	0.857	0.873	0.875	0.853	0.908	0.886	0.937	0.894	0.916	0.876	0.922
Na	0.033	0.031	0.035	0.038	0.037	0.039	0.048	0.048	0.047	0.043	0.037	0.044	0.024	0.047	0.028	0.048	0.033
End members																	
Ortho and Calcic Cpx																	
Wollastonite	47.72	49.33	47.49	47.54	47.37	47.41	46.34	47.25	47.38	46.14	48.4	47.85	49.020	48.130	48.219	47.792	48.594
Enstatite	35.78	37.56	35.52	34.31	35.27	33.24	32.97	33.97	33.65	33.77	37.45	36.27	36.258	35.037	36.971	36.066	37.955
Ferrosilite	16.5	13.11	16.99	18.15	17.35	19.35	20.69	18.78	18.97	20.09	14.15	15.89	14.721	16.834	14.810	16.142	13.451
Sodic and Calcic Cpx																	
Aegerine	4.909	8.543	1.728	3.503	3.646	7.08	7.395	7.302	6.45	7.722	5.761	7.325	2.928	3.900	3.367	7.911	3.757
Jaderite	-1.299	-5.299	1.985	0.595	0.71	-2.871	-2.139	-2.092	-1.399	-2.91	-1.892	-2.62	-0.424	1.060	-0.366	-2.724	-0.285
Diopside	96.391	96.756	96.288	95.902	95.983	95.792	94.743	94.79	94.949	95.188	96.131	95.295	97.496	95.040	96.999	94.813	96.528

Table 5.4. Microprobe data of garnet

	Garnetiferous pyroxene granulite															Garnetiferous foliated charnockite					
	J-11-22						SM-18									J-11-20					
	Rim	**Core**	**Rim**	**Rim**	**Core**	**Core**	**Rim**	**Core**	**Core**	**Rim**	**Core**	**Rim**	**Rim**	**Rim**	**Core**	**Rim**	**Core**	**Rim**	**Core**	**Rim**	**Rim**
SiO_2	38.9	38.28	37.92	38.07	38.37	38.5	38.41	38.41	38.4	38.03	38.78	38.36	37.51	36.15	38.03	37.91	37.82	38.34	38.21	37.97	38.29
TiO_2	0.02	0.02	0.04	0.05	0.06	0.04	0.08	0	0	0.09	0.05	0.08	0.31	0.1	0.02	0	0.02	0.06	0.08	0.04	0.09
Al_2O_3	21.49	21.21	21.17	20.77	21.36	20.98	21.17	20.92	20.88	21.1	21.2	21.29	20.71	19.72	21.2	20.42	21.02	21.12	20.57	20.33	20.81
Cr_2O_3	0.01	0	0.01	0.01	0.01	0.02	0	0.01	0.01	0.05	0.04	0.04	0.04	0	0.01	0.01	0.01	0.01	0	0.01	0
FeO	28.21	28.77	29.01	29.64	28.63	28.99	28.72	28.53	28.45	28.95	28.79	28.55	29.39	29.48	28.16	29.59	29.71	29.29	29.87	29.61	29.44
MnO	1.09	1.08	1.26	1.59	1.29	1.1	0.84	0.74	0.86	0.73	0.8	0.76	0.76	0.86	0.78	2.29	2.14	1.98	1.96	1.88	1.99
MgO	4.4	4.37	3.94	3.29	4.27	4.45	4.59	4.82	4.57	4.17	4.63	4.14	3.74	5.14	4.81	3.46	3.52	3.15	3.62	3.46	3.32
CaO	7.51	7.54	7.35	7.42	7.35	7.3	6.88	7.05	7.01	6.79	7.07	7.18	7.13	6.92	6.85	7	6.91	7.07	6.92	6.98	6.97
Na_2O	0.02	0.05	0	0.02	0.03	0.02	0	0	0.01	0	0	0.04	0	0.01	0	0.04	0.05	0.02	0	0	0.01
K_2O	0	0.02	0	0	0	0	0	0	0.01	0	0.01	0	0.04	0	0	0.01	0.01	0.05	0	0	0
Cations calculated based on 12(O)																					
Si	3.011	2.977	2.975	2.998	2.984	2.993	3.002	3.004	3.016	3.003	3.010	3.011	2.982	2.894	2.990	2.993	2.968	3.015	2.998	3.009	3.015
Ti	0.001	0.001	0.002	0.003	0.004	0.002	0.005	0	0	0.005	0.003	0.005	0.019	0.006	0.001	0.000	0.001	0.004	0.005	0.002	0.005
Al	1.960	1.944	1.957	1.928	1.958	1.922	1.950	1.928	1.933	1.963	1.939	1.969	1.941	1.861	1.964	1.900	1.944	1.958	1.902	1.899	1.931
Cr	0.001	0	0.001	0.001	0.001	0.001	0	0.001	0.001	0.003	0.002	0.002	0.003	0	0.001	0.001	0.001	0.001	0.000	0.001	0.000
Fe3	0.016	0.099	0.088	0.069	0.067	0.086	0.037	0.064	0.035	0.018	0.032	0	0.055	0.339	0.053	0.113	0.116	0.005	0.093	0.079	0.029
Fe2	1.810	1.772	1.815	1.883	1.795	1.799	1.840	1.802	1.834	1.894	1.837	1.874	1.899	1.635	1.798	1.841	1.834	1.922	1.867	1.884	1.910
Mn	0.071	0.071	0.084	0.106	0.085	0.072	0.056	0.049	0.057	0.049	0.053	0.051	0.051	0.058	0.052	0.153	0.142	0.132	0.130	0.126	0.133
Mg	0.508	0.507	0.461	0.386	0.495	0.516	0.535	0.562	0.535	0.491	0.536	0.484	0.443	0.613	0.564	0.407	0.412	0.369	0.423	0.409	0.390
Ca	0.623	0.628	0.618	0.626	0.612	0.608	0.576	0.591	0.590	0.574	0.588	0.604	0.607	0.594	0.577	0.592	0.581	0.596	0.582	0.593	0.588
End member																					
Almandine	60.095	59.504	60.960	62.734	60.086	60.065	61.20	59.99	60.80	62.96	60.959	62.203	63.282	56.370	60.125	61.49	61.772	63.663	62.188	62.556	63.234
Pyrope	16.856	17.012	15.477	12.870	16.570	17.217	17.78	18.70	17.74	16.31	17.781	16.079	14.772	21.152	18.848	13.60	13.869	12.234	14.101	13.574	12.903
Grossular	20.492	20.062	19.825	20.101	19.781	19.400	18.76	19.03	19.20	18.84	19.144	19.968	19.475	17.266	18.766	18.66	18.452	19.647	18.430	18.870	19.131
Spessartine	2.372	2.389	2.812	3.534	2.844	2.418	1.849	1.632	1.897	1.623	1.746	1.677	1.706	2.011	1.737	5.116	4.791	4.369	4.338	4.190	4.394
Uvarovite	0.006	0	0.006	0.006	0.006	0.012	0	0.006	0.006	0.030	0.024	0.025	0.025	0	0.006	0.006	0.006	0.006	0.000	0.006	0.000
Andradite	0.166	1.022	0.895	0.724	0.676	0.864	0.356	0.629	0.347	0.169	0.317	0.000	0.554	3.145	0.507	1.112	1.098	0.045	0.898	0.781	0.285
Ca-Ti Gt	0.012	0.012	0.024	0.031	0.035	0.024	0.045	0	0	0.051	0.029	0.048	0.186	0.056	0.011	0	0.011	0.036	0.046	0.024	0.053

Table 5.5. Microprobe data of Amphibole

	Gneiss			Foliated Charnockite									
	J-11-2			J-11-37									
	Rim	**Core**	**Rim**	**Rim**	**Core**	**Rim**	**Rim**	**Core**	**Rim**	**Rim**	**Core**	**Rim**	**Rim**
SiO_2	36.72	36.65	36.1	42.39	41.98	42.30	41.01	41.62	42.70	42.89	42.56	41.47	42.85
TiO_2	3.75	3.64	3.3	2.02	2.16	2.09	1.98	2.06	2.08	1.95	1.83	2.12	1.86
Al_2O_3	15.44	15.49	15.87	11.59	11.12	11.01	12.26	11.4	11.24	10.98	11.22	11.03	10.7
Cr_2O_3	0.02	0.01	0.02	0	0.02	0	0.02	0	0.04	0.01	0	0.03	0.01
FeO	19.57	19.93	19.79	16.5	16.59	15.44	15.71	16.61	15.36	15.57	15.47	15.70	15.43
MnO	0.18	0.19	0.02	0.28	0.24	0.29	0.26	0.22	0.19	0.26	0.18	0.19	0.21
MgO	9.85	9.71	9.66	10.58	10.61	10.81	10.34	10.73	11.22	11.02	11.34	11.01	11.31
CaO	0	0.05	0.02	11.49	11.54	11.69	11.86	11.47	11.86	11.84	11.72	11.98	12.13
Na_2O	0.09	0.03	0.04	1.5	1.6	1.56	1.19	1.65	1.40	1.21	1.51	1.53	1.41
K_2O	9.7	9.87	9.85	1.69	1.69	1.68	2.10	1.73	1.74	1.69	1.64	1.74	1.66
	Cations calculated based on 23(O)												
Si	5.366	5.356	5.317	6.307	6.300	6.385	6.218	6.242	6.360	6.411	6.348	6.284	6.417
Ti	0.412	0.400	0.366	0.226	0.244	0.237	0.226	0.232	0.233	0.219	0.205	0.242	0.210
Al	2.659	2.668	2.755	2.032	1.967	1.959	2.191	2.015	1.973	1.934	1.972	1.970	1.888
Cr	0.002	0.001	0.002	0	0.002	0	0.002	0	0.005	0.001	0	0.004	0.001
Fe(iii)	2.392	2.436	2.437	0.485	0.442	0.235	0.309	0.539	0.315	0.340	0.426	0.300	0.239
Fe(ii)	0.000	0	0	1.567	1.640	1.714	1.683	1.544	1.598	1.606	1.504	1.690	1.694
Mn	0.022	0.024	0.002	0.035	0.031	0.037	0.033	0.028	0.024	0.033	0.023	0.024	0.027
Mg	2.146	2.116	2.121	2.347	2.374	2.433	2.337	2.399	2.492	2.456	2.522	2.487	2.525
Ca	0.000	0.008	0.003	1.837	1.855	1.891	1.927	1.843	1.893	1.896	1.873	1.945	1.946
Na	0.025	0.008	0.011	0.433	0.466	0.457	0.35	0.48	0.404	0.351	0.437	0.449	0.409
K	1.808	1.840	1.851	0.321	0.324	0.323	0.406	0.331	0.331	0.322	0.312	0.336	0.317

Contd…..

	Foliated Charnockite									Garnetiferous Foliated Charnockite		
	J-11-37			J-11-32			J-11-19A			J-11-20		
	Rim	Core	Rim	Rim	Core	Rim	Core	Rim	Core	Rim	Core	Rim
SiO_2	43.15	42.44	42.63	35.47	36.67	32.67	36.28	42.21	42.58	41.31	41.8	41.54
TiO_2	1.9	2.09	2.45	4.49	5.25	5.21	4.65	1.95	2.14	2.19	2.3	1.95
Al_2O_3	10.41	11.14	11.61	12.23	13.49	12.19	13.91	11.17	10.91	11.43	11.17	11.16
Cr_2O_3	0	0.01	0	0.06	0.02	0.06	0.03	0	0.02	0.03	0.02	0
FeO	15.66	16.12	15.23	17.93	19.09	17.92	18.85	17.26	17.53	18.83	20.05	20.38
MnO	0.23	0.21	0.24	0.05	0.13	0.02	0.11	0.14	0.19	0.13	0.23	0.11
MgO	11.45	10.62	10.97	10.61	11.61	13.39	11.4	10.04	9.99	8.2	8.04	8.24
CaO	12.08	11.5	11.91	0.3	0.01	0.06	0.06	11.92	11.41	11.67	11.35	11.51
Na_2O	1.36	1.62	1.35	0.09	0.04	0.12	0.08	1.16	1.23	1.08	1.44	1.34
K_2O	1.54	1.69	1.85	8.02	9.67	8.7	9.08	1.5	1.47	1.64	1.62	1.64
Cations calculated based on 23(O)												
Si	6.432	6.368	6.337	5.479	5.302	4.94	5.297	6.354	6.379	6.353	6.344	6.31
Ti	0.213	0.236	0.274	0.522	0.571	0.593	0.511	0.221	0.241	0.253	0.263	0.223
Al	1.829	1.97	2.034	2.226	2.299	2.172	2.393	1.982	1.926	2.072	1.998	1.998
Cr	0	0.001	0	0.007	0.002	0.007	0.003	0	0.002	0.004	0.002	0
Fe(iii)	0.336	0.329	0.21	2.316	2.308	2.266	2.301	0.398	0.53	0.223	0.358	0.477
Fe(ii)	1.616	1.694	1.683	0	0	0	0	1.775	1.666	2.199	2.186	2.112
Mn	0.029	0.027	0.03	0.007	0.016	0.003	0.014	0.018	0.024	0.017	0.03	0.014
Mg	2.545	2.376	2.431	2.443	2.503	3.019	2.481	2.253	2.231	1.88	1.819	1.866
Ca	1.929	1.849	1.897	0.05	0.002	0.01	0.009	1.922	1.831	1.923	1.845	1.873
Na	0.393	0.471	0.389	0.027	0.011	0.035	0.023	0.339	0.357	0.322	0.424	0.395
K	0.293	0.323	0.351	1.58	1.783	1.678	1.691	0.288	0.281	0.322	0.314	0.318

Contd…..

	Garnetiferous pyroxene granulite													Pyroxene Granulite	
	J-11-22			SM-8-1										J-11-34	
	Rim	Core	Rim	Core	Rim	Rim	Core	Rim	Rim	Core	Rim	Rim	Core	Rim	Core
SiO_2	42.12	41.47	42.4	41.47	42.41	41.69	41.39	41.61	41.04	41.61	41.99	40.48	41.06	41.42	40.17	40.46
TiO_2	2.11	2.13	1.97	2.53	2.46	2.38	2.41	2.3	2.05	2.29	2.18	2.24	2.42	2.41	2.43	1.99
Al_2O_3	12.47	12.2	11.78	11.42	11.46	11.59	11.21	11.22	11.72	11.57	11.24	12.44	11.54	11.38	12.4	11.92
Cr_2O_3	0	0.02	0	0.06	0.07	0.04	0.05	0.05	0.07	0.06	0.06	0.05	0.06	0.06	0.24	0.18
FeO	17.04	17.29	16.79	19.14	18.99	18.71	19.13	18.79	18.44	19.57	19.2	18.81	19.08	19.05	18.64	18.48
MnO	0.09	0.1	0.11	0.19	0.39	0.19	0.16	0.3	0.27	0.15	0.25	0.13	0.16	0.21	0.04	0.19
MgO	9.67	9.07	9.6	8.19	8.39	8.4	8.31	8.3	8.26	8.44	8.52	7.64	8.06	8.21	8.3	8.44
CaO	11.5	11.63	11.78	11.38	11.49	11.15	11.33	11.48	11.6	11.09	11.38	11.88	11.54	11.54	11.58	11.79
Na_2O	1.31	1.32	1.34	1.67	1.47	1.58	1.67	1.48	1.27	1.59	1.49	1.18	1.47	1.4	1.46	1.33
K_2O	1.54	1.6	1.58	1.67	1.63	1.61	1.64	1.75	1.86	1.68	1.56	2.2	1.68	1.69	1.76	1.66
Cations calculated based on 23(O)																
Si	6.283	6.303	6.394	6.324	6.371	6.339	6.332	6.368	6.32	6.283	6.355	6.254	6.307	6.332	6.158	6.236
Ti	0.237	0.243	0.223	0.29	0.278	0.272	0.277	0.265	0.237	0.26	0.248	0.26	0.28	0.277	0.280	0.231
Al	2.192	2.185	2.093	2.052	2.029	2.077	2.021	2.024	2.127	2.059	2.005	2.265	2.089	2.05	2.24	2.165
Cr	0	0.002	0	0.007	0.008	0.005	0.006	0.006	0.009	0.007	0.007	0.006	0.007	0.007	0.029	0.022
Fe(iii)	0.42	0.232	0.17	0.176	0.226	0.286	0.224	0.159	0.176	0.47	0.352	0	0.166	0.2	0.271	0.262
Fe(ii)	1.706	1.965	1.947	2.264	2.159	2.093	2.223	2.246	2.199	2.002	2.078	2.43	2.285	2.235	2.119	2.120
Mn	0.011	0.013	0.014	0.025	0.05	0.024	0.021	0.039	0.035	0.019	0.032	0.017	0.021	0.027	0.005	0.025
Mg	2.151	2.055	2.158	1.862	1.879	1.904	1.895	1.894	1.896	1.9	1.922	1.76	1.846	1.871	1.897	1.939
Ca	1.838	1.894	1.903	1.859	1.849	1.816	1.857	1.882	1.914	1.794	1.845	1.966	1.899	1.89	1.902	1.947
Na	0.379	0.389	0.392	0.494	0.428	0.466	0.495	0.439	0.379	0.465	0.437	0.353	0.438	0.415	0.434	0.397
K	0.293	0.31	0.304	0.325	0.312	0.312	0.32	0.342	0.365	0.324	0.301	0.434	0.329	0.33	0.344	0.326

Table 5.6. Microprobe data of plagioclase

	Gneiss				Incipient charnockite								Foliated charnockite									
	J-11-2				J-11-27								J-11-37									
	Core	Rim	Rim	Core	Core	Rim	Rim	Core	Rim	Rim	Core	Rim	Core	Rim	Rim	Core	Core	Rim	Rim	Core	Rim	Core	Rim
SiO_2	63.89	64.25	63.42	64.32	65.15	68.22	68.91	64.79	65.43	76.64	65.41	65.34	60.87	60.37	60.86	61.56	61.38	60.98	60.82	61.28	59.76	61.81	60.99
TiO_2	0	0	0.02	0	0.06	0.07	0	0	0	0	0.04	0	0	0.09	0.03	0	0	0	0.02	0.06	0.01	0.02	0
Al_2O_3	22.79	22.79	22.59	22.77	21.73	19.79	19.66	21.49	21.87	13.88	21.56	21.57	24.51	24.74	24.87	24.47	24.14	24.89	24.84	24.33	24.1	24.36	24.57
Cr_2O_3	0	0	0.01	0.01	0.01	0.03	0	0.02	0.02	0.01	0	0.02	0	0	0	0	0.02	0	0	0.02	0	0	0
FeO	0.16	0.33	0	0.11	0.01	0	0	0	0	0.17	0.04	0.03	0.03	0.27	0.28	0.02	0.05	0.21	0.21	0	1.53	0.17	0.01
MnO	0	0	0.03	0.01	0	0	0	0.04	0	0.02	0	0	0.04	0	0.05	0	0	0	0	0	0.01	0.04	0
MgO	0	0.01	0	0	0	0.02	0.02	0.04	0	0.02	0	0	0	0	0	0.01	0.01	0	0	0	0.82	0.01	0.02
CaO	4.01	3.72	3.87	3.85	2.88	0.19	0.34	2.93	2.67	1.04	2.86	2.8	6.33	6.89	6.66	6.13	5.89	6.49	6.36	5.84	6.08	6.29	6.19
Na_2O	9.67	9.81	9.95	9.64	10.65	11.5	11.93	10.09	10.45	7.69	10.33	10.19	8.08	7.57	7.8	7.97	8.31	7.88	7.85	8.2	7.32	8.3	8.18
K_2O	0.12	0.15	0.09	0.1	0.08	0.11	0.07	0.11	0.07	0.08	0.14	0.14	0.54	0.47	0.35	0.46	0.5	0.41	0.64	0.47	0.45	0.21	0.23
Cations calculated based on 8(O)																							
Si	11.24	11.255	11.23	11.28	11.44	11.93	11.95	11.48	11.47	13.14	11.49	11.50	10.82	10.74	10.76	10.88	10.90	10.78	10.78	10.88	10.71	10.88	10.83
Ti	0	0	0	0	0.01	0.01	0	0	0	0	0.01	0	0	0.01	0	0	0	0	0	0.01	0	0	0
Al	4.72	4.705	4.71	4.70	4.50	4.08	4.02	4.49	4.52	2.80	4.46	4.47	5.13	5.19	5.18	5.10	5.05	5.19	5.19	5.09	5.09	5.05	5.14
Fe(ii)	0.02	0.048	0	0.02	0	0	0	0	0	0.02	0.01	0	0	0.04	0.04	0	0.01	0.03	0.03	0	0.23	0.03	0
Mn	0	0	0	0	0	0	0	0.01	0	0	0	0	0.01	0	0.01	0	0	0	0	0	0	0.01	0
Mg	0	0.003	0	0	0	0.01	0.01	0.01	0	0.01	0	0	0	0	0	0	0	0	0	0	0.22	0	0.01
Ca	0.76	0.698	0.73	0.72	0.54	0.04	0.06	0.56	0.50	0.19	0.54	0.53	1.21	1.31	1.26	1.16	1.12	1.23	1.21	1.11	1.17	1.19	1.18
Na	3.30	3.332	3.42	3.28	3.62	3.90	4.01	3.46	3.55	2.56	3.52	3.48	2.78	2.61	2.67	2.73	2.86	2.70	2.70	2.82	2.54	2.83	2.82
K	0.03	0.034	0.02	0.02	0.02	0.02	0.02	0.02	0.02	0.02	0.03	0.03	0.12	0.11	0.08	0.10	0.11	0.09	0.14	0.11	0.10	0.05	0.05
End members																							
Anorthite	18.52	17.18	17.60	17.98	12.95	0.90	1.54	13.74	12.32	6.91	13.17	13.08	29.31	32.58	31.43	29.05	27.37	30.56	29.82	27.50	30.61	29.17	29.11
Albite	80.82	81.99	81.91	81.46	86.63	98.48	98.08	85.64	87.29	92.46	86.06	86.14	67.71	64.77	66.61	68.35	69.87	67.14	66.61	69.87	66.69	69.67	69.61
Orthoclase	0.66	0.82	0.49	0.56	0.43	0.62	0.38	0.61	0.38	0.63	0.77	0.78	2.98	2.65	1.97	2.60	2.77	2.30	3.57	2.63	2.70	1.16	1.29

Contd…..

Foliated charnockite														
	J-11-32							J-11-19A						
	Core	**Rim**	**Rim**	**Core**	**Rim**	**Core**	**Rim**	**Core**	**Core**	**Rim**	**Rim**	**Core**	**Rim**	**Rim**
SiO_2	62.41	61.76	61.87	62.23	61.68	62.2	61.93	62.22	61.67	60.68	61.31	61.68	61.74	61.09
TiO_2	0.03	0.01	0.01	0	0.05	0	0	0.02	0.02	-0.02	0.02	0.06	0.04	0
Al_2O_3	23.58	22.37	24.52	24.05	23.75	23.57	24.47	23.77	23.28	23.2	24.05	23.87	23.33	24.02
Cr_2O_3	0	0.02	0	0.02	0.01	0.01	0.02	0	0	0	0	0.02	0.02	0
FeO	0.09	0.09	0.19	0.03	0.25	0.05	0.13	0.15	0.07	1.15	0.28	0.1	0.13	0
MnO	0	0.05	0	0	0.05	0	0	0	0.1	0	0.05	0.06	0.02	0.03
MgO	0.01	0	0.04	0	0.01	0.01	0	0.01	0	0.62	0	0	0	0.01
CaO	5.25	4.57	5.86	5.57	5.85	5.41	5.71	5.53	5.49	5.73	5.77	5.73	5.55	6.25
Na_2O	8.6	5.62	8.34	8.36	8.37	8.33	8.35	8.42	8.2	8.13	8.29	8.19	8.39	8.08
K_2O	0.48	5.48	0.4	0.58	0.63	0.5	0.38	0.51	0.55	0.29	0.49	0.5	0.48	0.38
Cations calculated based on 8(O)														
Si	11.040	11.16	10.88	10.97	10.94	11.04	10.91	11.00	11.03	10.88	10.90	10.95	11.02	10.89
Ti	0.004	0	0	0	0.01	0	0	0	0	0	0	0.01	0.01	0
Al	4.916	4.76	5.08	5.00	4.96	4.93	5.08	4.95	4.91	4.90	5.04	5.00	4.91	5.05
Fe(ii)	0.013	0.01	0.03	0	0.04	0.01	0.02	0.02	0.01	0.17	0.04	0.01	0.02	0
Mn	0	0.01	0	0	0.01	0	0	0	0.02	0	0.01	0.01	0	0
Mg	0.003	0	0.01	0	0	0	0	0	0	0.17	0	0	0	0
Ca	0.995	0.88	1.10	1.05	1.11	1.03	1.08	1.05	1.05	1.10	1.10	1.09	1.06	1.19
Na	2.949	1.97	2.84	2.86	2.88	2.87	2.85	2.89	2.84	2.83	2.86	2.82	2.90	2.79
K	0.108	1.26	0.09	0.13	0.14	0.11	0.09	0.11	0.13	0.07	0.11	0.11	0.11	0.09
End members														
Anorthite	24.55	21.49	27.35	26.04	26.90	25.66	26.84	25.87	26.16	27.56	27.02	27.10	26.05	29.31
Albite	72.78	47.83	70.43	70.73	69.65	71.51	71.03	71.29	70.72	70.77	70.25	70.09	71.27	68.57
Orthoclase	2.67	30.68	2.22	3.23	3.45	2.82	2.13	2.84	3.12	1.66	2.73	2.82	2.68	2.12

Contd…..

	Foliated charnockite						Pyroxene granulite								
	J-11-20						SM-18								
	Core	**Rim**	**Rim**	**Core**	**Rim**	**Rim**	**Core**	**Rim**	**Rim**	**Core**	**Rim**	**Rim**	**Rim**	**Core**	**Rim**
SiO2	61.85	61.37	60.44	61.95	60.67	64.38	59.08	58.06	59.56	59.24	57.67	55	59.36	58.36	58.75
TiO2	0.02	0	0.05	0.02	0	0.01	0.1	0.06	0	0.05	0	0.02	0	0.06	0.06
Al2O3	23.77	23.88	24.57	23.89	24.33	18.28	25.27	26.39	25.41	25.17	23.59	23.75	25.74	25.49	25.69
Cr2O3	0.01	0	0.02	0.01	0	0	0.01	0	0	0.01	0.02	0	0.01	0	0
FeO	0.09	0.13	0.26	0.09	0.35	0.4	0.05	0.3	0.34	0.14	1.42	2.14	0.15	0.01	0.14
MnO	0	0	0	0.03	0.07	0.08	0	0.07	0.01	0.05	0.06	0.01	0	0.04	0
MgO	0.02	0.03	0	0	0.02	0	0	0.01	0	0.01	0.83	0.86	0	0.02	-0.01
CaO	5.62	5.4	6.58	5.32	6.25	0.04	7.63	8.72	7.5	7.75	6.71	7.49	7.62	7.46	8.11
Na2O	8.62	8.53	8.18	0.31	8.3	14.77	7.54	6.78	7.62	7.43	6.84	7.1	7.25	7.32	7.11
K2O	0.24	0.25	0.14	8.51	0.16	1.09	0.24	0.23	0.17	0.28	0.26	0.24	0.29	0.31	0.29
Cations calculated based on 8(O)															
Si	10.97	10.95	10.76	11.16	10.81	11.67	10.58	10.37	10.60	10.60	10.63	10.34	10.57	10.54	10.51
Ti	0	0	0.01	0	0	0	0.01	0.01	0	0.01	0	0	0	0.01	0.01
Al	4.97	5.02	5.16	5.07	5.11	3.90	5.33	5.55	5.33	5.31	5.13	5.26	5.40	5.42	5.42
Fe(ii)	0.01	0.02	0.04	0.01	0.05	0.06	0.01	0.04	0.05	0.02	0.22	0.34	0.02	0.00	0.02
Mn	0	0	0	0	0.01	0.01	0	0.01	0	0.01	0.01	0	0	0.01	0
Mg	0.01	0.01	0	0	0.01	0	0	0	0	0	0.23	0.24	0	0.01	0
Ca	1.07	1.03	1.26	1.03	1.19	0.01	1.46	1.67	1.43	1.48	1.33	1.51	1.45	1.44	1.55
Na	2.96	2.95	2.82	0.11	2.87	5.19	2.62	2.35	2.63	2.58	2.45	2.59	2.50	2.56	2.47
K	0.05	0.06	0.03	1.95	0.04	0.25	0.05	0.05	0.04	0.06	0.06	0.06	0.07	0.07	0.07
End members															
Anorthite	26.13	25.55	30.53	33.22	29.12	0.14	35.39	41.01	34.90	36.00	34.59	36.32	36.14	35.40	38.04
Albite	72.54	73.04	68.69	3.50	69.99	95.23	63.29	57.70	64.16	62.45	63.81	62.30	62.22	62.85	60.34
Orthoclase	1.33	1.41	0.77	63.27	0.89	4.62	1.33	1.29	0.94	1.55	1.60	1.39	1.64	1.75	1.62

Contd…..

Pyroxene granulite																						
	J-11-34				J-11-22					SM-8-1												
	Rim	Core	Core	Rim	Core	Rim	Core	Rim	Rim	Rim	Core	Rim	Rim	Core	Rim	Rim	Core	Rim	Rim	Core	Rim
SiO_2	53.89	53.75	53.47	55.63	55.51	55.6	55.74	55.68	54.17	61.23	61.53	60.36	61.02	61.72	61.29	61.1	60.72	60.78	59.81	60.86	61.53
TiO_2	-0.07	0.03	0.02	0.01	0.06	0.03	0	0	0.01	0	0.01	0	0.02	0	0.03	0.07	0.04	0.02	0.02	0	0
Al_2O_3	28.8	28.94	28.58	26.64	28.06	28.06	27.96	27.88	27.24	25.18	23.96	24.53	24.53	24.12	24.63	24.72	25.03	24.68	24.6	23.91	24.64
Cr_2O_3	-0.03	0.01	0.01	-0.01	0.02	0	0	0	0.04	0	0	0	0	0.02	0	0	0.01	0.02	0	0.01	0.01
FeO	0.14	0.23	0.1	0.17	0.02	0.46	0	0.49	0.11	0.23	0.12	0.34	0.25	0.01	0.22	0.41	0.15	0.28	0.26	0.11	0.38
MnO	0	-0.05	0.01	-0.01	0.06	0	0	0	0.02	0	0.02	0	0.04	0	0.04	0	0	0	0	0	0.02
MgO	-0.01	0.01	0.01	0.01	0	0.02	0.01	0.03	0.02	0.01	0	0.17	0.01	0	0	0.02	0	0.01	0.03	0.05	0.01
CaO	11.81	12.09	12.24	10.19	10.7	10.74	10.73	10.62	10.7	6.53	6.09	6.76	6.49	6.14	6.49	6.6	6.57	6.56	7.03	6.07	6.43
Na_2O	4.9	4.89	4.8	5.89	5.53	5.72	5.67	5.7	5.93	8.17	8.01	7.6	7.66	7.95	8.12	7.98	7.73	7.77	7.92	8.08	8.01
K_2O	0.22	0.18	0.18	0.28	0.2	0.16	0.16	0.2	0.16	0.24	0.46	0.34	0.52	0.38	0.47	0.22	0.47	0.49	0.28	0.44	0.17
Cations calculated based on 8(O)																					
Si	9.79	9.73	9.75	10.15	9.99	9.97	10.02	10.00	9.96	10.75	10.93	10.76	10.82	10.93	10.81	10.78	10.75	10.78	10.71	10.89	10.83
Ti	0	0	0	0	0.01	0	0	0	0	0	0	0	0	0	0	0.01	0.01	0	0	0	0
Al	6.16	6.18	6.14	5.73	5.95	5.93	5.92	5.90	5.90	5.21	5.02	5.16	5.13	5.04	5.12	5.14	5.22	5.16	5.19	5.04	5.11
Fe(ii)	0.02	0.03	0.02	0.03	0.00	0.07	0.00	0.07	0.02	0.03	0.02	0.05	0.04	0.00	0.03	0.06	0.02	0.04	0.04	0.02	0.06
Mn	0	0	0	0	0.01	0	0	0	0	0	0	0	0.01	0	0.01	0	0	0	0	0	0
Mg	0	0	0	0	0	0.01	0	0.01	0.01	0	0	0.05	0	0	0	0.01	0	0	0.01	0.01	0
Ca	2.30	2.35	2.39	1.99	2.06	2.06	2.07	2.04	2.11	1.23	1.16	1.29	1.23	1.17	1.23	1.25	1.25	1.25	1.35	1.16	1.21
Na	1.73	1.72	1.70	2.08	1.93	1.99	1.98	1.99	2.11	2.78	2.76	2.63	2.63	2.73	2.78	2.73	2.65	2.67	2.75	2.80	2.73
K	0.05	0.04	0.04	0.07	0.05	0.04	0.04	0.05	0.04	0.05	0.10	0.08	0.12	0.09	0.11	0.05	0.11	0.11	0.06	0.10	0.04
End members																					
Anorthite	56.40	57.15	57.90	48.11	51.09	50.47	50.66	50.16	49.49	30.23	28.82	32.32	30.95	29.27	29.85	30.98	31.11	30.94	32.40	28.61	30.43
Albite	42.35	41.83	41.09	50.32	47.78	48.64	48.44	48.72	49.63	68.45	68.59	65.75	66.10	68.58	67.58	67.79	66.24	66.31	66.06	68.92	68.61
Orthoclase	1.25	1.01	1.01	1.57	1.14	0.90	0.90	1.12	0.88	1.32	2.59	1.94	2.95	2.16	2.57	1.23	2.65	2.75	1.54	2.47	0.96

Table 5.7. Microprobe data of K-feldspar

	Gneiss			Incipient charnockite									Foliated charnockite							
	J-11-2			J-11-27									J-11-37			J-11-20		J-11-19A		
	Rim	Core	Rim	Rim	Core	Rim	Rim	Core	Core	Rim	Rim	Core	Rim	Core	Rim	Rim	Core	Rim	Rim	Core
SiO_2	64.37	64.79	64.52	64.49	64.96	64.64	63.8	64.86	64.58	65.16	65.08	64.4	64.62	64.71	64.82	64.33	64.37	64.49	62.43	63.64
TiO_2	0	0	0	0	0	0	0	0.04	0	0	0	0	0.04	0	0.07	0.02	0	0.02	0.06	0
Al_2O_3	18.12	17.98	17.99	18.48	18.47	18.02	18.28	18.19	18.36	18.5	18	18.21	18.38	18.22	18.48	18.46	18.01	18.15	17.92	18.19
Cr_2O_3	0	0	0	0.02	0	0	0	0	0.03	0.02	0.01	0	0	0	0	0	0	0	0	0
FeO	0.05	0.03	0.05	0.07	0	0.01	0	0.08	0	0.1	0	-0.08	0.23	0.01	0.05	0.52	0.11	0	0	0.01
MnO	0	0.03	0	0	0.04	0	0.04	0.01	0	0	0	0	0	0.01	0	0.03	0.01	0	0	0.02
MgO	0.01	0	0	0	0	0.01	0	0	0.01	0	0.01	0.01	0	0	0.01	0.07	0	0	0	0
CaO	0.01	0.01	0	0.02	0.01	0	0.01	0	0.02	0	0	0.04	0.05	0.13	0.05	0.06	0.03	0.04	0.03	0
Na_2O	0.54	0.85	0.51	0.84	1.07	0.57	0.53	0.86	0.59	0.94	0.45	0.65	0.48	0.53	0.5	0.77	0.64	0.24	0.26	0.25
K_2O	15.83	15.47	15.99	15.48	15.07	15.88	16.05	15.47	15.99	15.39	16.04	15.6	15.88	15.77	15.84	15.22	15.27	15.5	15.42	15.53
Cations calculated based on 8(O)																				
Si	12.014	12.046	12.033	11.968	11.997	12.037	11.960	12.017	11.983	11.993	12.061	12.012	11.978	12.014	11.982	11.940	12.041	12.050	11.981	12.007
Ti	0	0	0	0	0	0	0	0.006	0	0	0	0	0.006	0	0.010	0.003	0	0.003	0.009	0
Al	3.985	3.940	3.954	4.042	4.020	3.955	4.038	3.972	4.015	4.013	3.931	4.003	4.015	3.987	4.026	4.038	3.970	3.997	4.053	4.045
Fe(ii)	0.008	0.005	0.008	0.011	0	0.002	0	0.012	0	0.015	0.000	-0.012	0.036	0.002	0.008	0.081	0.017	0	0	0.002
Mn	0	0.005	0	0	0.006	0	0.006	0.002	0	0	0	0	0	0.002	0	0.005	0.002	0	0	0.003
Mg	0.003	0	0	0	0	0.003	0	0	0.003	0	0.003	0.003	0	0	0.003	0.019	0	0	0	0
Ca	0.002	0.002	0	0.004	0.002	0	0.002	0	0.004	0	0	0.008	0.010	0.026	0.010	0.012	0.006	0.008	0.006	0
Na	0.195	0.306	0.184	0.302	0.383	0.206	0.193	0.309	0.212	0.335	0.162	0.235	0.172	0.191	0.179	0.277	0.232	0.087	0.097	0.091
K	3.769	3.669	3.804	3.664	3.550	3.772	3.838	3.656	3.785	3.613	3.792	3.712	3.755	3.735	3.735	3.603	3.644	3.694	3.775	3.738
End member																				
Anorthite	0.05	49.68	0.0	0.100	0.050	0.0	0.050	0.0	0.10	0.0	0.0	0.202	0.25	0.65	0.25	0.307	0.15	0.211	0.16	0.00
Albite	7.70	50.32	4.6	7.611	9.735	5.2	4.777	7.8	5.30	8.5	4.1	5.944	4.38	4.83	4.57	7.118	5.98	2.294	2.49	2.39
Orthoclase	92.25	0.00	95.4	92.289	90.214	94.8	95.174	92.2	94.60	91.5	95.9	93.854	95.37	94.52	95.18	92.575	93.87	97.494	97.35	97.61

Table 5.8. Microprobe data of illmanite

	Foliated charnockite		Pyroxene granulite				
	J-11-37	J-11-20	J-11-32		J-11-22	SM-18	
	Core	Core	Core	Rim	Core	Core	Rim
SiO_2	0.02	0.01	0	0.05	0.05	0.02	0.02
TiO_2	50.32	51.65	52.05	51.7	50.48	50.83	50.12
Al_2O_3	0	0	0	0.03	0.01	0.03	0.02
Cr_2O_3	0	0.02	0.01	0.03	0.04	0.05	0.03
FeO	46.36	47.63	44.34	44.92	47.14	48.02	48.02
MnO	0.78	0.32	2.67	2.56	0.37	0.17	0.2
MgO	1.01	0.12	0.55	0.47	0.62	0.52	0.25
CaO	0.02	0	0.01	0	0.03	0.02	0.14
			Cations				
Ti	1.947	0.493	0.973	1.972	0.986	0.247	1.945
Cr	0	0.001	0	0.001	0.001	0	0.001
Al	0	0.001	0	0.002	0.001	0.001	0.001
Nb	0	0	0	0	0	0	0
Fe	1.994	1.905	1.994	1.905	1.905	1.905	2.071
Mn	0.034	0.110	0.034	0.110	0.110	0.110	0.009
Mg	0.077	0.036	0.077	0.036	0.036	0.036	0.019
Ca	0.001	0	0.001	0	0	0	0.008
Si	0.001	0.001	0.001	0.003	0.001	0.000	0.001

Table 5.9. Microprobe data of Magnetite

	Foliated charnockite				Pyroxene granulite
	J-11-37	J-11-32	J-11-20	J-11-19A	J-11-22
	Core	Core	Core	Core	Core
SiO_2	0	0.01	0.02	0	0
TiO_2	0	0.11	0.08	0.07	0.04
Al_2O_3	0.16	0.41	0.13	0.26	0.16
Cr_2O_3	0.11	0.21	0.11	0.02	0.13
FeO	92.94	91.54	91.22	90.24	91.39
MnO	0.04	0.08	0.03	0.13	0.04
MgO	0.03	0.04	0.01	0.01	0
CaO	0.01	0	0.03	0.14	0.03
Na_2O	0	0.01	0.03	0	0.04
			Cat ions		
Ti	0	0.03	0	0	0
Al	0.1	0.15	0	0.1	0.1
Cr	0	0.05	0	0	0
Fe(iii)	15.9	15.74	15.9	15.9	15.9
Fe(ii)	8.0	7.99	8.0	7.9	8.0
Mn	0	0.02	0	0	0
Mg	0	0.02	0	0	0

Table 5.10. Two Pyroxene thermometry

		Brey and Kohler (1990)	Putirka (2008)
		T(ºC)	T(ºC)
J-11-19A	Core	699	864
	Rim	710	861
J-11-32	Core	783	901
	Rim	687	838
J-11-22	Core	770	935
	Rim	759	925
J-11-34	Core	754	935
	Rim	704	911
SM-8-1	Core	855	1013
	Rim	703	900

Table 5.11. Garnet-Pyroxene thermobarometry

Garnet- Orthopyroxene thermometry									
		Bhattacharya et al 1991	**Sen and Bhattachary 1998**	**Lee and Ganguly**	**Harley 1984**	**Carswell and Harley 1990**	**Aronovich and Berman 1997**	**Lal 1993**	
J-11-22	Core	747	725	801	657	686	994	719	
	Rim	734	707	784	643	672	984	708	
Grt-Opx-Barometry							**Grt-Opx-Pl-Qtz-Barometry**		
		Bhattacharya et al. (1991)		**Eckert et al. (1991)**	**Eckert et al. (1991)**	**Perkins + Chipera (1985)**	**Lal (1993)**	**Newton + Perkins, 82**	**Powell+Holland 88**
J-11-22	Core	Mg (kbar)	10.7	7.4	7	11.8	8.0	8.2	7.5
		Fe (kbar)	11.2			13.7	10.7		
	Rim	Mg (kbar)	10.5			11.6	7.8	8.0	7.3
		Fe (kbar)	11.3	7.1	6.8	13.7	10.7		

Table 5.12 Two feldspar Thermometry

	Putirka (2008) T(°C)	
J-11-2	Core	739
	Rim	727
J-11-27	Core	747
	Rim	745
J-11-19A	Core	905
	Rim	900
J-11-37	Core	929
	Rim	911

Table 5.13 Garnet-Cpx-Plg_ thermobarometry

		Garnet-Cpx thermometry				
		Krogh Ravna (2001)	**Ai (1994)**	**Krogh(1988)**	**Raheim and Green (1979)**	**Ellis and Green (1979)**
	Rim	631	629	618	633	676
	Core	652	655	640	653	697
J-11-20	Rim	573	577	570	595	632
J-11-22	Core	633	661	651	646	702
	Rim	544	565	563	580	621
SM-18	Core	612	645	632	645	690
	Rim	554	580	571	601	635

		Garnet-Cpx barometry		
		Eckert et al. (1991)	**Powell & Holland, 1988**	**Newton & Perkins (1982)**
	Rim	8.3	6.7	7.4
	Core	8.4	7	7.5
J-11-20	Rim	8.1	6	7.2
J-11-22	Core	7.8	7	7
	Rim	7.6	6.8	6.8
SM-18	Core	8.9	8.9	8.3
	Rim	8.5	8.3	7.8

Chapter - VI

FLUID INCLUSIONS

6.1. Introduction

Petrographic and micro-thermometric studies of fluid inclusions provide the essential chemical data on the composition of fluids, which are trapped during the formation of the rock or involved during subsequent transformation and/or deformation. The Study of fluid inclusions is the only way to obtain information on volatiles present during the formation of a rock. This study provides detailed information about the fluids associated with igneous, hydrothermal and metamorphic processes. Fluid inclusion study of metamorphic rock provides an insight into the possible metamorphic fluids involved during recrystallization of the mineral. Hence, the study of fluid inclusion, particularly, in medium to high-grade terrains, provides useful information of the metamorphic history of the rocks. The rocks belong to Granulite facies, especially the charnockites of granitic - tonalitic - trondjametic composition; have shown the presence of prominently CO_2 inclusions of varying densities, and the presence of different types of deep crustal fluids like CO_2, CO_2-H_2O, CO_2-CH_4-N_2, CH_4-N_2, H_2O-NaCl and melt+CO_2 (Santhosh, 1984; Hansen *et al.,* 1984; Ravindra Kumar *et al.,* 1985; Srikantappa *et al.,* 1985, 1987; Srikantappa and Zargar, 2009; Newton *et al.,* 2014). The granulite facies terrains are characterized by low H_2O and predominant CO_2 rich fluid activity when compared to CO_2-H_2O or H_2O rich amphibolite facies gneiss, and CO_2 influx is a major agent for creating zones of low water activity and formation of granulite (Touret, 1974, 1981, 2001; Janardhan *et al.,* 1982; Rudnick *et al.,* 1984; Hansen *et al.,* 1984; Roedder, 1984; Santhosh, 1985; Srikantappa *et al.,* 1985, 1992, 2008; Ravindra Kumar et al, 1995; Newton *et al.,* 2014). The CO_2 rich fluid inclusion in granulites is interpreted to be either

syn-metamorphic (Touret and Hortel, 1990; Srikantappa *et al*., 1992) or post metamorphic (Lumb et al, 1987; Lamb, 1990). To know, syn or post metamorphic nature of fluids in granulites, determination of relative entrapment of inclusions in metamorphic minerals, as well as, coincidence of isochores with the mineralogical P-T estimates is a pre-requisite. The Southern Indian granulite terrain is considered to be one of the good sites for fluid induced transformation of Amphibolite-Granulite facies rocks (Janardhan *et al.,* 1979; Hansen *et al.,* 1984; 1987; Santhosh, 1985; Srikantappa and Zargar, 2009; Rajesh *et al.,* 2011; Newton *et al.,* 2014). The process of arrested charnockite formation and presence of CO_2 and CO_2-H_2O inclusions have been reported from the Palghat region (Ravindrakumar and Srikantapp, 1995) and Halgur area (Srikantappa and Malathi, 2008; Srikantappa and Jargar, 2009) of south India

The Study of fluid inclusion in metamorphic rock is important in understanding various mineral reactions, mineral stability, heat flow, elemental transport and kinetics of crystal growth, also controls of external variables like; activity or partial pressure of volatile components, and melting and deformation of metamorphic rocks. Fluid inclusions are part of the mineral assemblage in metamorphic rocks and occupy roughly the same volume as most of the accessory phases. Therefore, fluid inclusions have an equal status as that of any rock forming minerals in metamorphic rocks. For these reasons, the type of fluid phase present in metamorphic rocks needs to be documented to understand their role in origin of metamorphic rocks. Therefore, in this chapter an attempt has been made to report the nature and composition of fluid inclusion, and to compare the data with P-T data obtained by using mineral chemistry to understand the transformation of amphibolite facies to granulite facies, and the possible conditions of entrapment.

6.2. Methodology

6.2.1. Sample preparation

Fluid inclusion studies were carried out on doubly polished thin wafers of about 0.3mm to 0.7mm thickness prepared for selected rock samples following the procedure of Roedder (1984). While, preparing doubly polished sections precautions were taken to avoid both, excessive heating and mechanical shattering of the sample. Temperature is maintained below 100^{o}C to avoid decrepitation of inclusions with high filling densities.

Heating and freezing studies were carried out for more than 200 inclusions present in gneisses, incipient and foliated charnockites and pyroxene granulite.

6.2.2. Instrumentation

The micro-thermometric studies were carried out on a Linkam THMSG 600 heating/freezing stage fitted on an Olympus BX 50 transmitted light microscope at PPOD laboratory, Geological Survey of India, Bangalore. A silver block (THMSB) is used for heating. The unit operates in the temperature range of -195° to + 600°C. The stage is periodically calibrated by pure H_2O (demineralized water, melting point 0°C) and pure CO_2 inclusions (synthetic CO_2 standard supplied by the stage manufacturer whose triple point -56.6°C). Estimated accuracy is ±0.1°C at temperatures below 30°C and ±1.00°C at temperatures above 30°C. Reproducibility of the results of heating above 300°C has been tested and found to be ± 2 to 3°C.

Freezing experiments were performed first on all sections/wafers to avoid decrepitation of inclusions followed by heating. The measurements taken during melting include final melting temperature of ice (Tm_{ice}) to determine the salinity of aqueous phase. During heating, attempts were made to measure the homogenization temperatures

of the CO_2 (T_hCO_2) to determine the density of CO_2 and the total homogenization temperature (T_hTotal). The salinity is calculated by using Linksys software (version 1.8) following the equations of Bodnar (1983), Zhang and Frantz (1987) and Brown and Lamb (1988).

6.3. Fluid inclusion characteristics

6.3.1. Fluid Inclusion in Gneisses

Fluid inclusion studies were carried out for three gneiss samples. Presence of mixed CO_2-H_2O biphase, and occasionally CO_2 rich fluid inclusions were recorded mainly in quartz and rarely in plagioclase grains. Temperatures of melting (T_m) and homogenization (T_h) of fluid inclusions of gneisses are presented in table 6.1. CO_2 inclusions in quartz and Plagioclase are generally monophase at room temperature. They occur as isolated, rounded to irregular shape with the size varying from 0.04 to 21.68um (Fig. 6.1- 6.3). Fluid inclusion of gneisses indicates the presence of different generation of inclusions.

CO_2 rich inclusions, on cooling develop a vapor phase around -60 to -80^{0}C and crystallize around -95 to -111^{0}C. Temperature of first melting of CO_2 obtained varies from -56.7 to -65.2^{0}C. Whereas, the melting point of pure CO_2 is -56.6^{o}C, which is close to the triple point. The higher range of melting point (-59 to -65.2^{0}C) obtained in the present study may indicate the presence of additional phases such as CH_4 and N_2, phases (Van den Kerkhof 1988; and Lamb 1990). The total Homogenization temperature of isolated CO_2 rich inclusions into liquid phase (T_h) ranges from -12.5 to 31.1^{0}C. 14 inclusions have the T_h range of -0.3 to -27^{o}C and 20 inclusions are in the range of 1.1 to 31.1°C, with respective densities of 0.929 to 1.0637 gm/cc and 0.466 to 0.921 gm/cc., and an average density of 0.870 gm/cc.

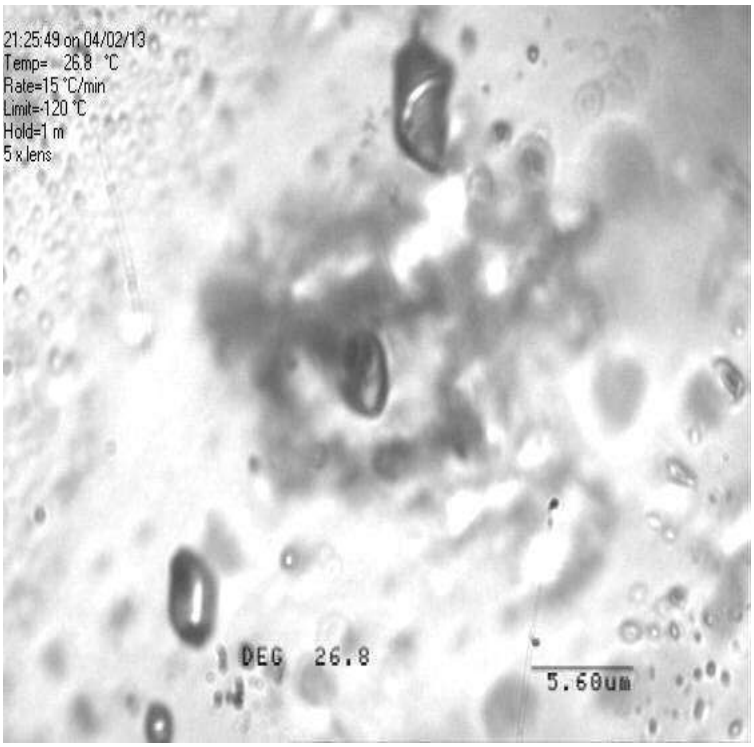

Fig. 6.1. Isolated rounded monophase CO_2 inclusion in gneiss

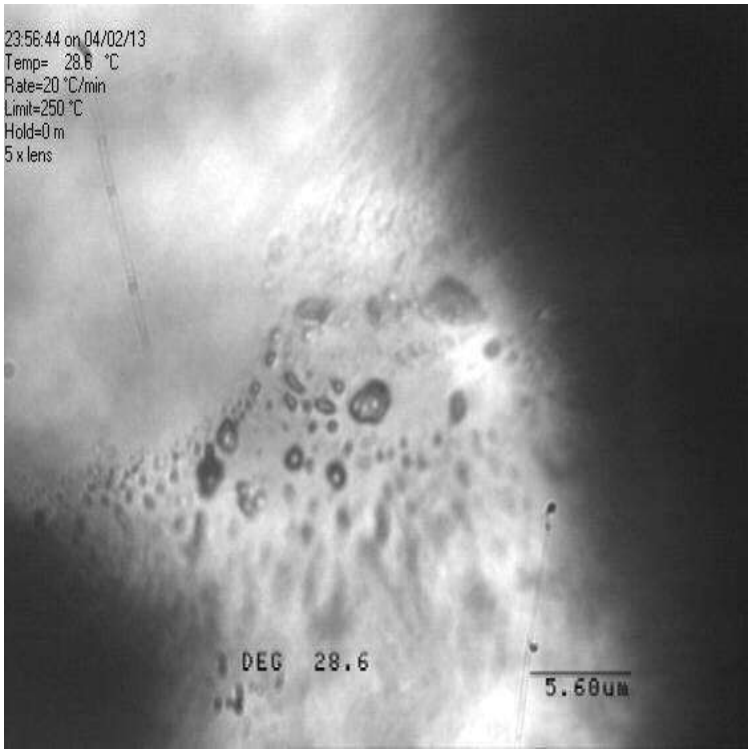

Fig. 6.2. Isolated primary monophase CO_2 inclusion in gneiss

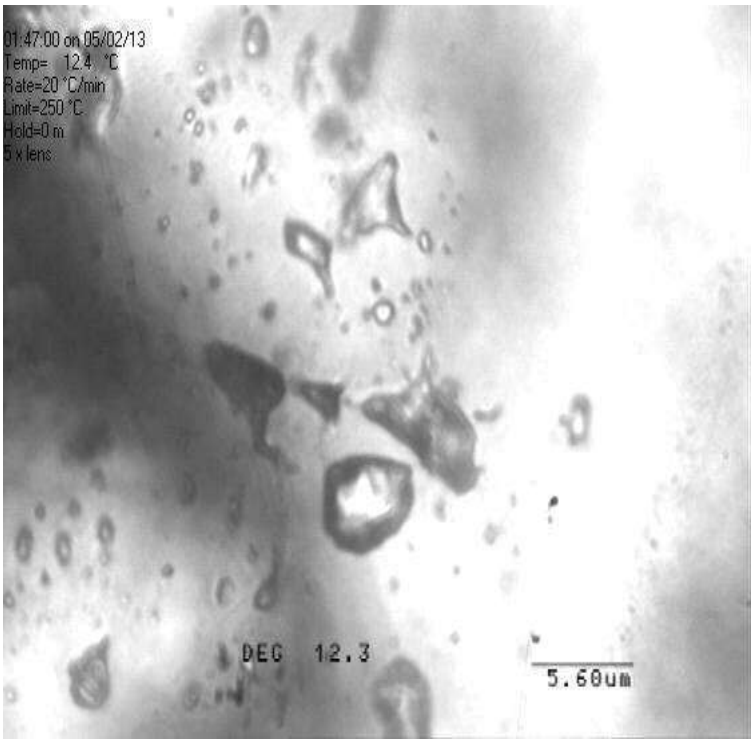

Fig. 6.3. Isolated irregular biphase CO_2-H_2O inclusion in gneiss

6.3.2. Fluid Inclusion in Incipient Charnockite

Fluid inclusion studies were carried out for three Incipient Charnockite samples and measurable inclusions were found mainly in quartz and plagioclase (Fig. 6.4 to 6.6). Temperature of melting (T_m) and temperature of homogenization (T_h) of fluid inclusion are given in table 6.2. In the incipient charnockite three types of fluids have been observed viz., CO_2, CO_2-H_2O, H_2O. CO_2 inclusion in quartz and plagioclase occur as oval to sub rounded in shape and size vary from 1.29 to 7.23um. Whereas, CO_2-H_2O rich biphase ranges from 2.95 to 11.4um and fill is 0.63 to 0.96um.

CO_2 inclusions in quartz grains of incipient charnockites on cooling develop a vapor phase around -95 to -110°C, and melting temperature (Tm) obtained varies from -56.5 to -57.7^{0}C, indicating pure CO_2 inclusion and without CH_4 and N_2 phase. The homogenization temperature ranges from -18.7 to 27.9°C with the density range from 0.850 to 1.026gm/cc.

The H_2O rich biphase inclusions found in incipient charnockites show, initial melting temperature in the range of -1.9 to -4°C and, final melting temperature of -24 to -28°C, this suggests, the major component of aqueous phase is NaCl in the fluid system. The range of total homogenization temperature varies from 230 to 350°C. The density of H_2O-NaCl (0.574 to 0.915g/cc) and H_2O (0.745g/cc) corresponds to the calculated salinity range of 1.036 to 14.97% NaCl equivalent of incipient charnockite, elsewhere (Ravindra Kumar and Srikantappa, 1995; Srikantappa, 2008).

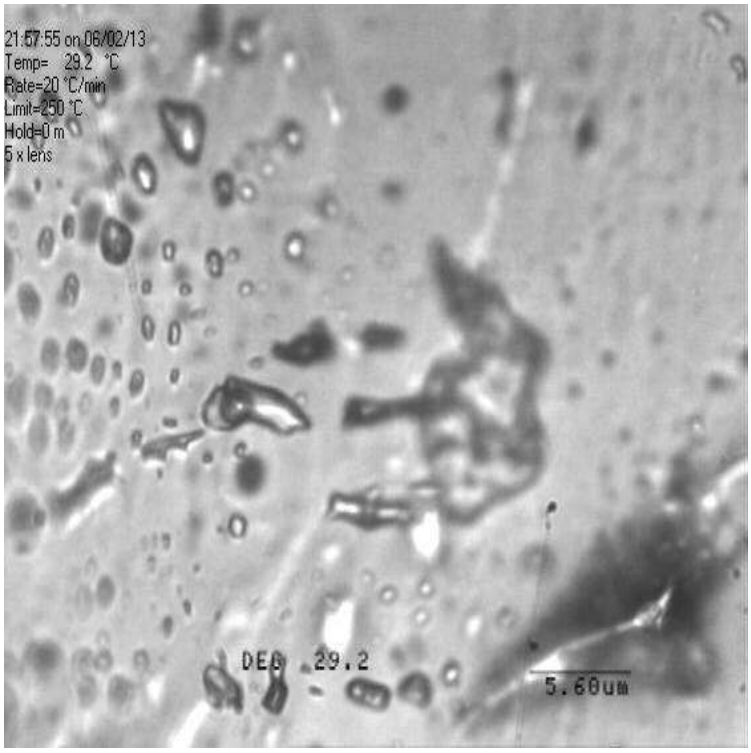

Fig. 6.4. Isolated irregular shaped biphase (CO_2-H_2O) inclusion in incipient charnockite

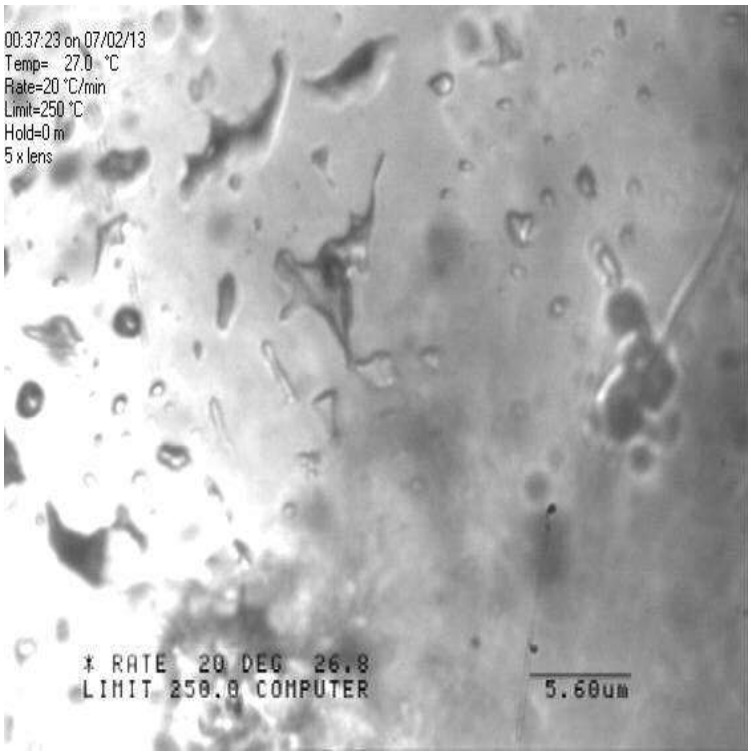

Fig. 6.5. Isolated irregular shaped biphase (CO_2-H_2O) inclusion in incipient charnockite

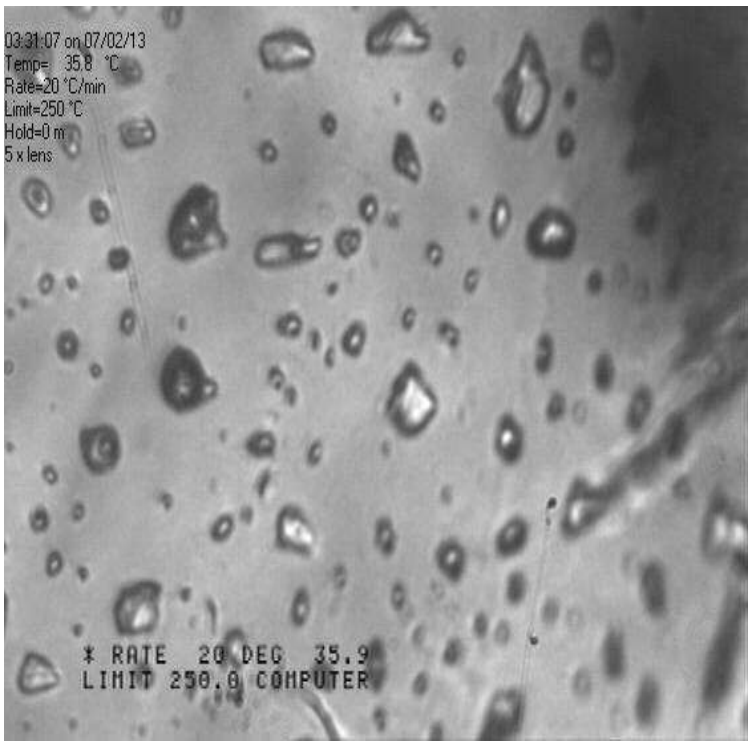

Fig. 6.6. Isolated rounded shaped biphase (CO_2-H_2O) primary inclusion in incipient charnockite

6.3.3. Fluid Inclusion in Foliated Charnockite

Fluid inclusion studies were carried out for three Foliated Charnockite samples. Presence of CO_2 rich fluid and occasionally mixed CO_2-NaCl biphase inclusions have been observed mainly in quartz and rarely in plagioclase grains. Melting (T_m) and homogenization temperatures (T_h) of fluid inclusions of foliated Charnockite are presented in table 6.3. CO_2 inclusions present in quartz and Plagioclase are generally monophase at room temperature. They occur as rounded, tabular to irregular shape with isolated (Fig. 6.7 – 6.9) or trail bound (Fig. 6.10 – 6.13), varying in size from 1.26 to 55.18um. The study indicates the presence of different generation of fluid inclusions in foliated Charnockite of Somvarpet area.

CO_2 rich inclusions are cross cut by a trail of low salinity inclusions (6.37-9.18 wt% NaCl equi.). Low salinity inclusions vary in size from 3.33-3.92um when compared to CO_2 rich inclusions. Another important features observed in the present study is, the presence of empty inclusions. Cavities, which appear like CO_2 inclusions were cooled up to -120^oC but no phase change was observed indicating that they are empty inclusions. Such inclusions are termed as 'exploded' inclusions and are characteristics of polymetamorphic terrains (Negri and Touret, 1978). These types of inclusions are also reported from South of B. R. Hills by Srikantappa *et al.*, (2008) and Basavarajappa *et al.*, (1992). The presence of exploded inclusions implies that the inclusions were naturally decrepited during intense deformation which the rock suffered.

Primary carbonic fluid inclusions in these samples occur typically in isolation and are mono-phase at room temperature. During cooling experiments, a vapor bubble nucleates and homogenizes in to liquid phase. Temperature of first melting of CO_2 range from -56.7°C to -60°C, indicating, fluid is dominated by CO_2. The maximum depression of melting temperature of CO_2 is close to the triple point, indicates pure CO_2 (-56.6^oC) inclusion. The remaining inclusions contain some amount of CH_4 in addition to CO_2. The

total homogenization temperature of CO_2 is in the range of -16.2 to 28°C. Within this, 21 inclusions have -4 to -16.2°C T_h, and 30 inclusions have 3.2 to 28°C T_h and the respective densities are 0.9513 to 1.0145 gm/cc and 0.6566 to 0.9084 gm/cc. The carbonic inclusions probably formed from trapping of the homogeneous vapor phase, but, their temperature of total homogenization couldn't be measured.

The range of homogenization temperature of aqueous and aqueous carbonic inclusions varies from 131°C to 280°C, which corresponds to a salinity range of 6.3737 to 9.1875 wt.% NaCl equivalent, (calculated using Linksys software, version 1.8) following the equations of by Bodnar (1983), Zhang and Frantz (1987) and Brown and Lamb (1988). The initial ice melting temperatures (T_{FM}) range from -30°C to -22°C. This suggests, in the fluid system, the major component of aqueous phase is NaCl. The final melting temperature of ice (T_m ice) ranges from -4°C to -6°C corresponds with salinities of 6.3737 to 9.1875 wt. % NaCl equivalent. The CO_2 density of inclusions studied varies from 0.81 to 0.9997 gms/cm^3.

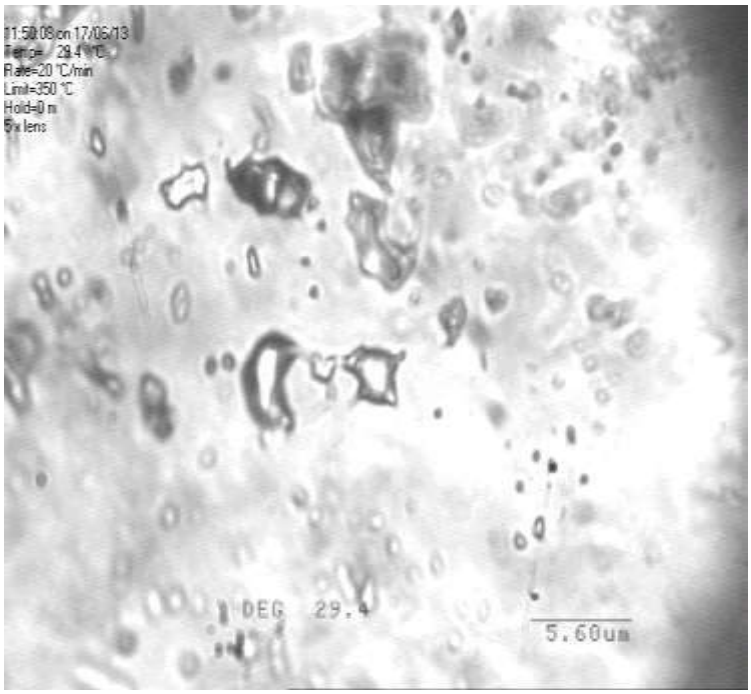

Fig. 6.7. Isolated irregular shaped biphase primary inclusion in foliated charnockite

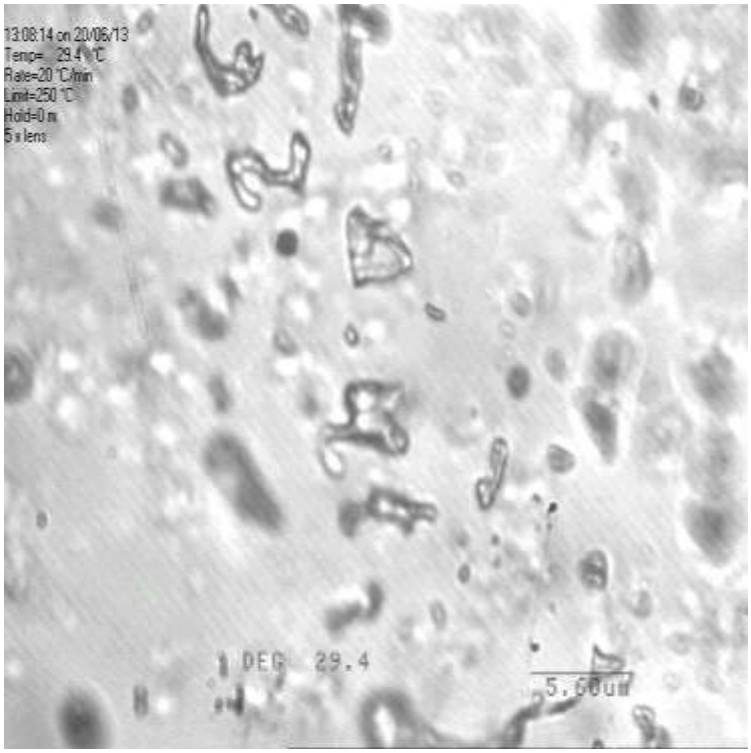

Fig. 6.8. Isolated irregular monophase primary inclusion in foliated charnockite

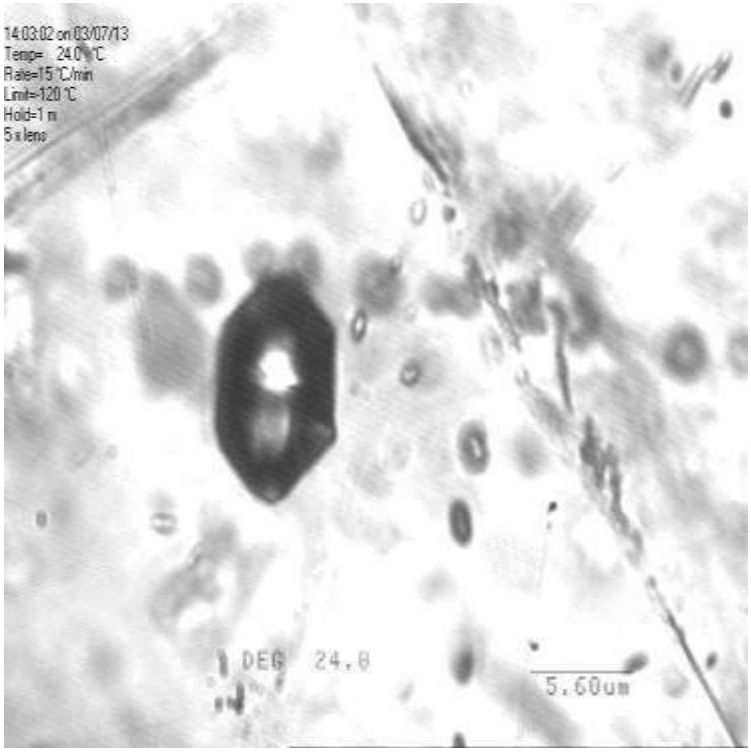

Fig. 6.9. Isolated monophase primary inclusion in foliated charnockite

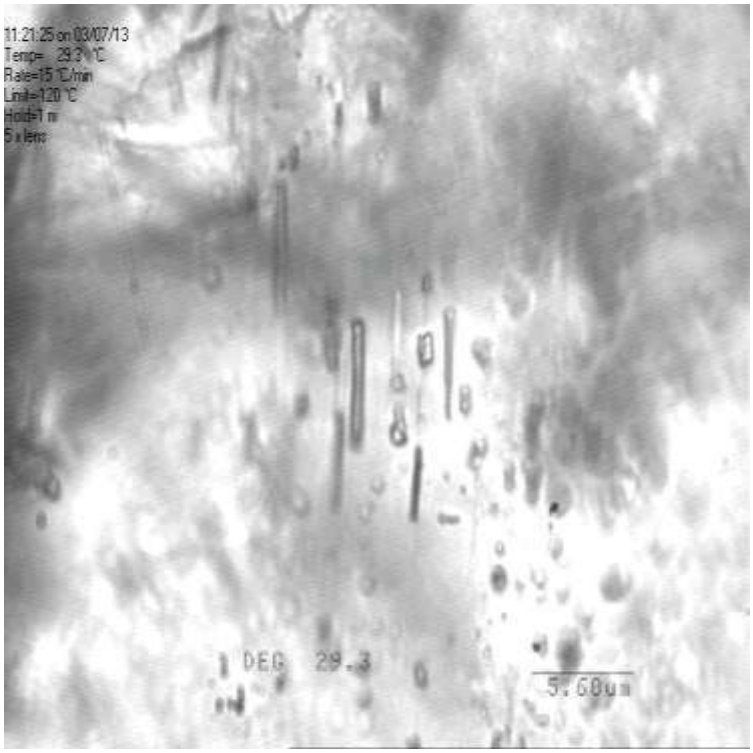

Fig. 6.10. Arrayed tabular shaped monophase inclusion in plagioclase grains of foliated charnockite

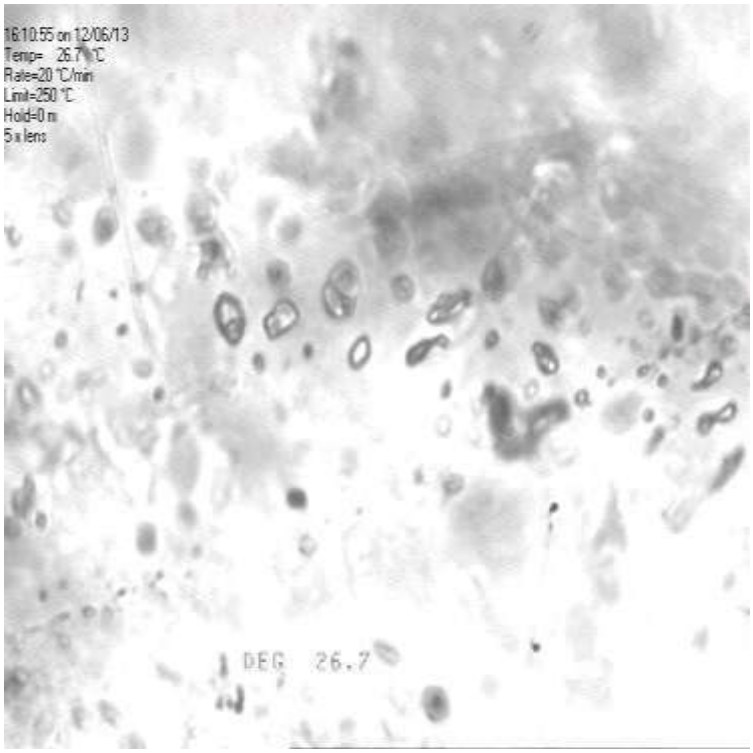

Fig. 6.11. Arrayed rounded shaped biphase inclusion in foliated charnockite

Fig. 6.12. Arrayed rounded shape monophase inclusion in foliated charnockite

Fig. 6.13. Arrayed rounded shape monophase inclusion in foliated charnockite

6.3.4. Fluid Inclusion in Pyroxene granulite

Fluid inclusion studies were carried out for four samples of Pyroxene granulites representing both garnetiferous and non-garnetiferous. Of these, only non-garnetiferous pyroxene granulites show the presence of CO_2 rich fluid inclusions mainly in plagioclase and rarely in quartz grains. Temperature of melting (T_m) and temperature of homogenization (T_h) of fluid inclusions of Pyroxene granulites are presented in table 6.4. CO_2 inclusions in quartz and Plagioclase are generally monophase at room temperature. CO_2 inclusion occur as isolated rounded to irregular shape with (Fig. 6.14 – 15), varying in size from 1.21 to 33.28 μm. The study reveals the presence of single generation of fluid inclusions and the presence of exploded inclusions similar to foliated charnockite.

CO_2 rich inclusions on cooling develop a vapor phase around -60 to -80°C and crystallize around -95 to -110°C. Temperature of first melting of CO_2 obtained in pyroxene granulite varies from -56.7 to -61.8°C, which is close to the triple point, indicating it to be pure CO_2 (-56.6°C). The homogenization temperature of 33 inclusions studied, range from -7.5 to 2.5°C T_h, and corresponding densities are 0.9128 to 0.9705gm/cc.

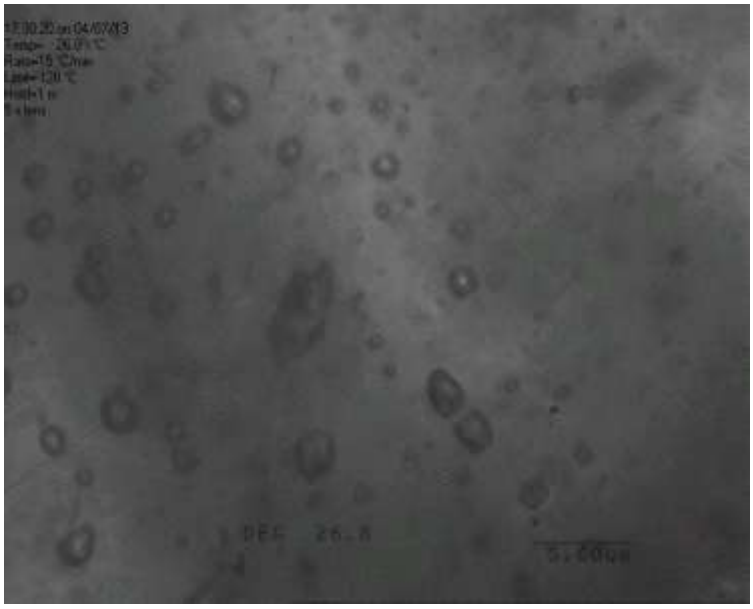

Fig. 6.14. Typical isolated rounded monophase CO_2 inclusion in Pyroxene granulite

Fig. 6.15. Typical isolated rounded monophase CO_2 inclusion in Pyroxene granulite

6.4. Interpretation of Fluid inclusion data

The occurrences of different types of fluids in metamorphic rocks is dependent on many factors like; lithology, mineral assemblage, character of protolith (ortho or para) and type of deformation. Evaluation of the textural relations between the host minerals and their fluid inclusions is important to constrain the entrapment of inclusions relative to mineral growth in granulites, which will be a first step in establishing evidences for either syn or post metamorphic nature of fluids in granulite facies rocks. The fluid inclusion studies in granulite facies rocks of southern India have revealed the presence only of syn-metamorphic carbonic fluids (Touret and Hansen, 1988; Ravindra Kumar *et al*., 1985; Srikantappa *et al*., 1992, 1993, 2008). Micro thermometric study of important lithounits of the amphibolite – granulite transmission zone of Somvarpet area revealed presence of CO_2 and CO_2-H_2O dominant fluids types.

6.4.1. Carbonic inclusion

The Mono-phase carbonic (CO_2) fluid inclusions are transparent to dark in color and more abundant than aqueous fluid inclusions. The Carbonic inclusions are mainly dominated by CO_2 with some variable amounts of other vapors such as CH_4, and N_2. Carbonic fluid inclusions appear to contain only one or two carbonic phases at room temperature. Theoretically, they must contain aqueous phase, which occur as a thin film near the inclusion wall, and may not be observable under microscope. Carbonic inclusions are commonly could not be homogenized at the same temperature as the aqueous inclusions. They are most likely trapped heterogeneous inclusions, and their homogenization temperatures are unusable.

6.4.2. CO_2 Inclusions in gneisses and incipient charnockites

The homogenization temperature obtained for the CO_2 inclusions in quartz grains of gneiss and incipient charnockites are plotted in fig.6.15-6.17 and fig 6.19-6.21. P-T data obtained for the gneiss from mineral thermobarometry indicate 738^{o}C metamorphic temperature. When this temperature data is intersected with CO_2 fluid density line, CO_2 isochore is developed in between 4.5 – 5 kb pressure (Fig. 6.18). Similarly, metamorphic temperatures obtained for incipient charnockite indicate 729 to 765^{o}C temperatures and 5.8 to 6.3 kb pressure (fig 6.22). P-T data obtained for the incipient charnockites of Somvarpet are relatively higher when compared P-T data of incipient charnockite of Mercara, Kabbaldurga and Ponmudi/Kottavattum granulites, which are in the range of 600-700^{o}C and 5-6kb (Janardhan *et al.,* 1979; Stahle *et al.,* 1987; Srikantappa *et al.,* 1985; Ravindarakumar *et al.,* 1985; Hansen *et al.,* 1987; Santhosh, 1991).

6.4.3. CO_2 Inclusions in charnockites and pyroxene granulite

The density data obtained for CO_2 inclusions for quartz grains of three samples of foliated charnockite are plotted in fig. 6.26. The data of individual samples is presented in fig. 6.24 & 6.25. The obtained T_h for CO_2 inclusion of charnockite show one at -4 to -16°C and the other at 3.2 to 28°C, and corresponding CO_2 densities are 1.0145 to 0.9513 and 0.908 to 0.6566gm/cc respectively. The density data obtained for CO_2 inclusions of charnockites shows two periods of deformation. The P-T data indicate temperature of 897.6-945.4°C, when this temperature data intersected on CO_2 density line, the CO_2 isochore falls on 6.3-6.7kb pressure area (fig. 6.27). When the temperature data of non garnetiferous pyroxene granulites (977.8°C) are intersected with CO_2 density line CO_2 isochore intersects at 6.7 – 7 kb pressure area. This P-T path shows that there may be Isothermal decompression path of metamorphism. All these observations suggest syn-metamorphic nature of CO_2 fluids. While considering the above, P-T paths and fluid characteristics of gneiss and incipient charnockite shows that the earlier syn-metamorphic fluids might have been re-trapped during the formation of incipient charnockite at slightly medium P-T conditions. Stahle *et al*., (1987) and Raith *et al*., (1989) have also come to similar conclusions for the CO_2 fluids present in the incipient charnockite of Kabbaldurga.

6.5. Source of CO_2

A number of theories have been proposed for the source of CO_2 in charnockitization and granulite facies metamorphism by many previous workers viz., Touret and Hartel (1990); Santhosh *et al.,* (1991); Newton, (1992); Srikantappa *et al.,* (1985, 1992, 2008); Raith and Srikantappa, (1993); Tsunogae *et al.,* (2008); Ohyama

et al., (2008); Newton *et al.,* (2014). According to Hansen *et al.,* (1995) under plating basaltic magmas appears to be the source for of CO_2 rich fluids in charnockites. The carbon isotopic data of Newton *et al.,* (1980), and Jachson *et al.,* (1988) also indicate mantle signatures. Basavarajappa, (1992); Srikantappa *et al.,* (1994) who have studied many south Indian granulites have suggested, CO_2 rich fluids could have been derived by the syn-metamorphic basic intrusives. Magmatic under plating of Bohlen, (1991) and mantle plumes of Peucat *et al.,* (1993) are the possible models that are used to explain the source of syn-metamorphic CO_2 pore fluids. Janardhan *et al.,* (1979); Newton, (1992) have suggested 'carbonic metamorphism' because of the presence of abundant mantle-derived CO_2 in the lower crustal rocks (granulite) of south India. In some instances, CO_2 appears to have been derived due to decarbonation reaction of carbonates. The enderbitic granulites in the Nilgiris are interpreted to have been derived from andesitic to dactic volcanic rocks and CO_2 has been stored in these rocks in the form of secondary carbonates during low-grade hydrothermal reaction with seawater. Decarbonation reaction of these carbonates, releasing CO_2, made available as pore fluids during high-grade metamorphism (Raith *et al.,* 1990). For the formation of some of the incipient charnockites in south India "fluid release" models have been proposed (Srikantapp *et al.,* 1985, 2008; Stahle *et al.,* 1987; Raith and Srikantapp 1993). Newton *et al.,* (2014) have said that there appears to be link between the Closepet granite, incipient charnockite and the underlying massif granulites. They said that they are the members of a single late Archaean process involving fluids of probable deep-crustal or upper mantle origin. In Somvarpet area close association of migmatitic gneisses, incipient charnockite, massif granulites also suggest source CO_2 could be either deep crust or upper mantle.

Table 6.1. Fluid inclusion in Amphibolite facies gneisses

Sample No.	Size (mm)	T_m of CO_2 (ºC)	T_h of CO_2 (ºC)	Density (g/cm^3)
J-11-2	3.25	-56.7	10.8	0.8559
	4.25	-62.1	26.2	0.6921
	1.2	-60.9	16.5	0.8087
	8.51	-60.5	18.2	0.7927
	9.37	-57.8	-0.3	0.9299
	0.04	-57.8	1.3	0.9202
	5.76	-57.7	1.1	0.9215
	5.8	-57.7	1.4	0.9196
	12.69	-59.9	-3.1	0.9462
	6.6	-59.9	-1.3	0.9358
	8.47	-59.9	-4.2	0.9524
	5.94	-65.1	2	0.9159
	5.76	-65	-12.5	0.9963
	21.68	-62	2.5	0.9128
	4.29	-59.6	2.2	0.9147
	6.32	-59.6	12.2	0.8451
	3.52	-59.5	27.5	0.6675
	4.39	-59.5	31.1	0.466
J-11-14	2.95	-58	30	0.5956
	0.91	-58	31.1	0.466
	13.17	-57.9	31.1	0.466
J-11-27	19.78	-58.3	-10.8	0.9877
	2.55	-58.3	-10.5	0.9862
	10.68	-58.2	-27	1.0636
	4.63	-58.2	-13	0.9988
	8.41	-61.1	-10.7	0.9872
	1.05	-61	-10.7	0.9872
	3.16	-61.1	-15.7	1.0121
	1.76	-61	-23	1.046
	8.2	-61	-15	1.0087
	3.69	-65.1	3.7	0.9052
	1.37	-65.2	3.7	0.9052
	1.73	-64.2	1.5	0.919

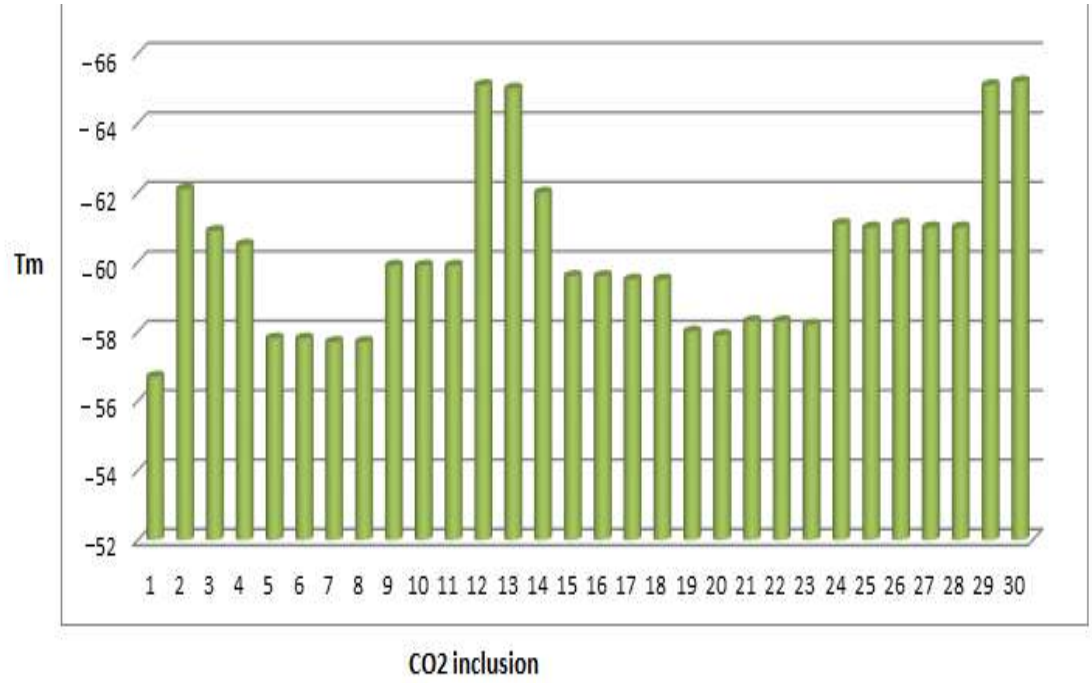

Fig. 6.16. CO_2 melting temperature in gneisses

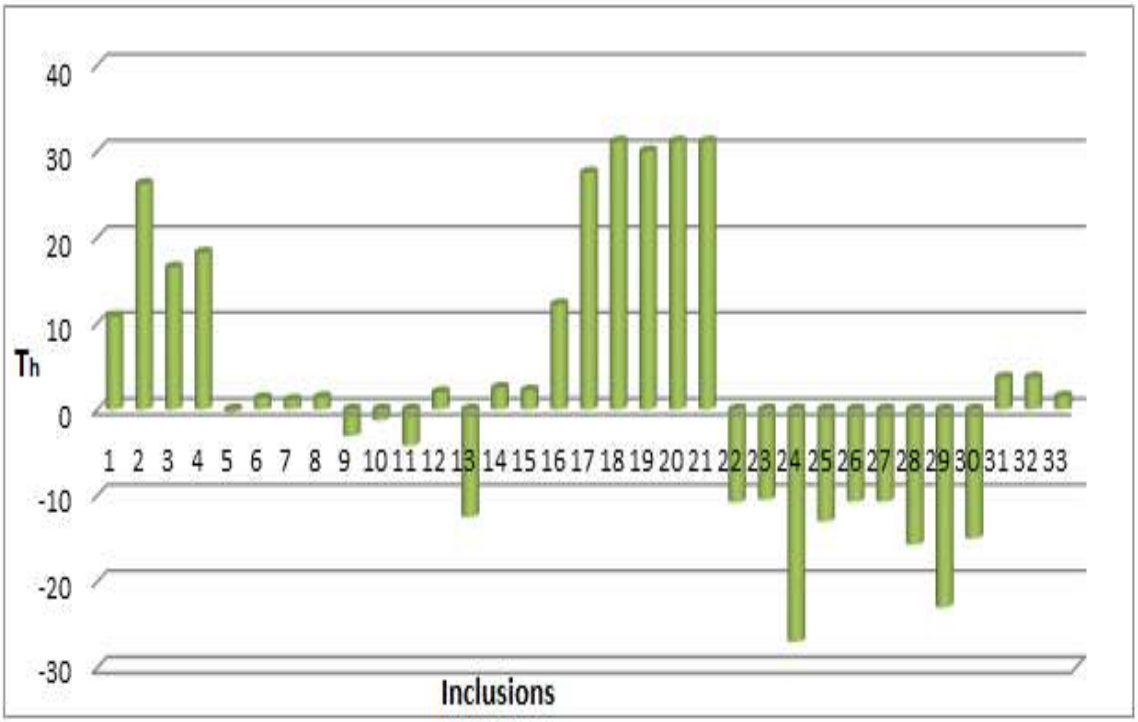

Fig.6.17. CO_2 homogenization temperature in gneisses

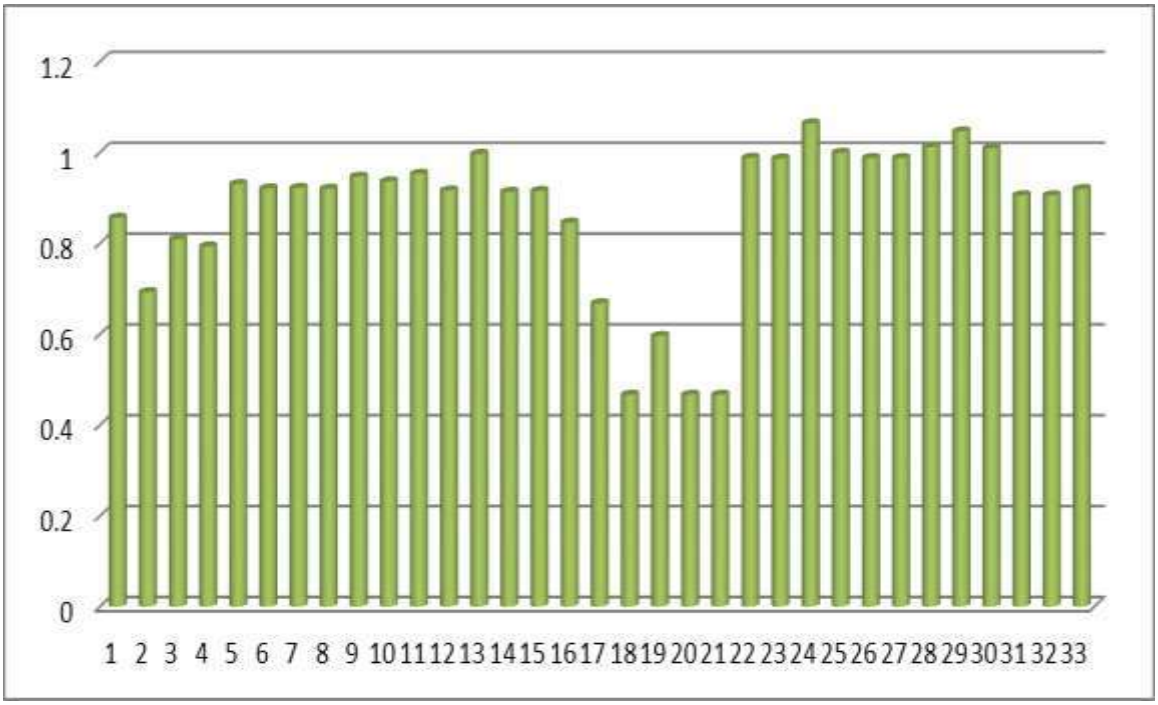

Fig. 6.18. CO_2 density (gm/cc) bar charts of gneisses

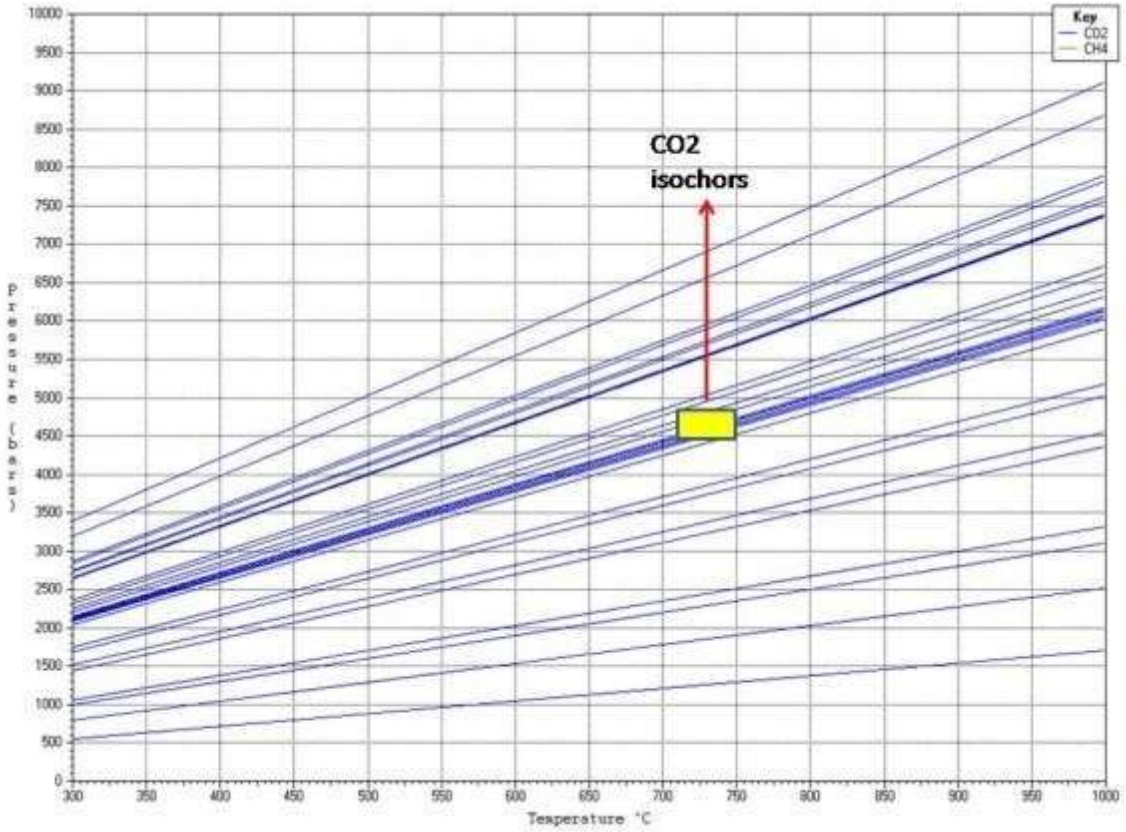

Fig. 6.19. CO_2 density data of gneisses intersected with mineral thermobarometry

Table 6.2. Fluid inclusion in Incipient charnockite

Sample No.	Size	Fill	T_{FM} (°C)	T_m Ice (°C)	T_h Aq (°C)	T_m CO_2 (°C)	T_h CO_2 (°C)	T_m clathrat (°C)	T_h Total (°C)	EqWt% NaCl	Density (gm/cm^3)
J-11-10	2.95	0.89			260				260		0.784
	2.74					-56.6	11.5				0.8505
	7.23					-56.6	11.5				0.8505
	6.48	0.88				-57.5	27.9	9.5		1.0365	0.6588
	7.56				300	-61.2	6.8	2.8	300		0.7125
	2.13				283				283		0.7453
	0.16		-28	-1.9	285				285	3.1168	0.7665
	1.86	0.94	-28	-2	283				283	3.2777	0.7718
	2.94	0.95	-27	-2	280				280	3.2777	0.7768
J-11-40	1.89		-25	-11	262				262	14.9768	0.9156
	3.49					-56.8	-18.6				1.0258
	2.26					-56.7	-18.7				1.0263
	1.29					-56.8	-17				1.0183
	7.3					-56.7	-18.1				1.0235
J-11-35	3.76	0.94			320			3.3	320		0.6672
	4.37	0.95			295			3.2	295		0.7226
	8.26	0.9			270			3.3	270		0.7679
	3.99	0.86			325				325		0.6544
	7.04	0.97			252			1.2	252		0.7962
	4.28	0.97			247			1.3	247		0.8036
	3.59	0.63			235			1.2	235		0.8205
	7.5	0.76			325			3	325		0.6544
	3.45	0.94	-25		350			4.2	350		0.5746
	3.24	0.96	-24		350			4.1	350		0.5746
	11.4	0.95			230			4.2	230		0.8273

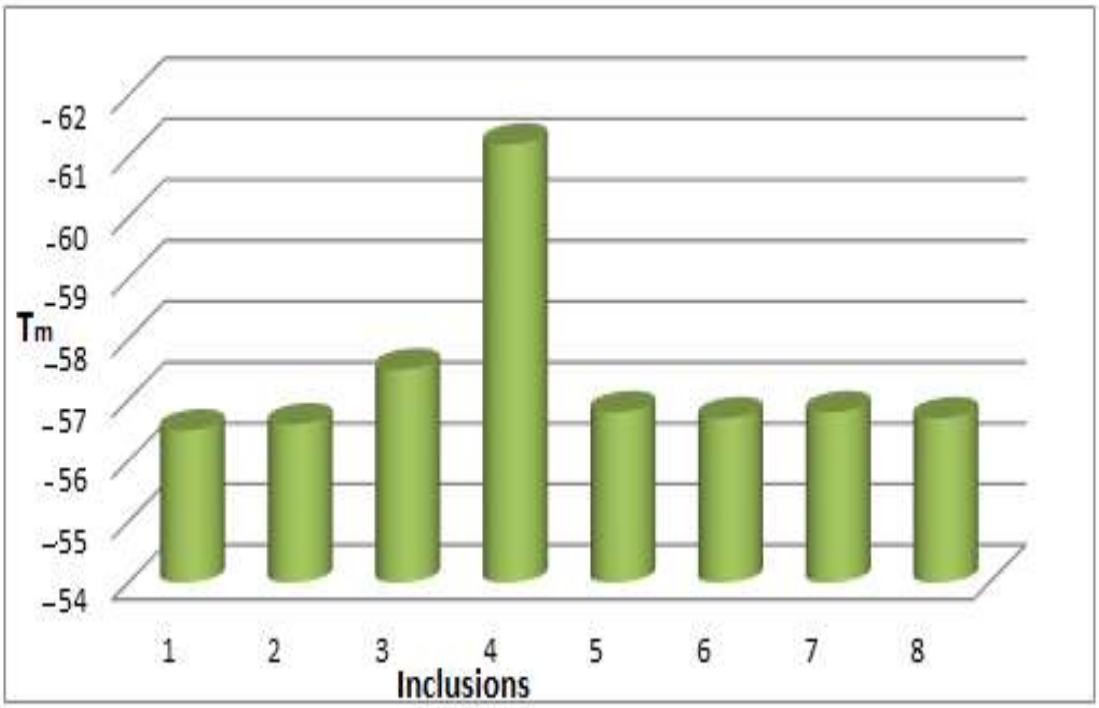

Fig. 6.20. CO_2 melting temperature in incipient charnockite

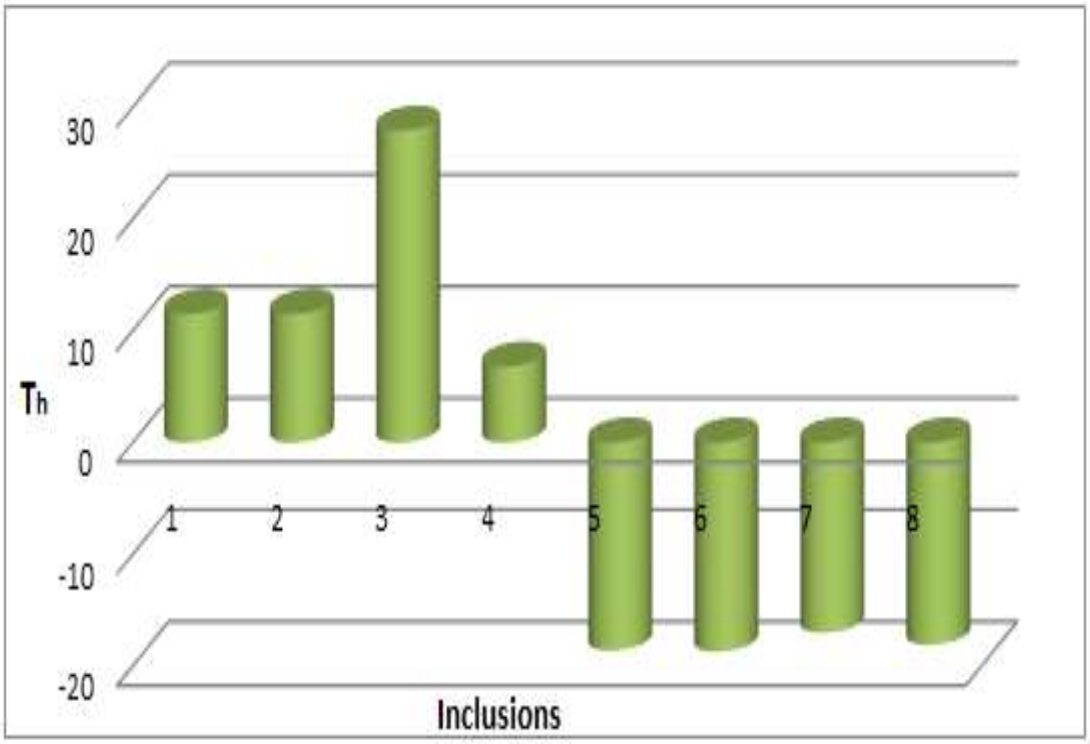

Fig. 6.21. CO_2 homogenization temperature in incipient charnockite

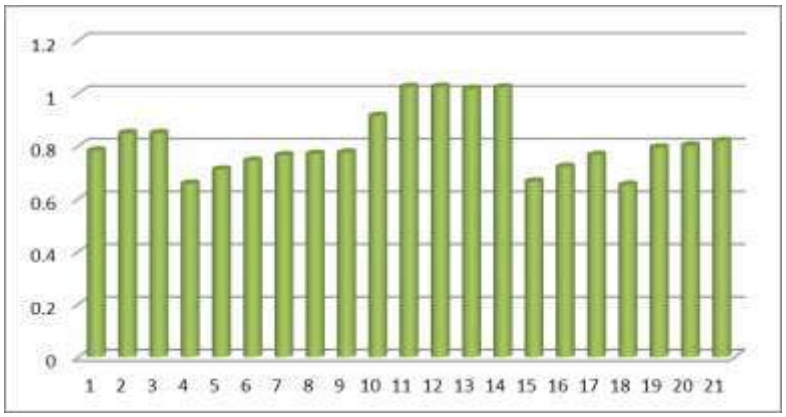

Fig. 6.22. CO_2 density (gm/cc) bar charts of incipient charnockite

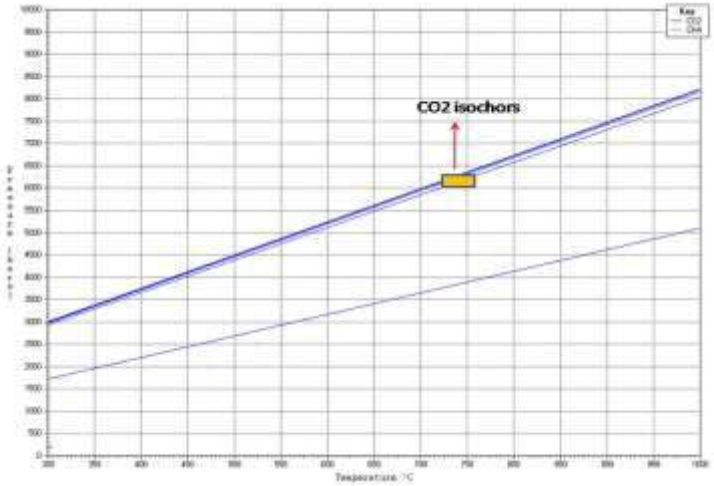

Fig. 6.23. CO_2 isochores of incipient charnockite intersected with P-T data of mineral thermobarometry

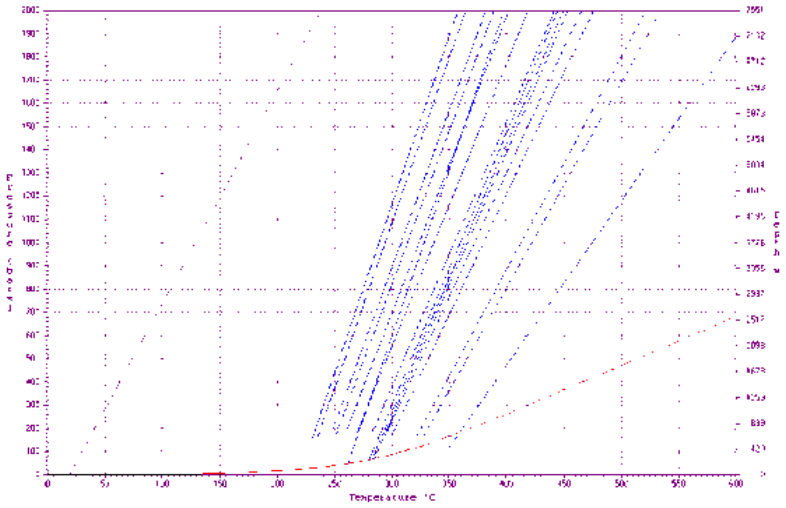

Fig. 6.24. H_2O density (gm/cc) plots of incipient charnockite

Table 6.3. Fluid inclusion in foliated charnockite

Sl.No	Size	Fill	T_{FM} in °C	T_m ice in °C	CO_2 (T_m) in °C	CO_2 (T_h) °C	T_m clathrat in °C	T_h total in °C	EqWt% NaCl	Density (gm/cm^3)
J.11.33	2.18				-57	9				0.8692
	2.55				-57.2	-15.6				1.0116
	5.29				-57.1	-15.4				1.0106
	6.78				-57.2	-15				1.0087
	2.58				-57	-15.2				1.0096
	53.3				-58	18.5				0.7897
	6.44				-60	18				0.7946
	3.33		-30	-4	-57.6	10.8	8	280	6.3737	0.81
J.11.19A	2.88				-57.1	11.9				0.8474
	1.64				-57.3	12.1				0.8459
	2.31				-56.9	12.5				0.8427
	9.12				-56.8	15.3				0.8194
	3.86				-56.7	-7.2				0.9689
	8.69				-56.8	18				0.7946
	7.1				-56.7	19				0.7847
	15.52				-57.1	8				0.8763
	2.02				-56.9	8.1				0.8756
	1.21				-56.8	7.5				0.8798
	26.53				-58	5				0.8967
	10.23				-58.2	5.2				0.8954
	6.66				-57.9	4.9				0.8974
	9.79				-56.7	3.2				0.9084
	15.83				-56.8	4.1				0.9026
	4.9				-56.8	3.6				0.9058
	55.18				-57	28				0.6566
	1.48				-57.2	-8				0.9731
	1.61				-56.7	-9.2				0.9794
	1.4				-56.9	-8.8				0.9773

Contd….

	1.41				-57.1	-9			0.9784
	1.74				-57	-10			0.9836
J.11.37	5.37				-57.2	-6.4			0.9645
	4.74				-56.8	-4			0.9513
	4.7				-56.9	-6.5			0.9651
	2.44				-57.2	-10.5			0.9862
	2.44				-57	-10.9			0.9882
	2.31				-56.8	-10			0.9836
	1.59				-57.2	-9.8			0.9826
	2.05				-57.2	-6			0.9624
	1.84				-57	-7			0.9678
	1.26				-57.5	-6.8			0.9667
	32.71				-56.8	16.2			0.8114
	5.76				-56.8	18.2			0.7927
	7.4				-57	-16.2			1.0145
	4.43				-57.1	19			0.7847
	7.01				-57.2	15			0.822
	1.75				-56.9	16			0.8132
	16.94				-57.21	10.3			0.8596
	6.4				-57	8			0.8763
	3.35				-61	8.6			0.872
	0.88				-57.9	9			0.8692
	1.94				-57.6	7.9			0.877
	3.92	0.95	-22	-6			131	9.1875	0.9997

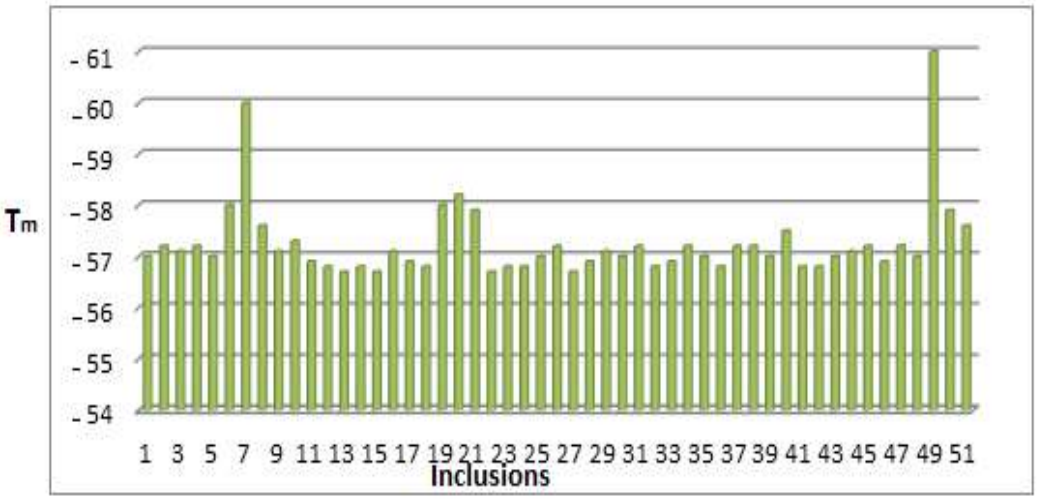

Fig.6.25. CO_2 melting temperature in foliated charnockite

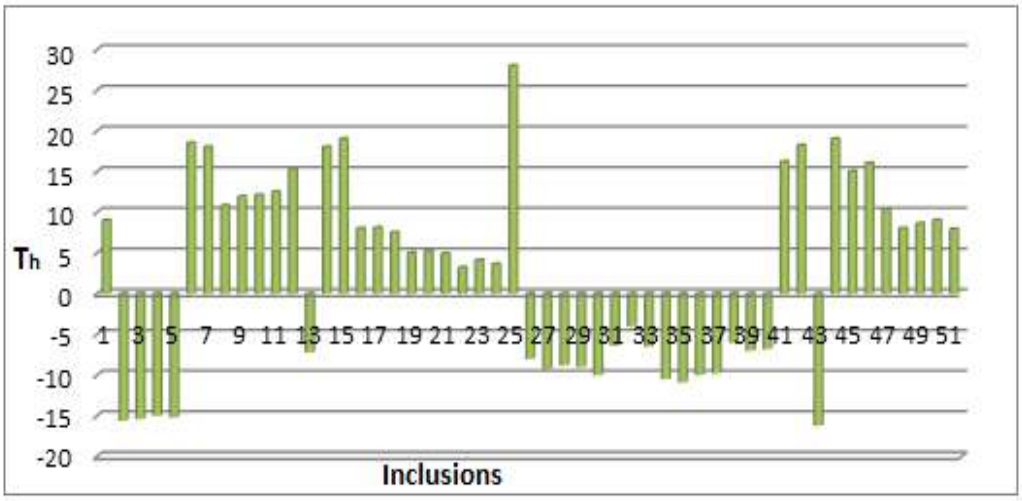

Fig. 6.26. CO_2 homogenization temperature in foliated charnockite

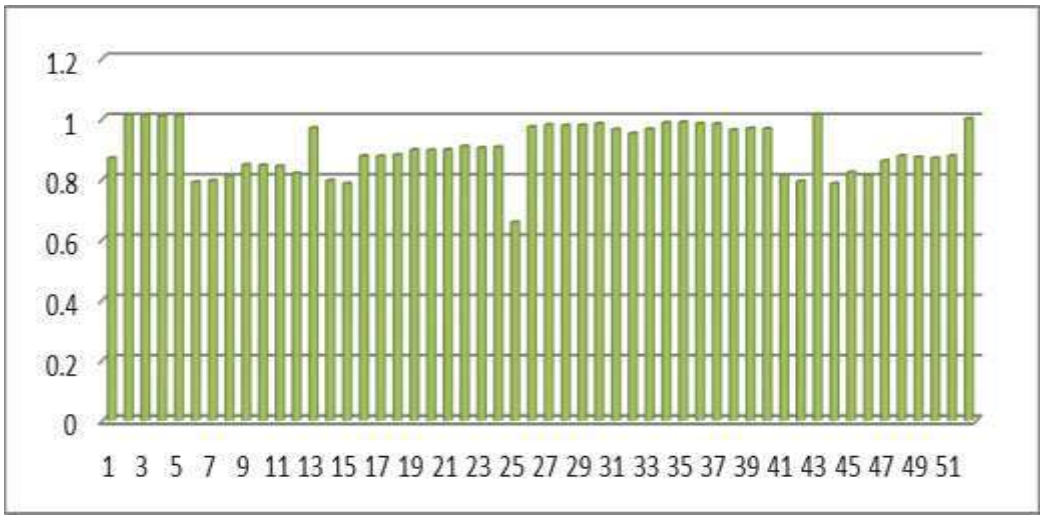

Fig. 6.27. CO_2 density (gm/cc) bar charts of foliated charnockite

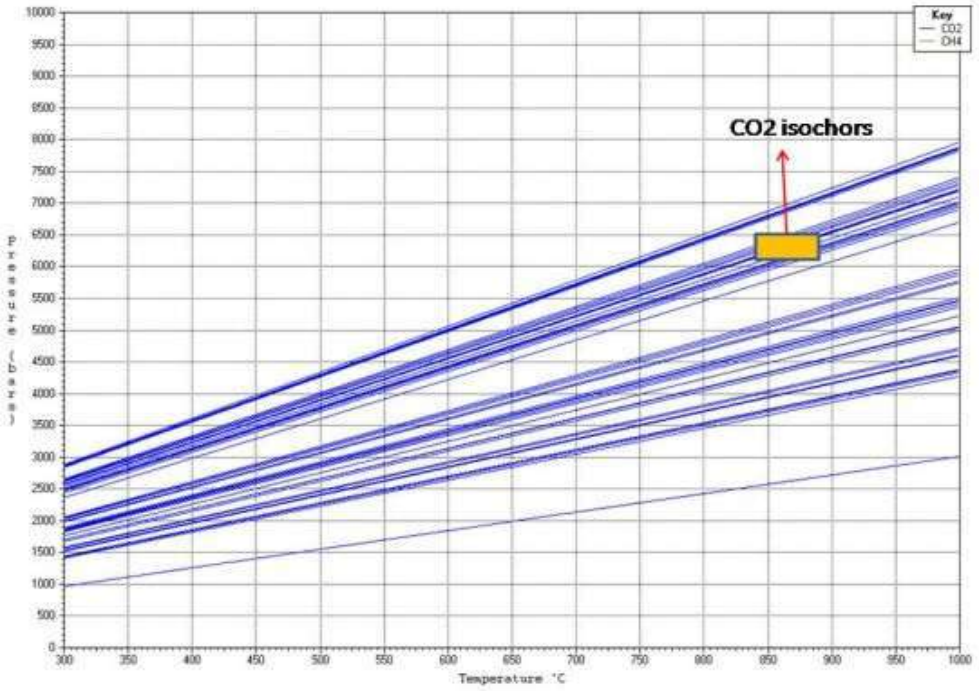

Fig. 6.28. CO_2 isochores of foliated charnockite intersected with mineral thermobarometry P-T data

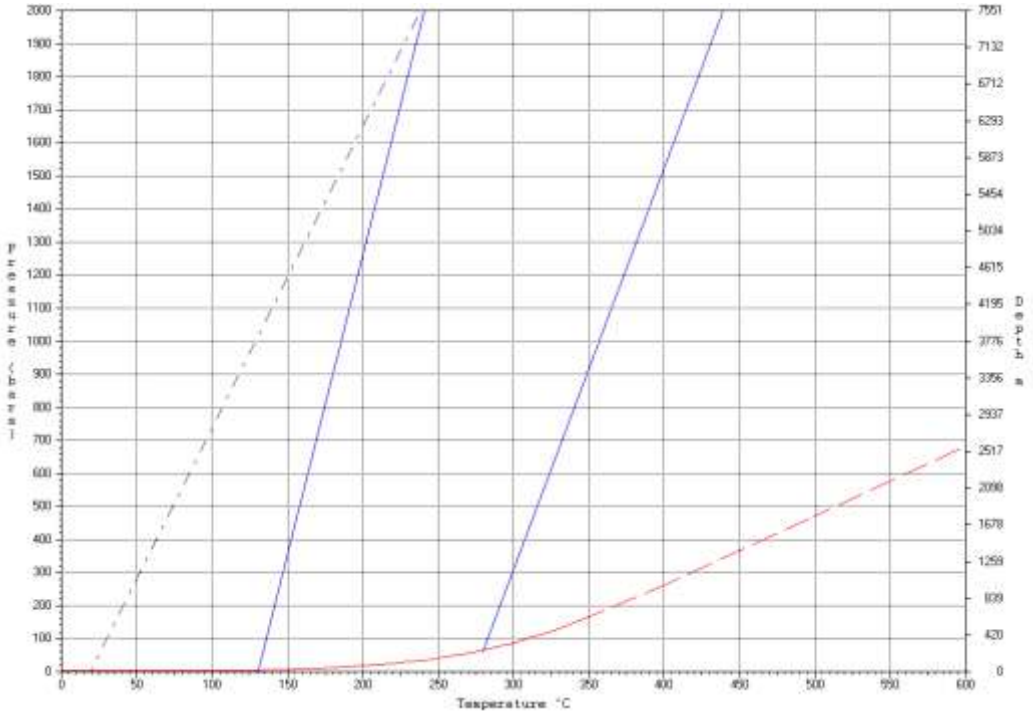

Fig. 6.29. H_2O density (gm/cc) plots of foliated charnockite

Table 6.4. Fluid inclusion of Pyroxene granulite

Sample No	Size	CO_2 (T_m) ºC	CO_2 (T_h) ºC	Density (gm/cm^3)
J.11.28	6.46	-61.8	2	0.9159
	3.38	-61.6	2.25	0.9144
	16.34	-61	2.1	0.9153
	33.28	-61.3	2	0.9159
	12.8	-61.5	2.5	0.9128
	2.03	-59.2	-6.2	0.9635
	2.41	-59	-6.5	0.9651
	6.52	-58.7	-6.1	0.9629
	2.89	-57	-7	0.9678
	1.51	-57.2	-7.5	0.9705
	2.01	-56.9	-6.9	0.9672
	3.38	-56.7	-7.2	0.9689
	1.79	-57	-7	0.9678
	1.44	-56.8	-5.6	0.9602
	1.69	-56.6	-5.8	0.9613
	1.65	-56.7	-5.3	0.9585
	7.13	-57.1	-4.6	0.9547
	1.63	-56.8	-5.2	0.958
	2.07	-56.9	-4.9	0.9563
	1.44	-57	-5	0.9569
	1.79	-57.2	-4.6	0.9547
	1.21	-56.9	-4.9	0.9563
	2.28	-56.7	-5.1	0.9574
	2.62	-57.3	-5	0.9569
	2.39	-57.2	-9	0.9784
	2.44	-57	-6.8	0.9667
	1.5	-57.5	-6.2	0.9635
	2.19	-57.1	-5.8	0.9613
	1.48	-56.9	-4	0.9513

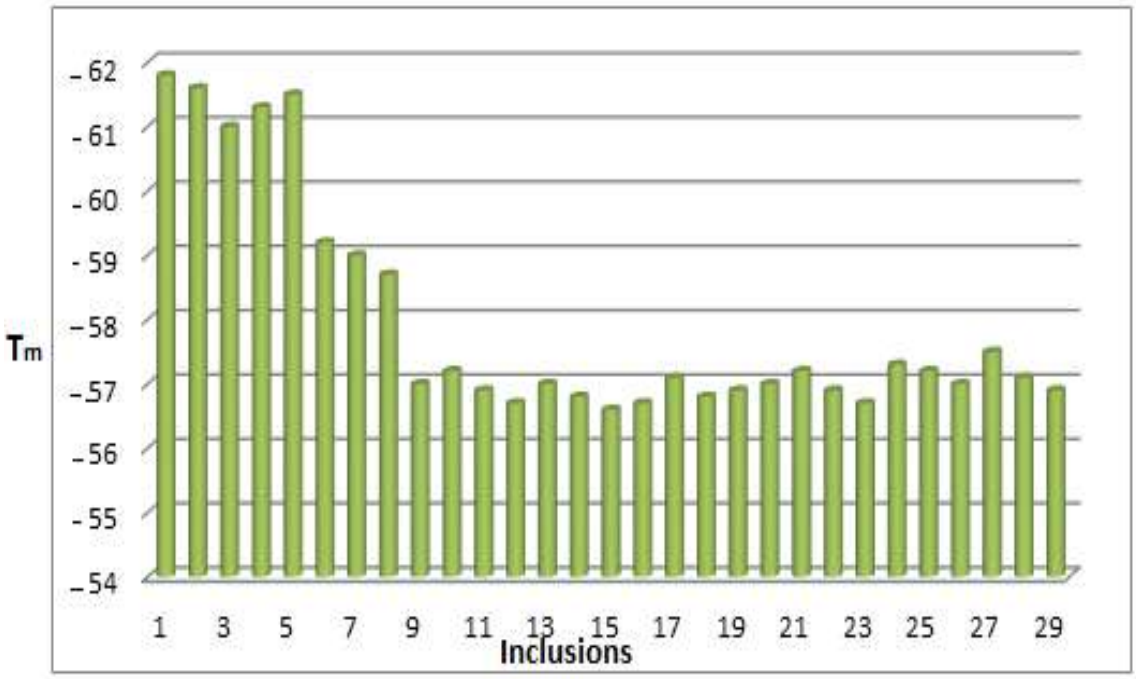

Fig. 6.30. CO_2 melting temperature in Pyroxene granulite

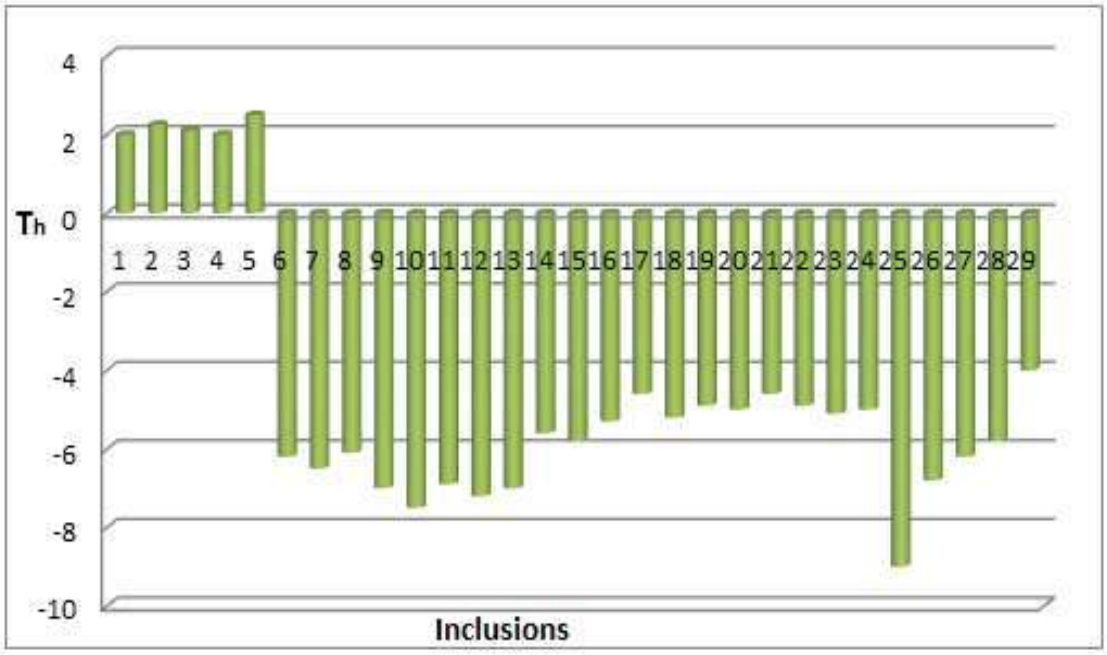

Fig. 6.31. CO_2 homogenization temperature in Pyroxene granulite

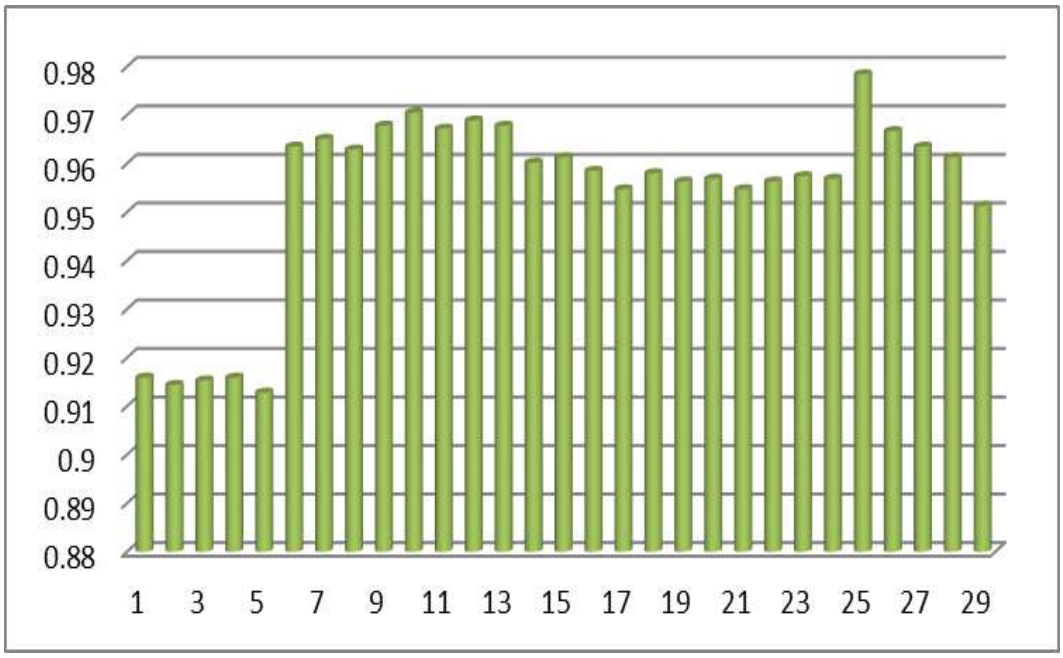

Fig. 6.32. CO_2 density (gm/cc) bar charts of Pyroxene granulite

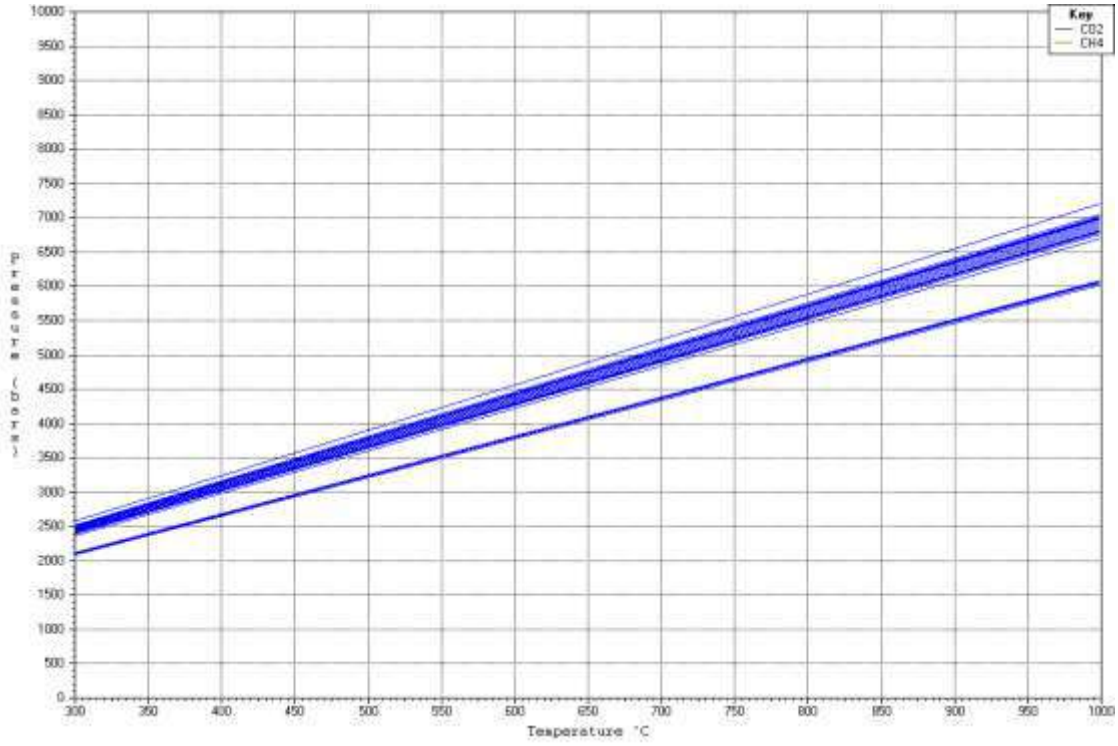

Fig. 6.33. CO_2 density (gm/cc) plots of Pyroxene granulite

Chapter - VII

GEOCHEMISTRY

7.1. Introduction

Granulite facies rocks represent the exhumed sections of the earth's middle and lower crust, hence; they have the record of chemical processes which occur within the deeper part of the crust. The distinct geochemical feature of granulite facies rocks is the depletion of LIL elements viz., U, Th, K, Rb and Ba, (Heier, 1973; Tarney and Windley, 1977, Rollinson and Windley, 1980). As, these elements appear to have been removed from high grade rocks during medium to high grade metamorphism, through the action of fluid, vapour or melt phases, and subsequently transported and concentrated in the upper crust. Geochemistry is an important tool to identify such depletions and the processes associated with them. Hence, a geochemical investigation in an unbroken gneiss-granulite succession is of fundamental relevance in quantifying element mobility. Fyfe (1973), Powell (1983) and Clemens and Vielzuf (1987) have considered, granulite facies rocks are "**restites**", as the granitic melt fraction has been removed from the system. Whereas, Weaver and Tarney (1983), Hansen *et al.*,, (1984, 1987) and Rudnick and Presper (1990) have opined that, CO_2 vapour phase has mobilized the LILE, and the rock is not restite. However, both the processes may have resulted in rather unusual chemical composition of lower crustal rocks. Identification of the protoliths is considered to be another important aspect in medium to high grade terrains. Since, the granulites forms an integral part of Archean high grade terrains (Stephenson, 1980; Weaver *et al.*,, 1982), its chemistry can provide insight into the crust-mantle interaction and the role of mafic magma in the development of the crust.

In this chapter, an attempt is made to present major, trace and REE elements geochemistry of the amphibolite facies gneisses, incipient charnockite, foliated

charnockite and pyroxene granulite and discuss their elemental abundance and elemental mobility in gneiss-granulite transformation and characterization of the protoliths.

7.2. Analytical Methods

The major oxides were analyzed by using Bruker (formerly Siemens) model S4 XRF at Geosciences division, Centre for Earth Science Studies (CESS), Trivandrum. Trace and REE were analyzed by using Perkin Elmer sciex ELAN DRC II Qudra pole ICP-MS at National Institute of Oceanography, Goa. .

For XRF analysis, fusion glass disks were prepared by using claisse Fluxy instrument. Wherein, one gram of the finely powdered sample is mixed with 5gm of flux (LiT/LiM/LiBR 49.75/49.75/0.50, pure) and fused in a platinum crucible. Fused disc are excellent for analyzing major elements as it reduces the effect of matrix and eliminates particle size effects; and provides a homogeneous specimen.

Samples preparation for trace and REE determination acid dilution method is fallowed. It involves digestion of 0.5gm powder of the sample in a Teflon beaker by adding acid mixtures HF: HNO_3 : $HClO_4$ in 7:3:1 ratio and dried the mixture on a Hotplate around 300°C till it becomes a dry paste. Next day, the dry paste is diluted with 1:1 HNO_3 and warm till the digestion is complete. Later, 1ml of Rhodium internal standards is added and the volume is made out to 100ml using double distilled water. From the prepared sample, 25ml was used for analysis by Perkin Elmer sciex ELAN DRC II Qudra pole ICP-MS. MRG-1, W-2, GSP-2 and JB-2 are used as reference standards.

The data obtained were analysed by using software namely; Min Pet and Petrography 2beta to prepare various discriminative diagrams.

7.3. Gneisses

Geochemical data of gneisses of the present study is given in table 7.1. Geochemically, Somvarpet gneisses do not show much variation in bulk chemistry, when compared with Gorur gneiss (Bhaskar Rao *et al.*,, 1991), and also do not show much variations in major oxides among the samples analysed except, SiO_2 content (66.9 to 73.3%). On the Harker's variation diagram (Fig.7.1a-i) the plots of CaO, TiO_2 and P_2O_5 exhibits negative correlation, whereas, Na_2O and K_2O exhibit positive correlation with SiO_2. On A-F-M diagram (fig.7.2), gneisses of the present study show calc-alkaline trend. On CIPW normative daigrams viz., Qtz-Ab-Or (fig 7.3) and of Barker and Arth, (1976) An-Ab-Or (fig.7.4) normative daigram, after O'Conner, (1965) gneisses of the study area falls in the fields of trondjamite and Tonalite – Trondjemite, respectively. Further, K_2O/Na_2O ratio of gneisses ranges from 0.31 to 1.22 which is typical of trondjamites (Bhaskar Rao et al, 1991). Al_2O_3 content of gneisses of Somvarpet ranges from 14.68 to 16.84% with an average of 15.44% can be classified as high Al-TTG (Barker and Arth, 1976).

The trace element data of Somvarpet gneisses is presented in table 7.2. The trace elements viz., Rb, Sr, Ba, Zr, Hf, Nb, Y, Th, U and Pb of Somvarpet gneisses show slight variation in their concentrations. The abundance of incompatible elements are presented in the Fig.7.7, (normalised after Wood *et al.*,,1979), show strong negative anomaly at Ti-P-Sc. LIL elements show unsystematic variation and enrichment viz., Rb from 21.2-104ppm (average of 58.98ppm), Sr from 230-466ppm (average of 339.43), Ba from 232-1293ppm (average of 623.4ppm), Th from 12.1-155ppm (average of 45.36ppm) and U content varies from 0.57-6.46ppm (average of 2.21ppm). The unsystematic variation of these LIL elements could be due to their instability during granite melting or presence of monazite. The average values of trace elements viz., Rb, Sr, Ba, Th and V have slightly

higher concentration and Cr, Zn, Zr, Nb, Y, Sc, Co show lower concentrations when compared to Gorur gneiss, but all these elemental concentrations are comparable to Kabbaldurga and B.R.Hills gneisses (P. Allen *et al.*,, 1984 and K.C.Condie *et al.*,, 1984). The average composition of many of the HFS and transition elements are comparable to Gorur gneiss (Bhaskar Rao *et al.*,, 1991), except few elements, viz., Nb, Y, Cr, Zn and Co, which shows lower concentration. There is a large variation in K/Rb ratios (500-1000) of Somvarpet gneisses (Fig.7.5) and low in Rb/Sr (0.04-0.1) ratios (Fig.7.6). However, Rb/Sr ratios of gneisses of the study area are higher than the upper mantle value (0.03), and are akin to that of continental trondhjemites (Sun, 1982).

The REE data of Somvarpet gneisses is presented in table 7.3. Chondrite normalised REE patterns (after Masuade *et al.*,, 1973) of gneisses presented in fig. 7.8 are charecterised by LREE enrichment and depleted HREE (Eu, Dy and Yb) compare to REE patterns of Gorur and Kabbaldurga gneisses (Bhaskar Rao *et al.*,, 1991; Bhattacharya *et al.*, 1991). The REE plot shows fractionated pattern with $(La/Yb)_N$ ratios ranging from 9.7 – 249.15. The slightly fractionated REE pattern is mainly due to LREE enrichment rather than the HREE depletion. While, the relatively flat REE patterns, especially in the HREE region may be due to the presence of garnet/ hornblende in the litho units. Whereas, the characteristic of negative europium anomaly may suggest that plagioclase is significant in residual phase (Bhaskar Rao et al, 1991).

7.4. Incipient Charnockite

Geochemical data of incipient charnockite of Somvarpet area is presented in table.7.4. The major oxides such as Fe_2O_3, CaO, P_2O_5 and TiO_2 content of incipient charnockite define negative correlation and K_2O positive correlation with SiO_2 (Harker's variation diagram, Fig.7.1a-i), whereas, MnO, MgO, Na_2O and Al_2O_3 do not show any definite trend. When compared with Kabbaldurga Incipient charnockite (Janardhan *et al.*,

1982) Somvarpet incipient charnockite do not show much variation in major oxides, except K_2O. The average K_2O (1.6%) content is slightly lower compared with the reported values of K_2O (3.67%) of Kabbaldurga incipient charnockite (Janardhan *et al.*, 1982). On AFM diagram (fig.7.2) the incipient charnockite display well defined calc-alkaline trend. The calc-alkaline nature of incipient charnockite is substantiated even Ab-Qtz-Or (fig.7.3), An-Ab-Or (Fig.7.4) diagrams. On CIPW normative trilinear diagrams, the rock follows trondjhemitic trend.

REE data of Somvarpet incipient charnockites is presented in table 7.5. The trace element concentrations of Somvarpet incipient charnockite show slight variation i.e., Sr ranges from 295.4-503ppm (average of 408.5ppm), Zr ranges from 25.6-222ppm (average of 116.5ppm), Hf ranges from 0.67-5.5ppm (average of 3.16ppm), Nb ranges from 3.45-14ppm (average of 5.52ppm), Y ranges from 4-21ppm (average of 11.15ppm), Th ranges from 0.3–23.6ppm (average of 12.15ppm), Ba ranges from 195.2-476ppm (average of 341.3ppm) and Pb ranges from 8-18.5ppm (average of 12.1ppm). The abundance of incompatible elements are presented in the daigram (fig.7.9, Chondrite normalized after Wood et al 1979b). The average values of HFS elements and LILE of incipient charnockite are depleted when compared to the Kabbaldurga charnockites (Janardhan *et al.*,, 1982; Stahle *et al.*,, 1987). Incipient charnockite of Somvarpet, show slightly higher contents of Sr, Ba, Zn and Th and lower Zr, Nb, Y, Rb and U. Among the transition elements (Ni, Co, Zn and Cr), Ni and Cr elements s how slight variation, and ranges from 4.5-6.9ppm and 2.6-4.9ppm respectively. The remaining elements such as Zn & Co don't show much variation. However, the average composition of the transition elements are comparable to Kabbaldurga charnockite except Cr, which is lower (Battacharya and Chaudhary, 2013). The incipient charnockites show large variation in K/Rb (800-1200) ratios (Fig.7.5) and low in Rb/Sr (0.03-0.04) ratios (Fig.7.6). Even, Rb/Sr ratios of incipient charnockite Somvarpet have higher values than that of Rb/Sr

values (0.03) the upper mantle (Sun. 1982). On K V/s Rb diagram, the incipient charnockites exhibit depleted granulite trend. This could be due to preferential depletion of Rb relative to K and Sr during granulite grade of metamorphism. The abundance of incompatible trace element patterns (fig.7.9), also indicate the depletion of LILE. The values of these elements are highly dependent on metamorphic grade (Wood *et al.*, 1979). In spider diagram (fig.7.9), the incipient charnockite show prominent Nb-Ti-P anomalies. The negative anomaly of P could be due to apatite fractionation.

REE data of Somvarpet incipient charnockites is presented in table 7.6. The normalized values, after Masuda et al, (1973) are in Fig.7.10. REE data of the study area has been compared with Kabbaldurga charnockite (Battacharya and Chaudhary, 2013). While, the average values of LREE (La and Ce) show slightly higher concentrations, whereas, HREE (Dy and Lu) show lower concentrations. REE plot shows slightly fractionated pattern with $(La/Yb)_N$ ratios ranging from 24.32 – 96.1. The La, Pr, Nd and Ce concentrations are slightly depleted in charnockites compare to gneisses of the area. The slight fractionated REE pattern is mainly due to LREE enrichment rather than the HREE depletion. The LREE enriched pattern observed for Somvarpet are quite similar to the REE patterns of Kabbaldurga charnockite (Bhattacharya *et al.*,, 1991; Friend and Numan, 1992).

7.5. Foliated Charnockite

Geochemical data of foliated charnockites is presented in table 7.7. The average major elemental composition of foliated charnockites of Somvarpet area do not show much variation, except SiO_2 (7% lower than BR hills) and CaO (2% higher than BR hills) when compared with BR hills charnockite (Condie and Allen, 1984). On the Harker's variation diagram (fig.7.1a-i) major elements viz., Fe_2O_3, MnO, CaO, MgO, P_2O_5 and TiO_2 show negative correlation, K_2O exhibits positive correlation with SiO_2, and Na_2O

and Al_2O_3 do not define any definite trend. On the AFM diagram (fig 7.2) of Irvine and Baragar (1971), the foliated charnockites fall well within the calc-alkaline fields. On An-Ab-Or CIPW normative diagram (fig.7.4) of Barker and Arth (1976) and Qtz-Ab-Or (fig.7.3) of Barker and Arth (1976), they plot in the field of tonalite and trondhjemite. Based on the Al_2O_3 content of the foliated charnockites of Somvarpet area can be classified as high Al-TTG, as all the samples have Al_2O_3 >15% (Barker and Arth, 1976). Relatively constant or low values of K_2O, may reflect K-depletion by a fluid phase during granulite facies metamorphism (Sheraton *et al.*, 1973; Tarney, 1976; Janardhan *et al.*, 1982 and Condie *et al.*, 1982).

The trace elements data of Somvarpet foliated charnockites is presented in table 7.8. The average values of trace elements of Somvarpet foliated charnockites show lower Sr, Ba, Zr, and higher Cr, Nb, Cs, Y, Pb, Sc concentrations, compared to B R Hills charnockites (Condie and Allen, 1984). Foliated charnockites of the area are depleted in LILE (Rb, Sr, Ba, Pb, Th and U) when compare to LILE of Incipient charnockite and amphibolite gneisses of the area. Depletion of LILE is a characteristic feature of the granulite facies rocks, and depletion of LILE appears to have developed fluid activity during metamorphism. Relatively constant or low values of K and extreme Rb depletion may reflect the presence of a fluid phase with relatively high CO_2/H_2O ratios (Heier, 1973; Janardhan *et al.*, 1979, 1982 and Condie *et al.*, 1984). The foliated charnockites of the study area have high K/Rb (2000-2500) ratios (fig.7.5), follows distinct depleted granulite trend (DGT). Depletion of Rb and to some extent Sr in the foliated charnockites of the present study has resulted in low to very low Rb/Sr (0.01-0.09) ratios (fig.7.6). The average values of incompatible elements of foliated charnockites are normalized after wood *et al.*, (1979) is given in fig.7.11. The normalized of trace elements abundance suggests strong depletion of Rb and to some extent, U. The strong depletion of Rb compare to K is also evident from higher K/Rb ratios, and comparable to K/Rb ratios reported from charnockites of B.R. Hill, Kabbaldurga and Satanuru – Halguru -

Sivanasamudrum areas (Janardhan *et al.,* 1994; Mahabaleshwar *et al.,* 1995). Ba/Sr ratios which ranges from 0.57 to 0.94 (0.73), are comparable to BR hills charnockites. The charnockites having highest Ba/Sr ratio may indicate high K-feldspar or biotite content. The content of transition metals viz., Ni ranges from 10.89-56.13ppm (20.75ppm), Co 36.13–44.71ppm (40.91ppm) and Cr ranges from 7.95-110ppm (43.96ppm), in the foliated charnockites of the area are relatively high, and also variable. A higher and variable concentration appears to be inherited by the tonalite and trondhjemites protoliths (Condie and Allen, 1984).

The trace elements data of Somvarpet foliated charnockites is presented in table 7.9. REE distribution in the foliated charnockites of the area is similar to those of BR hills charnockite (Condie and Allen, 1984), except Ce (73.42ppm) which is higher than the BR hills charnockite. REE patterns also resemble Archean TTG suite (Barker and Arth, 1976; Jahn *et al.*, 1981; Martin, 1987). Chondrite normalized (after Masuda *et al.*, 1973) REE plot (fig.7.12) indicates, LREE concentrations vary more than HREE with $(La/Yb)_N$ ratios ranging from 4.66-83.68.

7.6. Pyroxene Granulite

Geochemical data of pyroxene granulites of Somvarpet area presented in table.7.10, do not show much variation in bulk chemistry, when compare to BR hills mafic granulites (Janardhan *et al.,*, 1994). The major oxides viz., CaO, MgO, Al_2O_3 and Fe_2O_3, exhibit negative correlation with SiO_2 on Harker's diagram (Fig.7.13a-i). On AFM (Fig.7.14) and FeO^T/MgO Vs SiO_2 (Fig.7.19) diagrams of pyroxene granulites of Somvarpet show tholeiitic affinity with iron enrichment, which is the characteristic feature of Archean tholeiites (Ramachandra and Ray, 2001)? In (Na_2O+K_2O) Vs SiO_2 diagram (Fig.7.16), pyroxene granulites falls within the basaltic field. The oxides like Na_2O and K_2O are considered to be mobile during metamorphism (Stephenson. 1980). Therefore, TiO_2, MnO and P_2O_5 diagram of Winchester and Flooyd (1977) was used, in

which, the pyroxene granulites of study area plot well within the Island Arc tholeiitic field.

The trace elements data of Somvarpet pyroxene granulite is presented in table 7.11. The trace element concentrations pyroxene granulites of Somvarpet are slightly variable (Fig.7.17). The HFS elements viz., Nb, Hf, and Y, do not show much variation, whereas, Zr, show large variation (15.3 to 103.6ppm). The transition elements such as Ni and Cr are slightly variable in their content, and ranges from 76.92-274.1ppm and 38.6-509.2ppm, respectively. However, the average composition of the transition elements are little higher, when compared to BR Hill granulites (Janardhan *et al.,* 1994). Somvarpet pyroxene granulites are slightly enriched in Ni, but depleted in Cr when compare to the Archean tholeiites (Condie, 1985). LILE contents are low to moderate with variable and higher K/Rb (500-900) ratio (Fig.7.20) and low Rb/Sr (0.01-0.03) ratios, Fig.7.21). The Rb/Sr ratios are even lower than the upper mantle values (Sun, 1982). Rb (2-8.61ppm) and Pb (0.47-5.92ppm) values show unsystematic variation, and could be due to their instability during metamorphism. The average content of the Rb (6.60ppm) of Somvarpet pyroxene granulite is almost similar to the BR Hill granulites (Janardhan *et al.,* 1994), however, very low when compared to the average content of Rb (about 12ppm) in Archean tholeiites (Condie, 1985). This is probably due to the relative loss of Rb to K during granulite facies metamorphism. The same is substantiated by the K Vs Rb diagram, wherein, the pyroxene granulites follow depleted granulite trend. The La/Nb ratio of Somvarpet pyroxene granulites varies from 1.37 to 6.95, suggesting variable degree of crustal contamination of mantle derived magmas (Thomson *et al.,* 1984).

The REE data of Somvarpet pyroxene granulite is presented in table 7.12. REE plot (Fig.7.18) shows sub parallel to slightly fractionated pattern with $(La/Yb)_N$ ratios of 0.96-4.08. The fractionated pattern REE is mainly due to LREE enrichment rather than HREE depletion. The LREE enriched pattern of pyroxene granulites of the study area is quite similar to the LREE patterns of B.R. Hill mafic granulites (Janardhan *et al.,* 1994).

Table 7.1. Major oxides (%) of Gneisses

Major oxides	J.11.19C	J.11.2	J.11.27	J.11.11	J.11.41	J.11.35A	Min.	Max.	Average	***
SiO_2	71.47	69.96	72.68	73.32	72.35	70.52	69.96	73.32	71.71	76.31
TiO_2	0.39	0.10	0.08	0.09	0.20	0.483	0.08	0.48	0.22	0.59
Al_2O_3	15.93	16.84	15.52	14.89	14.81	14.68	14.68	16.84	15.44	12.1
Fe_2O_3	0.79	0.08	0.07	0.07	0.13	0.72	0.07	0.79	0.31	3.23
FeO	1.99	0.75	0.63	0.67	1.17	1.89	0.63	1.99	1.18	-
Mno	0.02	0.01	0.01	0.01	0.02	0.02	0.01	0.02	0.01	0.04
MgO	0.94	0.20	0.10	0.12	0.33	0.58	0.10	0.94	0.37	0.39
CaO	2.94	2.43	1.25	1.55	1.51	1.81	1.25	2.94	1.91	1.41
Na_2O	4.58	5.11	4.53	4.73	3.80	4	3.80	5.11	4.45	3.63
K_2O	1.42	3.44	4.44	3.55	4.64	3.78	1.42	4.64	3.54	1.02
P_2O_5	0.04	0.14	-	0.03	0.08	0.16	0.03	0.16	0.09	0.02

Note : *** = Gorur Gneiss (Bhaskar Rao *et al*., (1991)

Table 7.2. Trace elements (ppm) of Gneisses

Trace elements	J.11.19C	J.11.2	J.11.27	J.11.11	J.11.41	J.11.35A	Min.	Max.	Average	***
Rb	34	51.39	21.2	69.13	104.4	74	21.2	104.4	58.98	45
Sr	466	361.1	232	350.3	230.2	397	230.2	466	339.43	73
Ba	232	611.2	294.8	472.4	1293	837	232	1293	623.4	71
Cr		1.10	0.30	1.79	0.774		0.30	1.79	0.99	18.5
Zn	60					50	50	60	55	112
Zr	169	218.6	111.3	112.1	94.04	323	94.04	323	171.34	235
Hf	4.4	5.3	4.66	3.71	2.49	6.9	2.49	6.9	4.57	6
Nb	12	1.38	4.63	2.1	4.16	8	1.38	12	5.37	16.5
Cs	-	0.22	0.55	0.39	0.60	ND	0.22	0.60	0.44	-
Y	13	33.24	15.46	12.82	11.32	14	11.32	33.24	16.64	83
Th	23.3	155.7	16.77	36.89	12.14	27.4	12.14	155.7	45.36	3.8
U	1.3	1.78	6.46	2.05	0.57	1.1	0.57	6.46	2.21	3.4
Cu	20	-	-	-	-	20	20	20	20	-
Pb	15	49.93	28.48	24.68	12.86	19	12.86	49.93	24.99	-
Ga	19	33.66	22.65	19.71	16.41	17	16.41	33.66	21.40	20.5
Sc	4	0.58	2.19	1.04	1.43	3	0.58	4	2.04	8.5
V	42	9.32	23.42	13.49	14.19	32	9.32	42	22.40	7
Co	24	30.07	35.33	21.27	36.58	31	21.27	36.58	29.70	49
Ni	-	5.41	-	-	5.84	-	5.41	5.84	5.62	4.5

Note : *** = Gorur Gneiss (Bhaskar Rao *et al*., (1991)

Table 7.3. Rare Earth Elements (ppm) of Gneisses

REE	**J.11.19C**	**J.11.2**	**J.11.27**	**J.11.11**	**J.11.41**	**J.11.35A**	**Min.**	**Max.**	**Average**	***
La	62.2	444	21.14	54.8	36.14	101	21.14	444	119.88	23.3
Ce	130	462	107	211	119.0	183	107	462	202	52.5
Pr	13.4	83.61	4.80	11.26	6.10	17.7	6.10	83.61	22.81	5.9
Nd	47.5	336.7	19.83	45.91	25.12	58	19.83	336.7	88.84	27.5
Sm	8.2	40.06	4.92	8.06	23.65	8.1	8.06	40.06	15.49	8.15
Eu	1.51	2.33	0.62	1	1.24	1.33	0.62	2.33	1.33	3.65
Gd	5.9	29.69	3.65	6	2.82	5.6	2.82	6	8.94	8.3
Tb	0.7	2.92	0.58	0.78	0.38	0.6	0.38	2.92	0.99	1.3
Dy	3	8.97	2.73	2.97	1.80	3.1	1.80	8.97	3.76	8.05
Ho	0.5	1.07	0.40	0.39	0.30	0.5	0.30	1.07	0.52	-
Er	1.1	2.86	1.22	0.94	0.94	1.3	0.94	2.86	1.39	2.35
Tm	0.13	0.21	0.21	0.10	0.12	0.16	0.10	0.21	0.15	0.65
Yb	0.7	1.08	1.32	0.58	0.73	0.9	0.58	1.32	0.88	2.8
Lu	0.11	0.16	0.21	0.09	0.11	0.12	0.09	0.21	0.13	0.75
K_2O/Na_2O	0.31	0.67	0.98	0.75	1.22	0.94	0.31	1.22	-	-
$(La/Yb)_N$	112.55	249.15	9.70	57.26	30	68.01	9.70	249.15	-	-

Note : *** = Gorur Gneiss (Bhaskar Rao *et al*., (1991)

Table 7.4. Major oxides (wt %) of Incipient charnockite

Major oxides	J.11.19B	J.11.3	J.11.27A	J.11.10	J.11.40	J.11.35	Min.	Max.	Average	***
SiO_2	71.05	69.71	66.57	68.2	72.02	71.13	66.57	72.02	69.78	71.4
TiO_2	0.37	0.28	0.29	0.57	0.281	0.17	0.17	0.37	0.32	0.49
Al_2O_3	15.26	16.16	16.81	13.69	15.43	15.78	13.69	16.81	15.52	13.7
Fe_2O_3	0.66	0.22	3.44	2.05	0.70	0.44	0.22	3.44	1.25	1.6
FeO	1.75	2.04	0.34	5.49	1.75	1.33	0.34	5.49	2.11	3.13
Mno	0.02	0.02	0.09	0.041	0.052	0.03	0.02	0.09	0.04	0.06
MgO	0.41	0.68	1.06	0.52	0.69	0.47	0.41	1.06	0.63	0.79
CaO	2.97	3.10	4.26	2.54	2.6	2.77	2.54	4.26	3.04	1.95
Na_2O	4.33	5.20	5.38	4.21	4.89	5.20	4.21	5.38	4.86	3.76
K_2O	2.02	1.47	1.05	1.19	1.88	2.01	1.05	2.02	1.60	3.67
P_2O_5	0.09	0.37	0.26	0.09	0.09	0.12	0.09	0.12	0.17	0.12

Note : *** = Kabbaldurga (Janardhan *et al.,* 1982)

Table 7.5. Trace elements (ppm) of Incipient charnockite

Trace elements	J.11.19B	J.11.3	J.11.27A	J.11.10	J.11.40	J.11.35	Min.	Max.	Average	***
Rb	18	26.27	14.52	20	28	29.82	14.52	29.82	22.77	44
Sr	399	503.3	295.4	440	462	351.7	295.4	503.3	408.57	234.5
Ba	454	294.8	195.2	213	415	476.3	195.2	476.3	341.38	312.5
Cr	-	0.52	3.95	-	-	10.56	0.52	10.56	5.01	5.8
Zn	< 30	-	-	130	50	-	< 30	130	90.00	62.7
Zr	145	118.9	25.6	222	149	38.83	25.6	222	116.56	271.9
Hf	3.3	2.98	0.67	5.5	3.5	2.98	0.67	5.5	3.16	-
Nb	4	3.71	3.45	4	14	3.95	3.45	14	5.52	21.5
Cs	-	0.21	0.11	-	-	0.15	0.11	0.21	0.16	-
Y	4	21.1	9.88	15	9	7.93	4	21.1	11.15	26.5
Th	0.3	23.67	6.50	32	7.7	2.71	0.3	23.67	12.15	6.1
U	0.2	0.79	0.44	0.9	0.7	0.35	0.2	0.79	0.56	1.3
Cu	<10	-	-	<10	10	-	10	10	10.00	31.8
Pb	8	18.52	8.55	12	14	11.8	8	18.52	12.15	-
Ga	15	24.51	19.96	23	17	19.88	15	24.51	19.89	-
Sc	02	2.19	4.11	03	04	2.39	02	4.11	2.95	8.4
V	53	23.42	19.53	93	28	15.45	15.45	93	38.73	109.1
Co	32	58.42	36.9	35	26	42.93	26	58.42	38.54	71.8
Ni	-	5.16	9.57	-	-	15.87	5.16	9.57	10.20	8.7

Note : *** = Kabbaldurga (Janardhan *et al.,* 1982)

Table 7.6. Rare Earth Elements (ppm) of Incipient charnockite

REE	J.11.19B	J.11.3	J.11.27A	J.11.10	J.11.40	J.11.35	Min.	Max.	Average	***
La	18.2	85.04	51.3	111	37.5	20.87	18.2	111	53.99	44.3
Ce	28	376.7	199.8	213	72.9	111.6	28	376.7	167.00	81.5
Pr	2.59	17.33	8.46	21.9	6.3	3.69	2.59	21.9	10.05	8.7
Nd	8.9	72.03	34.25	76.9	21.3	15.34	8.9	76.9	38.12	30.1
Sm	1.3	11.07	3.87	1.2	2.9	2.44	1.2	11.07	3.80	5.5
Eu	1.14	1.86	1.11	1.64	1.04	0.95	0.95	1.86	1.29	1.2
Gd	01	8.66	3.19	7.6	2.2	1.92	01	8.66	4.10	5.7
Tb	0.1	1.13	0.39	0.8	0.3	0.29	0.1	1.13	0.50	0.8
Dy	0.7	4.60	1.70	3.7	1.5	1.29	0.7	4.60	2.25	7.5
Ho	0.1	0.65	0.28	0.6	0.3	0.22	0.1	0.65	0.36	1
Er	0.3	1.58	0.92	1.4	0.9	0.65	0.3	1.58	0.96	-
Tm	<0.05	0.16	0.13	0.14	0.13	0.09	<0.05	0.16	0.13	-
Yb	0.3	0.79	0.83	0.7	0.8	0.52	0.3	0.83	0.66	2
Lu	0.05	0.10	0.13	0.09	0.14	0.07	0.05	0.14	0.10	4
$(La/Yb)_N$	36.76	65.23	37.45	96.1	28.4	24.32	24.32	96.1	-	-

Note : *** = Kabbaldurga (Janardhan *et al.*, 1982)

Table 7.7. Major oxides (wt %) of Foliated charnockite

Major oxides	J.11.20	J.11.18	J.11.19A	J.2.4	J.11.37	J.11.32	J.11.33	Min.	Max.	Average	***
SiO_2	61.15	56.02	63.75	65.93	61.82	59.43	64.13	56.02	65.93	61.75	68.59
TiO_2	1.02	1.36	0.56	0.47	0.73	0.86	0.47	0.47	1.36	0.78	0.43
Al_2O_3	15.36	15.65	17.94	17.18	16.82	17.25	18.02	15.36	17.94	16.89	15.9
Fe_2O_3	2.61	3.18	-	-	-	-	-	2.61	3.18	2.90	3.09
FeO	6.51	8.19	4.21	3.72	5.79	6.41	3.84	3.72	8.19	5.52	-
Mno	0.13	0.15	0.06	0.05	0.09	0.08	0.05	0.05	0.15	0.09	0.03
MgO	2.41	3.34	1.03	0.94	1.75	2.33	1.19	0.94	2.41	1.86	1.25
CaO	5.92	6.97	4.93	4.09	5.87	6.09	4.14	4.09	6.97	5.43	3.46
Na_2O	4.22	4.27	5.58	5.51	4.81	5.07	5.74	4.22	5.74	5.03	5.22
K_2O	0.95	0.59	0.84	1.03	1.04	1.27	1.29	0.59	1.29	1.00	1.17
P_2O_5	0.25	0.23	0.27	0.21	0.32	0.40	0.22	0.21	0.40	0.27	0.13

Note : *** = BR hill charnockites (Condie and Allen, 1984)

Table 7.8. Trace elements (ppm) of Foliated charnockite

Trace elements	J.11.20	J.11.18	J.11.19A	J.2.4	J.11.37	J.11.32	J.11.33	Min.	Max.	Average	***
Rb	3	< 2	4.04	4.05	16.31	22.53	22.52	2	22.52	12.08	10.5
Sr	275	341	455.8	439	286.1	358.2	494.7	275	494.7	378.54	787
Ba	235	197	307	416.2	168	270.9	390.1	197	416.2	283.46	449.75
Cr	100	110	7.95	8.92	28.05	42.56	10.21	7.95	110	43.96	20.75
Zr	94	163	44.27	68.01	119.2	89.02	40.29	40.29	119.2	88.26	145
Hf	2.2	3.5	1.11	1.72	3.06	2.17	0.99	0.99	3.5	2.11	3.47
Nb	15	14	6.52	5.68	21	10.53	5.91	5.68	21	11.23	3.85
Cs	30	25	0.03	0.05	0.14	0.13	0.17	0.03	30	7.93	0.03
Y	0.1	0.4	12.39	6.64	50.8	24.39	9.49	0.1	50.8	14.89	3.3
Th	0.1	0.1	0.32	11.53	8.53	1.79	0.89	0.1	11.53	3.32	1.77
U	0.1	0.1	0.18	0.53	0.90	0.44	0.28	0.1	0.90	0.36	0.12
Pb	5	5	4.73	7.92	9.15	6.0	6.34	4.73	9.15	6.31	2
Ga	11	19	20.76	21.22	20.26	21.31	21.48	11	21.48	19.29	-
Sc	121	269	6.05	3.48	10.21	10.45	3.5	3.5	269	60.53	3.27
V	47	53	62.38	39.31	66.09	68.36	31.29	31.29	68.36	52.49	-
Co	-	-	40.76	38.29	44.71	44.68	36.13	36.13	44.71	40.91	-
Ni	17	18	12.77	21.99	30.22	56.13	10.89	10.89	56.13	23.86	20.75

Note : *** = BR hill charnockites (Condie and Allen, 1984)

Table 7.9. Rare Earth Elements (ppm) of Foliated charnockite

REE	J.11.20	J.11.18	J.11.19A	J.2.4	J.11.37	J.11.32	J.11.33	Min.	Max.	Average	***
La	20.8	27.8	25.94	73.18	41.26	30.1	29.78	20.8	73.18	35.55	30.5
Ce	45.4	59	58.26	155.2	253.5	206	105.8	45.4	253.5	126.17	52.75
Pr	5.42	6.86	4.58	10.04	10.5	7.10	5.07	4.58	10.5	7.08	-
Nd	22.4	27	18.98	41.95	41.73	29.45	21.45	21.45	41.95	28.99	-
Sm	4.9	5.3	2.97	3.37	8.10	5.55	3.07	2.97	8.10	4.75	2.4
Eu	1.5	1.72	1.53	1.20	1.58	2.01	1.21	1.20	2.01	1.54	1.22
Gd	5	5	2.71	3.03	7.03	4.84	2.56	2.56	7.03	4.31	-
Tb	0.8	0.8	0.381	0.32	1.23	0.73	0.34	0.32	0.8	0.66	0.16
Dy	5.1	4.7	0.92	1.25	6.99	3.76	1.58	1.25	6.99	3.47	-
Ho	1	1	0.36	0.20	1.34	0.69	0.27	0.20	1	0.69	-
Er	2.9	2.7	1.12	0.70	4.44	2.11	0.85	0.70	2.9	2.12	-
Tm	0.42	0.41	0.16	0.09	0.78	0.33	0.11	0.09	0.42	0.33	-
Yb	2.7	2.6	0.9	0.53	4.93	2.06	0.65	0.53	2.7	2.05	0.29
Lu	0.42	0.42	0.15	0.09	0.78	0.32	0.10	0.09	0.78	0.33	0.04
Ba/Sr	0.85	0.57	0.67	0.94	0.58	0.75	0.78	0.57	0.94	0.73	-
$(La/Yb)_N$	4.66	6.48	17.46	83.68	5.07	8.85	27.76	4.66	83.68	-	-

Note : *** = BR hill charnockites (Condie and Allen, 1984)

Table 7.10. Major oxides (wt %) of Pyroxene granulite

Major oxides	J-11-22	J-11-36	J-11-16	J-11-5	J-11-21	J-11-12	J-11-26	J-11-30	J-11-24	J-11-17	J.11.6	Min.	Max.	Average	***
SiO_2	51.81	50.03	51.03	50.98	49.87	50.28	50.68	49.72	50.06	50.49	49.99	49.72	51.81	50.45	49.65
TiO_2	1.06	0.85	1.03	1.27	0.93	1.32	1.18	1.05	0.89	0.98	1.12	0.85	1.32	1.06	0.86
Al_2O_3	13.22	16.01	12.34	15.57	15.95	14.56	16.0	15.96	11.90	11.25	15.48	11.25	16.01	14.39	14.12
FeO	13.80	9.94	10.81	11.85	11.38	13.99	12.27	11.11	11.64	11.69	12.09	9.94	13.99	11.87	12.39
Fe_2O_3	1.53	1.10	1.20	1.32	1.26	1.55	1.36	1.23	1.29	1.30	1.33	1.10	1.55	1.32	-
Mno	0.21	0.15	0.19	0.18	0.19	0.21	0.19	0.17	0.21	0.21	0.19	0.15	0.21	0.19	0.19
MgO	6.65	8.76	7.93	4.66	5.56	4.18	4.37	5.68	8.31	8.71	5.28	4.18	8.71	6.37	7.71
CaO	10.8	11	12.52	10.25	11.67	9.74	10.66	11.19	12.93	12.78	10.71	10.66	12.93	11.30	11.03
Na_2O	1.99	2.19	1.96	2.79	2.51	3.03	2.65	3.05	1.84	1.86	2.55	1.84	3.05	2.40	2.69
K_2O	0.22	0.17	0.22	0.28	0.20	0.53	0.22	0.22	0.19	0.21	0.24	0.17	0.53	0.25	0.52
P_2O_5	0.08	0.09	0.15	0.22	0.15	0.26	0.19	0.21	0.12	0.15	0.15	0.08	0.22	0.16	0.2

Note : *** = BR hill (Janardhan *et al.*, 1982)

Table 7.11. Trace elements (ppm) of Pyroxene granulite

Trace elements	J-11-22	J-11-36	J-11-16	J-11-5	J-11-21	J-11-12	J-11-26	J-11-30	J-11-24	J-11-17	J.11.6	Min.	Max.	Average	***
Rb	5	2	6.48	8.61	5.95	18.61	5.64	3.58	4.55	5.63	7.20	2	18.61	6.66	6
Sr	162	204	131.7	187.4	169.8	151.3	183.2	229.8	108	120.6	177.8	108	187.4	165.96	163.42
Ba	49	44	39.44	62.34	40.36	210.9	61.23	53.55	53.12	44.07	49.5	39.44	62.34	64.32	38.57
Zr	60	70	29.37	40.13	20.11	103.6	25.23	27.79	15.3	24	24.75	15.3	70	40.03	70.68
Hf	1.6	2	0.91	1.13	0.75	2.73	0.87	0.94	0.59	0.88	0.85	0.59	2	1.20	1.78
Nb	2	4	2.87	3.90	2.27	6.16	3.10	5.11	2.01	2.66	2.66	2	6.16	3.34	5
Y	18	18	26.48	32.48	21.69	47.94	27.16	30.36	20.72	23.35	25.69	18	47.94	26.53	-
Th	0.7	1.5	0.97	1.41	0.59	2.54	0.85	0.75	0.86	0.64	1.07	0.59	2.54	1.08	0.47
U	0.2	0.2	0.26	0.31	0.65	0.65	0.33	0.23	0.28	0.33	0.33	0.2	0.65	0.34	0.27
Pb	5	5	2.10	2.02	1.50	5.41	5.92	2.26	0.47	1.60	1.35	0.47	5.41	2.97	-
Ga	16	15	15.85	21.13	16.43	19.11	20.16	19.16	13	14.23	19.01	13	21.13	17.19	-
Sc	37	25	43.76	35.49	36.69	36.13	32.54	28.01	39.13	38.81	30.65	25	39.13	34.84	38.42
V	355	242	208.2	223.1	198.9	205.4	217.1	208.1	147.6	135.8	145.8	135.8	355	207.91	-
Co	68	58	59.32	70.1	66.52	71.04	79.23	83.46	71.68	76.55	82.85	58	82.85	71.52	53.28
Be	1	1	0.43	0.58	0.38	0.82	0.45	0.59	0.26	0.32	0.28	0.26	1	0.56	-
Cr	130	400	509.2	38.6	251.6	99.77	87.16	173.2	375.5	530.4	56.41	56.41	530.4	241.08	175.28
Ni	90	260	217.2	101.2	140.3	76.92	99.51	163.9	262.4	274.1	126.5	76.92	274.1	164.73	128.1
Cs	<0.5	<0.5	0.23	0.26	0.18	0.52	0.25	0.10	0.14	0.21	0.23	0.10	0.52	0.24	-

Note : *** = BR hill (Janardhan *et al.*, 1982)

Table 7.12. Rare Earth Elements (ppm) of Pyroxene granulites

REE	J-11-22	J-11-36	J-11-16	J-11-5	J-11-21	J-11-12	J-11-26	J-11-30	J-11-24	J-11-17	J.11.6	Min.	Max.	Average
La	5.2	11	5.67	8.55	4.47	12.87	5.98	9.11	4.69	5.58	6.39	4.47	11	7.23
Ce	12.9	27.2	15.41	23.12	12.35	33.9	18.17	26.6	20.62	34.94	42.27	12.9	42.27	24.32
Pr	1.8	3.1	1.98	2.85	1.57	3.9	2.16	2.95	1.58	1.88	2.18	1.57	3.9	2.36
Nd	8.7	13.4	8.49	12.19	6.74	16.53	9.19	12.63	6.83	8.46	9.44	6.83	16.53	10.24
Sm	2.7	3	2.86	3.78	2.35	4.75	3.16	3.80	2.47	2.95	3.34	2.47	4.75	3.20
Eu	1.01	1.1	1.05	1.35	0.93	1.52	1.18	1.47	0.91	1.07	1.27	0.91	1.52	1.17
Gd	3.2	3.3	3.44	4.41	2.90	5.62	3.72	4.24	2.83	3.20	3.67	2.83	5.62	3.68
Tb	0.6	0.6	0.65	0.81	0.56	1.06	0.71	0.77	0.56	0.64	0.72	0.56	1.06	0.70
Dy	3.7	3.5	3.90	4.79	3.38	6.62	4.35	4.56	3.27	3.85	4.13	3.27	6.62	4.19
Ho	0.7	0.7	0.77	0.96	0.65	1.38	0.83	0.91	0.63	0.70	0.76	0.63	0.96	0.82
Er	2	1.9	2.43	2.93	2.05	4.58	2.54	2.90	1.87	2.12	2.31	1.87	4.58	2.51
Tm	0.29	0.28	0.34	0.43	0.30	0.69	0.37	0.44	0.29	0.32	0.35	0.28	0.69	0.37
Yb	1.7	1.7	1.84	1.27	1.61	3.96	1.98	2.45	1.65	1.91	2.07	1.61	3.96	2.01
Lu	0.26	0.26	0.29	0.35	0.26	0.64	0.31	0.38	0.24	0.28	0.31	0.24	0.64	0.33
$(La/Yb)_N$	1.85	3.92	0.91	4.8	1.68	1.96	1.83	2.25	1.72	1.77	1.87	0.91	4.8	-

Note : Light Blue Square indicates gneiss, red circle indicates incipient charnockite and green triangle indicates foliated charnockite.

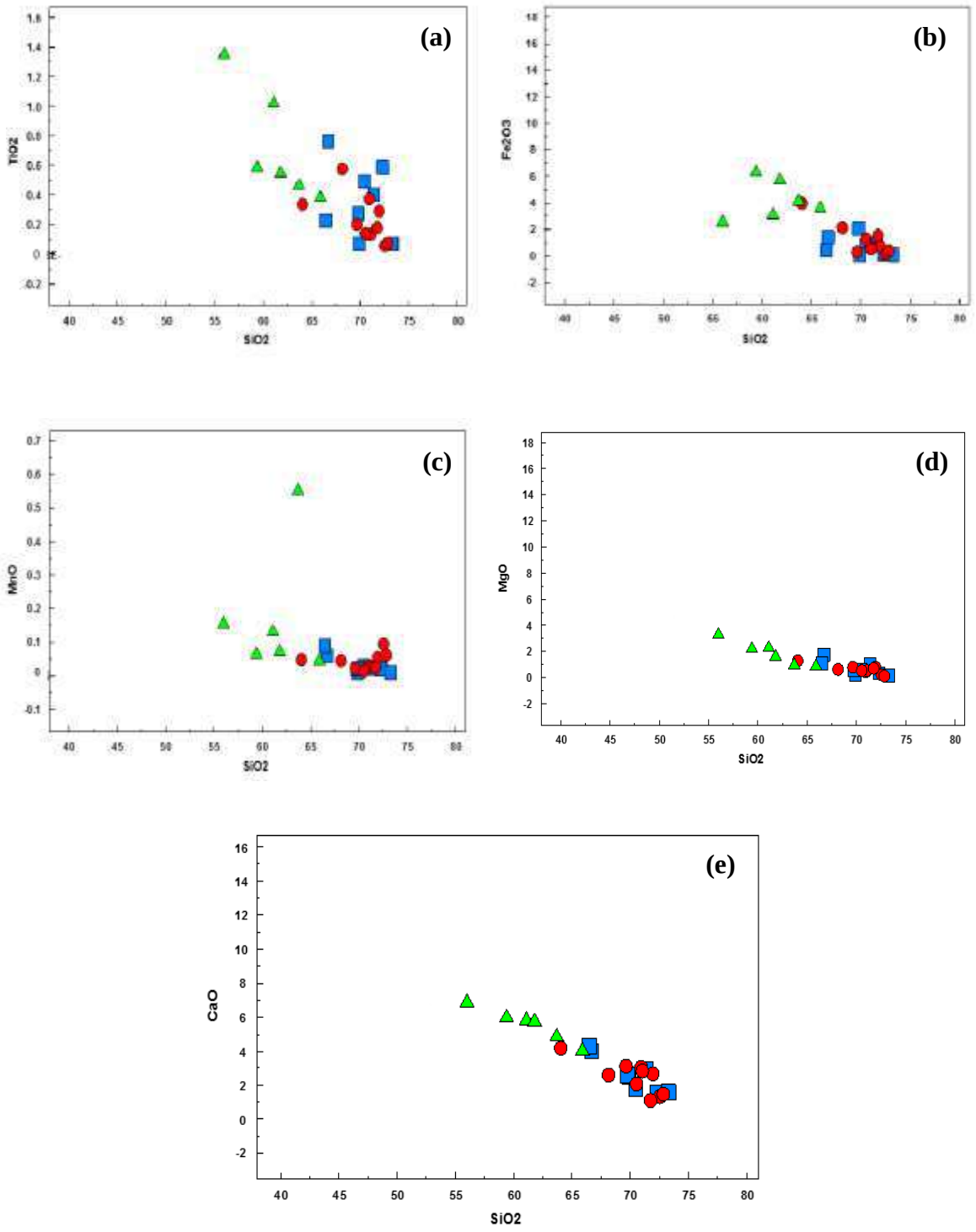

Fig. 7.1a-e. Harker's Variation diagram of gneisses, Incipient charnockite and foliated charnockite

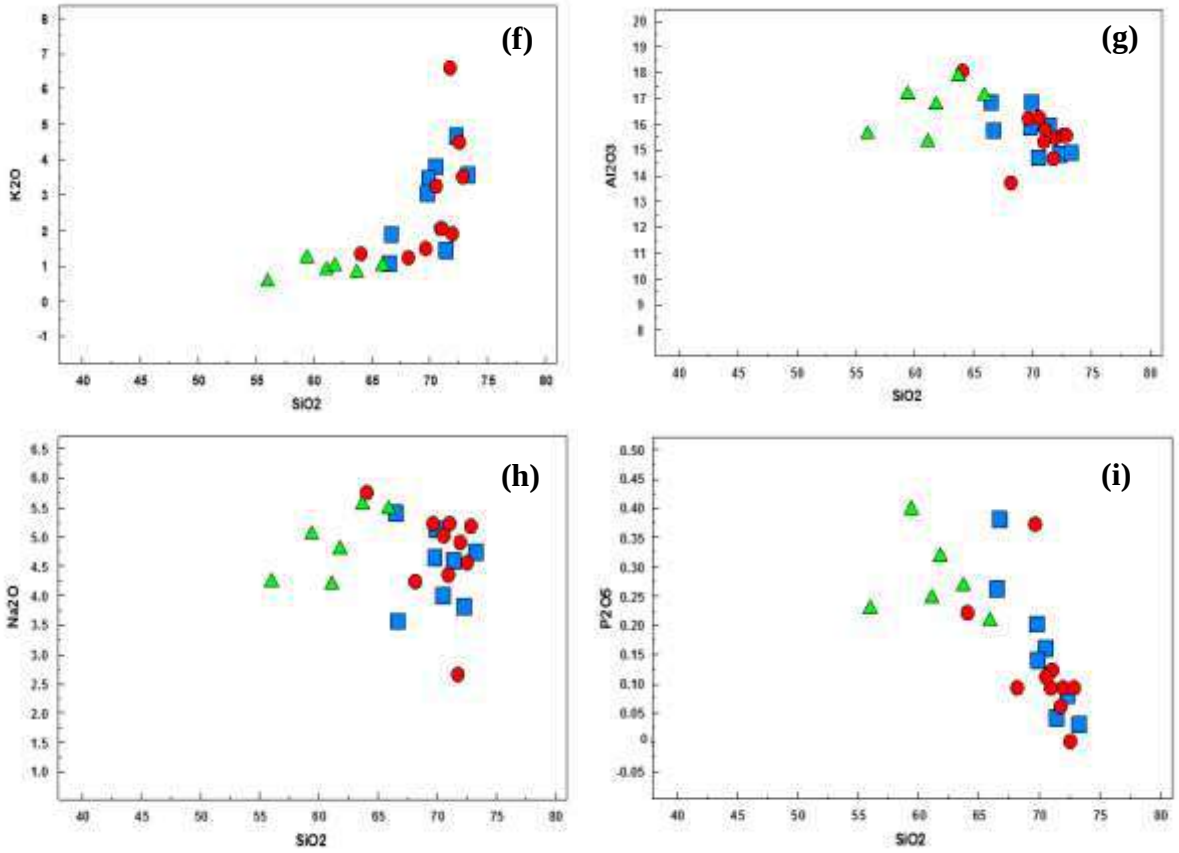

Fig. 7.1f-i. Harker's variation diagram of gneisses, Incipient charnockite and foliated charnockite

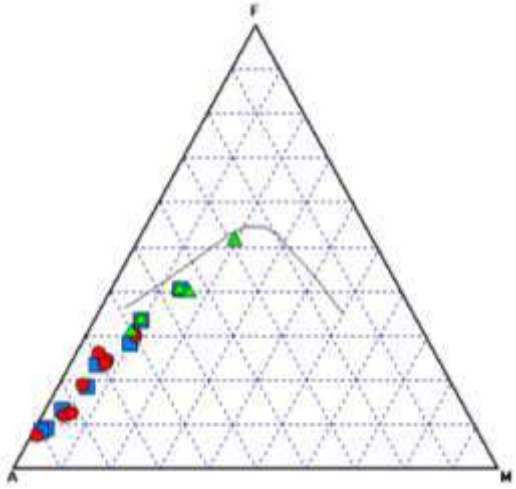

Fig.7.2. A-F-M diagram of gneisses, Incipient charnockite and foliated charnockite, after Irvine and Baragar (1971)

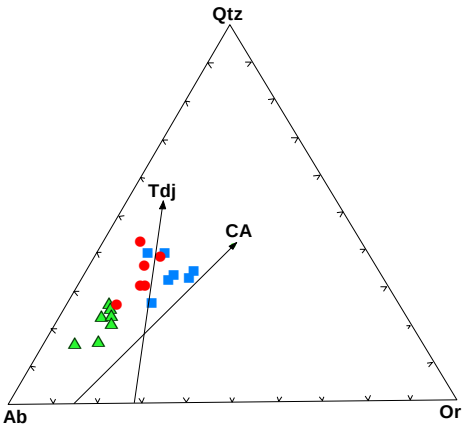

Fig.7.3. Qtz-Ab- Or normative diagram after Barker and Arth (1976) for gneisses, Incipient charnockite and foliated charnockite

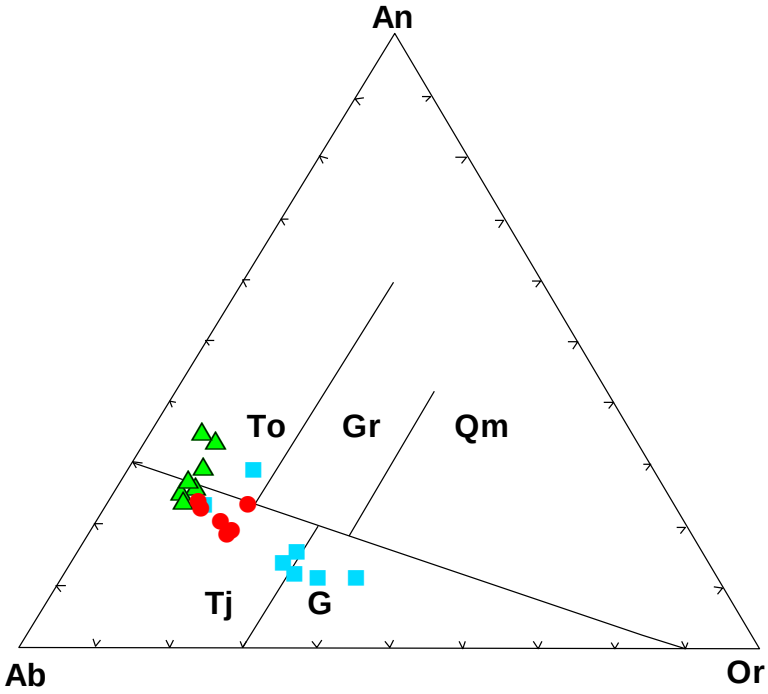

Fig. 7.4. An-Ab-Or normative diagram after O'Conner, (1965) for gneisses, Incipient charnockite and foliated charnockite.

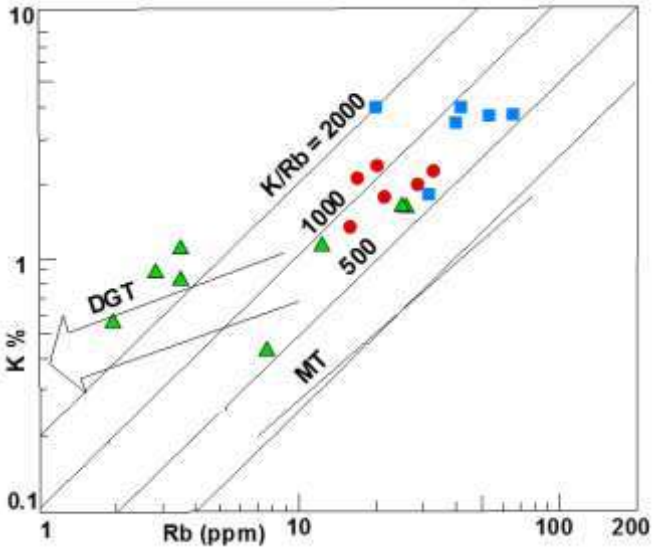

Fig.7.5. K-Rb distribution in gneisses, Incipient charnockite and foliated charnockite. MT (main trend for continental crust defines by Shaw, 1968). DGT (Depleted granulite trend)

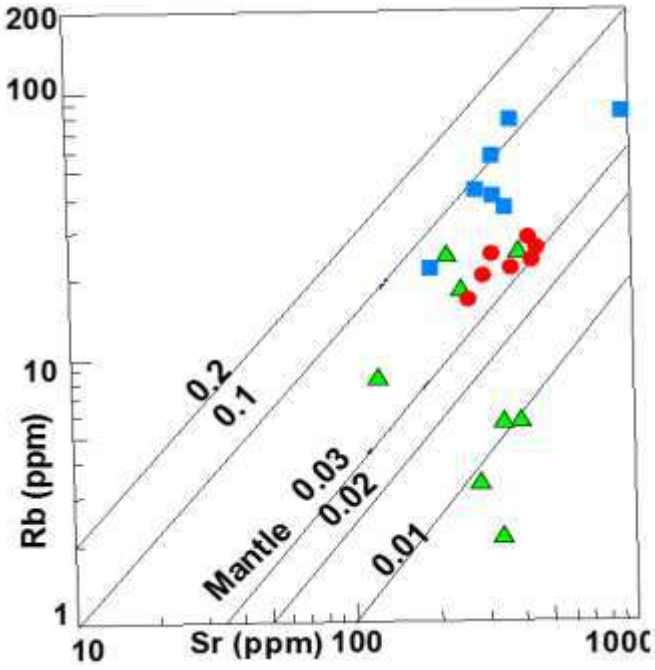

Fig.7.6. Rb-Sr distribution in gneisses, Incipient charnockite and foliated charnockite

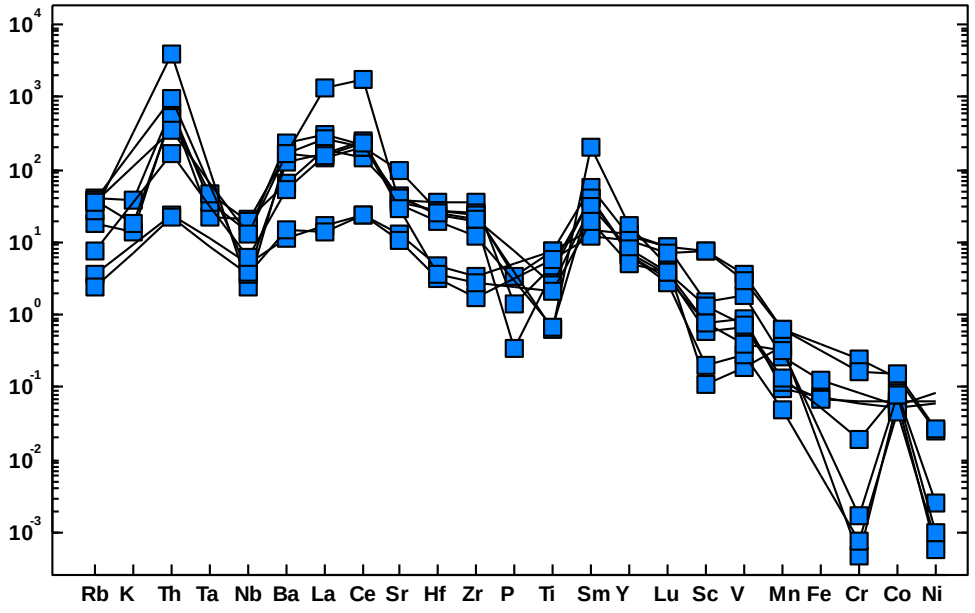

Fig. 7.7. Chondrite normalized value of trace element abundance pattern in gneisses, after Wood *et al*., (1979b)

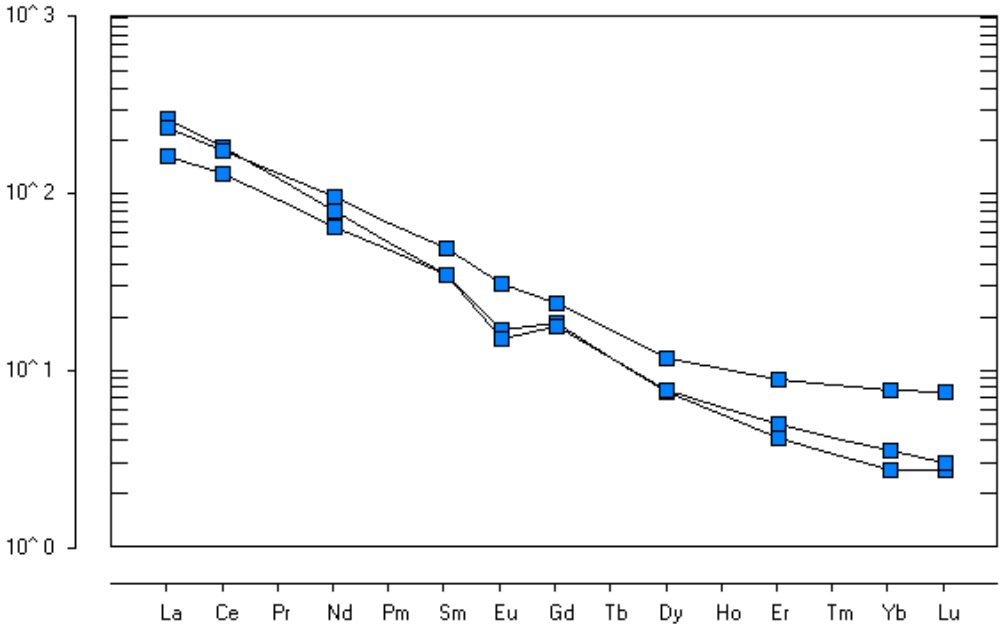

Fig. 7.8. Chondrite normalized value of REE pattern in Gneisses after Masuda *et al.*, (1973)

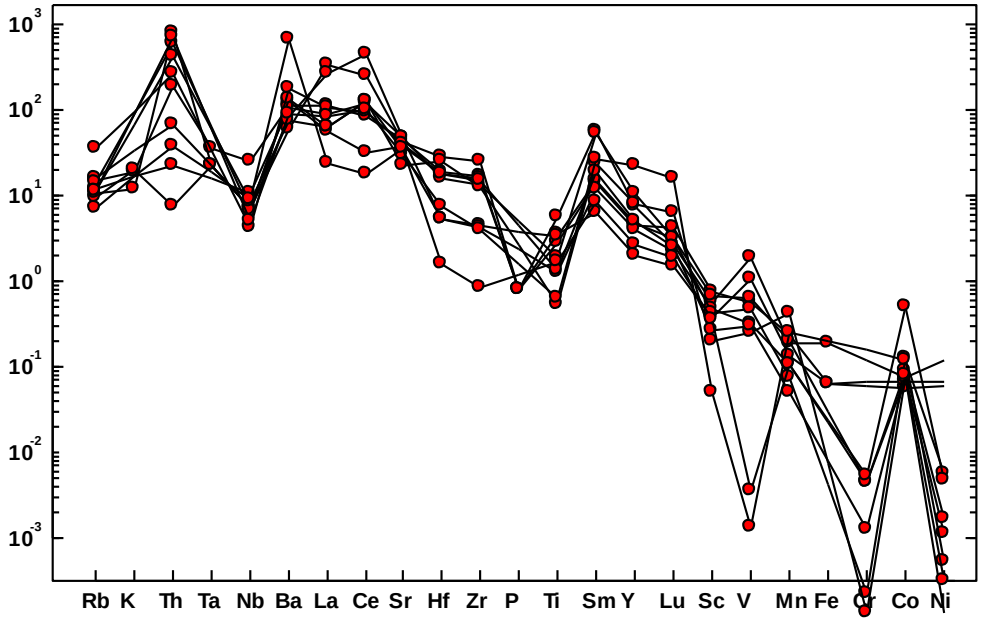

Fig. 7.9. Chondrite normalized value of trace element abundance pattern in Incipient charnockite after Wood *et al.*, (1979b)

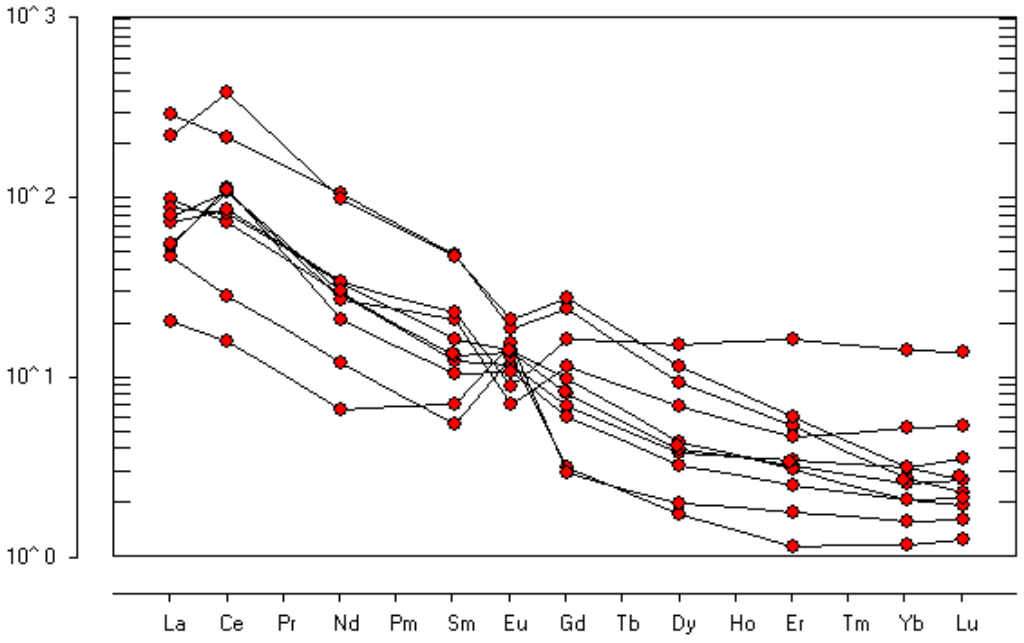

Fig.7.10. Chondrite normalized value of REE pattern in incipient charnockite after Masuda *et al.*, (1973)

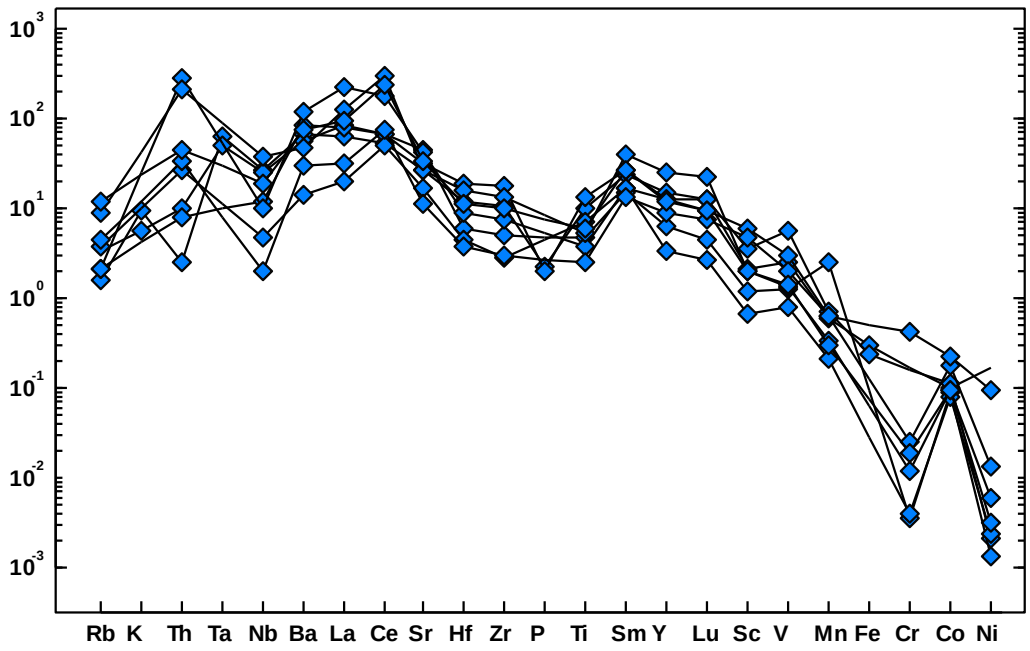

Fig. 7.11. Chondrite normalized value of trace element abundance pattern in foliated charnockite after Wood *et al.*, (1979b)

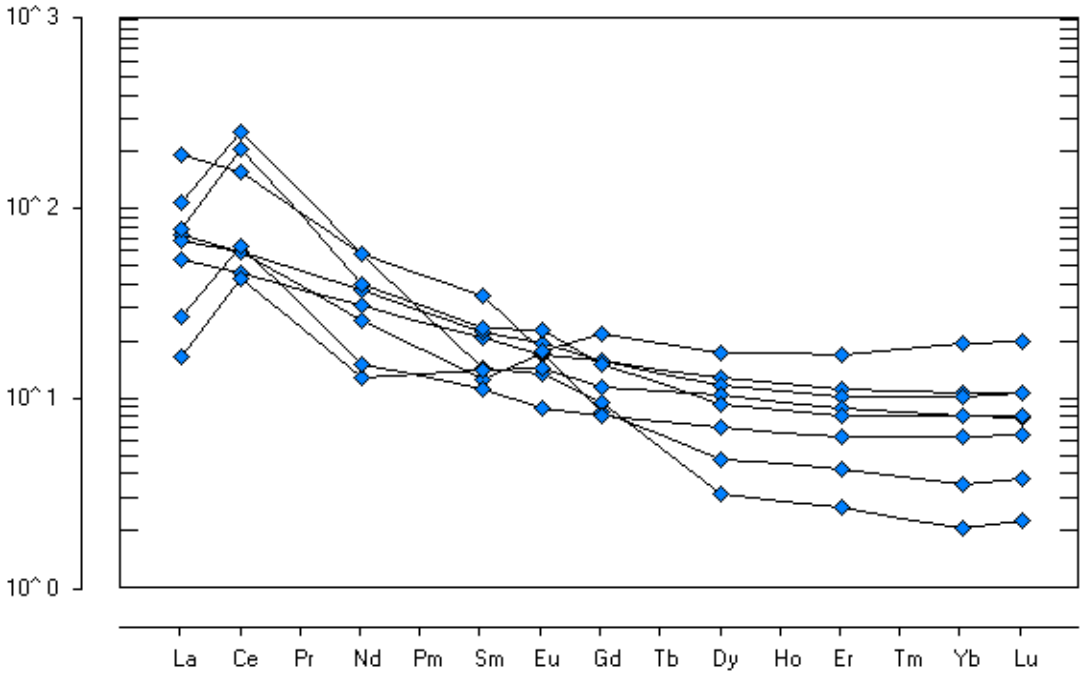

Fig.7.12. Chondrite normalized value of REE pattern in foliated charnockite after Masuda *et al.*, (1973)

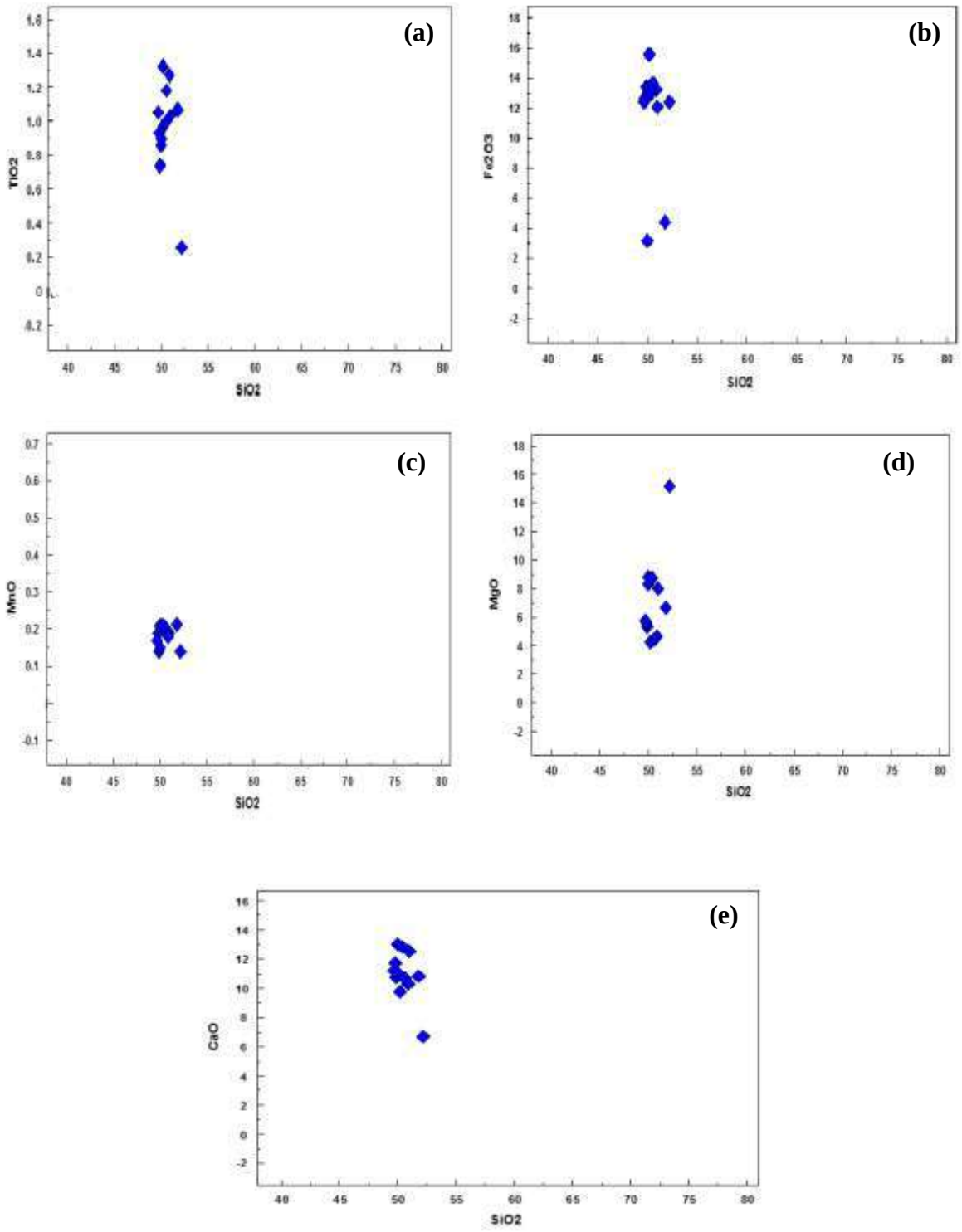

7.13a-e. Harker's variation diagram of pyroxene granulite

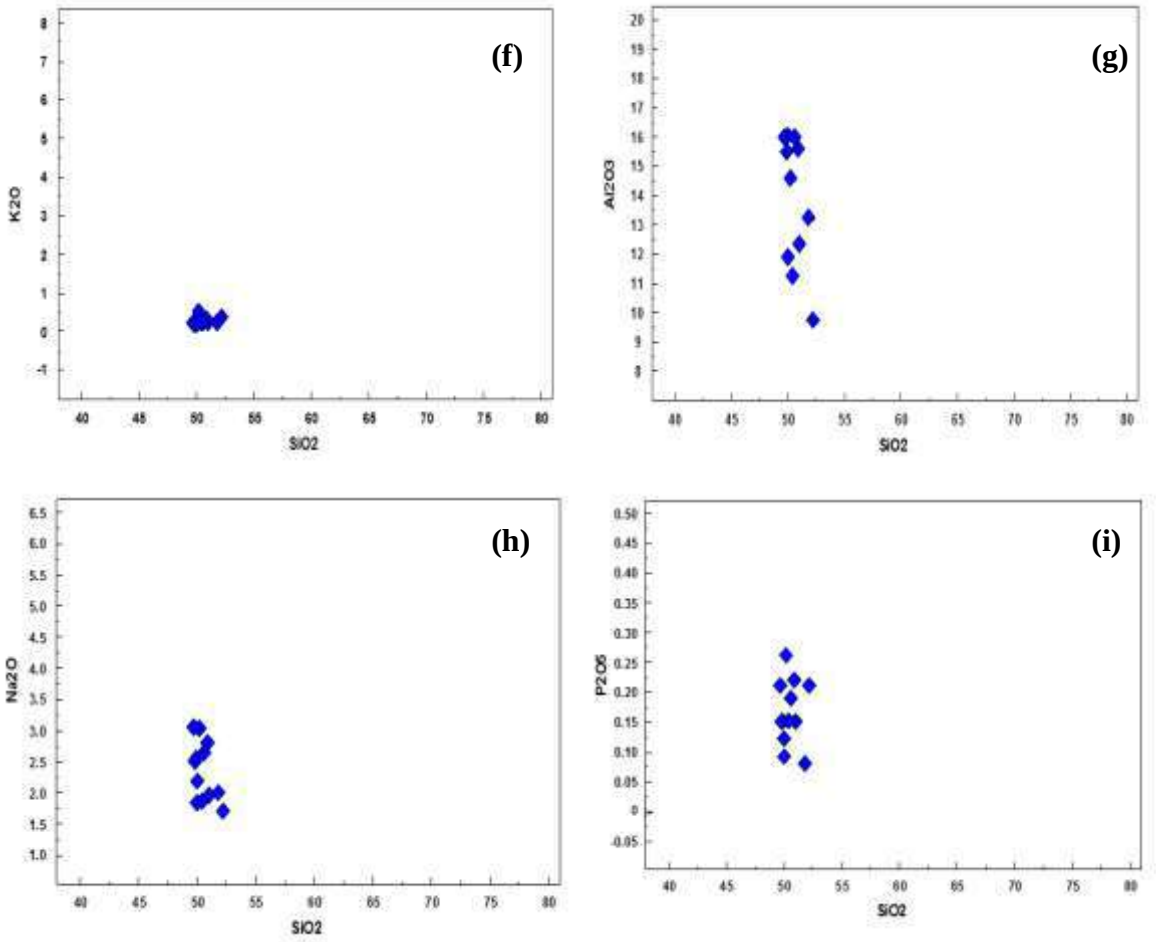

7.13f-i. Harker's variation diagram of pyroxene granulite

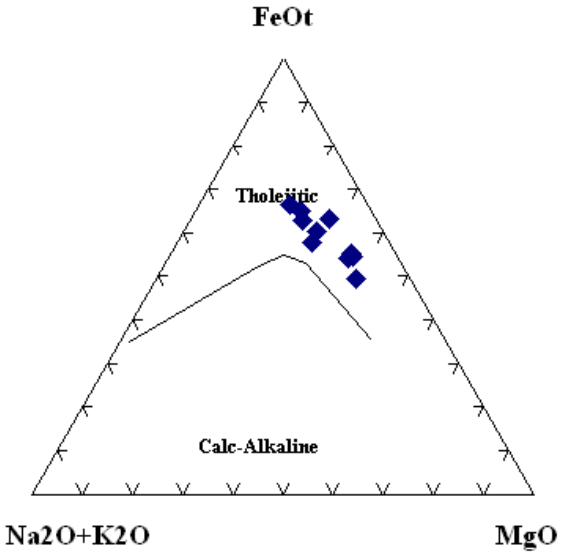

Fig.7.14. A-F-M diagram of pyroxene granulites (Winchester and Floyd, 1976).

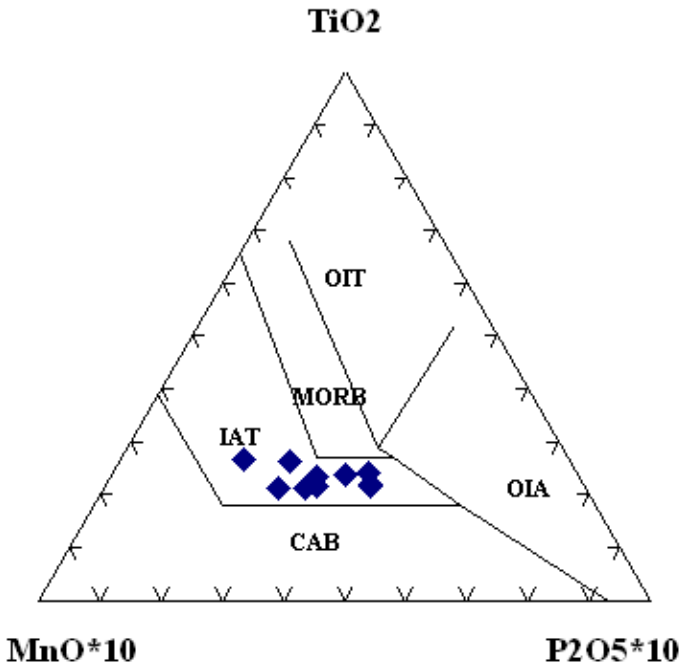

Fig. 7.15. TiO_2 - MnO*10 - P_2O_5*10 diagram (Wood, 1980) of pyroxene granulite

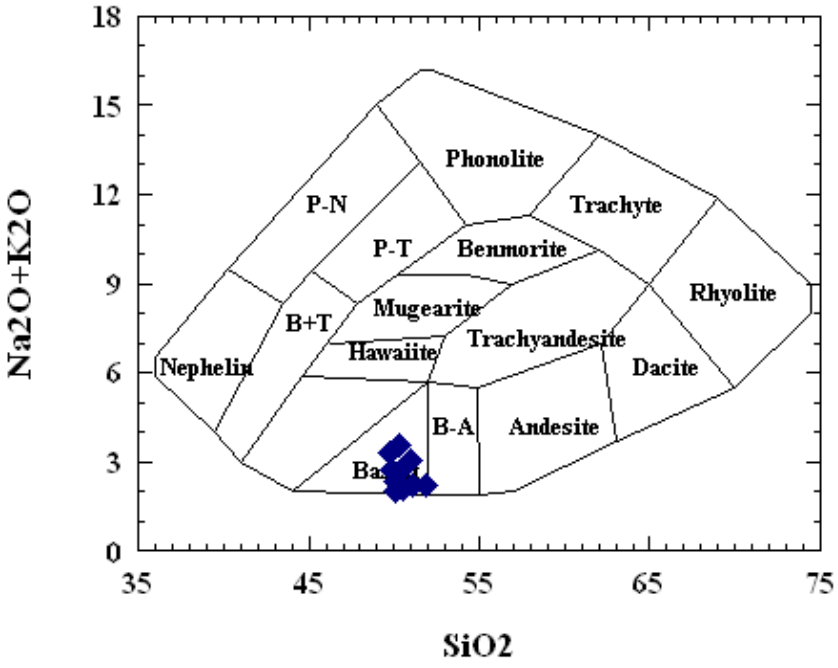

Fig. 7.16. (SiO_2-F/M) after Miyashiro (1974) of pyroxene granulite

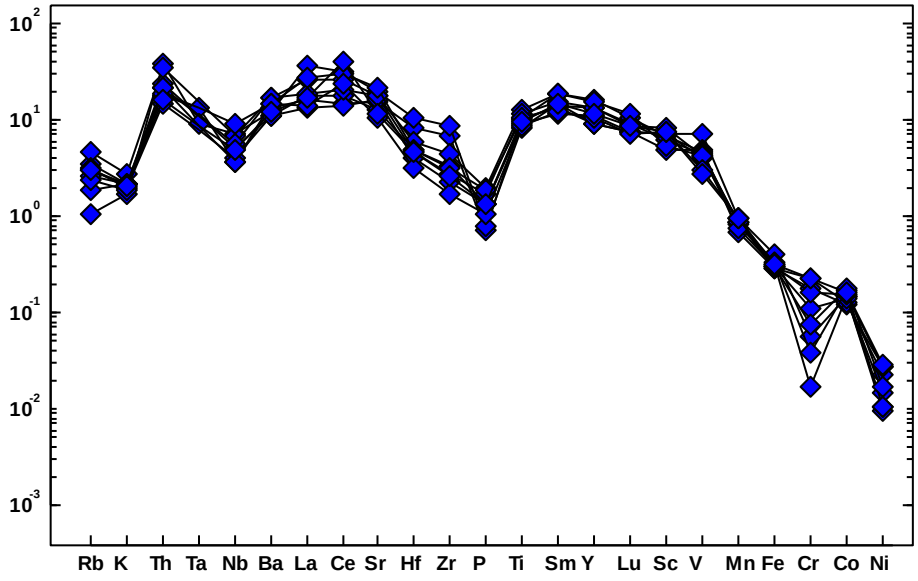

Fig. 7.17. Condrite normalized value of trace element abundance pattern in Pyroxene granulite, after Wood *et al.*, (1979b)

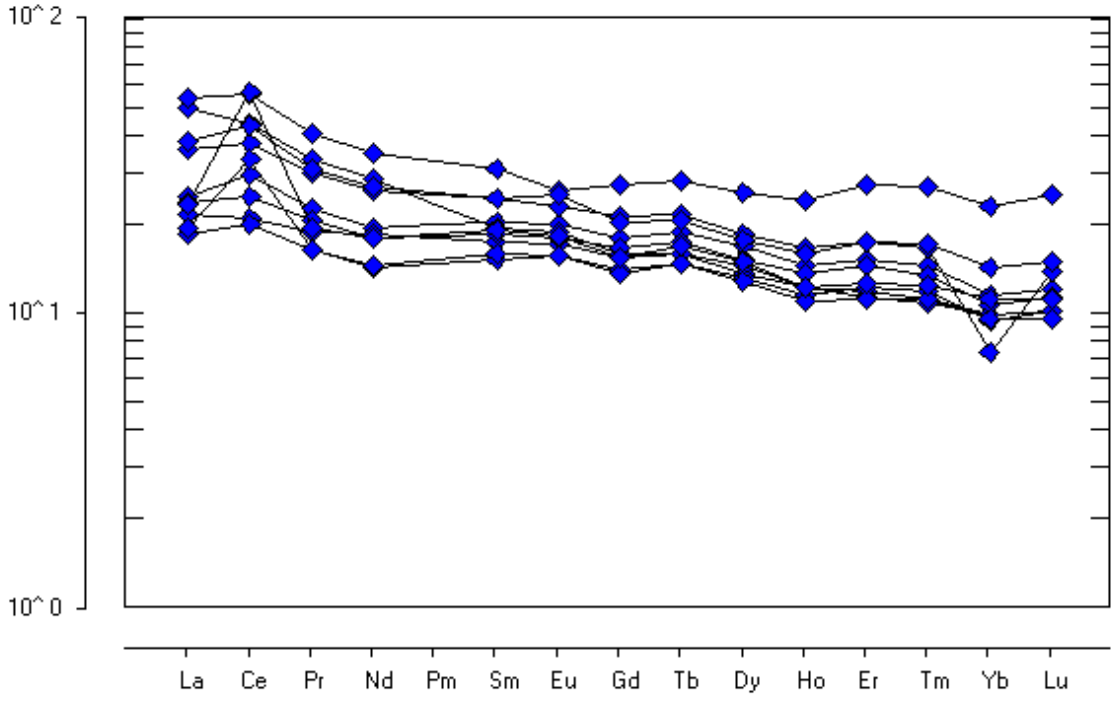

Fig.7.18. Condrite normalized value of REE pattern in pyroxene granulite, after Masuda *et al.*, (1973)

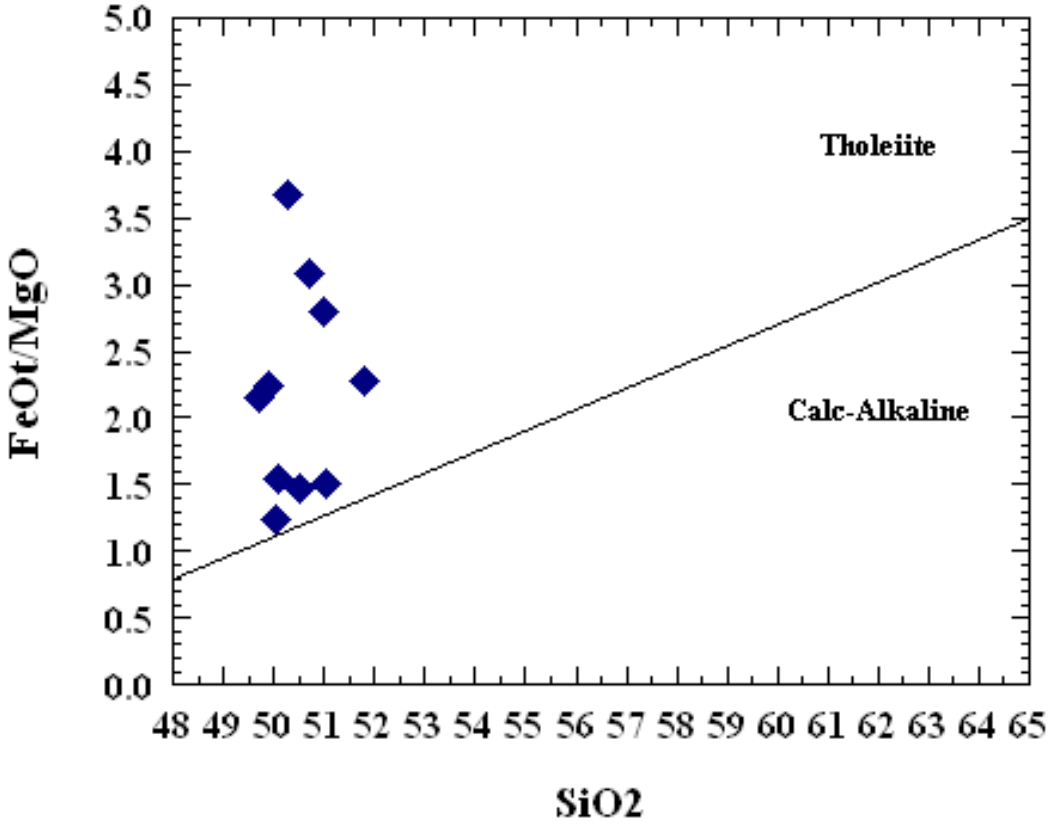

Fig. 7.19. FeO^T/MgO Vs SiO_2 plot (Barker, 1971) of pyroxene granulite

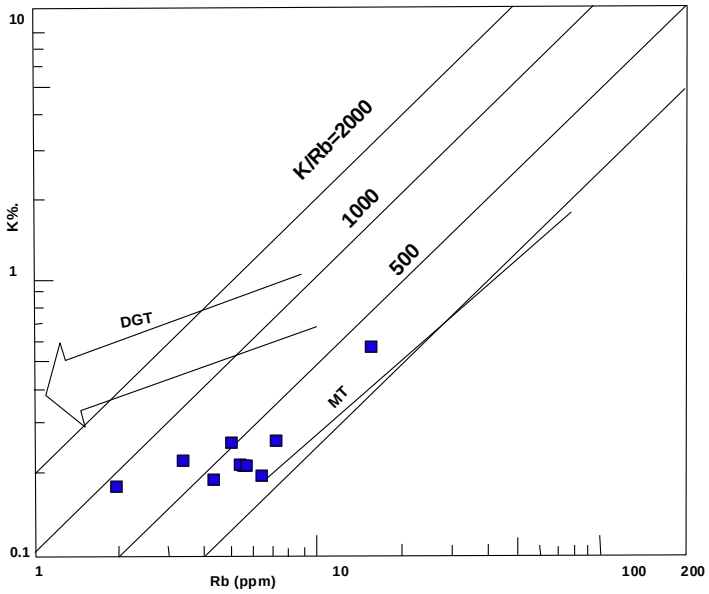

Fig.7.20. K-Rb distribution in Pyroxene granulites. Mt (Main trend for continental crust define by Shaw, 1968), DGT (Depleted granulite trend)

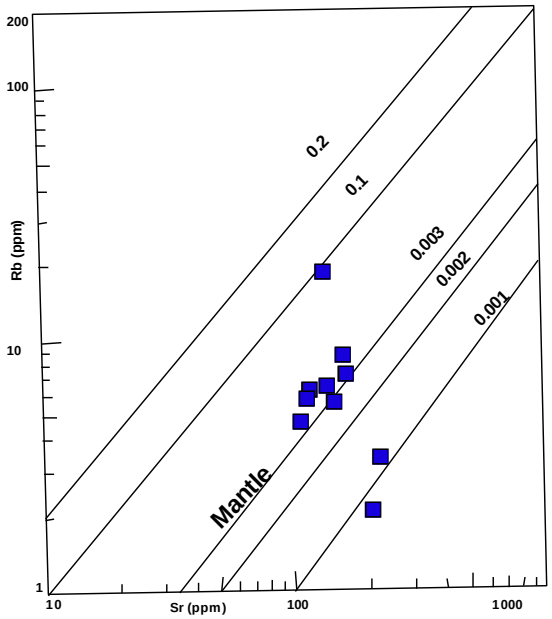

Fig. 7.21. Rb-Sr distribution in pyroxene granulites

Chapter - VIII

SUMMARY AND CONCLUSION

8.1. Summary

Nature and composition of the middle to lower crust is inferred from the study of amphibolite - granulite facies rocks. The studies of these rocks provide important constraints on the chemical and thermo tectonic processes that operated in the deep crust (Condie, 1981; Fountain and Salisbury, 1981; Harley, 1989; Bholen, 1991; Daczko *et al.*,, 2000; Bhattacharya and Sen, 2000). The Southern Indian shield exposes one of the largest granulite terrains of the world and the characteristic feature of this terrain is an unbroken transition from amphibolite to granulite facies with increasing P-T (Rasse *et al.*,, 1986). The terrain presents a cross section of events which have affected the crust at different levels and at different times. No single hypothesis can account for all the complexities noticed in charnockite (incipient and foliated) – gneiss – pyroxene granulite. An attempt has been made to constrain the metamorphic evolution of the Somvarpet area in particular and the gneiss-charnockite transformation in general.

Somvarpet area is a part of the amphibolite – granulite facies transition zone of the Western Dharwar Craton and covers the western most part of *Fermer's Orthopyroxene Isograde line*. Lithologies of the area include; amphibolite facies gneisses, incipient charnockite, foliated charnockite, pyroxene granulite, hornblende schist and mafic intrusives. Amphibolite facies gneisses are predominant in the northern part of the area and are migmatised to varying degrees and over printed by greasy brown patches of incipient charnockite. Quite often, the gneissic foliation is bent or swerved at the borders of the charnockite patches. The close observation reveals that the development of orthopyroxene along the set of conjugate shears trending $N30^0W$ to $N15^0E$ across the foliation. The foliated charnockite of the area is greasy looking and exhibits a granular texture. On fresh surface, the rock is massive in appearance, but, the

weathered surface show well developed foliation trending in NE-SW with moderate to steep dip due East. Pyroxene granulite is one of the major litho units in the southernmost part of the study area, and occurs as disrupted boulders, boudins and as enclaves within foliated charnockite and amphibolite facies gneisses. Hornblende schist is the minor litho unit and generally occurs in association with mafic granulites and also as enclaves within the gneisses and foliated charnockite. Mafic intrusives are represented mainly by dolerites, occur as bouldary outcrops with spheroidal weathering, they are dark coloured, fine to medium grained and exhibiting ophitic to sub-ophitic texture.

Based on petrography, gneisses of the study area are distinguished as non garnetiferous grey gneiss and garnetiferous leucocratic gneiss. The non garnetiferous gneiss essentially consists of quartz, K-feldspar and plagioclase feldspar in the felsic layers and, biotite/hornblende in the mafic layers, apatite, zircon and monazite occur as accessary phases. The garnetiferous gneiss comprises of quartz, plagioclase, microcline, biotite, and garnet. The incipient charnockite is coarse grained, exhibit xenoblastic texture with large plates of orthopyroxene. The petrographic study revealed the formation hypersthene at the expense of either biotite/hornblende.

Foliated charnockite exhibits granulitic texture and contain both the feldspars with quartz, hypersthene, biotite and hornblende. The pyroxene granulite is medium to fine grained and greenish black to black in colour, and exhibits granulitic texture. The rock essentially contains both ortho and clinopyroxenes and plagioclase with subordinate amounts of garnets.

The chemistry of pyroxenes indicates the moderate content of Al_2O_3 of Opx may be due to its formation at medium P-T conditions. Various discriminate diagrams indicate Opx from charnockites falls in the field of transition zone, and of pyroxene granulites in the metamorphic field. The Cpx from the pyroxene granulite and charnockites of

Somvarpet area are wollastonite or diopside in composition. Concentrations of Ti, Cr and Mn are very low. Ca and Mg content of Cpx increases towards the margin with decreasing Fe, Al, Ti and to a lesser extent Na, which reflects slight compositional zoning in Cpx. The garnets are mainly almandine in composition. Chemically, there is a variation from core to rim. Towards core, pyrope content increases with decrease in spessartine. This represents the typical retrograde diffusion zoning of garnet. The amphiboles are found to be calcic sub group. Ti content of the amphiboles varies from 0.3 - 0.41 in gneisses, 0.2 – 0.57 in foliated charnockite and 0.24 – 0.28 in pyroxene granulite. The variation in Ti content of amphiboles of different lithounits may be related to bulk chemistry. The plagioclase feldspars are characterised by low K-content, and most of them are albite rich, only few plagioclase of pyroxene granulite are anorthite in composition. High Ca content of plagioclase in pyroxene granulite is probably due to the grade of metamorphism and bulk chemistry of the rock.

The temperatures estimates using chemistry of the co-existing pyroxenes for the foliated charnockites, garnetiferous and non-garnetiferous pyroxene granulite by two pyroxene thermometers have given the following temperatures with respect to Brey and Kohler (1990) and Putrika (2008) respectively ;

- Foliated charnockites – 811 and 773°C
- Garnetiferous pyroxene granulites – 893 and 822°C
- Non-garnetiferous pyroxene granulite – 847 and 808°C

Gt-Cpx-Plg thermometers of Krogh (1988, 2001), Raheim and Green (1979) and Ellis and Green (1979) and Ai (1994) have yielded the following temperatures for core and rim respectively;

- Foliated charnockites - 659 and 613°C
- Pyroxene granulite - 652 and 581°C

The estimated mean temperature by using Plagioclase-K-feldspar thermometer of Putrika (2008) have given the temperature of core and rim for gray gneiss 738 - 732°C, incipient charnockite 747 - 745°C and foliated charnockite 917 - 905°C respectively.

P-T-t paths are believed to be of prime evidence, which can describe the tectonic settings for the granulite formation. The type (i) path is characteristics of continent-continent collision environments, the type (i) and (ii) some times of continental magmatic arc regions and (ii) and (iii) representing rift environments and hot spots (Bholen, 1991). Harley (1989) and Holger *et al.,* (2008), in his review on the types of P-T paths of granulites and their implications for the origin of granulite terrains has recognized a path of nearly isothermal decompression (ITD) and a path of nearly isobaric cooling (IBC). Bohlen (1987) argues that most of the granulite terrains follow the IBC path. Nevertheless both ITD and IBC paths occur equally in many of the granulite terrains.

Calculated P-T conditions of different rock types combined with textural studies are used to constrain P-T-t path. The temperatures estimated from pre-exsolution composition of co-existing plagioclase and K-feldspar of gneiss which yields 738 – 732^{o}C and the incipient charnockite of the same exsolution of co-existing minerals which yields 747 – 744^{o}C for rim to core respectively. Whereas, foliated charnockites exhibits varied temperature and pressure. Feldspar thermometry of Putrika, (2008) has yield temperatures of 917 – 911^{o}C and 811– 773^{o}C for core to rim respectively. Garnet-Cpx-Plagioclase thermometry of Raheim and Green, (1979) and Krogh (2001) have yield temperatures of 699 – 901^{o}C peak metamorphic temperature Whereas, Powell & Holland, (1988) and Eckert *et al.,* (1991) yield pressures of 6.9 – 8.4 kb peak metamorphic pressure.

The estimated temperatures for non garnetiferous pyroxene granulites by using Putrika (2008) two pyroxene thermometer yield 1017 – 939°C (avg. 978°C) for core and

rim respectively. This temperature seems to be higher and probably this temperature is of metamorphic or magmatic cooling temperature of pyroxene granulite intrusion. This assemblage was equilibrated at or near isobaric cooling as indicated by P-T data obtained using garnet- pyroxene thermometry. Gt-Opx thermobarometry of Sen and Bhattacharya, (1998) indicate 747 - 734°C temperature for core and rim and 10.6 – 11 kb peak pressure. The Gt-Cpx-plg thermobarometry of Krogh (2001) indicates 583°C temperature and pressure of 8.7 kb. Newton and Perkins (1982) barometer for the assemblage Opx-Gt-Pl-Qtz of pyroxene granulites yields 8.2 kb and 8 kb pressure for core and rim respectively. Mineral chemistry and thermobarometric study of pyroxene granulites exhibits isobaric cooling P-T path followed by isothermal decompression path. The above evidences indicate IBC and ITD P-T path for the Somvarpet area.

Fluid inclusion petrographic study indicates the presence of CO_2, CO_2-H_2O, and H_2O-NaCl and H_2O inclusions in different rock types. Presence of mixed CO_2-H_2O biphase inclusions and occasionally CO_2 rich biphase fluid inclusions were recorded mainly in quartz and rarely in plagioclase grains of gneisses, incipient and foliated charnockites and mafic granulites. The density of primary CO_2 inclusions in gneisses, incipient charnockite and foliated charnockite ranges from 0.905 to 1.063 g/cc, 0.850 to 1.026 g/cc and 0.951 to 1.014 g/cc respectively. The density of CO_2 of CO_2-H_2O biphase inclusion ranges between 0.574 to 0.712 gm/cc. Salinity of H_2O inclusions ranges from 1.036 to 14.976% NaCl equivalent in incipient charnockite. The primary CO_2 inclusions in charnockites are cross cut by a trail of low salinity (6.37-9.18 wt% NaCl equi.) inclusion. The homogenization temperatures of CO_2 in incipient charnockite range from -16.2 to 28°C and respective densities are 0.574 to 1.026gm/cc. High density CO_2 inclusions are the characteristics granulite facies rocks. Low density of CO_2 inclusions in the incipient charnockite suggest release and re-entrapment of inclusion along structurally

controlled weak zones. The density data obtained for CO_2 inclusions of foliated charnockites correlated with the P-T data and it indicates, the fluids might have entrapped at 897.6 to 945.4^oC temperature and 6.3 to 6.7 kb pressure which indicates syn-metamorphic nature of fluids. Correlation of CO_2 and H_2O fluid density plot and P-T data of gneisses indicate entrapment of fluids at 738^oC temperature and 4.5 – 5 kb pressure. Correlation of density values of CO_2 inclusions of incipient charnockite with the mineral P-T data indicate, CO_2 entrapment is at 729 to765^oC temperatures and 5.8 to 6.3 kb pressure. Relatively low density carbonic inclusion and their entrapment at relatively low P-T compared to CO_2 inclusion of incipient charnockite compare to foliated charnockite may be attributed to re-entrapment of earlier CO_2 during the formation incipient charnockite. Srikantappa *et al.,* (2008) and Jacques *et al.,* (2012) had same conclusions for the low density CO_2 inclusions in incipient charnockites.

Geothermobarometry, mineral stability, mineral isograde and fluid inclusion demonstrate that the P-T conditions along N-S traverse in the study area increase gradually from 738^oC/4.5-5kb in amphibolite facies gneisses to 764^oC/5.8-6.3kb in incipient charnockite; 898 – 945^oC/6.3-6.7kb in foliated charnockite further south. This is not only reflects increasing temperature and pressure of metamorphism but also a change in the fluid regime from amphibolite – granulite facies (Raase *et al.,* 1986).

Despite the mineralogical differences between gneisses and incipient charnockite of the Somvarpet area, they are broadly similar in terms of the major element geochemistry and they exhibit calc-alkaline trend. In contrast to major elements, the incipient charnockite is depleted in LIL elements, and it is a characteristic feature of granulite facies rocks, and suggests the passage of a fluid phase which extracted these elements. High K/Rb (2-2.5) and low Rb/Sr (0.01-0.09) ratios from gneisses to incipient charnockite follows distinct depleted granulite trend (DGT). The concentrations of HFS

elements show slight variation between gneiss and incipient charnockite respectively. Both gneisses and incipient charnockite display slightly variable REE patterns. Among the REE, HREE (La, Pr and Ce) is slightly depleted in incipient charnockite and overall concentration of the other REE is similar in both gneisses and incipient charnockite. REE patterns suggest the magmatic history of gneisses and incipient charnockite are similar to the classical Archaean tonalitic to trondjhemitic suites.

On Harker's diagram Al_2O_3, FeO, CaO, MgO and TiO_2 of foliated Charnockite show negative correlation with SiO_2. Whereas, K_2O and Na_2O do not define any definite trend, this may probably due to remobilization of these elements during granulite facies metamorphism. On the AFM diagram of Kuno (1968), the foliated charnockites plots well within the calc-alkaline fields. On An-Ab-Or and Qtz-Ab-Or, CIPW normative diagrams of Barker and Arth (1976) foliated charnockite fall in trondjametic field. Their Al_2O_3 content (>15%) they belong to high Al_2O_3 TTG group. The foliated charnockites of Somvarpet area are depleted in LIL elements when compare to incipient charnockite and exhibit high K/Rb ratios (2000-2500) and follows distinct depleted granulite trend (DGT). Depletion of Rb and to some extent Sr in the foliated charnockites of the present study has resulted in low to very low Rb/Sr ratios (0.01-0.09). The strong depletion of Rb relative to K is also evident from higher K/Rb ratios and similar higher K/Rb ratios are also reported for B.R.Hill, Kabbaldurga and Satanuru-Halguru-Sivanasamudrum charnockites (Janardhan *et al.,* 1994; Mahabaleshwar *et al.,* 1995). The foliated charnockites are characterized by moderate to high content of REE and display slightly fractionated REE pattern with $(La/Yb)_N$ ratios of 5.52-99.28, and REE patterns resemble the REE patterns of Archean TTG suite.

Major oxide geochemistry of the pyroxene granulites indicates they are derived from metamorphism of tholeiitic basalts. The negative correlation of CaO, MgO, Al_2O_3

and Fe_2O_3 with SiO_2 on Harker's diagram suggest fractionation of ferromagnesian and feldspars minerals from the melt during crystallization. The LIL elements contents are low to moderate and almost similar to BR Hill granulites (Janardhan *et al.,*, 1994). However, they are very low when compared to the average Archean tholeiites (about 12ppm; Condie, 1985) and Proterozoic mafic dykes (Radhakrishna and Joseph., 1998). This is probably due to the loss of Rb relative to K during granulite facies metamorphism. The transition metal (Ni and Cr) contents are slightly variable in Somvarpet pyroxene granulites. However, the average composition of these elements is slightly higher when compared to BR Hill granulites (Janardhan *et al.,*, 1994). The higher content of transitional trace metals in pyroxene granulites indicates high degree of mantle melting i.e. 20-30% (Janardhan *et al.,*, 1994). HFS elements behave as incompatible elements during mantle melting and enter preferentially into the melt (Saunders *et al.,*, 1988). The low to moderate content of these elements in Somvarpet pyroxene granulite suggest they have derived from near chondrite or depleted mantle source. The REE patterns of Somvarpet granulites are similar to Archean tholeiites reported elsewhere, and broadly comparable to the REE patterns of low-K, Island arc tholeiitic magma. The absence of negative Eu anomaly of Somvarpet pyroxene granulites may be attributed to deep source of melt precursors in which plagioclase is either absent during partial melting.

8.2. Conclusion

Recently Chetty *et al.,* (2012) have mapped the shear zones in the western part of the Dharwar craton. In this map the Somvarpet is located in the north of Kasaragod Mercara shear zone and to the east of Balehonnur shear zone. Santosh *et al.,* (2015) have demarcated the Coorg massif through Mercara shear zone to the south of western Dharwar craton and they defined it as an exotic block. Amaldev *et al.,* (2016) have said the Mercara shear zone is terrain boundary between Coorg block and western Dharwar

craton and they said it is a deeply eroded zone of subduction based on the geochemistry of magmatic suits of rocks and together with high P-T of metasedimentary rocks occurring within Coorg block. Very recently Ratheesh *et al.,* (2016) proposed a crustal thickness map for Biligirirangan hill and the surrounding areas by using gravity and flexure inversion technique. Based on integrated study (petrologic, isotope geochemistry, geochronology), they said that the eastward subduction of Western Dharwar craton beneath the Biliogirangan Mesoarchean continent and they have attributed spatial variation in the subduction to more thickened crust in Niligiri block. Hence, an integrated study (petrologic, isotope geochemistry, geochronology) is needed to understand the thickness of the crust and crust mantle interaction.

The present study contributes new petrological, geochemical, P-T estimates and fluid inclusion data base for the amphibolite to granulite facies transition zone of Somvarpet area. However, based on the data generated during the course of the study following conclusions are arrived;

- Amphibolite facies gneisses are predominant in the northern part of the area and are over printed by greasy brown patches of incipient charnockite along the shears.
- The development of orthopyroxene in incipient charnockite is at the expense of either biotite/hornblende.
- The foliated charnockite and mafic granulite are the dominant lithounits in the south indicating the gradual increase in grade of metamorphism from north to south.
- Relatively low density carbonic inclusion and their entrapment at relatively low P-T in incipient charnockite compared to foliated charnockite attributed to re-entrapment of earlier CO_2 during the formation incipient charnockite.
- The chemistry of amphibolite facies gneisses, incipient charnockite and foliated charnockite indicate they are high Al_2O_3 TTG.

- The relatively higher contents of LIL elements in incipient charnockites compared to foliated charnockite attributed to their enrichment during fluid induced metamorphism.
- Geothermobarometry, mineral stability, mineral isograde and fluid inclusion demonstrate that the P-T conditions along N-S traverse in the study area increase gradually from 738ºC/4.5-5kb in amphibolite facies gneisses to 764ºC/5.8-6.3kb in incipient charnockite; 898 – 945ºC/6.3-6.7kb in foliated charnockite further south. This is not only reflects increasing temperature and pressure of metamorphism but also a change in the fluid regime from amphibolite granulite facies.

REFERENCES

REFERENCES

Ai, Y. (1994) A revision of the garnet-clinopyroxene Fe^{2+} - Mg exchange geothermometer. *Contr. Min. and Petrol., v. 115, pp. 467–473.*

Allen, P. (1984) Origin of Archean charnockites from Southern India. *In A.Kroner, G.N.Hansen and A.M.Goodwin (Eds), Archean Geochemistry. Spr. verlag Berlin. 182-203.*

Amaldev, T., Santhosh, M. and Baiju, K. R. (2016) Convergent margin magmatism in the Mercara shear zone: terrane boundary between the Coorg block and the Western Dharwarn Craton, Southern India. *28th Kerala Sci. Cong, pp. 505-514.*

Aranovich, L.Y., Newton, R.C. (1997) H_2O activity in concentrated KCl and KCl-NaCl solutions at high temperatures and pressures measured by the brucite periclase equilibrium. *Cont. Min. Petrol., v. 127, pp. 261-271.*

Barker and Arth (1976) Generation of trondjamite-tonalite-liquids and archean bimodal trondjamite-basalt suits. *Jour. Geo., v.4, pp. 219-240.*

Basavarajappa, H. T. (1992) Petrology, Geochemistry and fluid inclusion studies of charnockites around B.R.Hills, Southern Karnataka, India. *Min. Petrol., v. 60, pp. 127-142.*

Bhaskar Rao, Y. J., Naha, K., Srinivasan, R. and Gopalan, K (1991) Geology, Geochemistry and geochronology of the Archean Peninsular gneiss around Gorur, Hassan district, Karnataka , India. *Proc. Of Indian Aca. Sci. (Ear. Plan. Sci.), v. 100, pp. 399-412.*

Bhaskar Rao, Y. J., Sivaraman, T. V., Pantulu, G. V. C., Gopalan, K. and Naquvi, S. M. (1992) Rb-Sr ages of late Archean metavocanics and granites, Dharwar Craton, South India and evidence for early Proterozoic thermotectonic events. *Prec. Res., v. 59, pp. 145-170.*

Bhattacharya and Sen (1986) Granulite metamorphism, fluid buffering and dehydration melting in Madras charnockites and metapelites. *Jour. Petrol., v. 27, pp. 1119-1141.*

Bhattacharya and Sen (2000) New insights into the origin of Kabbaldurga Charnockites, Karnataka, South India. *Gond. Res., v. 3, No. 4, pp. 489-506.*

Bhattacharya, S. and Chaudhary, A. (2013) Kabbaldurga charnockites revisited: Incipient growth or anatectic melt?. *Natu. Sci., v. 5, pp. 419-436.*

Bholen, S.R., Wall, V.J. and Boettcher, A. L. (1983) Experimental investigation and application of garnet granulite equilibria. *Cont. Min. Petrol., v. 28, pp. 310-318.*

Bodnar, R. J. (1983) A method of calculating fluid inclusion volumes based on vapour bubble diameter and P-V-T-X properties of inclusion fluids. *Econ. Geol., v. 78, pp. 535-542.*

Bohlen, S. R. (1987) Pressure-temperature-time paths and a tectonic model for the evolution of granulites. *Jour. Geol., V. 95, pp. 617-632.*

Bohlen, S. R. (1991) On the formation of granulites. *Jour. of Meta. Geol., V. 9, No. (3), pp. 223-229.*

Brey, G.P. and Kohler, T. (1990) Geothermobarometry in four-phase. New thermobarometers, and practical assessment of existing thermobarometers. *Jour. Petrol., v. 31, pp. 1353–1378.*

Brown and White (2008) Processes in granulite metamorphism. *Jour. Met. Geol., v. 26, pp. 121-124.*

Brown, P. E. and Lamb, W. M. (1988) P-V-T properties of fluids in the system H_2O + CO_2 + NaCl: new graphical presentations and implications for fluid inclusion studies. Geochimica. *Cosmochemica Acta., v. 53, pp. 1209-1221.*

Carswell, D.A. and Harley, S.L. (1990) Mineral barometry and thermometry. *In Carswell, D.A. (eds.): Eclogite facies rocks. Glasgow, London: Blackie, pp. 83–110.*

Chacko. T, Ravindra Kumar. G.R. and Newton R. C (1987) Metamorphic P-T conditions of the Kerala Khondalite belt, a granulite facies supracrustal terrain. *Jour. of Geo., vol. 95, pp. 343-358.*

Chadwick, B. and Enibley, R. W. (1993) Lava flows from a mid – 1980s submarine eruption on the cleft segment. Jamn de Fuca Ridge. *Jour. Geophy. Res., v. 99, pp. 4761-4776.*

Chadwick, B., Vasudev, V.N., Krishna Rao, B. and Hegde, G. V. (1989) The Dharwar super group: Basin development and implications for late Archean tectonic setting in western Karnataka, southern India. In: The Archean terrain, processes and metallogeny. *Glover J. E and Ho S. E. (eds.). The University of Western Australia, Publ., No.22, pp.3-15.*

Chadwick, B., Vasudev, V.N., Krishna Rao, B., Hegde, G.V. (1992) The Dharwar supergroup: Basin development and implications for Late Archean tectonic setting in western India, southern India. *In The Archean: Terrains, Processes and Metallogeny. (Ed.) Glover, J.E., and Ho, S., University of Western Australia.*

Chetty, T. R. K., Mohanty, D. P. and Yellappa, T. (2012) Mapping of shear zones in the Western Ghats, Southwestern part of Dharwar craton. *Jour. Geol. Soc. India. V. 79, pp. 151-154.*

Clemens, J. D. and Vielzuf, D. (1987) Constraints on melting and magma production in the crust. *Earth and planetary Science letters v. 86, pp. 287-306.*

Condie, K. C. (1981) Geochemical and isotopic constraints on the origin and source of Archean granulite. *Geol. Soc. Aust. Spec. Publ. No 7, pp. 469-479.*

Condie, K. C. and Allen, P. (1984) origin of Archean charnockites from Southern India. *In: A. Kroner (Edi.), Archean geochemistry. Springer Berlin, pp. 182-203.*

Condie, K. C., Allen, P. and Narayana, B. L. (1982) Geochemistry of the Archean low to high grade transition zone, southern India. Co*nt. min. petrol., v. 81, pp. 157-167.*

Condie, K. C. (1985) Secular variation in the composition of basalts: an index to mantle evolution. *Jour. Petrol., v. 26, pp. 545-563.*

Daczko, N.R., Clarke, G.L., and Klepeis, K.A. (2000) Transformation of two-pyroxene hornblende granulite to garnet granulite involving simultaneous melting and fracturing of the lower crust, Fordland, New Zealand: *Jour. Meta. Geol., v. 19, p. 549–562.*

Drury, S. A and Holt, R. W. (1980) The tectonic framework of the South India Craton: A reconnaissance involving landsat imagery. *Tectanophysics, v.65, pp. T1-T15.*

Drury, S. A., Harris, N. B. W., Holt, R. W., Reeves-Smith, G. J. and Wightman, R. T. (1984) Precambrian tectonics and crustal evolution in South India. *Jour. Geol., v. 92, pp. 1-20.*

Eckert, J. O. and Newton, R. C. (1993) Paleopressures of South Indian two-pyroxene garnet granulites from thermochemically calibrated CMAS barometers. *Jour. Met. Geol., v. 11, pp. 845-854.*

Eckert, J. O., Newton, R. C. and Kleppa, O. J. (1991) The ΔH of reaction and recalibration of garnet-pyroxene-plagioclase-quartz geobarometers in the CMAS system by solution calorimetry. *Am. Min., v. 76, pp. 148-160.*

Ellis, D. J. and Green, D. H. (1979) An experimental study of the effect of Ca upon garnet-Clinopyroxene Fe – Mg exchange equilibria. *Cont. Min. Petrol., v. 71, pp. 13-22.*

Ellis, D. J. and Green, D. H. (1985) Garnet- forming reactions in mafic granulites from Enderby Land, Antarctica Implications for geothermometry and geobarometry. *Jour. Petrol. v. 26, pp. 633-662.*

Fitzsimons, I. C. and Harley, S. L. (1994) Garnet coronas in scapolite – wollastonite calc-silicates from East Antarctica: the application and limitations of activity corrected grids. *Jour. Met. Geol., v. 12, pp. 761-777.*

Fountain, D. M and Salisbary, M. H. (1981) Exposed cross sections through the continental crust. Implication for crustal structure and evolution. *Ear. plan. Sci. Lett., v.56, pp.263-277.*

Friend, C. R. L. (1981) Charnockite and granite formation and influx of CO_2 at Kabbaldurga. *Nature (London) 294, pp. 550-552.*

Friend, C. R. L. and Nutman, A. P. (1992) Response of zircon U-Pb isotopes and whole rock geochemistry to CO_2 fluid induced granulite facies metamorphism, Kabbaldurga, Karnataka, South India. *Cont. Min. Petrol., v. 111, pp. 299-310.*

Fyfe, W. S. (1973) The generation of batholiths. *Technophysics, v. 17, pp. 273-283.*

Gopalkrishna, D., Hansen, E. C., Janardhan, A. S. and Newton, R. C. (1986) the southern margin of the Dharwar craton. *Jour. Geol., v. 94, pp. 247-260.*

Hansen, E. C. and Green, D. H. (1993) Experimental study of the stability of Cordierite and garnet in politic compositions at high pressure and temperature. III synthesis of experimental data and geological applications. *Cont. Min. petrol., v. 38, pp. 151-166.*

Hansen, E. C., Janardhan, A. S. Newton, R. C., Prame, W. K. B. N. and Ravindra Kumar, G. R. (1987) Arested Charnockite formation in southern India and Sri Lankha. *Contr. Min. Petrol., v. 96, pp. 225-244.*

Hansen, E. C., Janardhan, A. S., Newton, R. C., Prame, W. K. B. N. and Ravindra Kumar, G. R. (1986) Charnockites in the making in south India and Sri Lankha. *Contr. Min. Petrol., v. 26, pp. 79-95.*

Hansen, E. C., Newton, R. C. and Janardhan, A. S. (1984) Pressure, temperature and metamorphic fluids across an unbroken amphibolite facies transition in southern Karnataka, India; (*eds) Akroen, A. M. Goodwin and E. C. Hansen, Arch. Geochem. (Berlin: Springer-Verlag), pp. 161-181.*

Hansen, E. C., Newton, R. C., Janardhan, A. S. and Lindenberg, S. (1995) Differentiation of late Archean crust in the eastern dharwar craton, Krishnagiri-Salem area, South India. *Jour. Geo., v. 103, pp. 629-651.*

Harley, S. L. (1989) The origin of granulites: a metamorphic perspective. *Geol. Mag. 126, pp. 215-247.*

Harley, S. L. (1998) Ultrahigh temperature granulite metamorphism (1050^{o}C, 12 kb) metamorphism and decompression in garnet (Mg 70) – orthopyroxene – sillimanite gneisses from the Raucer group, East Antarctica. *Jour. Meta. Geol., v. 16, pp. 541-562.*

Harris, K. S. and Jayaram, S. (1982) Metamorphism of cordierite gneisses from the Bangalore region of the Indian Archean. *Cont. Min. Petrol., v. 34, pp. 341-353.*

Heier, K. S., (1973) Geochemistry of granulite facies rocks and problems of their origin. *Philos. Trans. Soc. London, A-273, pp. 429-442.*

Holger, S., Christoph. H., alfred, K. and Sospeter, M. (2008) Isothermal decompression history in the "Western granulite" terrain, central Tanzania: Evidence from reaction textures and trapped fluids in metapelites. *Jour. Afr. Ear. Sci., v. 51, pp. 123-144.*

Indares, A. and Martignole, J. (2003) Towards the upper limits of the granulite facies. *Jour. Meta. Geol., v. 21, pp. 1-2.*

Jachson, D. H., Metty, D. P. and Harris, N. B. W. (1988) Carbon isotope compositions of fluid inclusion in charnockites from southern India. *Nature, v.2, pp. 167-170.*

Jacques, L. R., Touret, J. L. and Martin, H. (2012) Fluid assisted granulite metamorphism: A continental journey. *Gond. Res. V. 21, pp. 224-235.*

Jahn, B. M. and Zhang, Z. Q. (1981) Radiometric ages (Rb-Sr, Sm-Nd,U-Pb) and REE geochemistry of Archean granulite gneisses from eastern Hebei Provinces, China. *Jour. China. vol. 6, pp. 204-234.*

Janardhan, A. S., Newton, R. C. and Hansen, E. C. (1982) The transformation of amphibolite facies gneiss to charnockite in southern Karnataka and northern Tamil Nadu, India. *Contri. Min. Petrol., v. 79, pp. 130-149.*

Janardhan, A. S., Newton, R. C. and Smith, J. V. (1979) Ancient crustal metamorphism at low H_2O. Charnockites formation at Kabbaldurga, South India. *Nature London, 278, pp. 511-514.*

Janardhan.A. S., Jayanada, M. and Shankar, M. A. (1994) Formation and Tectonic evolution of Granulites from the Biligiri Rangan and Nilgiri Hills, India: Geochemical and Isotopic constraints. *Jour. Geol. Soc. Ind, v, 44(1), pp. 27-40.*

Jayanada, M., Janardhan, A. S., Sivasubramanian, P. and Peucat, J. J. (1995) Geochronological and isotopic constraints on the granulite formation in the Kodaikanal area, southern India. *Geol. Soc. India Mem. V. 34, pp. 373-390.*

Jayananda, M. and Mahabaleshwar, B. (1991) The generation and emplacement of the clospet granite during the late Archean granulite metamorphism in south eastern Karnataka. *Jour. Geol. Soc. India, v.38, pp.418-426.*

Jayananda, M., Kano, T., Peucat, J. J. and Channabasappa, S. (2008) 3.35 Ga komatiite volcanism in the western Dharwar craton, southern India: constraints from Nd isotopes and whole-rock geochemistry. *Prec. Res., v. 162, pp. 160–179.*

Jayananda, M., Peucat, J. J., Chardon, D., Krishna Rao, B. and Corfu, F. (2013) Neoarchean greenstone volcanism, Dharwar craton, Southern India: constraints from SIMS zircon geochronology and Nd isotopes. *Preca. Res., v. 227, pp. 55–76.*

Kalia, K. L., Roy Choudary, K., Reddy, P., Krishna, V. G., Narain, Hari, Subotin, S. T. (1979) Crustal structure along the Kavali – Udupi profile in the Indian peninsular shield from deep seismic sounding. *Jour. Geol. Soc. India, v. 20, pp. 307-333.*

Kamineni, D. C. (1986) Distribution of Uranium thorium and rare earth elements in the Eye – Dashwa Lakes plutons study of some analog elements. *Jour. Chem. Geo., v. 55, pp. 361-373.*

Krogh, E. J. (1988) The garnet – Clinopyroxene Fe –Mg geothermometer – a reinterpretation of existing experimental data. *Cont. Min. Petrol., v. 99, pp. 44-48.*

Kuno, H. (1968) Differentiation of basalt magmas. In: Hess, H. H. and Poldervaart, A. *A. (eds.)* Basalts: The Poldervaart Treatise on Rocks of Basaltic Composition, 2*nd New York: Inter. Sci., pp. 623–688.*

Laird, D. and Albee, A. L. (1981) High pressure metamorphism in mafic schist from northern Vermont. *Am. Jour. Sci., v. 281, pp. 97-126.*

Lamb, W. M. (1990) Fluid inclusion in granulites. *In: granulites and crustal evolution. (Eds), Vietzeuf, D. and Vidal, P. H., pp. 68-70.*

Lamb, W. M. and Valley, J. M. (1987) Post metamorphic CO2 rich fluid inclusions in granulites. *Contr. Min. Petrol., v. 96, pp. 485-495.*

Leake, B. E. (1978) Nomenclature of amphiboles. *Cont. Min. Petrol., v. 16, pp. 501-520.*

Lee, H. Y., Ganguly, J. (1988) Equilibrium compositions of coexisting garnet and orthopyroxene: experimental determinations in the system FeO-MgO-Al_2O_3-SiO_2, and applications. *Jour. Petrol., v. 29, pp. 93–113.*

Lingadevaru. M, Shadakshara Swamy. N, Anantha Murthy. K.S and Mahabaleswar. B. (2007) Metamorphic P-T conditions of Hanur granulites, Karnataka, Southern India. *Kuv. Univ. Sci. Jour, pp. 123-131.*

Mahabaleshwar, B. and Peucat, J. J. (1988) 2.9 b.y Rb-Sr age of the granulite facies rocks of Satanur-Halgur and Sivanasamudram areas, Karnataka, South India. *Jour. Geol. Soc. India, v. 28, pp. 56-69.*

Mahabaleshwar, B., Jayananda, M., Peucat, J. J. and Shadakshara Swamy, N. (1995) Archean high grade gneiss complex from Satanur-Halgur-Sivansamudram area, Karnataka, Southern India; Petrogenesis and crustal evolution. *Jour. Geol. Soc. India, v. 45, pp. 33-49.*

Martin, H. (1987) Effect of steeper Archean geothermal gradient on geochemistry of subduction-zone magmas. *Jour. Geol., v. 14, pp. 753-756.*

Masuada, A., Nakumura, N. and Tanaka, T. (1973) Fine structures of mutually normalized REE patterns of chondrites. *Geochem. Cosmochim. Acta. 37: 239-248.*

Moorbath, S. and Windley, B. F. (1981) The Origin and Evolution of the Earth's Continental Crust. *The Royal Society, London (eds.), pp. 303.*

Naha, K., Srinivasan, R., Gopalan, K., Pantulu, G. V. C., Subba Rao, M. V., Vrevsky, A. B. and Bogomalov, Y. S. (1993) The nature of the basement in the Archean Dharwar craton of Southern India and the age of the Peninsular gneiss. *Proc. Indian Acd. Sci. (Ear. Pla. Sci.), v. 102, pp. 547-565.*

Newton, R. C. (1980) Carbonic metamorphism, granulites and crustal growth. *Nature, 288: pp. 5-49.*

Newton, R. C. (1989) Metamorphic fluids in the deep crust. *Annual reviews in earth sciences, v. 17, pp. 385-412.*

Newton, R. C. (1992) Charnockite alteration: evidence for CO_2 infiltration in granulite facies metamorphism. *Lour. Met. Geol., v. 10, pp. 383-400.*

Newton, R. C. and Perkin, D. (1982) Thermodynamic calibration of geobarometers based on the assemblage's garnet-plagioclase-orthopyroxene-clinopyroxenes-quartz. *Am. Min., vol. 67, pp. 203-222.*

Newton, R. C., Touret, J. L. R., and Arnovich, L. Y. (2014) Fluid and H_2O activity at the onset of granulite facies metamorphism. *Prec. Res., v. 253, pp. 17-25.*

Nutman, A.P., Chadwick, B., Krishna Rao, B. and Vasudev, V. N. (1996) SHRIMP U/Pb zircon ages of acid volcanic rocks in the Chitradurga and Sandur groups and granites adjacent to the Sandur schist belt, Karnataka. *Jour. Geo. Soc. India, V. 47, pp. 153-164.*

Nutman, A.P., Chadwick, B., Ramakrishna, M. and Viswanatha, M. N. (1992) SHRIMP U-Pb ages of detrital zircon in Sargur supracrustal rocks in western Karnataka, southern India. *Jour. Geol. Soc. of India, v. 39, pp. 367–374.*

O'conner, J. T. (1965) A classification for quartz rich igneous rocks based on feldspar ratio. *Us Geol. Surv., v. 525, pp. 79-84.*

Ohyama, H., Tsunogae, T., and Santhosh, M. (2008) CO_2-rich fluid inclusions in staurolite and associated minerals in a high-pressure ultrahigh-temperature granulite from the Gondwana suture in Southern India: *Lithos, v. 101, pp. 177-190.*

Perkins, D. and Chipera, S. J. (1985) Garnet – Orthopyroxene – plagioclase – quartz barometry: refinement and application to the English river subprovince and the Minnesota River valley. *Cont. Min. Petrol., v. 89, pp. 69-80.*

Peucat, J. J., Bouhallier, C., Fanning, C. M. and Jayananda, M. (1995) Age of Holenarsipur greenstone belt, relationship with the surrounding gneisses, Karnataka, South India. *Jour. Geol., v. 103, pp. 710-726.*

Peucat, J. J., Jayanada, M., Chardon, R., Capdevila, C., Fanning Marc. and Jean-Louis Paquette (2013) The lower crust of Dharwar craton, south India: patchwork of Achaean granulitic domains. *Jour. Prec. Res., v. 58, pp. 1-25.*

Peucat, J. J., Mahabaleswar, B. and Jayanada, M. (1993) Age of younger tonalitic magmatism and granulite metamorphism in the south Indian transition zone (Krishnagiri area): comparision with older peninsular gneiss from Hassan-Gorur area. *Jour. Meta. Geol., v. 11, pp. 879-888.*

Peucat, J. J., Videll, P., Bernard, G. J. and Condie, K. C. (1989) Sr, Nd and Pb isotopic systematic in the Archean low to high grade transition zone of Southern India: sun-accretion Vs post accretion granulite. *Jour. Geol., v. 97, pp. 537-550.*

Pichamuthu, C. S. (1960) Charnockites in the making; *Nature (London) 188, pp. 135-136.*

Pichamuthu, C. S. (1965) Regional metamorphism and Charnockitization in Mysore state, India. *Min. India. V. 6, pp. 119-126.*

Pichamuthu, C. S. and Srinivasan, R. (1984) The dharwar craton, perspective report series. *7th Indian National Sci. Aca., pp. 3-34.*

Powell, R. (1983) Fluids and melting under upper amphibolite facies conditions. *Jour. Geol. Soc. Lon. V. 140, pp. 629-633.*

Powell, R. and Holland, T. J. B. (1988) An internally consistent dataset with uncertainties and correlation; 3, application to geobarometry, worked examples and a computer program. *Jour. Met. Geol., v. 6, pp. 173-204.*

Pride, C. and Muecke, G.K. (1980) Rare earth element geochemistry of the Scourian Complex, NW Scotland - evidence for the granite-granulite link. *Cont. Min. Petrol., v. 73, pp. 403-412.*

Putirka, K. D. (2008) Thermometers and barometers for volcanic systems. *In: Putirka, K. D., and Tepley, F. (eds.), Minerals, Inclusions, and Volcanic Processes, Reviews in Mineral and Geochemistry, MSA, v. 69, pp. 61-120.*

Raase, P. (1974) Al and Ti contents of hornblende, indicators of pressure and temperature of regional metamorphism. *Cont. min. petrol., v. 45, pp. 231-236.*

Raase, P., Raith, M., Aackermand, D and Lal, R. K. (1986) Progressive metamorphism of mafic rocks from green schist to granulite facies in the Dharwar craton of South India. *Jour. Geol., v.94, pp.261-282.*

Radhakrishna, B. P. (1983) Archean granite-greenstone terrain of the south Indian shield, In: *Precambrian of South India. S. M. Naqui and J. J. W., Rogers (Eds.), Mem. Geol. Soc. India, No. 4, pp. 314-315.*

Radhakrishna, B. P. and Naqvi, S. M. (1986) Precambrian continental crust of India and its evolution. *Jour. Geol., v. 94, pp. 145-166.*

Radhakrishna, B. P. and Ramakrishna, M. (1988) Archean Proterozoic boundary in India. *Jour. Geo. Soc. India, v. 32, pp. 263-278.*

Radhakrishna, T. and Joseph, M. (1998) Geochemistry and petrogenesis of the Proterozoic dykes in Tamilnadu, south India: Another example of the Archaean Lithospheric mantle source. *Geo. Sci. Rundschau, v. 87, pp. 268-282.*

Raheim, A. and Green, D. H. (1979) Experimental determination of the temperature and pressure dependence of the Fe-Mg partition coefficient for coexisting garnet and clinopyroxene. *Cont. Min. Petrol., v. 48, pp. 179–203.*

Raith, M., Raase, P., Ackermand, D. and Lal, R. K. (1982) Regional Geothermobarometry in the granulite terrane of South India. *Tran. Res. Soc. Edinbergh. V. 73, pp. 221-244.*

Raith, M., Hoerness, S., Sthale, H. J. and Klate, E. (1989) Contrasting mechanisms of Charnockite formation in the amphibolite to granulite transition zones of Southern India. *In: Bridgwater, D. (Eds.) Fluid movements, element transport and the composition of the deep crust. NATO ASI series, v. 281, pp. 29-38. Kalwar academic publisher.*

Raith, M. and Srikantappa, C. (1993) Arrested charnockite formation at Kottavattam, South India. *Jour. Met. Geol., v. 11, pp. 815-832.*

Rajesh, H. M. and Santhosh, M. (2004) Charnockitic magmatism in southern India. Proc. *Indi. Aca. Sci. earth and planetary sci., v. 113, pp. 565-585.*

Rajesh, H. M. and Santhosh, M., Yoshikura, S. (2011) The Nagercoil charnockite: a magnesian, calcic to calc-alkalic granitoid dehydrated during a granulite-facies metamorphic event. *Jour. Petrol., v. 52, pp. 375–400.*

Ramachandra, H.M. and Abhinaba Rao (2001) Evolution of the Bhandara- Balghat granulite belt along the southern margin of the Sausar Mobile belt of central India. *Indian Acad. Sci. Earth planet Sci., v. 110(4), pp.351-368.*

Ramakrishnan, M. and Vaidyanadhan, R. (2008) Geology of India, Volume 1, Geological Society of India, Bangalore, 556p.

Rathees-Kumar, R. T., Santhosh, M., Qiong-Yan Yang, Ishwar Kumar, C., Neng Song Chen and Sajeev, K. (2016) Archean tectonics and crustal evolution of the Biligiri Rangan Block, Southern India. *Prec. Res., v. 275, pp. 406-428.*

Ravindra Kumar, G. R., Srikantappa, C. and Hansen, E. C. (1985) Charnockite formation at Ponumudi, Kerala, South India. *Nature (London), v. 313, pp. 207-209.*

Ravindra Kumar, G.R., and Srikantappa, C. (1995) Arrested charnockite formation in Palghat region, south India. *Jour. Geol. Soc. India, v. 45, pp. 147-164.*

Ravna, E. J. K. (2000) The garnet-clinopyroxene geothermometer: an updated calibration. *Jour. Meta. Geol., v. 18, pp. 211–219.*

Roedder, E. (1984) Fluid inclusions. *Reviews in mineralogy, Mineralogical Association of America, v. 12, 644p.*

Rollinson, H. R. and Windley, B. F. (1980) An Archean granulite-grade tonalite-trondjemite-granite suite from scouria, NW Scotland: geochemistry and origin. *Contr. Min. petrol., v. 72, pp. 265-281.*

Rudnick, R. L. and Presper, T. (1990) In crustal and crustal evolution (Kluwer, Dordrecht), *pp. 523-550.*

Rudnick, R. L., Mclennan, S. M. and Taylor, S. R. (1984) Large ion lithophile elements in rocks from high-pressure granulite facies terrains. *Geochim. Cosmochim. Acta., v. 49, pp. 1645-1655.*

Santhosh, M. (1984) Fluid inclusion and petrography of charnockites from the granulite facies terranes of Southern Kerala, South India. *Jour. Min., v. 8, pp. 337-345.*

Santhosh, M. (1985) Carbonic inclusion metamorphism of charnockites in the southwestern India shield: a fluid inclusion study. *Lithos, v. 19, pp. 1-10.*

Santhosh, M. (1991) Role of CO_2 in granulite petrogenesis: evidence from fluid inclusion. *Jour. Geosci. Oskha city univ., v. 34, pp. 1-53.*

Santhosh, M. (2013) Evolution of continents, cratons and supercontinents: building the habitable Earth. *Curr. Sci., V. 104, No. 7, pp. 871-879.*

Santhosh, M., Jayanada, M. and Mahabaleshwar, B. (1992) Fluid evolution in the clospet granite: a magmatic source for CO_2 in charnockite formation at Kabbaldurga. *Jour. Geol. Soc. Indi., v. 38, pp. 55-65.*

Santhosh, M., Kusky, T. and Wang, L. (2011) Supercontinental cycles, extreme metamorphic processes, and changing fluid regimes. *Intr. Geol. Rev., v. 53, pp. 1403-1423.*

Santhosh, M., Tagawa, M., Taguchi, S And Yoshikura, S. (2003) The Nagercoil granulite block, Southern India: petrology, fluid inclusions and exhumation history. *Jour. Asi. Ear. Sci., v. 22, pp. 131-155.*

Santhosh, M., Tanaka, K. and Yoshimura, Y., (2006) Carbonic fluid inclusions in ultrahigh temperature granitoids from southern India. *Comptes Rendus Geoscience, v. 337, pp. 327-335.*

Santhosh, M., Yang, Q. Y., Teng and Tang, L. (2015) Paleoproterozoic crustal growth in the North China cratonic: Evidence from the Luliang complex, *Prec. Res., v. 263, pp. 197-231.*

Saunders, A. D., Noory, M. J. and Tarney, J. (1988) Origin of MORB and chemically depleted mantle reservoir: trace element constraints. *Jour. Petrol., v. 29, pp. 415-445.*

Sen, S. K. and Bhattacharya, S. (1998) Dehydration melting of micas in the Chilka Lake Khondalites: The link between the metapelites and granitoids. *Proc. Indian Acad. Sci. (Earth Planet Sci), v. 106, pp. 277-297.*

Sheraton, J. W., Skimmer, A. C. and Tarney, J. (1973) The geochemistry of the Scourian gneisses of the Assynt district. *In R. G. Park and J. Tarnney (Eds.). The early Precambrian of Scotland and related rocks of greenland, University of Keele, pp. 13-30.*

Spear, F. S. (1981) An experimental study of hornblende stability and compositional variability in amphibole. *Am. Jour. Sci., v. 281, pp. 697-734.*

Srikantappa, C. (1987) Carbonic inclusions from the Niligiri charnockite massif, Tamil Nadu, India. *Jour. Geol. Soc. Ind., v. 30, pp. 72-76.*

Srikantappa, C. (1992) Syn-metamorphic carbonic inclusions in the Satanuru-Halagur granulites, Karnataka, India. *Jour. Geol. Soc. India. 39:502-508.*

Srikantappa, C. (1993) High pressure charnockites of the Nilgiri Hills, Southern India. In: B. P. Radhakrishna (Eds.) continental crust of South India. *Geo. Soc. India. Mem., v. 25, pp. 95-110.*

Srikantappa, C., Malathi M. N. (2008) Solid inclusions of magmatic halite and CO_2-H_2O inclusions in Closepet granite from Ramanagaram, Dharwar craton, India, *The Indian Min., v.42, no.1, pp.84-98.*

Srikantappa, C., Raith, M. and Spiering, B. (1985) progressive charnockitization of a Leptynite - Kondalite suitein Southern kerala, India- evidence for formation of charnockite, througha dcrease in fluid pressure. *Jour. geol. Soc. Ind., Vol. 26, pp.849-872.*

Srikantappa. C, Venugopal. L, Devaraju. J. and Basavalingu. B. (1994) P-T conditions of metamorphism and fluid inclusion characteristics of the Coorg granulites, Karnataka. Jour. Geol. Soc. India, v. 44, pp. 495-504.

Srikantappa. C. and Arash Zargar, S. (2009) First report on the halite bearing fluid inclusions in the Precambrian granulites around Halaguru, Dharwar Craton, India. *Indian Min., v. 43, pp. 77-80.*

Stahle, H. T., Raith M, Hoernes, S. and Dects, A. (1987) Element mobility during incipient charnockite formation at Kabbaldurga, Southern India. *Jour. Petrol., v. 28, pp. 803-834.*

Subramaniam, A. P. (1967) Charnockites and granulites of southern India. A review. Dan. *Geol. Foren., v. 17, pp. 473-493.*

Swami Nath, J. and Ramakrishnan, M. (1981) Early Precambrian supracrustals of Southern Karnataka. *Geol. Survey India Mem., v. 112, pp. 328.*

Swamin Nath, J., Ramakrishnan, M. and Vishwanatha, M. N. (1976) Dharwar stratigraphic model and Karnataka Craton evolution. *Rec. Geol. Surv. India, v. 107(2), pp. 149-175.*

Tarney and Windley (1977) Chemistry thermal gradient and evolution of the lower crust. *Jour. Geol. Soc. Lond, v. 134, pp. 153-172.*

Tarney, J. (1976) Geochemistry of Archean high-grade gneisses, with implications as to be the origin and evolution of the Precambrian crust. *In: Windley, B. F. (eds.) the early history of the earth. Wiley, London, pp. 405-417.*

Thompson, A. B. (1984) Fluid absent metamorphism. *Jour. Geo. Soc. Land., v. 140, pp. 533-547.*

Toriumi, M. and Akiko Nomizo. (2000) Difusion-controlled garnet growth during Sambagawa metamorphism. *Jour. Tect. Res. Japan, v. 44, pp. 47-57.*

Touret, J. L. R. (1971) granulites facies fluids inclusions in Les, Leen Norwage meridionale. *Lithos, v. 4, pp. 423-436.*

Touret, J. L. R. (1981) Fluid inclusion in high grade metamorphic rocks. *In: Hollister, L. S., Crawford, M. L. (eds.) short course in fluid inclusion: application to petrology. Mineral. Assoc. Can. Pp. 182-208.*

Touret, J. L. R. (2001) Fluids in metamorphic rocks. *Lithos, v. 55, pp. 1-25.*

Touret, J. L. R. and Hansen, E. C. (1988) Geothermobarometry and fluid inclusions in a rock from the Doddabetta charnockite complex, southwest India. *Rec. Soc. Ita. Min. Petrol., v. 43, pp. 65-82.*

Touret, J. L. R. and Hortel, T. H. D. (1990) Synmetamorphic fluid inclusion in granulites. *In vielzeuf, D. and Vidal, Ph. (Eds.) Granulites and crustal evolution, NATO ASI series, C-311, Kluwer Acad. Pub. pp. 397-490.*

Trendall, A. F., Laeter, D. E., Nelson, D. P. and Mukhopadhyay (1997) A precise zircon U-Pb age for the base of the BIF of Mulaingiri formation (Bababudan group, Dharwar supergroup) of the Karnataka Craton. *Jour. Geo. Soc. India., v. 50, pp. 161-170.*

Tsunogae, T., Santhosh, M., Ohyama, H. and Sato, K. (2008) High-pressure and ultra-high temperature metamorphism at Komatri, northern Madurai block, southern India. *Jour. Asi. Earth Sci., v. 33, pp. 395-413.*

Tylor, P. N., Chadwick, B., Friend, C. R. L, Ramakrishnan, M., Moorbath, S. and Vishwanatha, M. N. (1984) Petrography, chemistry and isotopic ages of peninsular gneiss, Dharwar acid volcanic rocks and Chitradurga granite with special reference to the late Archean evolution of the Karnataka craton, Southern India. *Prec. Res., v. 23, pp. 349-375.*

Valley, J. W. (1984) Fluid heterogeneity during granulite facies metamorphism in the Adirondacks: stable isotope evidence. *Contr. Min. Petrol., v. 85, pp. 158-173.*

Vanden Kerkhof, A. M. (1988) The system CO_2-CH_4-N_2 in fluid inclusion. Theoretical modelling and geological applications. Geochem. Cosmochem. *Acta., v. 54, pp. 621-629.*

Waters, D.J. and Whales, C.J. (1984) Dehydration melting and the granulite transition in metapelites from southern Namaqualand, South Africa. *Contr. Min. Petrol., v. 88, pp. 269-275.*

Weaver, B. L. and Taeney, J. (1982) Lewisian gneiss geochemistry and Archean crustal development models. *Earth planet Science Letters, 55, pp. 171-180.*

Weaver, B. L. and Tarney, J. (1983) Elemental depletion in Archean granulites facies rocks. *In migmatites melting and metamorphism (eds.) Atherton, M. P. and Gribble, C. D., Shiva publ. co. Nantwich, pp. 250-263.*

Wickham, S. M. (1987) The segregation and emplacement of granitic magmas. *Jour. Geol. Soc. Lond., v. 144, pp. 281-297.*

Winchester J.A. and Floyd P.A. (1977) Geochemical discrimination of different magma series and their differentiation products using immobile elements. *Chem. Geol., v., 20, pp. 325—343.*

Wood, B. J. and Banno, S. (1979) Activity – compositions in Ca(Mg, Fe)Si_2O_6 – $CaAl_2SiO_6$ clinopyroxene solid solutions. *Am. Jour. Sci., v. 279, pp. 854 -865.*

Zhang, Y. J. and Frantz, J. D. (1987) Determination of the homogenization temperature and densities of supercritical fluids in the system NACl-KCl-CaCl-H_2O using synthetic fluid inclusions. *Chem. Geol., v. 64, pp. 335-350.*

APPENDIX

Appendix– I

Sample Details of the Study Area

Sl. No	Sample No	Rock type	Location	Latitude	Longitude
1	J-11-1	Garnetiferous Gneiss	Kenchammana Hoskote quarry	12° 52' 01.3"	75° 50' 48.1"
2	J-11-2 & J-11-3	Gray Gneiss & Incipient charnockite	Kumbarhalli quarry	12° 48' 09.8"	75° 50' 03.4"
3	J-11-07	Gray Gneiss	2km NE of Kodlipet	12° 48' 37.6"	75° 54' 09.6"
4	J.11.10 & J-11-11	Gray Gneiss & Incipient charnockite	Kodlipet Junior College quarry	12° 48' 09.6"	75° 53' 47"
5	J-11-13	Gray Gneiss	Magge quarry	12° 52' 13.7"	75° 55' 12.2"
6	J-11-14	Garnetiferous Gneiss	Near Nidagarhalli	12° 52' 28.6"	75° 55' 22.3"
7	J-11-19C & J-11-19B	Gray Gneiss & Incipient charnockite	Shanthalli quarry	12° 38' 37.1"	75° 47' 20.8"
8	J-11-25	Gray Gneiss	Sulgod Somvar quarry 3km North of Alur.	12° 38' 56.5"	75° 56' 21.4"
9	J-11-27 & J-11-27A	Garnetiferous Gneiss & Incipient charnockite	Banavar quarry	12° 35' 48.0"	75° 56' 01.5"
10	J-11-35A & J-11-35	Gray Gneiss & Incipient charnockite	Thakeri quarry	12° 34' 28.9"	75° 48' 44.6"
11	J-11-41 & J-11-40	Gray Gneiss & Incipient charnockite	Jakkanhalli quarry	12° 39' 07.2"	75° 46' 38.7"
12	J-11-44	Garnetiferous Gneiss	Byadarvalli quarry	12° 52' 42.5"	75° 46' 26.9"
13	J-11-18	Foliated Charnockite	Road cutting between kutti and Shettalli	12° 39' 59.3"	75° 48' 29.2"
14	J-11-19A	Foliated Charnockite	Shanthalli quarry	12° 38' 37.1"	75° 47' 20.8"
15	J-11-20	Garnetiferous Foliated Charnockite	Vanaguru road cutting, 3km East of Patla	12° 43' 39.5"	75° 44' 40.4"
17	J-11-32	Foliated Charnockite	Road cutting between Somvarpet and Surlabi	12° 35' 31.6"	75° 49' 46.8"
18	J-11-33	Foliated Charnockite	Road cutting between Hangal and Surlabi	12° 34' 49.6"	75° 49' 53.9"
19	J-11-37	Foliated Charnockite	Road cutting between Garvale and Surlabi	12° 34' 11.8"	75° 45' 40.4"
20	J-2-4	Garnetiferous foliated charnockite	Road cutting between Somvarpet and Banavar	12° 36' 41.1"	75° 57' 26.7"
21	J.11.04	Pyroxene granulite	Road cutting between Doddakunda and Mallipatna	12° 47' 14.1"	75° 54' 28.5"

Contd...

22	J.11.05	Pyroxene granulite	Road cutting in between Doddakunda to Nirgod	12° 47' 14.1"	75° 54' 28.5"
23	J.11.06	Pyroxene granulite	Near Doddakunda	12° 47' 22.5"	75° 54' 27.3"
24	J.11.12	Pyroxene granulite	Kaganur road cutting	12° 50' 19.7"	75° 53' 19.1"
25	J.11.16	Pyroxene granulite	Near Magge	12° 52' 03.4"	75° 56' 24.8"
26	J.11.17	Pyroxene granulite	Near Basavarahalli	12° 51' 31.7"	75° 56' 38.6"
27	J.11.21	Pyroxene granulite	Rudragiri betta, 1km south of Uchangi village	12° 43' 36.6"	75° 48' 56.1"
28	J.11.22	Garnetiferous Pyroxene granulite	BTCS college campus, Somvarpet	12° 36' 26.3"	75° 51' 10.5"
29	J.11.24	Pyroxene granulite	In between the Alenirgundi and Alur road near Malambi	12° 41' 02.0"	75° 54' 06.4"
30	J.11.26	Pyroxene granulite	Adjacent Sulgod Somvar quarry	12° 38' 56.5"	75° 56' 21.4"
31	J.11.28	Garnetiferous Pyroxene granulite	Banavar	12° 36' 40"	75° 57' 25"
32	J.11.30	Pyroxene granulite	Hegatturu quarry	12° 39' 10.2"	75° 58' 29.6"
33	J.11.34	Pyroxene granulite	Gurvale village	12° 34' 54.3"	75° 46' 33.7"
34	J.11.36	Pyroxene granulite	5km behind Garvale village near coffee estate	12° 34' 54.3"	75° 46' 33.7"
35	SM-18	Garnetiferous Pyroxene granulite	Road cutting between Banavar and Bannur	12° 36' 41.1"	75° 57' 26.7"
36	SM-8-1	Pyroxene granulite	Malambi betta	12° 41'	75° 54' 06"
37	J-11-23	Hornblende schist	Road cutting between Alenirgundi and Alur	12° 41' 02.0"	75° 54' 06"
38	J-11-31	Hornblende schist	Adjacent to the Hegatturu quarry	12° 39' 09"	75° 58' 29"
39	J-11-38	Hornblende schist	Road cutting between Garvale and Surlabi	12° 34' 11"	75° 45' 39.4"
40	J-11-43	Hornblende schist	Jakkanhalli quarry on the way to Shanthalli	12°39' 05"	75° 46' 36"
41	J-11-42	Hornblende schist	Road cutting between Byadarvalli and Sakaleshpur	12° 52' 39.5"	75° 46' 24"
42	J.11.26A	Dolerite dyke	Adjacent Sulgod Somvar quarry	12° 38' 56.5"	75° 56' 21.4"
43	J-11-27C	Dolerite dyke	Banavar quarry	12° 35' 48.0"	75° 56' 01.5"
44	J-11-14A	Dolerite dyke	Nidagarhalli	12° 52' 28.6"	75° 55' 22.3"
45	J-11-19D	Dolerite dyke	Shanthalli quarry	12° 38' 37.1"	75° 47' 20.8"
46	J-11-4A	Dolerite dyke	Road cutting between Doddakunda and Mallipatna	12° 47' 14.1"	75° 54' 28.5"
47	J-11-24A	Dolerite dyke	Road cutting between Alenirgundi and Alur	12° 41' 02.0"	75° 54' 06.4"

LIST OF PUBLICATION

- **Jayaram, G. N.,** Anantha Murthy, K. S., Lingadevaru, M. and Govindaraju, **(2015)**: Fluid inclusion studies of Gneisses – Charnockite of Somvarpet area, South Western part of Dharwar Craton. *Abstract has been published in National seminar on earth resource assessment and management, pp. 52, November 24th – 25th at Kuvempu University, Shimoga.*

- **Jayaram, G. N.,** Anantha Murthy, K. S., Lingadevaru, M. and Govindaraju, **(2015)**: Geochemistry of Amphibolite – Granulite facies gneisses of Sakaleshpur-Somvarpet Area, Western Dharwar Craton. *International Jour. Of Research, vol. 2, Issue 3, pp 488-502.*

- **Jayaram G N,** Anantha Murthy K S, Lingadevaru M and Govindaraju, **(2015):** Geochemistry of Amphibolite – Granulite facies gneisses of Sakaleshpur – Somvarpet area, Western Dharwar Craton. *Abstract has been published published in XIV convention of Mineralogical society of India and National Seminar on recent advances in research on Precambrian terrains in India, pp. 20, 31st March 2015 at University of Mysore, Mysore*.

- **Jayaram G N,** Anantha Murthy K S, Lingadevaru M and Govindaraju, **(2014):** Geochemistry of Pyroxene granulite around Somvarpet, South Western Dharwar Craton, Karnataka, India. *Jour. Of Indian Mineralogist, vol. 48, No. 1, pp. 108-123*.

- Anantha Murthy K S, **Jayaram G N,** Lingadevaru M and Govindaraju, **(2013):** Petrology and Geochemistry of Pyroxene granulite around Somvarpet, South Western Dharwar Craton. *Extended abstract has been published in Goldsmidt Geochemistry 2013, International conference at Italy on 25th - 30th August 2013*.

- **Jayaram G N,** Lingadevaru M, Anantha Murthy K S and Govindaraju, (**2012):** Petrology of Amphibolite – Granulite facies transition zone around Sakaleshpur – Somvarpet area, Western Dharwar Craton. In: **Frontiers of Earth Science research'** (Eds; *Syed Asfaq and Ali Raza Moosvi), pp. 30-34* ISBN: 978-81-909728-4-0.